THE
PHYSICAL REVIEW
A Journal of Experimental and Theoretical Physics Established by E. L. Nichols in 1893
VOL. 52, NO. 5 SEPTEMBER 1, 1937 SECOND SERIES

The Electrodynamic Force Equation in its Bearing upon the Evidence for the Existence of a New Cosmic-Ray Particle

W. F. G. SWANN
Bartol Research Foundation of the Franklin Institute, Swarthmore, Pennsylvania
(Received July 6, 1937)

It is shown that the force in the force equation of electrodynamics may be multiplied by a relativistic invariant which leaves the equation practically unaltered for low velocities but which becomes important as the velocity of light is approached. The application of the invariant does not affect the constancy of the ordinarily assumed relativistic kinetic energy for motion in a pure magnetic field. The presence of the invariant referred to would result in one obtaining an erroneous value for the momentum if he interpreted the results of his experiments by the ordinary force equation. Moreover, the momentum which such an erroneous calculation would yield would depend, in the example cited, upon the magnetic field in which the measurements were made. Certain tentative remarks are made concerning the relationship of these matters to the evidence for the existence of the neutrino.

THE evidence for the existence of a new cosmic-ray particle goes back, ultimately, to measurements whose interpretation depends upon the Force equation

$$(d/dt)(m\mathbf{u}) = e(\mathbf{E}+[\mathbf{uH}]/c), \tag{1}$$

where $\mathbf{E}$ and $\mathbf{H}$ are the electric and magnetic fields, $\mathbf{u}$ the velocity, e the charge, and m the relativistic mass of the particle, and where c is the velocity of light. The mass m is related to the rest mass m_0 by the equation

$$m = km_0,$$

$$\text{where} \quad k=(1-\beta^2)^{-\frac{1}{2}} \quad \text{and} \quad \beta = u/c. \tag{2}$$

Equation (1) conserves $T-e(\mathbf{E}\cdot\mathbf{u})$ where

$$T=(k-1)m_0c^2. \tag{3}$$

T is the kinetic energy of the particle. In the case where $\mathbf{E}$ is zero, T itself is conserved.

Equation (1) is relativistically invariant, and would remain so if the right-hand side were multiplied by an invariant J. Moreover, in this case it would still follow that T as given by (3) would be conserved for $\mathbf{E}=0$. In other words k would be conserved for this case. Let us replace (1) therefore, by

$$(d/dt)(m\mathbf{u}) = Je(\mathbf{E}+[\mathbf{uH}]/c). \tag{4}$$

It is our purpose to show that invariants J can be constructed which would be unity for particles of low velocity moving in a pure magnetic field but which would differ from unity as the velocity of light is approached. The presence of such an invariant in the force equation would result in erroneous conclusions as to the rest mass being drawn by an interpretation of experimental results which neglected the invariant.

The product of any two 4-vectors gives an invariant. 4-vectors may be constructed from the

TABLE I. *Specifications of 4-vectors.*

4-VECTOR	COMPONENTS				DEGENERATE FORMS	
	x	y	z	4th	Resultant 3-vector	4th Component
I_1	ku_x	ku_y	ku_z	kic	$kr\omega$) ↓	kic
I_2	$(d/ds)(ku_x)$	$(d/ds)(ku_y)$	$(d/ds)(ku_z)$	$(d/ds)(kic)$	$k^2r\omega^2$ ←)	0
I_3	$(d^2/ds^2)(ku_x)$	$(d^2/ds^2)(ku_y)$	$(d^2/ds^2)(ku_z)$	$(d^2/ds^2)(kic)$	$k^3r\omega^3$) ↑	0
I_4	$(d^3/ds^3)(ku_x)$	$(d^3/ds^3)(ku_y)$	$(d^3/ds^3)(ku_z)$	$(d^3/ds^3)(kic)$	$k^4r\omega^4$ →)	0
I_5	etc.	etc.	etc.	etc.	$k^5r\omega^5$) ↓	0

field, as in the case of the 4-vector comprising the three components of the vector potential and the scalar potential, or they may be constructed from the motional elements alone. It is not our intention to determine a unique invariant to attach to the force equation, but simply one which *illustrates* our contention.

For our 4-vector material we may consider the 4-vectors I_1, I_2, etc., given in Table I, where $ds \equiv dt/k$, and where, under degenerate forms, we have given the values to which the resultant 3-vectors, and the 4th components degenerate for the case where the particle moves in a pure magnetic field, so that, as already stated, k is conserved in spite of the incorporation of the invariant J in (4). Here ω stands for angular velocity, and r, for radius of curvature.

The arrows give the direction of the resultant degenerate 3-vector for a clockwise motion along the element of path shown.

The scalar product of any of the two 4-vectors listed gives an invariant. However, we can readily see from the direction of the degenerate 3-vectors and from the fact that all the 4th components are zero except the first, that any scalar product of a 4-vector of odd order with one of even order is zero. Only scalar products of odd or of even 4-vectors survive, and these are obtained immediately in degenerate form by multiplying together the corresponding quantities in the column next to the last.

Now consider the invariant I defined by

$$I=[(I_1\cdot I_3)^{7/4}]/[(I_3\cdot I_5)^{3/4}].$$

It is, of course, zero when the velocity is zero, or as a matter of fact, when certain of the higher derivatives are zero. It degenerates to $-kr^2\omega$, i.e., to $-kur$ for the case of a pure magnetic field. Thus, if we should write for J

$$J=1-a_1I+a_2I^2\cdots\text{etc.},$$

our invariant would degenerate, for a pure magnetic field, to

$$J'=1+a_1kur+a_2k^2u^2r^2+\cdots,$$

where, of course, the a's are constants which may be positive or negative, and u for motion in the pure magnetic field is constant and is, as a matter of fact, nearly equal to c for high energy particles.

Equation (4) leads, for the case of a pure magnetic field, to

$$m_0k(u^2/r)=J'uHe/c$$

or writing m_0ku as the resultant momentum M *of the particle*, we have

$$\frac{M}{r}=\frac{J'He}{c}=\frac{He}{c}\left(1+\frac{a_1}{m_0}Mr+\frac{a_2}{m_0^2}(Mr)^2+\cdots\right).$$

Now by a suitable choice of the a's, we can make the coefficient of H/c practically any function of Mr we please. Thus, we can make it decrease with Mr indefinitely, as it would do if we chose the a's so as to make it e^{-Mr}. We can make it decrease with Mr and approach asymptotically some value different from unity. Thus, suppose that it approached asymptotically the value 0.25. Then if one measured the curvature of a high energy particle in a magnetic field and neglected the faster J', he would find a value of M too large by a factor of 4.[1] The extent of the error in M would depend upon Mr and these errors would reflect themselves upon the rest

[1] This matter has significance in relation to the particles of apparently abnormal mass reported by Street and Stevenson, Abstract no. 40, Meeting of the American Physical Society, Apr. 29, 1937.

mass, if there were other means of arriving at the velocity. They would, in fact, tempt one in certain cases to predict a continuous range of rest masses.

It is to be observed that J' depends upon M *and* r. This would mean that for the same M, we could, by altering H, realize a different value of J'. Under these conditions, if we should allow the same particle to pass through different magnetic fields and measure its momentum by cloud chamber observations in each case, we should, if we used the classical equation without J', obtain two different values for the apparent momentum. An experiment founded upon this principle should serve to test the idea here tentatively proposed.

It is perhaps worth while to point out that the classical electrodynamic equation has no very reputable ancestry such as would be likely to protest against the modification here suggested. Its origin, along with the electromagnetic equations from the Lagrangian equations, is simply a result of the adjustment of the relativistic Lagrangian function to a form designed to give that end. The fact that the Schroedinger equation leads to it as a statistical result applicable to the motion of a wave pocket applies, as far as I know, only to the case where relativistic considerations are neglected, and so has no bearing upon the problem here considered. There appears to be no case where the modification here suggested would come into conflict with principles already established.

In weighing the possibilities inherent in the foregoing considerations, one must attend to certain matters. S. H. Neddermeyer and C. Anderson,[2] by measurements of deviations in a magnetic field, have divided cosmic-ray particles into two categories, those associated with showers, and those associated with single rays. While the points of their graph are very scattered, there is a reasonably definite indication that the shower particles lose energy more rapidly in passing through matter than do the single particles; and, the energy loss for the former is consistent with the Bethe-Heitler theory. Anderson's measurements are interpreted in energy through the assumption of the normal electronic mass. If, therefore, we admit that two particles can show the same magnetic field deviation, but lose energy differently in passing through matter, we are in some difficulty, at first sight at any rate, in avoiding recognition of the existence of two different kinds of particles. It is true that the invariant in our force equation can be periodic in character, so that it does not change monotonically with the velocity; and, if such were the case one could have particles of different energy showing the same magnetic deflection and with the same rest mass. However, such an assumption seems rather radical in scope. The alternative is to admit that there is more than one kind of particle and then the advantage of providing for the constancy of the mass in the various particles becomes dubious. One could, of course, have the constant a's in the expression for J dependent upon the spin, or indeed an invariant might be constructed which involved the spin more obviously. In either case one would insure a condition in which although the particles had the same charge, the same rest mass, and obeyed the same laws for production of ionization, they had different force equations.[3]

It may be of interest to observe that if the force equation does in actuality involve an additional invariant J of the kind we have discussed in relation to the mass of the particle reported by Street and Stevenson, we should, in general, have a situation in which the energy as measured without regard to that invariant would be in error by a factor which increased with increase of the energy. The result would be that percentage losses in passing through lead divided by the average energy in the lead would come out too small; and, consequently, the apparent increase of energy loss with energy would come out too small.

One cannot help contemplating whether considerations of the foregoing kind may not have a bearing upon the evidence for the existence of the neutrino, since such evidence comes ultimately from the measurements of kinetic energies of electrons through assumption of the classical force equation. If the invariant J were incorpo-

[2] S. H. Neddermeyer and C. Anderson, Phys. Rev. **51**, 884 (1937).

[3] It must be remarked, however, that a modification of the force equation of the kind cited might permit even a proton of high energy, and consequently of low ionizing power, to masquerade as the particle reported by Street and Stevenson.

rated, it would not be $T-e(\mathbf{E}\cdot\mathbf{u})$ which would be conserved. We should, in fact, have

$$(1/J)(dT/dt)=e(\mathbf{E}\cdot\mathbf{u}).$$

It is true that the neutrino manifests itself in connection with particle energies far below those concerned in cosmic-rays, energies comparable with a million electron volts. It is to be observed, however, that there is nothing to require that J should change monotonically with increase of the velocity of the particle.

It must further be pointed out that there is little to *necessitate* regarding the ordinary expression (3) as having anything to do with the quantity which we speak of in energy transitions in atomic structure problems. The assignment of energy levels in atoms, and the subsequent determination of frequencies by their differences, for example, are things which do not involve T as given by (3) having any relation to that which should be conserved in the processes involved. The energy magnitudes concerned in atomic structure problems come, for the most part, from a consideration of magnitudes of constants which determine the characteristic solutions of ψ equations. It is quite true that experiments on critical potentials and the like form a bridge between kinetic energy as born of the force equation and energy as it occurs in problems of atomic structure; but, this bridge can hardly be considered to have been established for energies as high even as a million electron volts. However, it is not our purpose here to stress to the realm of the neutrino the considerations here presented. The main purpose of the paper concerns the cosmic-ray particles.

SEPTEMBER 1, 1937 PHYSICAL REVIEW VOLUME 52

The Disintegration of Lithium by Deuterons

JOHN H. WILLIAMS, WILLIAM G. SHEPHERD AND ROBERT O. HAXBY
University of Minnesota, Minneapolis, Minnesota

(Received June 21, 1937)

The following disintegrations have been studied in the range of deuteron energy from 100 to 250 kv:

$$_3Li^7+{}_1H^2\rightarrow{}_2He^4+{}_2He^4+{}_0n^1+Q_1 \quad (1)$$
$$_3Li^6+{}_1H^2\rightarrow{}_2He^4+{}_2He^4+Q_2 \quad (2)$$
$$_3Li^6+{}_1H^2\rightarrow{}_3Li^7+{}_1H^1+Q_{3a} \quad (3a)$$
$$_3Li^6+{}_1H^2\rightarrow{}_3Li^{7*}+{}_1H^1+Q_{3b} \quad (3b)$$
$$_3Li^{7*}\rightarrow{}_3Li^7+h\nu$$
$$_3Li^7+{}_1H^2\rightarrow{}_2He^5+{}_2He^4+Q_4 \quad (4)$$

Efficiency curves for (1), (2) and (3a) are regular. It is concluded that the Oppenheimer-Phillips process is not applicable to (3a). The relative yield of (3b) to (3a) increases with increasing deuteron energy. The return of the excited Li nucleus in (3b) to its normal state is shown by the emission of a gamma-ray of 400 kv energy as determined by absorption measurements. The existence of a homogeneous group of particles from (4) is interpreted as evidence for the instability of He^5, which has a mean life of approximately 6×10^{-20} sec. and is unstable by 0.93 Mev, disintegrating into an alpha-particle and a neutron. Absolute yields for the five disintegrations studied are given for a deuteron energy of 212 kv.

INTRODUCTION

STUDIES of the disintegration of lithium by deuterons over a wide range of energies have been made by various workers.[1-3] These researches, particularly with targets of separated isotopes, have established the identity of the disintegration processes and the reaction products.

The present paper reports a systematic study of the disintegration efficiency and the energy distribution of products of the following reactions in the deuteron energy range 100 to 250 kv.

$$_3Li^7+{}_1H^2\rightarrow{}_2He^4+{}_2He^4+{}_0n^1+Q_1, \quad (1)$$

$$_3Li^6+{}_1H^2\rightarrow{}_2He^4+{}_2He^4+Q_2, \quad (2)$$

[1] Cockcroft and Walton, Proc. Roy. Soc. **A144**, 704 (1934); Oliphant, Shire and Crowther, Proc. Roy. Soc. **A146**, 922 (1934); Oliphant, Kempton and Rutherford, Proc. Roy. Soc. **A149**, 406 (1935); Kempton, Browne and Maasdorp, Proc. Roy. Soc. **A157**, 372 (1936).
[2] Rumbaugh and Hafstad, Phys. Rev. **50**, 681 (1936).
[3] Alexopoulos, Helv. Phys. Acta **87**, 60 (1935).

$$_3Li^6+{}_1H^2\rightarrow{}_3Li^7+{}_1H^1+Q_{3a}, \quad (3a)$$

$$_3Li^6+{}_1H^2\rightarrow{}_3Li^{7*}+{}_1H^1+Q_{3b}, \quad (3b)$$

$$_3Li^{7*}\rightarrow{}_3Li^7+h\nu,$$

$$_3Li^7+{}_1H^2\rightarrow{}_2He^5+{}_2He^4. \quad (4)$$

The discovery of the existence of the postulated[2] gamma-ray following (3b) and the He^5 reaction (4) are also described.

Since Oliphant, Shire and Crowther[1] and Rumbaugh and Hafstad,[2] working with the separated isotopes of lithium, have already established the correct assignment of all the reactions except (4), these experiments were made using ordinary *thick* targets containing both lithium isotopes. To establish the nature of (4), targets of the separated isotopes Li^6 and Li^7 were used.

Apparatus

The transformer kenetron set, ion source, and accelerating tube described by Williams, Wells, Tate and Hill[4] were used. A new voltmeter consisting of 250 10 meg resistors similar to the one described by Hafstad, Heydenberg, and Tuve[5] served to measure voltages which were manually controlled and held to fluctuations in the output of less than 1 percent.

Charged particles were collected by means of a parallel plate ionization chamber connected to a Dunning type[6] amplifier. The output of this was fed into a thyratron scale of 8 counter[7] and a mechanical counter through a potentiometer. By adjusting this potentiometer and the depth of the ionization chamber, the counter could be made to respond only to particles whose specific ionization in the ionization chamber was above any desired amount. The amplifier power was supplied from a commercial voltage stabilizer and the gain was constant from day to day.

Due to the fact that the ion current is not steady and it is tedious and inaccurate to read a meter and average readings, a current integrator was constructed as shown in Fig. 1. The current from the Faraday cage charges a condenser

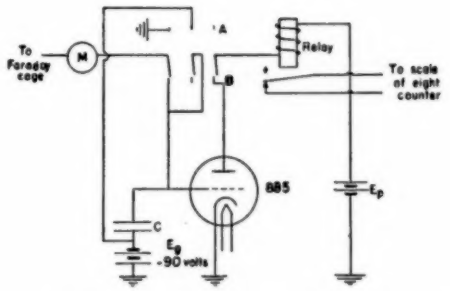

FIG. 1. Circuit diagram of current integrator. $C=22$ μf; A, B are positions of triple-pole double-throw switch; M is a microammeter, $E_p\sim150$ volts.

until the potential on the grid is sufficient to trip an 885 tube. When the tube fires the plate current of the 885 passes through a relay opening the input circuit of the scale of 8 counter. When the triple-pole double-throw switch is thrown to A it resets the circuit and when it is thrown to B the condenser charges from the collected ion beam. Thus, by taking readings of the counter before throwing the switch and again after the relay has opened, one obtains the number of counts for a definite amount of charge. As it is very essential to avoid leakage current W. E. 21L 2 μf paper condensers were used, since they were found to have inappreciable leakage conductance and bound charge. When the switch is first thrown to B the potential of the Faraday cage is about -90 volts. As the condensers charge this increase to about -12 volts when the thyratron fires. Because ions formed in the residual gas could produce a spurious current to the Faraday cage, a guard ring at a potential of about 45 volts was placed between the Faraday cage and the grounded part of the accelerating tube. With this precaution the spurious current collected was very small and in both directions so that the errors in a set of readings are less than one percent. The circuit was operated from a power pack connected to the stabilizer in order to eliminate errors due to voltage fluctuations.

Efficiency Curves

Since the concentration of deuterium in the mass two spot of the accelerating apparatus may change with time, measurements of the efficiency of a disintegration process as a function of deuteron energy are most readily made by comparing the yield to that at some standard

[4] Williams, Wells, Tate and Hill, Phys. Rev. **51**, 434 (1937).
[5] Hafstad, Heydenberg and Tuve, Phys. Rev. **50**, 504 (1936).
[6] Dunning, Rev. Sci. Inst. **5**, 387 (1934).
[7] Shepherd and Haxby, Rev. Sci. Inst. **7**, 425 (1936).

voltage. Our procedure was to take alternate readings of yield at a predetermined standard voltage, 212 kv. A further source of error arises from the deposition of hydrocarbons on the target under bombardment. To minimize this effect the LiCl thick targets were mounted on a disk holder which could be rotated to present a fresh target after each exposure of approximately three minutes duration.

The method employed in determining the efficiency curve for (1) is as follows. The amplifier detector system was made sufficiently differential to reject the α-particles of 8.4 cm range arising from molecular hydrogen in the mass two spot [the number of such α-particles was always less than 1 percent of those from (1)], as well as the α-particles from (2). With absorbing material of 2.8 cm air equivalent between the target and the ionization chamber the yield from (1) was determined as a function of voltage. In order to determine the numerical yield from this disintegration the area under a numbers *vs.* range curve at the standard voltage was compared to the yield from (2) under identical experimental conditions. As the minimum range was 2.8 cm a linear extrapolation of the numbers to zero absorber may introduce an error of 25 percent or less in the numerical yield determination.

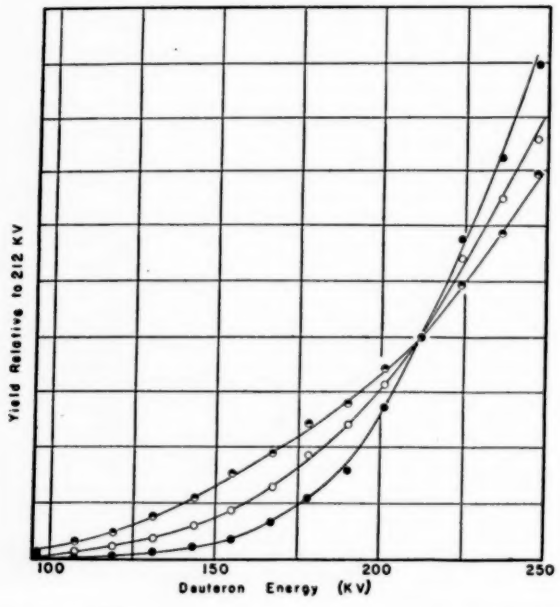

FIG. 2. Efficiency curves as a function of deuteron energy. Full circles, (1); half-full circles, (2); open circles, (3a). These curves are arbitrarily fitted at 212 kv.

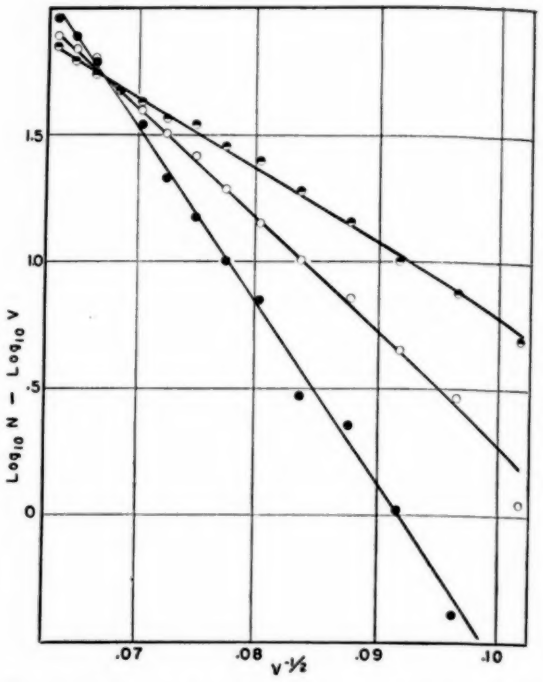

FIG. 3. Gamow plots of reactions (1), (2) and (3a) with same symbols as Fig. 2 from thick target data assuming $R \sim V^4$.

The α-particles from (2) were distinguished from the contamination deuterium-deuterium protons and other products by interposing an equivalent air path of 10 cm and by adjusting the potentiometer of the recording apparatus to count only α-particles.

In the case of the protons from (3a) sufficient absorbing material was introduced to remove the short range group from (3b). The counting mechanism was made sufficiently integral to record the protons without confusion due to increasing range with increasing bombarding deuteron energy.

In calculating the absolute yields from these disintegrations we have made reasonable assumptions as to the solid angle employed and have assumed an isotropic angular distribution which Neuert[8] has found to apply to (3a). The uncertainty in the concentration of deuterium in the mass two spot could be minimized by counting the number of α-particles of 8.4 cm range arising from molecular hydrogen bombardment and combining these numbers with the well-known yields from this proton reaction. We

[8] Neuert, Physik. Zeits. **38**, 122 (1937).

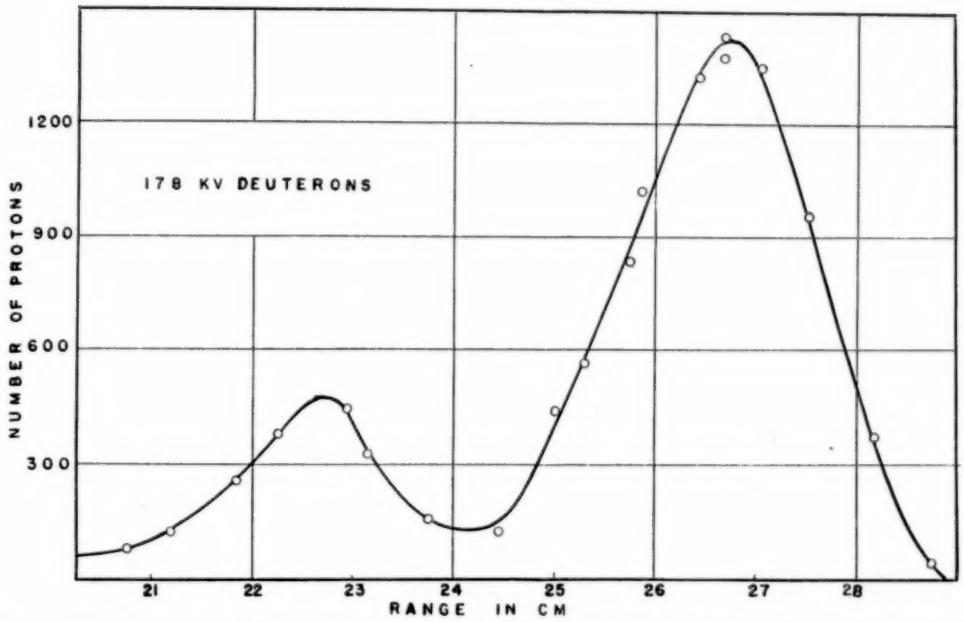

FIG. 4. Numbers *vs.* range curve for the protons from (3b) and (3a). The absolute range scale is not accurately determined.

estimate that our measured current is at least 90 percent deuterium. We have calculated our results on the basis of a thick target of lithium by multiplying the observations on LiCl by 20/3. Yields in disintegrations per deuteron of 212 kv energy are: (1) 4×10^{-7}, (2) 2×10^{-9}, (3a) 7×10^{-9}, (3b) 2×10^{-9}, (4) 3×10^{-9}. The estimated accuracy is ±50 percent.

The yields for (3b) and (4) were calculated from comparison measurements with the (3a) and (2), respectively, using the data described in later sections of this paper.

The efficiency curves for reactions (1), (2) and (3a) are shown in Fig. 2 where the curves are fitted at the standard voltage of 212 kv. It is seen that the yields increase smoothly with increasing deuteron energy with no evidence for resonance effects or other peculiarities. Increasing deuteron energy causes a more rapid increase in yield for (1) than for (2) while that for reaction (3a) falls intermediately.

Gamow plots, constructed from the thick target data following Oppenheimer's[9] integration which assumes range proportional to $V^{\frac{1}{2}}$, are shown in Fig. 3. It is evident that the data can be well fitted by three straight lines, as might well be expected for (1) and (2) since these processes are of the simple capture type discussed by Gamow. Conversely, reaction (3) is of the Oppenheimer-Phillips[10] type envisioned as a dissociation of the deuteron with the rejection of the proton. Since the data do fit Gamow plots assuming $R\sim V^{\frac{1}{2}}$, or $R\sim V^{1.2}$ as indicated by Mano's[11] data (the assumption is apparently not critical), one would conclude that the Oppenheimer-Phillips process is not important for this case.

A qualitative explanation for this conclusion follows. From the experimental evaluation of the exponent in the Gamow formula (assuming $R\sim V^{1.2}$) one can calculate a reasonable nuclear radius for (3a) of 4.5×10^{-13} cm. From the Oppenheimer-Phillips theory one concludes that if the deuteron is to be dissociated by the field of the nucleus the most probable distance to which the center of mass of the deuteron penetrates from the center of the nucleus should be roughly given by $X=Ze^2/2I$, where I is the binding energy of the deuteron ($\geqq2\times10^6$ ev). This gives $X\geqq1\times10^{-13}$ cm. Consequently one sees that for the lithium nucleus the deuteron would have already penetrated the potential barrier before dissociation would be probable. The Oppen-

[9] Henderson, Phys. Rev. **43**, 98 (1933).

[10] Oppenheimer and Phillips, Phys. Rev. **48**, 500 (1935).
[11] Mano, Ann. de physique **11**, 407 (1934).

heimer-Phillips process therefore does not occur for light nuclei where the potential barrier is less than the dissociation energy of the deuteron and the Gamow penetration theory should apply to these cases.

Protons from Li^6 and the Associated Gamma-Rays

Rumbaugh and Hafstad[2] have established the existence of two proton groups (3a) and (3b) of range approximately 26 cm and 30 cm by examining the disintegration products from targets of the separated isotope Li^6. The relative probability of these disintegrations has been examined throughout our voltage range. To measure the separate groups the ionization chamber and amplifier were set sufficiently differentially to almost completely resolve the two groups on an exploratory numbers *vs.* range plot as shown in Fig. 4. Several readings of the relative heights of the peaks were obtained by taking consecutive readings of numbers on the peaks. At each different deuteron energy the range position of the peaks was redetermined and relative peak readings taken at the appropriate amounts of absorbing material. The results are shown in Fig. 5, where the ratio of the yield of (3b) to (3a) is plotted as a function of deuteron energy.

The increase in relative yield is not linear and agrees in absolute value with the determinations of Rumbaugh, Roberts and Hafstad[12] at higher voltages. This increase might be expected on the general grounds that at higher bombarding energies (e.g., alpha-particle bombardment) the disintegration in which the nucleus is left in an excited state becomes relatively more probable.

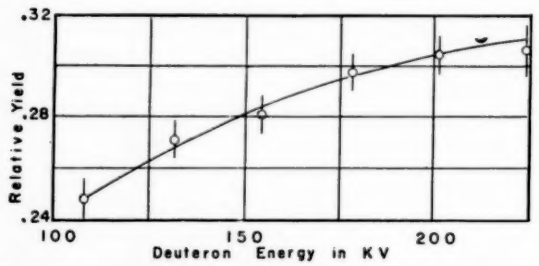

Fig. 5. Relative yield of protons from (3b) to protons from (3a) as a function of bombarding deuteron energy.

[12] Rumbaugh, Roberts and Hafstad (private communication). (We are indebted to these authors for the privilege of discussing their results prior to publication.)

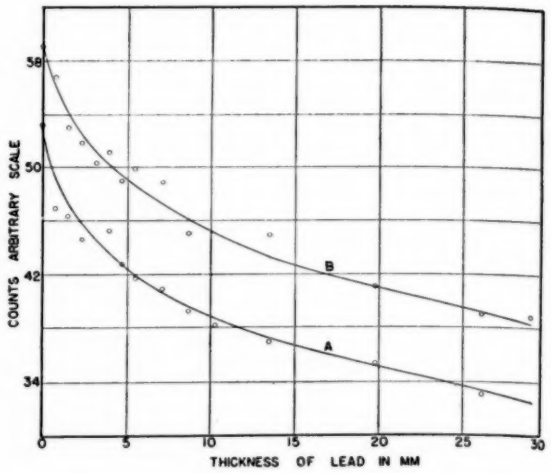

Fig. 6. Number of Geiger counter counts to an arbitrary scale as a function of thickness of lead absorber.

The interpretation of the two groups as due to the product nucleus being left in an excited state for (3b) leads to the prediction[2] of a gamma-ray of approximately 400 ± 40 kv energy being emitted as a secondary process.

To make absorption measurements of this radiation we have used a Geiger counter mounted in a tubular lead shield of 3 cm wall thickness. A port cut in the side of this shield allowed the counter to view the LiOH target without being exposed to any x-rays that were not scattered. Lead absorber sheets could be placed between the port and the target. The absorption measurements were complicated not only by the soft x-rays (primary rays less than 200 kv, scattered at least once) but by the copious neutrons emitted from the Li and contamination deuterium in the target under deuteron bombardment.

Two typical absorption curves are shown in Fig. 6. It is seen that the first millimeter of lead removes most of the x-rays and the absorption curve at large thicknesses of absorber allows an extrapolation to subtract the background effect of the neutrons present at lesser thicknesses of absorber. After the subtraction of the neutron background the logarithm of the remaining counts is a linear function of the thickness of lead as is shown in Fig. 7.

The absorption coefficient of this radiation in lead is calculated from our data to be 2.42 ± 0.20 cm^{-1}. This absorption coefficient indicates the presence of a gamma-ray of energy 400 to within

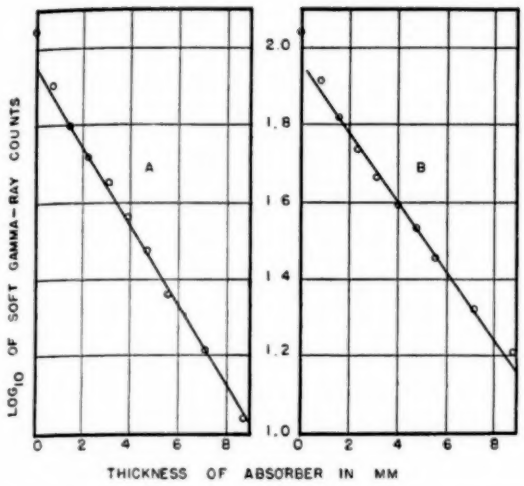

FIG. 7. Logarithm of counts not attributed to extraneous sources as a function of thickness of lead absorber.

an accuracy of 25 kv. It is only because the absorption coefficient is such a rapidly varying function of the energy of the radiation in this region that one can set such narrow limits on the energy. The evidence is thus in good agreement with the interpretation of the two proton groups. The failure of Alexopoulos[3] to observe the gamma-ray may be attributed to lack of intensity after absorption by 2 cm of lead.

THE INSTABILITY OF He^5

We have reported in a previous publication[13] evidence for the instability of He^5 from a study of the reaction

$$_3Li^7+{}_1H^2\rightarrow{}_2He^5+{}_2He^4+Q_4. \qquad (4)$$

Our measurements established the presence of a homogeneous group of alpha-particles of mean range 7.10 cm from Li^7 as shown in Fig. 8. This group was interpreted as the He^4 from reaction (4). The absence of a comparable homogeneous group of He^5 particles at 4.35 cm is to be expected since the substitution of mass-energy data in Eq. (4) gives He^5 a mass of 5.0140 which is unstable by 0.93 Mev.

We interpret the disintegration process as He^5 existing for a sufficient time to give the He^4 a somewhat definite energy in the disintegration. The He^5 then disintegrates into a neutron and an alpha-particle which share the initial energy of the He^5 and its negative energy of binding. One would then expect to observe these secondary alpha-particles with a calculable energy distribution. The energy of the alpha-particles may be written

$$E=4/5\epsilon+1/5Q+4(\epsilon Q)^{\frac{1}{2}}\cos\theta_r/5, \qquad (5)$$

where ϵ is the energy of the He^5 nucleus in the initial disintegration, Q is the disintegration energy of the He^5 into an alpha-particle and a neutron, and θ_r is the angle between the resultant He^4 and the initial He^5 in a coordinate system referred to the center of mass. Substituting the experimentally determined values, $\epsilon=6.25$ Mev and $Q=0.93$ Mev, one obtains values of E from 3.26 Mev to 7.12 Mev. The continuum of alpha-particle ranges would then extend from 1.90 cm to 6.06 cm.

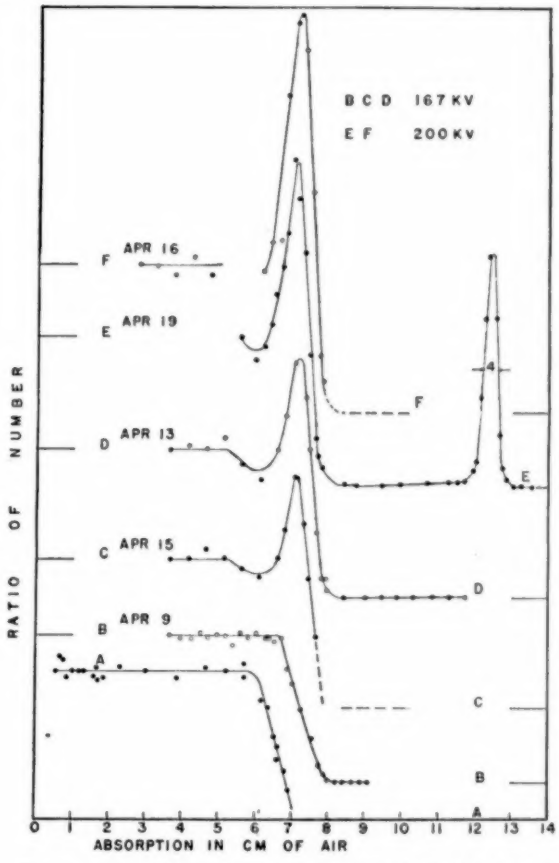

FIG. 8. Ratio of number of particles detected at a given absorption to the number at minimum absorption. The lettered scale marks on the left are unity and the corresponding marks on the right are zero. Curve *A* is from Oliphant, Kempton and Rutherford, reference 1. Increasing peak height at a given voltage is evidence of increasing differentiality of detecting apparatus.

[13] Williams, Shepherd, and Haxby, Phys. Rev. **51**, 888 (1937).

Assuming isotropic angular distribution of the secondary disintegration products with respect to the He^5 at rest, this continuum would present a plateau on the numbers *vs.* range curve between these limits. Our observations serve to indicate such a plateau by the dip in the numbers curve at 6 cm range. The experimentally allowable minimum range is not sufficiently small to enable a search for the corresponding decrease at small range. The evidence for the existence of this continuum is partially vitiated by uncertainty as to the exact distribution of particles in the background from (1).

Further evidence for the validity of our hypothesis arises from the extended width of the "homogeneous" alpha-particle group of 7.10 cm range as compared to the homogeneous alpha-particle group of 12.4 cm range from reaction (2). If we assume the shape of the underlying continuum due to (1) as extending horizontally to intercept the vertical portion of the total curve and attribute the residue to reaction (4), we find the width at half-maximum of the resultant peak is 6 mm. The half-width at half-maximum is thus 1 mm greater than is observed in the simple reaction (2).

This additional width corresponds to a variation in energy of 0.07 Mev and applying the uncertainty principle one calculates the mean life of He^5 to be approximately 6×10^{-20} sec.

ACKNOWLEDGMENTS

We wish to express our indebtedness to Dr. L. H. Rumbaugh of the Bartol Research Foundation who kindly supplied the separated isotopes of Li. We also wish to express our appreciation to Professor E. L. Hill for his stimulating and elucidating discussions and to Professor John T. Tate for his continued interest and encouragement.

This research was supported in part by a grant from the Graduate School.

SEPTEMBER 1, 1937 PHYSICAL REVIEW VOLUME 52

On the Comparison of Proton-Proton and Proton-Neutron Interactions

G. BREIT AND J. R. STEHN
University of Wisconsin, Madison, Wisconsin

(Received June 30, 1937)

Based on the data of Tuve, Heydenburg and Hafstad for the scattering of protons by protons and that of Amaldi and Fermi for the scattering of neutrons by protons a comparison of the two interactions is made. The present comparison is made more accurately than previously and allows for the uncertainty in the chemical factor C which is used in the interpretation of the neutron-proton experiments. The results are substantially in agreement with those of Breit, Condon and Present, the two interactions being very nearly equal. A slight excess of neutron-proton attraction over that between protons is indicated by the present calculation. Fermi's conclusion that the singlet S level of deuterium is virtual is reexamined by taking into account the effect of the range of force and of the chemical factor on the mean life of neutrons in an atmosphere of protons. Experiment agrees better with a virtual than with a real level. Nevertheless the evidence for its virtual character is not so good as to exclude completely the possibility that it is real. Tests by means of which a real level could be found if present are discussed.

A COMPARISON of the proton-proton and proton-neutron singlet S interactions using the experiments of Tuve, Heydenburg, Hafstad[1] on protons and of Amaldi, Fermi[2] on neutrons has already been made.[3] This comparison was not as complete as is desirable because: (a) Only Fermi's conclusion[4] that the lowest proton-

[1] M. A. Tuve, N. P. Heydenburg and L. R. Hafstad, Phys. Rev. **50**, 806 (1936).

[2] E. Amaldi and E. Fermi, Ricerca Scient. **7** *I*, 310 (1936); E. Amaldi and E. Fermi, Phys. Rev. **50**, 899 (1936).

[3] G. Breit, E. U. Condon and R. D. Present, Phys. Rev. **50**, 825 (1936).

[4] E. Fermi, Ricerca Scient. **7** *II*, 13 (1936). The extension of Fermi's formula used here is obtained by calculating without approximations, the transition probability due to

neutron singlet S level is virtual was used, and (b) only one value of Fermi's chemical factor was taken into account. This incompleteness is overcome in Table I, wherein we give values obtained for the proton-neutron interaction using the Amaldi-Fermi thermal neutron elastic scattering cross section of 43×10^{-24} cm^2. According to Fermi,[4] this experimental value should be set equal to $C(\pi a_1^2+3\pi a_3^2)$, where a_1 and a_3 are respectively the values in cm of the intercepts of straight line portions of the singlet and triplet wave functions for zero energy on the axis representing the distance between proton and neutron, while C is the chemical factor which would be 4 for very tight chemical binding of the hydrogen atoms. Fermi estimated $C=3.3$, while Bethe[5] has estimated that in paraffin C might be as low as 2.5. In the calculations a_3 was obtained using the empirical deuteron binding energy. The values tabulated correspond to 2.14 Mev for this energy. A change of this to 2.18 Mev makes no appreciable difference in the results below. In the calculations we used the newer values $e=4.8036\times10^{-10}$ e.s.u., $c=2.9986\times10^{10}$ cm/sec., $m=0.9115\times10^{-27}$ g, $h=6.638\times10^{-27}$ g cm^2/sec. These differ somewhat from the values used in the previous calculations on proton-proton scattering. The possible errors in the latter resulting from the change in units have been estimated and found to be within the experimental error with the exception of the Mev. The unit of depth of the potential well in Table I is 1.0080 Mev in terms of the newer units and is the same as that used in making the proton-proton calculations; to distinguish it from the Mev unit the depths D carry a prime. The values $(D_1)_{np}'$ are the depths in 1.0080 Mev of the proton-neutron interaction in the singlet S state; $(D_1^c)_{pp}'$ are the corresponding depths of the proton-proton interaction acting in addition to the Coulombian repulsion. It is seen from this table that within the reasonable range of values of r the proton-neutron interaction is slightly greater than the proton-proton interaction if the ^1S level is virtual and is appreciably greater if that level is real.

TABLE I. *Values of proton-proton and proton-neutron well depths.*

r (mc^2/e^2)	$\frac{1}{4}$	1	2	3	C	SINGLET LEVEL
$(D_1)_{np}'$	48.2	11.3	2.48	0.94	3.3	Virtual
	54.6	14.7	4.49	2.86	3.3	Real
	48.7	11.6	2.60	1.02	2.5	Virtual
	54.1	14.4	4.17	2.32	2.5	Real
$(D_1^c)_{pp}'$	48.7	11.1	2.42	0.98		

The revised comparison of energies of isobaric nuclei made by Feenberg and Wigner[6] and later by Feenberg and Phillips[7] and by Wigner[8] shows that a change of a neutron into a proton increases the energy of a nucleus somewhat more than would be expected from the Coulomb energy alone. This indicates that the attraction between two protons is weaker than that between two neutrons by more than merely the Coulomb energy. Similarly the values of Table I indicate a relatively stronger attraction between a proton and a neutron than between a proton and a proton.

By a slight extension of Fermi's formula[4] for the mean life τ of a neutron one finds:

$$\frac{1}{\tau}=\frac{128\pi^5 n}{h}\left(\frac{\nu}{c\alpha_3}\right)^3(\mu_p-\mu_n)^2\frac{D_3+E_3'}{D_3(1+\alpha_3 r)}\times\left(\frac{D_3-D_1}{D_3+E_3'-D_1}\right)^2[1+\alpha_3(r+a_1)]^2.$$

Here n = number of hydrogen atoms per cm^3, ν = frequency of emitted radiation, D_1 and D_3 are respectively the depths of square potential wells in singlet and triplet states, E_3' = energy of deuteron $\cong -2.14$ Mev, μ_p and μ_n are the respective magnetic moments of proton and neutron, r = radius of potential well, $\alpha_3=(-ME_3'/\hbar^2)^{+\frac{1}{2}}$. Using $n=7.8\times10^{22}$ cm^{-3}, $(\mu_p-\mu_n)=5.01\ e\hbar/2Mc$, $E_3'=-2.14$ Mev, and other units as in the comparison of proton-proton and proton-neutron depths, one obtains Table II.

From Fermi's theory, Amaldi and Fermi[2] conclude that $10^4\tau=1.7$ sec. experimentally. This value agrees best with the numbers obtained

magnetic dipole radiation for an interaction potential represented by a square well. The accurate value of the integral of the product of initial and final functions is used. If $r\to0$ Fermi's formula is obtained as a limiting case of the one used here.

[5] H. A. Bethe, private communication.

[6] E. Feenberg and E. Wigner, Phys. Rev. **51**, 95 (1937).

[7] E. Feenberg and M. Phillips, Phys. Rev. **51**, 597 (1937); especially reference 9 on p. 604.

[8] E. Wigner, Phys. Rev. **51**, 947 (1937); reference 11.

above for a virtual level and for $C=2.5$. An increase in the range of force from 0 to 1 or 2 times e^2/mc^2 is seen to improve the agreement slightly. However this agreement is not necessarily strong evidence for concluding that the level is virtual because: (a) Fermi's theory for the interpretation of the *albedo* may not be sufficiently accurate, as has been pointed out by Halpern, Lueneburg and Clark.[9] According to them a 50 percent or 100 percent correction may have to be applied to the experimental value. An increase in τ of 100 percent would spoil the agreement with a virtual level for $C=2.5$ without giving good agreement with a real level, although it would leave the agreement with a virtual level about the same for $C=3.3$. (b) There may be other processes besides the emission of magnetic dipole radiation which would involve the absorption of neutrons. The τ due to magnetic dipole radiation alone would then be larger than the experimental value; this might agree better with a real ^1S level. (c) It is assumed in the calculation of the capture cross section that the magnetic moments of proton and neutron have constant values unaffected by the mutual proximity of the particles. A partial justification of this assumption can be given as follows. The magnetic field at the proton due to the neutron is of the order μ_n/r^3, where r is the distance between proton and neutron. The proton, pictured as a small electrically charged sphere, will begin to spin about its axis when brought into this field with the frequency $\omega\sim e\mu_n/Mcr^3$. M here is the mass of the proton. The magnetic moment resulting from this precession is $\sim\omega e r_p^2/c=\Delta\mu_p$, where r_p=proton radius. The ratio of the induced magnetic moment to the original is $\Delta\mu_p/\mu_p\sim(\mu_n/\mu_p)(e^2/Mc^2r)\sim m/M$. Although on this basis no serious correction to the moments of elementary particles should be expected inside nuclei, the essentially classical picture above may not be sufficiently good.

In view of the present disagreements between theory and experiment it will perhaps be worth while to have some way of testing whether the ^1S level of the deuteron is real or virtual. One method available for this purpose is that of

TABLE II. *Values of $10^4\tau$; τ=mean life in seconds.*

r (mc^2/e^2)	0	½	1	2	C	SINGLET LEVEL
$10^4\tau$	2.77	2.72	2.67	2.62	3.3	Virtual
	7.2	8.6	10.7	20.7	3.3	Real
	2.14	2.09	2.04	1.94	2.5	Virtual
	4.8	5.5	6.4	9.8	2.5	Real

Teller.[10] It may also be possible to detect a real singlet level by excitation using bombardment with heavy particles, measuring their absorption as a function of velocity or else perhaps determining their energy loss directly.

Still another possibility is offered by the selective absorption of γ-rays. For a band of γ-rays having a width $\Delta\nu$ considerably greater than the natural breadth of the absorption line and an average frequency ν, the effective collision cross section due to magnetic dipole absorption from a stable ^3S state to a stable ^1S state is

$$\sigma=\frac{8\pi^3\nu}{3ch\Delta\nu}(\mu_p-\mu_n)^2\left(\int_0^\infty 4\pi u_1u_3dr\right)^2$$

$$\leqq 2.64\times10^{-28}\frac{\nu}{\Delta\nu}\left(\int_0^\infty 4\pi u_1u_3dr\right)^2 \text{ cm}^2.$$

Here u_1/r and u_3/r are respectively the radial wave functions for singlet and triplet states, normalized so that $\int_0^\infty 4\pi u^2dr=1$. For square wells of radius r one obtains

$$\left(\int_0^\infty 4\pi u_1u_3dr\right)^2=\frac{4(E_1'E_3')^{\frac{1}{2}}}{[(-E_1')^{\frac{1}{2}}+(-E_3')^{\frac{1}{2}}]^2}$$

$$\times\frac{(D_1+E_1')(D_3+E_3')(D_1-D_3)^2}{(1+\alpha_1r)(1+\alpha_3r)D_1D_3(D_1+E_1'-D_3-E_3')^2}.$$

The notation is the same as in the formula for $1/\tau$. The second factor in this formula is nearly unity for short range forces, so that $\sigma\leqq1.6(\nu/\Delta\nu)\times10^{-28}$ cm^2 if $E_1'=-0.10$ Mev. In pure deuterium the absorption cross section for 2 Mev radiation due to the Compton effect is $\sim1.5\times10^{-25}$ cm^2. In order that the nuclear absorption be at least as great as the electronic it is thus necessary that $(\nu/\Delta\nu)\sim1000$, or that the γ-ray band be no more than 2000 volts wide. This band would

[9] O. Halpern, R. Lueneburg and O. Clark, Phys. Rev. **51**, 775 (1937).

[10] J. Schwinger and E. Teller, Phys. Rev. **51**, 775 (1937); E. Teller, Phys. Rev. **49**, 420 (1936).

have to be chosen so as to include the presumably 2.0 Mev absorption frequency. Such a source of γ-rays would probably be difficult to find, unless it should prove possible to use the radiation emitted in the transition $^1S \rightarrow {}^3S$ itself. This could be attempted by bombarding H^2 with H^1 or n^1. The energy of the bombarding particles would then have to be at least $4/3 \times 2$ Mev $= 2.7$ Mev, whereas if H^2 were bombarded with H^2 one would need at least 4 Mev incident particle energies. It would be interesting to know whether there are γ-rays emitted in such experiments that show selective absorption by H^2.

Note added in proof: Dr. R. D. Present has made the following comment in connection with the above note: "Assuming the level to be real and to be situated at about -125 kv and using A_{tt} as determined from *THH* the discrepancy in He^4 obtained by Rarita and myself[11] would disappear because the range of forces would increase to the Feenberg-Share[12] value. Then all the experimental facts for the 2, 3, and 4-body problems would be consistent with the nuclear model, with the possible exception of the Coulomb energy of He^3 which would return to Share's[13] value approximately. This would tend to support the conclusion mentioned in your paper that $A_{tt} < A_{ss}$." In connection with Dr. Present's comment it is of interest to note that Westcott[14] using an independent set of experiments reaches the same conclusion concerning the mean life of neutrons as Fermi reaches. Westcott's method depends essentially on the use of boron as a standard absorber and is thus rather independent of complicated calculations on the diffusion of neutrons. It appears therefore that one is faced with a dilemma between the calculations of Rarita and Present with the above comment of Present on the one hand and the measurements on the mean life of slow neutrons on the other. The easiest solution of this apparent contradiction would be to suppose that the questionable point (c) in the application of standard theory to the calculation of τ is of importance and that, therefore, the magnetic moments of the proton and neutron in their free state do not give the correct result for the calculation of the mean life. Theoretical considerations by Willis E. Lamb on how this might come about from the point of view of the electron neutrino theory, which we have seen in manuscript, will appear shortly in the *Physical Review*.

We are indebted to the Alumni Research Foundation of the University of Wisconsin for a grant.

[11] W. Rarita and R. D. Present, Phys. Rev. **51**, 788 (1937).
[12] E. Feenberg and S. Share, Phys. Rev. **50**, 253 (1936).
[13] S. Share, Phys. Rev. **50**, 488 (1936).
[14] C. H. Westcott, Proc. Camb. Phil. Soc. **33**, 122 (1937).

Radioactive Isotopes of Scandium from Calcium and Potassium by Alpha-Particle Bombardment

HAROLD WALKE*
Radiation Laboratory, University of California, Berkeley, California
(Received June 21, 1937)

A study has been made of the radioactive isotopes of scandium formed from calcium and potassium by bombardment with alpha-particles. Sc^{43} has been separated chemically from calcium, its half-life being 4.0 ± 0.1 hours. No evidence has been obtained of Sc^{46} or Sc^{47}. Two radioactive isotopes of scandium, *viz.* Sc^{42} and Sc^{44}, have been isolated from potassium, these having half-lives of 4.1 ± 0.1 hours and 52 ± 3 hours, respectively. Cloud chamber studies of the positrons emitted by Sc^{43} and Sc^{42} show that the upper limits of the two spectra are 1.3 (8) and 1.6 (3) Mev, respectively.

INTRODUCTION

THE radioactivity induced in calcium by alpha-particle bombardment was first studied by Frisch[1] who observed the formation of Sc^{43} in the reaction

$$Ca^{40}+He^{4}\rightarrow Sc^{43}+H^{1};\quad Sc^{43}\rightarrow Ca^{43}+e^{+}.$$

The emitted protons have been studied by Pollard and Brasefield.[2]

A radioactivity induced in potassium by activation with alpha-particles was detected by Zyw,[3] who reported that it decayed to half-value in three hours. Zyw concluded that the radioactive isotope was Sc^{42} or Sc^{44} formed in one or other of the reactions

$$K^{39,\,41}+He^{4}\rightarrow Sc^{42,\,44}+n^{1};\quad Sc^{42,\,44}\rightarrow Ca^{42,\,44}+e^{+}.$$

No second period was detected.

In a preliminary account of some results obtained by activating potassium with 11 Mev alpha-particles it was suggested[4] that both Sc^{42} and Sc^{44} are formed and, moreover, it was concluded that Sc^{42} and Sc^{43} have very similar half-lives. This observation was somewhat unexpected so that a careful investigation of the alpha-particle induced radioactivities of calcium and potassium was undertaken. It is the purpose of the present paper to report the more extended results obtained.

APPARATUS

The alpha-particles of 11 Mev energy were produced by accelerating doubly charged helium ions in the Berkeley cyclotron under conditions already described.[4] The alpha-particle and deuteron peaks were well resolved so that there was no deuteron contamination of the alpha-particle beam. This was verified by bombarding paper with the alpha-particles. No activity was observed though the characteristic period of N^{13} can be readily detected when there is any deuteron contamination. The bombarding currents used varied from 0.1 to 0.2 microampere.

The decay of the radioactive samples was measured by means of a Lauritsen quartz fiber electroscope.

CHEMICAL SEPARATION OF THE ACTIVE SCANDIUM

Calcium was activated in the form of metal and potassium as potassium fluoride and chloride. After irradiation the calcium was dissolved in dilute HCl, the potassium salts being dissolved in water. Inactive scandium chloride was then added followed by ammonium hydroxide. The precipitated scandium hydroxide was filtered off, washed and thoroughly dried.

DECAY OF THE SCANDIUM PRECIPITATE FROM CALCIUM

In a previous paper[4] the decay curve of the radioactivity induced in calcium by alpha-particle bombardment was shown. This decay curve corresponded to a single period of 4.0 hours,

* Commonwealth Fund Fellow.
[1] Frisch, Nature **136**, 220 (1935).
[2] Pollard and Brasefield, Phys. Rev. **51**, 8 (1937).
[3] Zyw, Nature **134**, 64 (1934).
[4] Walke, Phys. Rev. **51**, 439 (1937) (note added in proof).

though there was evidence of a tail which suggested that there might be some deuteron contamination. In the present experiments, using a pure alpha-particle beam, the decay of the chemically separated scandium was observed. The decay curve shown in Fig. 1 is strictly linear for 50 hours, the half-life being 4.0 hours. A slight departure from linearity occurs when the corrected intensity is close to the background of the electroscope but, as can be seen, the initial intensity of any longer period must be less than 10^{-4} of that of the 4-hour period. It is thus clear that the period of 4.0 ± 0.1 hours must be associated with Sc^{43} formed thus

$$Ca^{40}+He^{4}\rightarrow Sc^{43}+H^{1};\quad Sc^{43}\rightarrow Ca^{43}+e^{+}.$$

There is no definite evidence for any longer periods and, moreover, the enlarged portion of the early decay curve of calcium metal (Fig. 1) suggests that there are no short periods present (unless the half-lives are of the order 1–2 minutes or less).

These facts are of interest in connection with other reactions which might be expected to occur. As previously observed transmutations using alpha-particles are such that protons or neutrons are ejected from the resulting compound nuclei, one would anticipate that the following reactions might take place

$$Ca^{42,\,43,\,44}+He^{4}\rightarrow Sc^{45,\,46,\,47}+H^{1},$$
$$Ca^{40,\,42,\,43,\,44}+He^{4}\rightarrow Ti^{43,\,45,\,46,\,47}+n^{1}.$$

Of the product nuclei Sc^{45}, Ti^{46} and Ti^{47} are stable, but one would expect that radioactivity due to the scandium isotopes Sc^{46} and Sc^{47} might be detected. However, unpublished experiments on the activation of scandium with deuterons have shown that the half-life of Sc^{46} is of the order 80 days and this fact together with the low abundance of Ca^{43} (0.17 percent) explain why no evidence of the reaction

$$Ca^{43}+He^{4}\rightarrow Sc^{46}+H^{1}$$

has been obtained. Nothing as yet is known of the properties of Sc^{47}, and assuming that it might be formed in these experiments, we may conclude that its half-life is either very short or very long. The same would appear to be true of Ti^{43}, unless the reaction in which it is formed is an improbable one, as it would then not be readily observable in the presence of Sc^{43}.

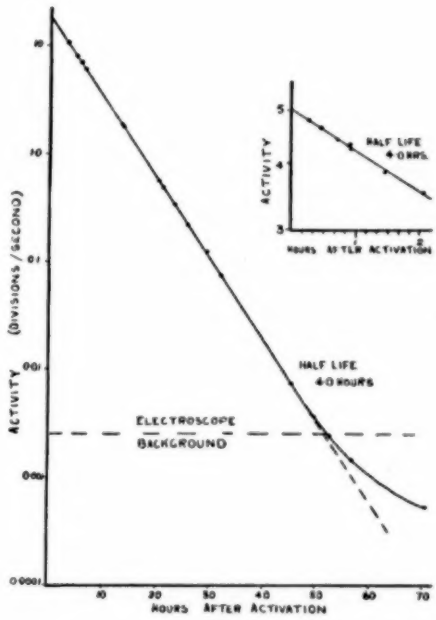

FIG. 1. Decay of the activity of a scandium precipitate from calcium metal after activation with 11 Mev alpha-particles. The inset figure shows on an enlarged time scale the early decay of the activity of calcium metal.

DECAY OF THE SCANDIUM PRECIPITATE FROM POTASSIUM

The usual reactions in which a proton is ejected from a nucleus after capture of an alpha-particle suggest that the stable nuclei Ca^{42} and Ca^{44} will be formed in the reactions

$$K^{39,\,41}+He^{4}\rightarrow Ca^{42,\,44}+H^{1}.$$

On the other hand the ejection of a neutron will lead to the formation of the radioactive scandium isotopes Sc^{42} and Sc^{44} which then decay by emitting positrons to give rise to the stable calcium isotopes with the same mass numbers.

In the present experiments samples of KF and KCl were bombarded with alpha-particles, the decay of the chemically separated radioactive scandium being measured. In the case of KCl only two periods were observed having half-lives of 4.1 ± 0.1 hours and 52 ± 3 hours, respectively. With KF, however, a trace of an additional very long period was detected, this being due to the occlusion of small amounts of Na^{22} in the scan-

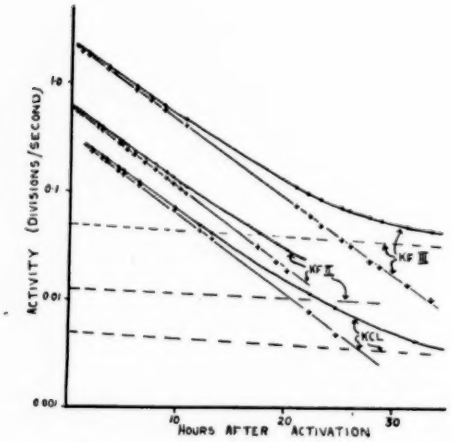

FIG. 2. Early decay of the activity of several scandium precipitates from various potassium salts after activation with 11 Mev alpha-particles. The points · represent total activity. Those marked + have been corrected for the activity due to the 52-hour period which is shown by the lines denoted thus - - - -.

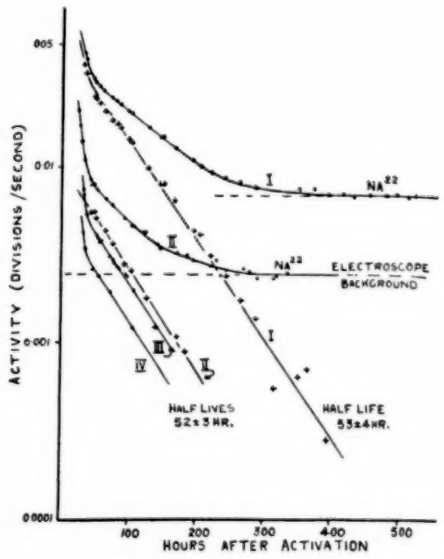

FIG. 3. Long period activities of several precipitates from various potassium salts. The points marked · represent total activity. Those denoted by + have been corrected for the activity due to Na^{22}. I and II are from KF. III and IV from KCl.

dium hydroxide (no carrier sodium was added). The Na^{22} is formed in the reaction[5]

$$F^{19}+He^{4}\rightarrow Na^{22}+n^{1}.$$

In Fig. 2 are shown the early portions of the decay curves of several such samples, and in Fig. 3 the decay curves of the longer period activities.

Since a radioactive isotope of scandium with half-life 52±2 hours has been separated from calcium after deuteron activation,[4] it is apparent that this period must be associated with Sc^{44} as this is the only radioactive scandium isotope which can be formed by reactions of already well-known types both from calcium+deuterons and potassium+alpha-particles. Thus we have

$$Ca^{43}+H^{2}\rightarrow Sc^{44}+n^{1}, \quad K^{41}+He^{4}\rightarrow Sc^{44}+n^{1}.$$

The 4.1 hour period would then be associated with Sc^{42}.

(These experiments thus enable the mass numbers of the three radioactive scandium isotopes formed by activating calcium with deuterons[4] to be determined. The 4.0 hour period has already been shown to be due to Sc^{43}. The 52±2 hour period must now be associated with Sc^{44} and the 53±3 minute period with Sc^{41} and not *vice versa* as tentatively suggested in the previous paper.)

[5] Frisch, Nature **136**, 220 (1935).

The thick target saturation yields of these radioactive bodies corrected for the finite period of bombardment are

4.1 hour period
10^{7} alpha-particles per active atom,
52 hour period
3.5×10^{9} alpha-particles per active atom.

The greater probability of the formation of the isotope with the 4.1 hour period suggests too that this period should be associated with the reaction involving the more abundant isotope *viz.* K^{39}. Hence for equal abundances of both isotopes we have

Sc^{42}	1×10^{7} alpha-particles per active atom,
Sc^{44}	0.6×10^{7} alpha-particles per active atom.

The half-life of Sc^{42} is then very little different from that of Sc^{43} (though all the measurements made suggest that it is longer by approximately 10 minutes). In consequence it was at first suspected that the effect was due to calcium contamination (since the calcium reaction is so much more probable than that involving potassium). However, all the samples used were of reagent quality, the KF being stated to be free from all impurities except a trace of chloride, and

the KCl containing less than 0.005 percent of Ca, Mg and NH_4, whereas it would be necessary to assume a minimum calcium content of approximately 5 percent to account for the observed intensity. Thus the activity obtained is 1000 times as great as can be accounted for by the known amount of calcium impurity.

It is then necessary, if the 4.1 hour period is due to Sc^{43}, that it should be formed from one of the known isotopes of potassium. The following reactions might be possible

$$K^{39}+He^4 \rightarrow Sc^{43}+\gamma, \qquad \text{I}$$

$$K^{40}+He^4 \rightarrow Sc^{43}+n^1, \qquad \text{II}$$

$$K^{41}+He^4 \rightarrow Sc^{43}+2n^1. \qquad \text{III}$$

Reaction I would require the radiative capture of an alpha-particle with 11 Mev energy, a form of reaction which has not yet been detected and which would appear to be highly improbable. Reaction II can be excluded since K^{40} is present in an abundance of only one part in 8500. On the other hand the third reaction might be possible according to the nuclear model proposed by Bohr.

However, absorption measurements suggested that the positrons emitted by the isotope with the 4.1 hour period are more penetrating than those emitted by Sc^{43}, so that it was thought that a definite decision concerning the mass number of the isotope formed in the potassium reaction would be reached by comparing the energy distributions of the positrons emitted by the two samples.

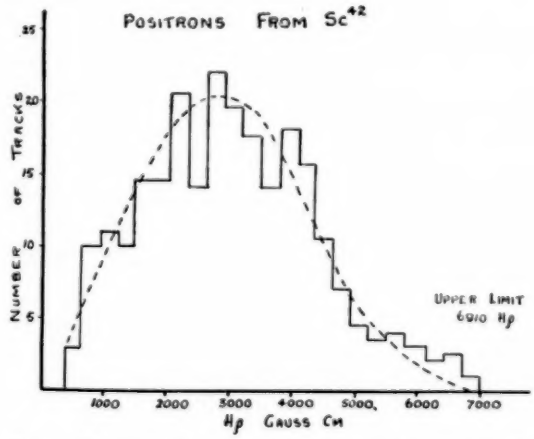

FIG. 4. Momentum distribution of positrons from Sc^{42}. Magnetic field 288 gauss. Number of tracks measured 480. Upper limit by inspection 6910 $H\rho$ 1.6 (3) Mev.

ENERGY DISTRIBUTIONS

The energy distributions were obtained by photographing the tracks produced by the emitted particles in traversing a large hydrogen filled expansion chamber 12″ in diameter. The chamber had been designed so that the magnetic field in which the particles were deflected was very uniform throughout the whole volume of the chamber.[6] The positrons from Sc^{43} were photographed in a field of 328 gauss, the distribution being based on measurements on 258 tracks. Those from Sc^{42} were bent in a magnetic field of 288 gauss, the distribution being based on 480 tracks.

The scandium precipitates were of approximately the same size and mass and were supported on small pieces of wood. The positrons entered the cloud chamber through a thin mica window 0.0006″ in thickness, $\frac{3}{4}$″ in length and $\frac{3}{16}$″ in width. No collimating slits were used.

The energies of the particles were obtained by the method adopted by Kurie, Richardson and Paxton,[7] the film being replaced in the camera, the radius of curvature ρ of the reprojected images of the tracks being measured. In this way a distribution of particles as a function of ρ (and thus of $H\rho$ since H was known) was obtained. From the maximum value of $H\rho$ obtained by inspection of the distribution curve the energy of the end point of the β-ray spectrum was calculated.

As a result of these experiments it was found

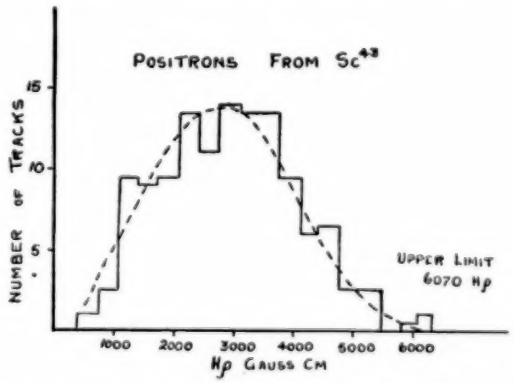

FIG. 5. Momentum distribution of positrons from Sc^{43}. Magnetic field 328 gauss. Number of tracks measured 258. Upper limit by inspection 6070 $H\rho$ 1.3 (8) Mev.

[6] Details of this chamber have not yet been published.

[7] Kurie, Richardson and Paxton, Phys. Rev. **49**, 368 (1936).

that the energy of the positrons emitted by the isotope with the half-life 4.1 hours is greater by approximately 250,000 ev than that of the positrons from Sc^{43}. It is thus clear that the 4.1 hour period must be associated with Sc^{42} and not with Sc^{43} formed by one of the reactions I, II and III.

The energy distributions of the positrons from Sc^{42} and Sc^{43} are shown in Figs. 4 and 5. The upper limits of the two spectra are 1.6 (3) and 1.3 (8) Mev, respectively. The end point of Sc^{43} agrees well with the value 1.4 Mev deduced from the absorption measurements in aluminum previously reported.[4]

The upper limit of Sc^{43} is, however, considerably higher than that obtained by Jacobsen[8] using an air-filled expansion chamber.

In Fig. 6 are shown sample photographs of the positrons emitted by the two isotopes, and in Fig. 7 is shown a comparison between the decay of the activities of the scandium precipitates from calcium and potassium after activation under similar conditions. In spite of the similarity between the half-lives of Sc^{43} and Sc^{42} it can be seen that the decay curves are quite different.

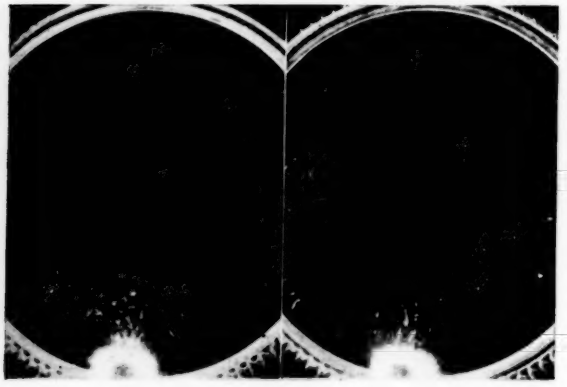

FIG. 6. Sample photographs of positrons from Sc^{42} (*A*) and Sc^{43} (*B*).

SUMMARY

In summarizing we may state that the evidence now presented, together with that obtained in the previous investigation,[4] indicates that four positron radioactive isotopes of scandium have been detected, namely Sc^{41}, Sc^{42}, Sc^{43} and Sc^{44} these being formed in the reactions:—

Sc^{41} (half-life 53±3 min. energy 1.8×10^6 ev)

$$Ca^{40}+H^2\rightarrow Sc^{41}+n^1.$$

Sc^{42} (half-life 4.1±0.1 hr. energy 1.6 (3)$\times10^6$ ev)

$$K^{39}+He^4\rightarrow Sc^{42}+n^1,$$

Sc^{43} (half-life 4.0±0.1 hr. energy 1.3 (8)$\times10^6$ ev)

$$Ca^{42}+H^2\rightarrow Sc^{43}+n^1,$$
$$Ca^{40}+He^4\rightarrow Sc^{43}+H^1.$$

Sc^{44} (half-life 52±2 hr.)

$$Ca^{43}+H^2\rightarrow Sc^{44}+n^1,$$
$$K^{41}+He^4\rightarrow Sc^{44}+n^1.$$

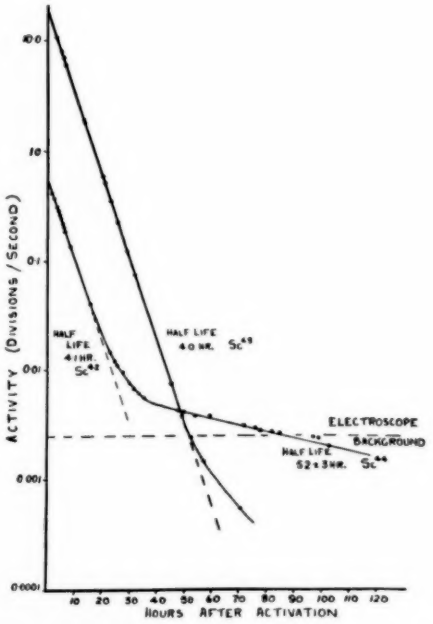
ACTIVITY (DIVISIONS / SECOND)
HALF LIFE 4.0 HR. Sc43
HALF LIFE 4.1 HR. Sc42
ELECTROSCOPE BACKGROUND
HALF LIFE 52±3 HR. Sc44
HOURS AFTER ACTIVATION

FIG. 7. Comparison between decay curves of scandium precipitates from potassium and calcium after activation with alpha-particles.

ACKNOWLEDGMENTS

It is a pleasure to acknowledge the cooperation and friendship of the staff of the Radiation Laboratory. The author is especially grateful to Professor E. O. Lawrence for continued encouragement and to Dr. Hugh C. Paxton who very kindly photographed the positrons of Sc^{42} and Sc^{43}.

This research has been aided by grants to the laboratory from the Research Corporation, the Chemical Foundation and the Josiah Macy, Jr. Foundation.

[8] Jacobsen, Nature **139**, 879 (1937).

Nuclear Transformations Produced in Copper by Alpha-Particle Bombardment

W. B. MANN
Radiation Laboratory, Physics Department, University of California, Berkeley, California
(Received June 11, 1937)

The radioactivity produced by bombardment of copper with 11 Mev alpha-particles has been investigated. Activities having half-lives of 1.10±0.05 hours and 9.2±0.2 hours have been found to belong, respectively, to the radioactive isotopes of gallium Ga^{68} and Ga^{66}. Both these isotopes have been found to be positron active. Absorption measurements gave values of respectively 1.8 and 3.1 Mev for the maximum energies of the short and long period positrons. Measurements of the positron tracks photographed in a cloud chamber gave, however, corresponding values of 1.9 and 3.9 Mev. The excitation function for alpha-particles and copper has also been investigated.

COPPER has been bombarded with 11 Mev alpha-particles from the cyclotron in the Radiation Laboratory at the University of California. It exhibited a strong consequent radioactivity which decayed with two periods corresponding to half-lives of 1.10±0.05 hours and 9.2±0.2 hours. These values were determined with a quartz fiber electroscope.

Radioactive Products

The only probable reactions which would explain the production of two activities would involve the conversion of each of the isotopes of copper into a radioactive isotope of gallium by the capture of an alpha-particle and emission of a neutron. Such reactions would result in the transformation of Cu^{63} and Cu^{65} into the radioactive isotopes Ga^{66} and Ga^{68}. Accordingly, by the method of ether extraction from hydrochloric acid, a chemical separation was made for gallium from a sample of copper which had been activated by alpha-particle bombardment. Both the 1.10 and the 9.2 hour activities separated out with the gallium precipitate. The copper and zinc were precipitated from solution by hydrogen sulphide and showed no activity. By the following consideration of the results which have already been obtained for the radioactive isotopes of gallium it has been possible to assign the half-lives of 9.2 and 1.10 hours to Ga^{66} and Ga^{68}, respectively. Irradiating gallium with slow neutrons, Fermi and his collaborators[1] found activities having half-lives of 20 minutes and 23 hours. These activities correspond to the radioactive isotopes Ga^{70} and Ga^{72} formed by neutron capture, from the two stable isotopes Ga^{69} and Ga^{71}. It is not possible, however, to assign either of these two periods to the appropriate radioactive isotope. Bothe and Gentner[2] have, however, recently activated gallium using the 17 Mev γ-radiation produced by proton bombardment of lithium resulting in the ejection of a neutron from each of the two stable gallium isotopes. They found activities decaying with half-lives equal to 20 minutes and 60 minutes which must, therefore, correspond to the radioactive isotopes Ga^{70} and Ga^{68}, respectively. It is, therefore, possible to assign the half-life of 9.2 hours to the new radioactive isotope Ga^{66}.

Disintegration Positrons

Both the isotopes of gallium produced by alpha-particle bombardment of copper have been found to be positron active, resulting in the formation of Zn^{66} and Zn^{68}. Absorption measurements were made with the use of aluminum absorbers and the resultant curves are shown in Figs. 1 and 2. The former is for Ga^{68} (1.10 hours) and the end point gives, using Feather's empirical formula, a value of 1.8 Mev for the maximum energy of the positrons. The absorption curve for Ga^{66} (9.2 hours), shown in Fig. 2 gave an end point corresponding to positrons having a maximum energy of 3.1 Mev.

To confirm these results, Dr. H. C. Paxton kindly took a series of Wilson photographs of the positrons emitted, using a cloud chamber fitted with a thin mica window at one side. Immedi-

[1] E. Amaldi *et al*, Proc. Roy. Soc. **A149**, 522 (1935).

[2] W. Bothe and W. Gentner, Naturwiss. **25**, 191 (1937).

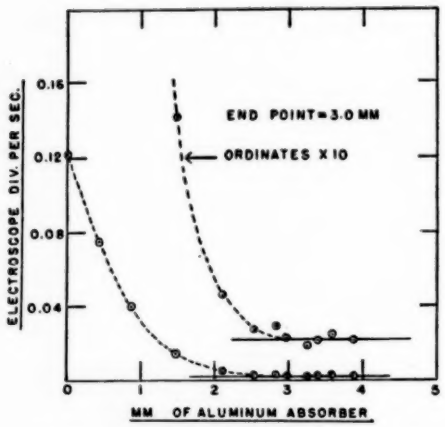

FIG. 1. Copper+11 Mev alpha-particles. Absorption curve for positrons emitted by radioactive Ga^{66} (half-life 1.10 ± 0.5 hours). End point corresponds to an energy of 1.8 Mev.

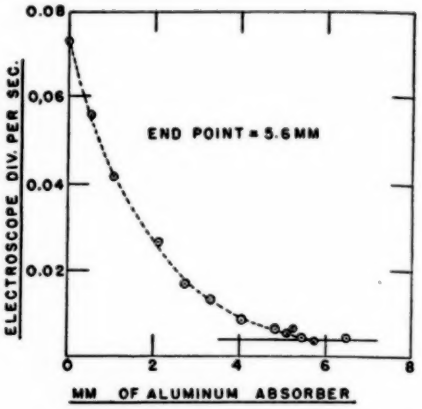

FIG. 2. Copper+11 Mev alpha-particles. Absorption curve for positrons emitted by radioactive Ga^{66} (half-life 9.2 ± 0.2 hours). End point corresponds to an energy of 3.1 Mev.

ately after bombardment the copper specimen, consisting of a small piece of foil, 0.001 in. thick, was placed about 4 cm from the mica window of the cloud chamber; part of the specimen was covered in order to reduce the intensity, and 114 photographs were taken. From these 351 positron tracks were measured and their energy distribution is shown plotted in Fig. 3. No correction for the long period activity has been made. Eighteen minutes were required for taking the photographs during which time the intensity of the short period activity was of the order of ten times the intensity due to the long period activity. The end point shown in Fig. 3 corresponds to positrons of 1.81 Mev energy, which when corrected for the stopping power of the mica window, equivalent to about 0.05 Mev, gives a value of 1.9 Mev for the maximum energy of the disintegration positrons.

Twelve hours after bombardment a further series of 140 photographs was taken, the specimen this time being held close to the mica window of the cloud chamber. The activity due to the short period would now have decayed to about one-fiftieth the intensity of that due to the long period. Three hundred tracks were measured and plotted and gave an end point at $H\rho$ equal to 14,300 gauss cm and a minimum at $H\rho$ equal to about 5000 gauss cm. The end point corresponds to a positron energy of 3.81 Mev. Another series of 150 photographs of these high energy positrons was taken twenty-seven hours after bombardment. From these 450 tracks were measured and the results are given in the histogram shown in Fig. 4. The minimum in the neighborhood of $H\rho$ equal to 5000 gauss cm is still apparent. From these measurements, which were primarily concerned with determining the maximum energy of the positrons, it cannot be said with certainty whether this minimum is real and the spectrum complex. The end point in Fig. 4, at $H\rho$ equal to 14,500 gauss cm, corresponds to a positron energy of 3.87 Mev. Correcting the values of 3.81 and 3.87 Mev for the decrease in energy of about 0.05 Mev, due to the mica window, gives a value in each case of 3.9 Mev. This value is not in very good agreement with the value of 3.1 Mev given by the absorption measurements with the use of Feather's formula. An energy of 3.1 Mev would correspond to an end point at $H\rho$ equal to 11,900 gauss cm. On the other hand, an energy of 3.9

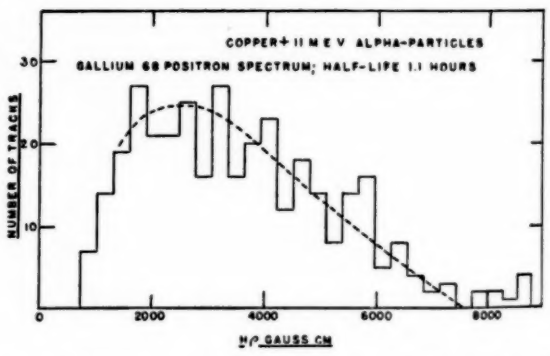

FIG. 3. Positron spectrum for Ga^{68}. End point corresponds to energy of 1.9 Mev.

Mev would correspond to an end point at 7.0 mm of aluminum in Fig. 2.

Excitation Function

Finally measurements were made for the purpose of determining the excitation function of copper. A preliminary experiment was made in which a pile of ten copper foils, each 0.0001 in. thick, were exposed so that the alpha-particle beam fell normally on the first foil. Only the first five foils were found to be active.

A second experiment was performed with five 0.0001 in. copper foils and the activities were followed on an electroscope for 35 hours. The stopping power of the foils was determined by observing visually the decrease in range of the alpha-particle beam in air on introducing the five foils into its path. The range was found to be decreased by 5 cm and, accordingly, it was assumed that each foil was equivalent to 1 cm of air. The range of the beam in air was 11.5 cm.

The results for the short and long periods were corrected to infinite bombardment (after twenty minutes bombardment the first foil showed initial activities of 1.5 and 0.165 electroscope divisions per second for the short and long periods, respectively) and are shown plotted in Fig. 5. The preliminary results are also shown by the diagonal crosses in Fig. 5; these preliminary results have been adjusted by multiplying the ordinates by a factor of 2.39 in order to bring them to the same scale as the subsequent results. A Gamow excitation function of the form

$$G\alpha\frac{1}{E}\exp-\left\{\frac{4Ze^2}{\hbar v}(2u-\sin 2u)\right\},$$

where $\cos^2 u = r_0E/2Ze^2$ has been fitted to the experimental data. E is the energy of the alpha-particles of velocity v while r_0 and Z are the radius and atomic number, respectively, of the bombarded nucleus. The curve shown in Fig. 5 is for r_0 equal to 7×10^{-13} cm. Shown also for comparison is the curve obtained taking r_0 equal to zero. The shape of the curve is quite sensitive to changes in r_0 in the neighborhood of r_0 equal to 7×10^{-13} cm. Thus for r_0 equal to 6×10^{-13} and 8×10^{-13} cm the ordinates at 9 cm mean range are, respectively, equal to 1.9 and 3.9 electroscope divisions per second.

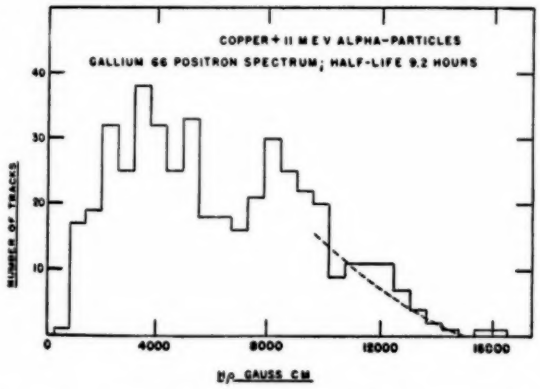

FIG. 4. Positron spectrum for Ga^{66}. End point corresponds to energy of 3.9 Mev.

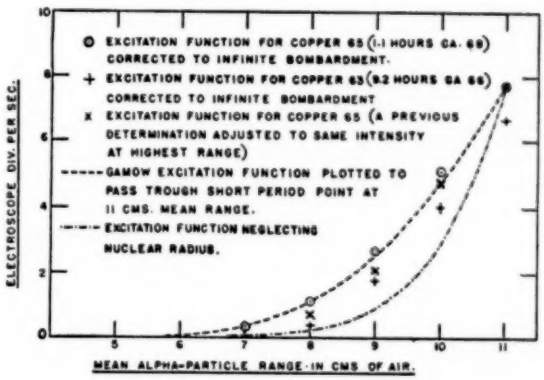
EXCITATION FUNCTION FOR COPPER 65 (1.1 HOURS GA. 66) CORRECTED TO INFINITE BOMBARDMENT.
EXCITATION FUNCTION FOR COPPER 63 (9.2 HOURS GA 66) CORRECTED TO INFINITE BOMBARDMENT
EXCITATION FUNCTION FOR COPPER 65 (A PREVIOUS DETERMINATION ADJUSTED TO SAME INTENSITY AT HIGHEST RANGE)
GAMOW EXCITATION FUNCTION PLOTTED TO PASS THROUGH SHORT PERIOD POINT AT 11 CMS. MEAN RANGE.
EXCITATION FUNCTION NEGLECTING NUCLEAR RADIUS.
ELECTROSCOPE DIV. PER SEC.
0
2
4
6
8
10
5
6
7
8
9
10
11
MEAN ALPHA-PARTICLE RANGE IN CMS OF AIR.

FIG. 5. Excitation function; copper+alpha-particles.

In conclusion I should like to express my thanks to Professor E. O. Lawrence for extending to me the facilities of the Radiation Laboratory and to him, to Professor J. R. Oppenheimer and to the staff of the Radiation Laboratory for so much friendly help and cooperation. I would also thank the Commonwealth Fund of New York for making possible my sojourn here. The research has also been aided by grants to the laboratory from the Research Corporation, the Chemical Foundation and the Josiah Macy, Jr. Foundation.

Inelastic Scattering of Fast Neutrons

G. T. SEABORG, G. E. GIBSON AND D. C. GRAHAME
Department of Chemistry, University of California, Berkeley, California
(Received May 28, 1937)

The radiation observed in the presence of a source of fast neutrons is found to be due chiefly to the excitation of gamma-rays in the lead block used in these experiments. The true absorption of fast neutrons in several elements is less than previous measurements had indicated, and hence an absorption process cannot account for the soft gamma-rays produced by the action of fast neutrons on matter. The capacity of fast neutrons to produce gamma-rays in lead and copper is considerably diminished as a result of their passage through various substances. Therefore the energy of the gamma-rays must be derived from the kinetic energy of the fast neutrons by a process of inelastic scattering.

INTRODUCTION

IT is found that most substances emit soft gamma-rays under the action of fast neutrons.[1–3] Aoki has reported that of forty-one elements bombarded by fast neutrons all but five produce some gamma-rays. It has often been supposed that these gamma-rays arise by inelastic scattering of the fast neutrons, but conclusive proof of this has been lacking. As an alternative explanation it may be supposed that the capture of a fast neutron occurs with the emission of the excess energy in a cascade process as a considerable number of low energy gamma-rays. If the apparent absorption of fast neutrons in several elements reported by Dunning, Pegram, Fink and Mitchell is a true absorption, such a process could easily account for the observed gamma-rays.[4] However, as pointed out by them, the results are more probably due in large part to large neutron energy losses through inelastic collisions. In this paper experiments will be described which show that inelastic scattering is responsible for practically all of the soft gamma-rays produced by fast neutrons (§§2–3).

In the following experiments a Geiger-Müller counter has been employed. Such a counter in the path of fast neutrons from which x- and gamma-rays and slow neutrons have been removed by the interposition of suitable absorbers gives a count much in excess of that due to unabsorbed gamma-rays. As it will be necessary to refer to this effect repeatedly in what follows it will be termed the "fast neutron effect." Section 1 of this paper is concerned with the identification of this effect.

§1. IDENTIFICATION OF THE "FAST NEUTRON EFFECT"

It is natural to suppose that this "fast neutron effect" arises from the interaction of fast neutrons with lead (which is usually present in these experiments) to form gamma-rays. In an early paper Lea reported finding such gamma-rays,[1] but repeated investigations of this matter by Kikuchi, Aoki and Husimi, using both a "deuteron-deuteron" and a Ra-Be source of neutrons had failed to confirm his results.[2,5] More recently Kikuchi and co-workers have reported the detection of gamma-rays from the action of fast neutrons on lead, but of too small an intensity to account for more than a few percent of their rather large "fast neutron effect."[6] In order to account for this radiation, Kikuchi and co-workers have postulated a hitherto unknown direct interaction of fast neutrons with extra-nuclear electrons to produce beta-particles with a maximum energy of about 1 Mev.[6,7] As alternative explanations, Kikuchi has suggested that the neutron may disintegrate spontaneously or in the neighborhood of a nucleus with the

[1] Lea, Proc. Roy. Soc. (London) **A150**, 637 (1935).
[2] Kikuchi, Aoki, Husimi, Proc. Phys.-Math. Soc. Japan **18**, 115 (1936).
[3] Aoki, Nature **139**, 372 (1937).
[4] Dunning, Pegram, Fink and Mitchell, Phys. Rev. **48**, 265 (1935).
[5] Kikuchi, Aoki, Husimi, Proc. Phys.-Math. Soc. Japan **18**, 297 (1936).
[6] Kikuchi, Aoki, Husimi, Proc. Phys.-Math. Soc. Japan **18**, 727 (1936).
[7] Kikuchi, Aoki, Husimi, Nature **138**, 841 (1936).

emission of a beta-particle or a gamma-ray. Measurements to be described in §2 on the absorption of fast neutrons in matter prove that the latter of these processes cannot occur to a measurable extent, and measurements of Gilbert, Smith and Fremlin[8] failed to reveal any appreciable spontaneous disintegration of the neutron.

The possibility of explaining the effect in terms of a short-lived radioactivity in lead was eliminated as follows: A Geiger-Müller counter was enclosed in lead and operated near a "deuteron-deuteron" source of neutrons. This "deuteron-deuteron" source of neutrons used a 60-cycle a.c. accelerating voltage on the target which made it possible to look for an induced radioactivity of very short half-life. An induced radioactivity would produce counts during both halves of the accelerating voltage cycle. Actually, visual observation of the cathode-ray oscilloscope (which used the same 60-cycle a.c. for sweep voltage) showed that the kicks occurred during the negative half of the accelerating voltage cycle. Hence it is probable that no radioactivity of half-life greater than 0.01 second is induced in lead under these conditions.

As mentioned above, experiments performed by Kikuchi and co-workers in an effort to measure the intensity of the gamma-rays produced by the action of fast neutrons on lead, led them to the conclusion that such gamma-rays were entirely inadequate to account for their rather large "fast neutron effect." These measurements were complicated, however, by the possibility that a considerable amount of radiation might arise from the action of neutrons on the x-ray shield and walls of the room; consequently, it was thought desirable to measure the intensity of the gamma-rays produced by the action of fast neutrons on lead with a different arrangement in which the effects of stray radiations could be positively eliminated. In particular, it was desired to determine whether or not the intensity of the gamma-rays from lead was sufficient to account for the entire radiation observed under these conditions.

This measurement was carried out with the arrangement shown in Fig. 1. A Ra-Be source of neutrons was encased in a lead block of sufficient

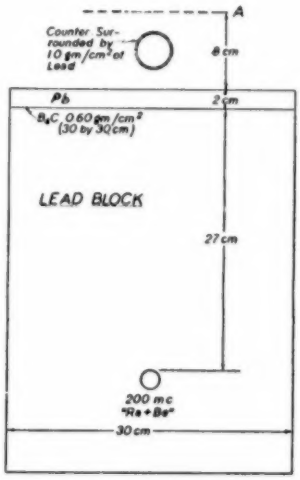

FIG. 1. Experimental arrangement for the detection of gamma-rays from the action of fast neutrons on lead.

size to absorb nearly all of the primary gamma-rays from the radium, and the assembly was mounted out-of-doors on a steel table 175 cm above the ground. A layer of B_4C (0.6 g/cm²) was interposed, as shown, in order to absorb the few slow neutrons that might be coming from the source and from the ground below the source. Two centimeters of lead above the B_4C absorbed the gamma-rays which are known to be formed[9, 10] in small intensity when slow neutrons are captured by boron. A steel Geiger-Müller counter of dimensions 3.7 cm×12 cm with a wall thickness of 0.20 mm and filled with argon to a pressure of 15 cm Hg was surrounded with a lead foil (1.0 g/cm²) and placed as shown. The absence of slow neutrons in the region above the counter was proved by the fact that a thin sheet of cadmium (0.4 mm×13×25 cm) placed at A in Fig. 1 caused no appreciable increase in the counting rate.

When the Ra-Be was introduced into the large lead block under these conditions the counting rate changed from the natural background of 65 per minute to 126 per minute. The primary gamma-rays coming directly from the Ra-Be source were responsible for about 3 per minute of this increase, as estimated by a method described in §3. The "fast neutron effect" is therefore $126-65-3=58$ counts per minute.

[8] Gilbert, Smith, Fremlin, Nature **139**, 796 (1937).

[9] Kikuchi, Aoki, Husimi, Proc. Phys.-Math. Soc. Japan **18**, 188 (1936).

[10] Fleischmann, Zeits. f. Physik **100**, 307 (1936).

Additional "test lead" (in plates 15×30 cm) was placed above the counter (position *A* in Fig. 1) and produced a further increase in the counting rate. Fig. 2 gives this increased counting rate as the percentage increase over the fast neutron effect with no lead at *A*. Allowance has been made for the change in natural background of the counter caused by the addition of the lead at *A*.

The curve in Fig. 2 gives direct proof of the existence of gamma-rays produced by the action of fast neutrons on lead. The shape of the curve affords a rough estimate of the average energy of these gamma-rays, indicating a value somewhat less than 1 Mev. The largest thickness of lead at *A* gave an increase amounting to 21 percent of the fast neutron effect with no lead at *A*. Upon the assumption that the fast neutron effect was entirely due to gamma-rays from the action of fast neutrons on the large lead block in Fig. 1, it was determined that the increase caused by the test lead at *A* should be approximately 30 percent. Hence it follows that in these experiments roughly two-thirds of the fast neutron effect is due to gamma-rays excited in the large lead block.

The remainder of the fast neutron effect must arise in the lead foil surrounding the counter or in the counter wall or counter gas. It could not be identified with certainty, but there are several processes which could contribute to it. An appreciable part will be due to recoil argon atoms within the counter. Internal conversion of gamma-rays produced in the counter wall and in the lead foil surrounding the counter may also contribute to the unidentified radiation. If neutrons excite a hitherto undetected, very soft, gamma-radiation in lead, this could likewise be responsible for the residual effect. Although no figure is available for the ionization produced by fast neutrons traversing a gas, an upper limit of one ion pair in 3 meters' path of air at NTP has been set by Dee.[11] Since the production of one ion pair in 50 meters' path of argon at NTP would be sufficient to account for the remainder of the fast neutron effect in these experiments, the possibility that neutron primary ionization is contributing to the count cannot be eliminated. In view of these multifold possibilities it is impossible to say whether the process proposed by Kikuchi plays any part in this small residual count.

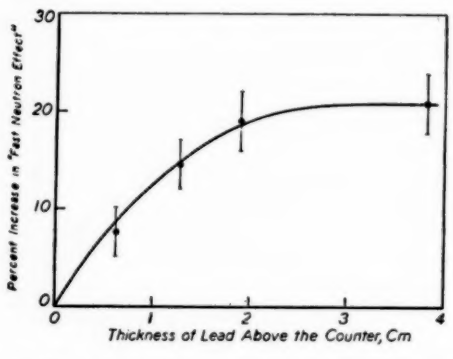

FIG. 2. Intensity of gamma-rays from the action of fast neutrons on "test lead" at *A* (Fig. 1) *vs.* thickness of lead.

In the experiments described in §§2–3 of this paper, however, the gamma-rays from lead or other elements always constitute the major part of the fast neutron effect. The conclusions to be drawn will not be affected by the presence of a small number of counts from any other process.

§2. Measurements on the Absorption of Fast Neutrons

When *slow* neutrons are absorbed in matter, the excess energy of the transformation is usually emitted as one or more gamma-rays. It is of interest to determine whether the gamma-rays produced by the action of fast neutrons on matter arise in a similar manner. The absorption of fast neutrons in several elements has been measured by Fleischmann[12] and by Dunning, Pegram, Fink and Mitchell.[4] Fleischmann used a method in which the loss of neutrons by scattering could not be avoided, whereas the results of Dunning and co-workers could be interpreted as being due either to absorption or to the slowing of the fast neutrons.

In the present work the absorption of fast neutrons has been measured with cylindrical absorbers to minimize the loss of neutrons by scattering and with a method of detection which made any change in the energy spectrum of the fast neutrons relatively unimportant.

The source of neutrons (Be+200 mg Ra) was mounted in the center of a cavity *A* (Fig. 3) within a large lead block. Measurements were

[11] Dee, Proc. Roy. Soc. (London) **A136**, 727 (1932).
[12] Fleischmann, Zeits. f. Physik **97**, 265 (1935).

made alternately with and without cylindrical absorbers around the source at A. The fast neutrons were detected by slowing them in 5.7 cm of paraffin at B and counting by means of a Geiger-Müller counter the gamma-rays produced by the absorption of these slow neutrons in cadmium and lead. A screen of B_4C, (0.6 g/cm^2) used as a shutter, could be inserted as shown in the figure, and the difference in counting rate with and without the shutter gave directly a measure of the intensity of slow neutrons incident upon the counter system, and hence also a measure of the intensity of *fast* neutrons incident upon the paraffin at B.

Pyrex glass at the left of the paraffin slabs (Fig. 3) served to prevent slow neutrons originating in or behind the source from reaching the counter system. The lead between the paraffin and counter absorbed the gamma-rays produced by the capture of slow neutrons in the paraffin. The entire assembly was mounted on a steel table 175 cm from the floor in the center of a large room. The Geiger counter was enclosed in a lead block in order to absorb gamma-rays produced in the floor and walls of the room by slow neutrons.

The absorbing cylinders used in these experiments were 17.8 cm long and approximately 10 cm in diameter. The exact thickness of the absorbing wall is stated for each element in Table I. Ideally, one should use a small spherical source of neutrons and spherical absorbers, but since the source of neutrons available was in the form of a cylinder 13 cm long and 1.8 cm in diameter, absorbers of the sort used were appropriate.

With the above arrangement, the results presented in Table I were obtained.

From Table I one sees that within the limitations of the experimental method no absorption outside of the probable error has been detected in the elements studied and that the calculated transmission of fast neutrons through several elements appears even to exceed one hundred percent. This excess may be attributed to the slowing of fast neutrons in the absorbers (§3). If the neutrons are slowed in the absorber without being captured there, the number of slow neutrons subsequently emerging from a layer of paraffin of a given thickness will be slightly increased. To this extent the method of detection

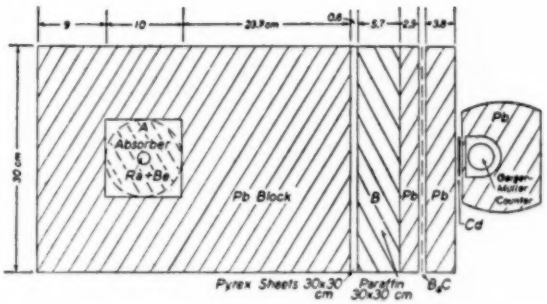

FIG. 3. Experimental arrangement for measuring absorption of fast neutrons in matter.

used was evidently affected by changes in the energy spectrum of the fast neutrons as they traversed the absorbers.

Dunning and co-workers found considerable apparent absorption of fast neutrons in several elements, but as they have pointed out, a slowing of fast neutrons in the absorbers could also produce their experimental results.

The experiments described in §3 show that whatever real absorption may occur is not responsible for any important part of the gamma-rays produced by the action of fast neutrons. Hence a capture process followed by the emission of soft gamma-rays in a cascade cannot be the origin of the gamma-rays observed.

It is well known that fast neutrons produce induced radioactivity and other nuclear transformations in many elements. Thus it is certain that some absorption of fast neutrons occurs in these elements, but such absorption was evidently too small to have been measured by the method described above. The increase due to slowing in the number of slow neutrons emerging tends to compensate for the decrease due to true absorption within the material. Since these two factors cannot be separated by such experiments, and in view of the obtained precision, it is clear

TABLE I. *Measurements on the absorption of fast neutrons.*

ABSORBER	WALL THICKNESS (cm)	FRACTION TRANSMITTED
C	4.1	1.00±0.02
Al	4.2	1.03±0.02
S	4.0	0.99±0.02
CCl_4	4.0	0.98±0.02
Fe	4.0	1.02±0.02
Cu	3.4	1.05±0.02
Cd	4.3	1.00±0.02
Pb	4.2	1.04±0.02

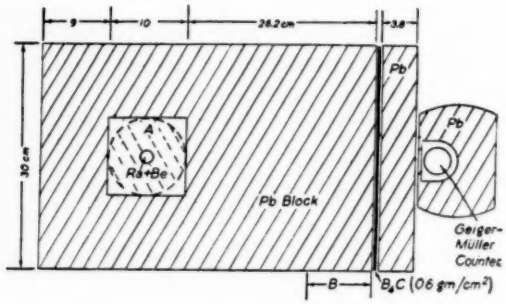

FIG. 4. Experimental arrangement for measuring the intensity of primary gamma-rays reaching the counter; also, arrangement for demonstrating inelastic scattering of fast neutrons.

that true capture cross sections of the order of 10^{-25} cm^2 are not ruled out.

§3. Slowing and Inelastic Scattering of Fast Neutrons

In the experiments of §1 and in the experiments to be described presently, an accurate knowledge of the intensity of primary gamma-rays penetrating the large lead block and tripping the counter is imperative. For this purpose a set of measurements was made in which the 200 millicuries of Ra-Be was replaced by 55 millicuries of pure radon. It was proved in this manner that scattered gamma-rays had been reduced to negligible proportions, and it was estimated that with 30 cm of lead between the Ra-Be source and the counter only 1.1 ± 0.3 counts per minute could be attributed to gamma-rays from the radium itself. Another determination of this quantity has been made as follows. The experimental arrangement used is shown in Fig. 4. It is the same as that used for the experiments on inelastic scattering to be described below. The Ra-Be source of neutrons was in the center of the empty cavity *A*. The lead housing around the counter was surrounded by Pyrex glass in order to eliminate stray slow neutrons formed in the walls of the room. Counts were taken with various thicknesses of lead between the source and counter. The excess lead was removed at *B*.

The curve so obtained is plotted logarithmically in Fig. 5. It has been resolved into two straight lines by making use of the known absorption coefficient of RaC gamma-rays in lead. One line gives the intensity of such gamma-rays acting on

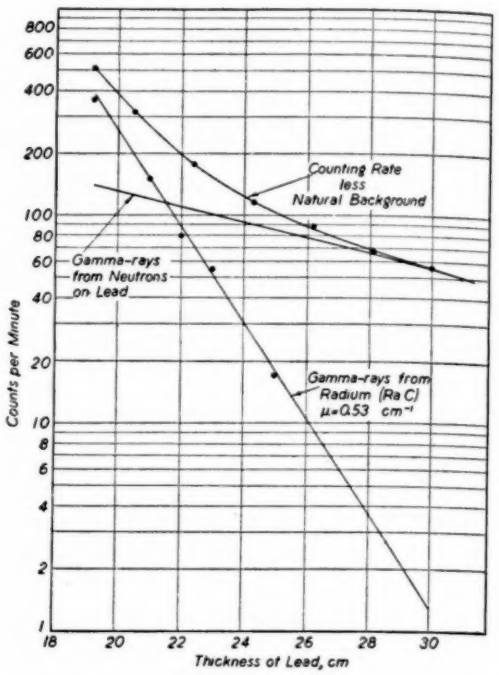

FIG. 5. Variation of counting rate with thickness of lead between source and counter. Straight lines show resolution of curve into its components.

the counter, the other gives the intensity of gamma-rays produced by the fast neutrons on the lead surrounding the counter. The slope of the latter curve is due partly to the loss of neutrons by scattering, and partly to the process of inelastic scattering next to be described. In all of the following work the corrections for the primary gamma-rays reaching the counter have been taken from Fig. 5.

The value obtained with pure radon referred to above (1.1 ± 0.3 counts per minute) is in agreement with the curve in Fig. 5. With 30 cm of lead between the Ra-Be source and the counter the counts due to the primary gamma-rays amount to less than 3 percent of the fast neutron effect.

It was proved in the following manner that the soft gamma-rays excited by fast neutrons are the result of inelastic scattering. The experimental arrangement was again as shown in Fig. 4, but in these experiments the full thickness of lead remained at *B*. Measurements were made alternately with and without cylindrical absorbers at *A*. The counts recorded by the Geiger-Müller counter (after subtracting the natural back-

ground) were due chiefly to gamma-rays excited in the lead by fast neutrons as described in §1. When the cylindrical "absorbers" were placed around the source at A, a marked decrease in the counting rate was observed. The results so obtained are listed in Table II.

In order to show that these effects did not arise solely from changes in that part of the "fast neutron effect" which could not be positively identified (§1), the counter was removed from its lead housing and placed in a copper cylinder of 2.8 cm wall thickness. This assembly replaced the lead housing shown in Fig. 4. Because of its small gamma-ray absorption and large cross section for the production of gamma-rays under the action of fast neutrons, copper gives a much larger yield of gamma-rays than does lead. When the gamma-rays from copper were used as the detector, the counting rate was twice as great as in the measurements using the gamma-rays from lead, and hence it is certain that in this case nearly all of the counts were due to gamma-rays excited in the copper. The results of these experiments are also listed in Table II. The results obtained by the two methods of detection are nearly the same, although close agreement was not necessarily to be expected.

Although it was shown in §2 that nearly all of the fast neutrons are transmitted through the "absorbers" (except H_2O), the results presented in Table II show that the capacity of these neutrons to produce gamma-rays in lead or copper is considerably diminished as a result of their passage through the "absorbers." Since the neutrons are not absorbed, the energy of the gamma-rays must be derived from the kinetic energy of the fast neutrons. In producing these gamma-rays the neutrons must lose energy and be slowed down. The results show, however, that below a certain energy, perhaps 0.5 Mev, the neutrons are no longer capable of exciting gamma-rays, and hence no further slowing is to be expected.

TABLE II. *Measurements on the inelastic scattering and slowing of fast neutrons.*

Element	Wall Thickness	Fraction Transmitted		Average Cross Section $\times 10^{25}$ cm^2
		Pb γ-ray Detection	Cu γ-ray Detection	
C ($\rho=1.3$)	4.1 cm	0.97±0.02	0.96±0.02	1.2±0.8
Al	4.2	0.90±0.02	0.94±0.02	3.3±0.9
S ($\rho=2.0$)	4.0	0.92±0.02	0.91±0.02	5.8±1.4
Cl(CCl_4)	4.0	0.92±0.02	0.94±0.02	7.3±2.1
Fe	4.0	0.78±0.02	0.78±0.02	7.4±0.8
Cu	3.4	0.75±0.02	0.78±0.02	9.4±0.9
Cd ($\rho=7.3$)	4.3	0.79±0.02	0.81±0.02	13.4±1.5
Hg	3.9	0.82±0.02	0.79±0.02	14.0±1.6
Pb	4.2	0.85±0.02	0.83±0.02	12.2±1.7
H_2O	4.0	0.84±0.02	0.86±0.02	

It is demonstrated, therefore, that many of the collisions of fast neutrons with nuclei are inelastic, leaving the nuclei in an excited state. This process has recently been discussed by Bohr and others.[13, 14]

The cross sections given in the right-hand column of Table II have been calculated in a purely formal manner from the experimental mean free paths corresponding to the transmissions observed. No correction has been attempted for the small amount of real absorption that must occur, nor for the diffusion of neutrons throughout the lead block. The values so obtained are several times smaller than the scattering cross sections found by Dunning, from which one concludes that only a part (1/2–1/10) of the impacts of fast neutrons with nuclei are inelastic. The ratio of the inelastic to elastic scattering cross section is doubtless dependent upon the energy of the incident neutrons.

Fleischmann looked for the production of thermal neutrons by the action of fast neutrons on lead and found an effect just outside of his probable error.[12] In a more sensitive experimental arrangement, Fink has confirmed the fact that fast or residual neutrons passing through several elements produce a detectable number of thermal neutrons.[15] Wertenstein, Ehrenberg, and Collie and Griffiths have observed that when fast neutrons traverse various substances, their capacity to induce artificial radioactivity in silver and iodine is enhanced.[16–18] These observations are in accord with the results of this paper.

[13] Bohr, Nature **137**, 344 (1936).
[14] Bethe and Placzek, Phys. Rev. **51**, 450 (1937).
[15] Fink, Phys. Rev. **50**, 738 (1936).
[16] Danysz, Rotblat, Wertenstein, Zyw, Nature **134**, 970 (1934).
[17] Ehrenberg, Nature **136**, 870 (1935).
[18] Collie and Griffiths, Proc. Roy. Soc. (London) **A155**, 434 (1936).

The inelastic scattering process gives rise to neutrons of low energy. A small fraction will have energies of a few hundred volts or less; of these an even smaller fraction will have energies within the cadmium resonance band. Owing to the extremely high efficiencies with which these two classes of neutrons can be detected, the production of both classes of neutrons has been observed.

We take this opportunity to thank Professor Gilbert N. Lewis and Dr. W. F. Libby of the chemistry department and Professor Edwin McMillan of the physics department for valuable advice and discussions.

SEPTEMBER 1, 1937 PHYSICAL REVIEW VOLUME 52

The Compton Effect with Gamma-Rays

ROBERT S. SHANKLAND
Case School of Applied Science, Cleveland, Ohio
(Received June 24, 1937)

This paper summarizes the results of recent studies of the Compton effect using Geiger-Müller counters. The results show that no time lag as great as 10^{-4} second can exist in the Compton scattering process and that the angular relationship given by the photon theory is verified to within $\pm 20°$.

THE results of several recent experiments[1] have seemed to indicate that in the Compton scattering of x-rays or gamma-rays the recoil electron appears at the same instant that the quantum is scattered. The angular relationship predicted by the theory of Compton-Debye[2] between the directions of the recoil electron and scattered photon pairs is, however, more difficult to establish. The original cloud chamber experiments of Compton and Simon[3] made with hard x-rays scattered by air indicated an agreement with theory. More recently, the counter experiments of Bothe and Maier-Leibnitz[1] and the cloud chamber experiments of Crane, Gaerttner and Turin[4] have seemed consistent with the angular relationship predicted by theory. Some experiments by the present writer[5] which attempted to fix the angular relationship sharply, yielded results that did not support the theoretical predictions. The publication of these findings aroused an active interest in the subject which resulted in several new experiments[6] and theoretical discussions[7] that have added greatly to the knowledge of these phenomena.

An experiment to check the angular relationship between the paths of the recoil electrons and scattered photons has been made with the apparatus shown schematically in Fig. 1. The beam of gamma-rays is directed against the scatterer at *S*, which in this experiment is an aluminum foil of thickness 0.00165 cm. The source is a radon tube giving off the gamma-rays of Ra C which are filtered through 0.32 cm of lead. The collimating system consists of a series of lead shields surrounding a brass tube 0.8 cm in diameter and 28 cm long. The end of this system as shown in Fig. 1 is designed to prevent most of the gamma-rays scattered from the brass tube from going

[1] W. Bothe and H. Maier-Leibnitz, Zeits. f. Physik **102**, 143 (1936), Gött. Nachr. **2**, 127 (1936), Phys. Rev. **50**, 187 (1936); J. C. Jacobsen, Nature **138**, 25 (1936); W. E. Burcham and W. B. Lewis, Proc. Camb. Phil. Soc. **32**, 637 (1936); R. S. Shankland, Phys. Rev. **50**, 571 (1936), Phys. Rev. **51**, 1024 (1937).
[2] A. H. Compton, Phys. Rev. **21**, 483 (1923); P. Debye, Physik. Zeits. **24**, 161 (1923).
[3] A. H. Compton and A. W. Simon, Phys. Rev. **26**, 289 (1925).
[4] H. R. Crane, E. R. Gaerttner and J. J. Turin, Phys. Rev. **50**, 302 (1936).
[5] R. S. Shankland, Phys. Rev. **49**, 8 (1936).
[6] Ibid. also A. Piccard and E. Stahel, J. de phys. **7**, 326 (1936); E. J. Williams and E. Pickup, Nature **138**, 461 (1936).
[7] P. A. M. Dirac, Nature **137**, 298 (1936); N. Bohr, Nature **138**, 26 (1936); F. Cernuschi, Comptes rendus **203**, 777 (1936); M. Taketani, Kagaku, 6 (1936); B. Hoffmann, A. G. Shenstone and L. A. Turner, Phys. Rev. **50**, 1092 (1936); E. J. Williams, Nature **137**, 614 (1936); R. Peierls, Nature **137**, 904 (1936).

directly to the counters. The gamma-ray counter G is set at an azimuth $\phi=90°$.

As the gamma-rays from Ra C consist of a line spectrum, it is necessary to compute the angle θ at which the recoil electron is ejected by each component of the incident radiation, when the scattering angle ϕ is 90°. The calculation is made by the Compton-Debye formula:

$$\cot\theta=(1+\alpha)\tan\tfrac{1}{2}\phi,$$

where $\alpha\equiv h\nu/mc^2$. A weighted mean of the values of θ computed from these equations is 22.5°. The electron counter R is mounted on an arm pivoted directly under the scatterer so that it can be set in the azimuth $\theta=22.5°$, and also be moved to the setting indicated by $-\theta$ in Fig. 1. The conservation of momentum in the scattering process will make it impossible for a recoil electron to be ejected to the counter R in the $-\theta$ position by a quantum scattered to the gamma-ray counter at G. The value of $-\theta$ chosen was $-22.5°$ since in this position the background discharge rate in the counter will be the same as in the $+\theta$ position. This fact was verified by an auxiliary experiment.

During the experiments the electron counter R was alternated from one position to the other every half-hour and the coincident discharges in the counters G and R were recorded. Table I gives the observed coincidence rates in the counters after they have been corrected for the decay of the radon tube during the course of the observations. The average strength of the source was 93 millicuries. The first and third columns give the coincidence rates observed with the electron counter R set in the position $+\theta$, demanded

TABLE I. *Observed rates of coincident discharges in counters G and R corrected for decay of gamma-ray source.*

R at $+\theta$ (min.$^{-1}$)	R at $-\theta$ (min.$^{-1}$)	R at $+\theta$ (min.$^{-1}$)	R at $-\theta$ (min.$^{-1}$)
1.24	0.78	1.08	0.98
1.22	1.07	1.09	0.85
1.46	0.88	1.19	0.82
1.30	0.79	1.78	0.71
1.50	1.11	0.99	0.50
1.50	0.89	1.22	0.62
1.19	0.91	1.51	0.61
		1.21	0.92
Mean Rates		1.30 min.$^{-1}$	0.83 min.$^{-1}$
Natural Uncertainty of Mean		±0.09	±0.07
Mean Error of Mean		±0.05	±0.05
Total Coincidences		195	141

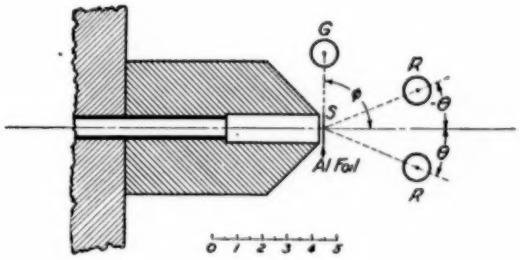

FIG. 1. Schematic diagram of apparatus.

by the photon theory of scattering. The second and fourth columns give the values observed with R set in the symmetrically opposite position $-\theta$. The mean coincidence rates are given, together with the natural uncertainty and the mean error of the mean.

The difference between the mean coincidence rates observed in the two positions shows a surplus of 0.47 min.$^{-1}$ in the position predicted by the theory. The natural uncertainty in this quantity is 0.12 min.$^{-1}$ while the mean error of the mean is 0.07 min.$^{-1}$, as computed by the Bessel formula. The criterion usually given in the theory of errors for an effect to be significant is that its magnitude should be at least three times the mean error of the mean. Here the effect is nearly seven times this quantity.

The data of Table I are plotted in Fig. 2 in the form of histograms. The abscissae give the observed coincidence rates, and the ordinates show the number of groups that were observed in the various ranges. A statistical analysis of these data has been made[8] which gives the following results. The data taken with the electron counter set in the $-\theta$ position show that the average $\bar{n}=0.835$ min.$^{-1}$; the standard deviation $\sigma=0.166$; and the asymmetry factor $\beta_1^{\frac{1}{2}}=0.11$. These quantities suggest that the observations approximate the normal distribution law: $[(2\pi)^{\frac{1}{2}}\sigma]^{-1}\times\exp[-(n-\bar{n})^2/2\sigma^2]$ where n is the observed coincidence rate. A smooth curve of this form has been drawn in the upper graph of Fig. 2. It is not unexpected that the residual coincidences should be distributed according to the normal law since they are due principally to the chance juxtaposition in time of the discharges of the separate counters.

[8] T. C. Fry, *Probability and Its Engineering Uses*, pp. 299–305; 470–471.

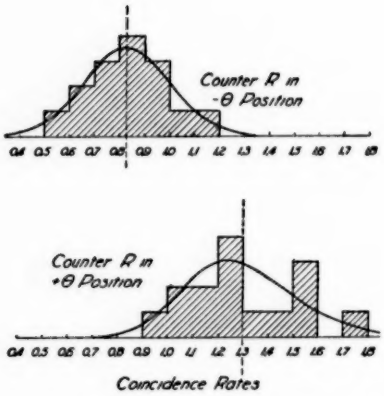

FIG. 2. Histograms of coincidence rates for different counter positions.

The data when the counter R is in the $+\theta$ position yield the average $\bar{n}=1.30$ min.$^{-1}$; the standard deviation $\sigma=0.214$; and the asymmetry factor $\beta_1^{\frac{1}{2}}=0.67$. The large asymmetry exhibited by these data suggests that they may be distributed according to the Poisson law: $\epsilon^n e^{-\epsilon}/n!$ Here ϵ is the expectation, and n is the coincidence rate measured from the background rate. Since the effect producing the shift of the second set of data with respect to the first is superimposed on the background coincidence rate, the origin for the Poisson function will be at 0.835 min.$^{-1}$. The smooth curve in the lower graph of Fig. 2 is of the Poisson type. The true coincidences due to the Compton effect should follow the Poisson law[9] and it is interesting that the data themselves suggest such a distribution. The greater value of σ found in the $+\theta$ position is due to the fact that the background and the true coincidences are here superimposed. Although the data are hardly extensive enough to base any further conclusions on the shapes of these curves, yet it is interesting to note that when they are graduated by the usual methods,[10] smooth curves result which are very similar to those drawn in Fig. 2.

The mean coincidence rates given in Table I are the sum of true coincidences and background coincidences. The latter are due principally to the finite resolving time of the electrical adding circuit used to record the coincidences. Cosmic-ray showers and other factors may also contribute a few coincidences in both the $+\theta$ and $-\theta$ positions. The residual coincidence rate was determined experimentally in two ways. First, the scattering foil was removed and the coincidence rate measured with the Ra C source in place and the electron counter set in the azimuth $-\theta$. The observed coincidence rate was 0.68 ± 0.10 min.$^{-1}$. Then, with the Ra C source removed, the counters were stimulated with old radon tubes so that the individual discharge rates in the counters were nearly the same as in the principal experiment, and the coincidence rate was again determined. The result of this comparison experiment gave a rate of 0.57 ± 0.09 min.$^{-1}$. The average of these determinations is used in the calculations below. The time constant of the adding circuit has not been further reduced since it is possible that the real coincidences may be missed in so doing; while theory indicates that there should be no lag in the scattering process itself of sufficient magnitude to be determined experimentally, yet the possibility exists that small time lags will be introduced by the amplifying circuits themselves which would vitiate the results. Other factors contributing to the background rate are the increased single counting rate in the electron counter due to scattered gamma-rays and to secondary beta particles ejected from the walls of the collimating system by the primary gamma-ray beam. Some of these will reach the electron counter and tend to raise the background coincidence rate. However, this will not obscure the principal effect looked for if the electron counter is operating near its maximum efficiency. That this was the case was shown by placing a radioactive source near the electron counter while the main experiment was in progress; the very large increase observed in both the single counting rate and the coincidence rate proved that the apparatus was functioning properly.

With the background coincidence rate determined above and the data of Table I, the following values for the rates of true coincidences observed in the two positions of the electron counter R are given: In the $+\theta$ position the observations give $1.30-0.62=0.68$ min.$^{-1}$; and in the $-\theta$ position the rate is $0.83-0.62=0.21$ min.$^{-1}$. The true coincidences observed in the $-\theta$ position can hardly be ascribed to chance.

[9] T. C. Fry, *Probability and Its Engineering Uses*, pp. 214–240.

[10] E. T. Whittaker and G. Robinson, *The Calculus of Observations*, pp. 285–316.

They are probably due to recoil electrons that have been deflected through an angle of about $2\theta°$ in leaving the foil. If the angle of deflection suffered by a recoil electron from its direction of ejection from an atom is given by Δ, and $P(\Delta)$ is the probability of a deflection of this magnitude, then the relation between Δ and $P(\Delta)$ may be given by the normal distribution function:

$$P(\Delta)=\frac{0.4769}{\pi^{\frac{1}{2}}\Delta_m}\exp\left[\frac{-(0.4769)^2\Delta^2}{\Delta_m{}^2}\right],$$

where Δ_m is the angle of half-scattering. For the position $+\theta$ the value of Δ is zero and $P(0)$ has a value proportional to 0.68 min.$^{-1}$. For the $-\theta$ position, Δ equals 45° and $P(45°)$ is here proportional to 0.21 min.$^{-1}$. A substitution of these values in the equation gives $\Delta_m=\pm 20°$ as the experimental value of the "angle of half-scattering" of the distribution function. This indicates that half of the recoil electrons ejected in the initial direction $+\theta$ are deflected by less than 20° in leaving the scatterer.

The value of Δ_m determined from this experiment can be compared with the value computed with the formula given by Bothe[11] for the multiple scattering of electrons passing through a thin foil: $\Delta_m=2.6e^2E^{-1}Z(\pi nt)^{\frac{1}{2}}$. Here t is the thickness of the foil, n is the number of atoms per cubic centimeter, Z is the atomic number, and E is the energy of the electron. This equation, however, applies to the case where the electron passes through the entire foil. In the present experiment the recoil electrons are liberated within the foil itself. This means that the equation would be correct for electrons passing through the entire foil, while those liberated on the side of the foil near the counter would suffer a negligible deflection. For sufficiently thin foils, the formula should be correct if t is used as half the foil thickness. For the foil as actually used, it works out that $\Delta_m=\pm 11.4°$.

Several factors are present which would tend to make the observed value of Δ_m greater than that computed by the Bothe formula. These are the nonhomogeneity of the gamma-rays used, the scattering by the gas in the chamber, and the finite angles subtended by the counters. The net effect of these factors would be to diminish the number of coincidences observed in the predicted direction, although the number observed in the other position would not be appreciably increased by this cause. It has been suggested[7] that the true coincidences observed in the $-\theta$ position might be related to a double Compton effect or to other mechanisms that would make the usual application of the laws of conservation of energy and momentum inadequate, but the essential features of the present experiments require no such interpretation. The wave mechanics suggests that, as in the case of the ejection of photo-electrons, the spread of the electrons about the most probable direction of ejection must be greater than that predicted by the simple corpuscular picture of the process. The experiments of Kirchner[12] support this view. In any event there seems no reason to doubt that the present experiment supports the angular relationship given by the theory of Compton-Debye to within ±20°.

Four other experiments have been performed by the writer which have shown a directional effect in the emission of recoil electrons. These experiments have been summarized in Table II. The first column gives the material of the scatterer; the second column gives the angle Δ between the predicted position of the electron counter and the comparison position; while the third column gives the angle θ of the Compton-Debye theory. The fourth and fifth columns give the thickness of the scatterer in centimeters and the initial energies of the recoil electrons expressed in million electron volts, respectively. The sixth column gives a quantity which should determine the relative number of recoil electrons deflected to the electron counter when it is in the comparison position where theory predicts no

TABLE II. *Results of six experiments which show a directional effect in the emission of recoil electrons.*

SCATTERER	Δ	θ	t	F	$\frac{Z}{E\sin(\Delta/2)}\left(\frac{t'\rho}{A}\right)^{\frac{1}{2}}$	$\frac{R_+-R_0}{R_--R_0}$
Aluminum	45°	22.5°	0.00165	0.35	1.30	3.24
Aluminum	45°	22.5°	0.0038	0.35	1.96	2.52
Air	60°	45°	1.5	0.18	1.07	5.5
Cellophane	12°	30°	0.0028	1.1	0.95	6.22
Paraffin	60°	45°	0.05	0.18	3.44	1.74
Beryllium	60°	45°	0.04	0.18	4.80	1.38

[11] W. Bothe, Zeits. f. Physik **13**, 368 (1923).

[12] F. Kirchner, Physik. Zeits. **27**, 385, 799 (1926); Ann. d. Physik **81**, 1113 (1926).

coincidences should be observed. The last column gives the ratio between the true coincidences observed in the predicted position and in the comparison position of the electron counter.

The first line of the table summarizes the experiment with aluminum as described above in some detail. The second line gives a similar experiment with a somewhat thicker aluminum foil. The average strength of the radon tube used in this experiment was 82 millicuries. The fourth line summarizes the experiment of Bothe and Maier-Leibnitz[1] with the more homogeneous gamma-rays from Th C″. The experiments in the third, fifth, and sixth lines were performed with the counters in a somewhat different arrangement than shown in Fig. 1. Here they were placed parallel to the axis of the gamma-ray beam. This allows beta-particles with a wider range of θ values to enter the electron counter, thus minimizing the effect of the nonhomogeneity of the gamma-ray source. The predicted position for the electron counter was therefore in the plane containing the quantum counters and the incident beam; while in the comparison position the electron counter was rotated 90° out of this plane about the incident beam as an axis. In the latter position, the conservation of momentum would not be satisfied and no coincidences should be observed except those due to the disturbing factors discussed above. In these experiments four gold-walled counters were used to record the scattered photons; these counters have a higher efficiency for gamma-rays than those with walls made of elements of lower atomic number. The average strength of the radon tube was 120 millicuries. Since the several experiments were performed under such different conditions, the only practicable way of attempting to correlate them is by means of the ratios given in the final column of Table II.

Figure 3 shows the relationship between this ratio for the several experiments and the electron diffusion factor given in column five of the table.

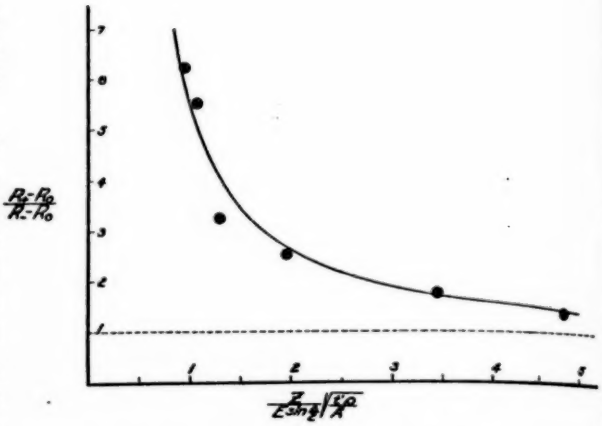

FIG. 3. Correlation of the data in Table II.

The circles represent the six experiments and a smooth curve of the form $(y-1)=cx^{-b}$ has been drawn to emphasize the general tendency. The two points that fall below this simple smooth curve represent the experiments in which the nonhomogeneity of the source would have the greatest effect in diminishing the angular effect. It is interesting to note that a more definite positive effect is observed with the paraffin scatterer than with a thinner scatterer of beryllium under the same conditions. This is of course due to the lower average atomic number of the paraffin. The fact that six distinct experiments may be correlated in this fashion gives strong additional evidence that the surplus of coincidences observed in the predicted position is due to the Compton effect and not to any spurious cause.

Taken as a group, these experiments lead to the conclusion that no time lag as great as 10^{-4} second can exist in the Compton scattering process, and that the angular relationship given by the theory of Compton-Debye is verified to within $\pm 20°$. The limit in the time factor is set by the nature of the electrical circuits used, while the angular resolution is determined very largely by the diffusion of the recoil electrons.

A Direct Spectrum of the Structure and Shift of the Compton Line with Helium Gas as the Scatterer

JESSE W. M. DUMOND AND HARRY A. KIRKPATRICK
California Institute of Technology, Pasadena, California, and Occidental College, Los Angeles, California

(Received April 15, 1937)

The characteristic K lines from a molybdenum target x-ray tube were scattered almost directly backward by helium gas at fourteen atmospheres in a chamber provided with a celluloid window. Entry and exit of radiation was provided through distinctly separate regions of the window to avoid window scattering. The scattered radiation was spectrally resolved with a Cauchois focusing curved (quartz) crystal spectrograph on a curved photographic film after an exposure of 2059 hours. The structure and breadth of the modified line obtained with a recording microphotometer are in excellent agreement with the theoretical predictions of DuMond's theory in which the modified line is regarded as broadened by the Doppler effect of the motion (momentum) of the electrons in the scattering substance. The momentum distribution for the helium atom and the consequent modified line structure have been computed by B. Hicks. The slight defect in the shift (discovered by Ross and Kirkpatrick) caused by the momentum imparted to the whole mass of the atom in the process of ejecting the recoil electron is also verified. All previous reliable studies with solid scatterers have shown the structure of the modified line much broader than DuMond's theory predicts for the electron momenta to be expected in a *free* atom of the scattering substance although the functional dependence of the breadth on the scattering angle and the primary wave-length were shown by the authors to be in good accord with their Doppler interpretation. The supposition that this excess breadth for solid scatterers is an effect of the higher electron momenta required in the solid state by the Pauli exclusion principle is thus verified in the present work by the fact that with this gaseous scatterer the modified line breadth shows no such excess over the value computed for the free atom. The authors believe this to be the first time a direct spectrum of radiation scattered by a gas has ever been obtained. A brief review of work to date on the structure and shift of modified scattered radiation is given to serve as a background against which to emphasize the interesting questions answered by this investigation and to point out the erroneous character of currently accepted results of certain previous investigations. The experimental details and the methods of reducing the data are fully given. A discussion is given of focusing x-ray spectrographs in general, operating on the geometrical principle first enunciated by the present authors. Advantages and disadvantages of the transmission type with curved crystalline lamina are discussed. Formulae and convenient methods are given for computing the dispersion at any point from reference lines recorded on the film thus automatically correcting for instrumental aberrations. The relativistic correction to the shift formula as derived by DuMond in 1929 is shown to be too small to require consideration here. Conclusive internal evidence from the extreme faintness of the unmodified scattered lines relative to the modified band, proves that the modified scattering here obtained has been scattered by helium only.

I. INTRODUCTION

Two distinct effects associated with scattering

A ROUGH and forceful description of the mechanism whereby radiation is spectrally modified by scattering from matter can be made as follows. An initially monochromatic line observed after scattering by matter under a well-defined scattering angle suffers a change of wave-length as the result of two distinct types of Doppler shift. The first of these two shifts can be understood as the result of the velocity (more accurately the momentum) *imparted* to a single electron as the scattering agent in each individual process *by the radiation itself*. This effect, commonly known as the Compton effect, is a systematic shift always toward longer wave-lengths, since the electron always recoils *away* from the source of radiation.

The second of these two Doppler shifts can be understood as the result of the initial *proper motion* (momentum) of the scattering electron. This linear momentum may be that of an electron in some particular atom or that of an electron more or less "free" in the crystal lattice of a solid body such as an electrical conductor or, conceptually at least, that of an electron in perfectly free motion in space. Since, as it turns out, most assemblages of electrons sufficiently numerous to give an observable spectrum of scattered radiation may be expected to have these momenta isotropically distributed as to direction in space, the second Doppler shift results statistically in a *broadening* of the shifted Compton line with a definite structure which is a key to the momentum distribution of the assemblage of scattering electrons.

While the first mentioned (Compton) shift is emphatically a quantum phenomenon, the second shift which produces the broadening of the modified line is much closer to the classical Doppler effect and indeed the formula for the magnitude of this broadening involves the action quantum, h, only in small unimportant correction terms.

Historical review

J. A. Gray[1] was the first to establish beyond doubt that the scattering process changes the wave-length of substantially homogeneous gamma radiation to a greater extent the greater the scattering angle, the change in wave-length when it occurs being independent of the scattering material. This he did by carefully designed absorption measurements interpreted with admirable critical skill.

The mechanism of the scattering of radiation in discrete quanta with recoil of the scattering electron under the impulse from both primary and unidirectionally emitted scattered quanta and with a consequent Doppler change of wave-length of the scattered radiation appears first in the literature in October, 1922 in an article by A. H. Compton. This article also presents the first experimental evidence in the form of a spectrum to show the change of wave-length of scattered radiation.[2]

The more precise mathematical formulation of the above effect appears in a famous paper by Compton[3] in May, 1923. In March P. P. Debye published an identical theory[4] but without experimental evidence of his own. He refers to Compton's paper[2] as one of his sources of information as to the experimental facts.

Regarding the second effect associated with modified scattering (broadening of the shifted line by the initial momenta of the scattering electrons) the first reference to this in the literature appeared in a paper by P. A. Ross, remarkable for its insight, compactness and content. This paper[5] appeared in July, 1923 and was communicated June 6 of that year. It contains the observation from one of his photographic spectra that the modified line is broader than either the unmodified or the primary line and gives qualitatively what the authors of the present paper have since shown to be the correct interpretation of this in terms of the initial momenta of the scattering electrons. It also gives the first direct evidence for the unmodified scattered line and the correct qualitative explanation for the mechanism of its production. It also gives the kernel of the idea later so fruitfully applied by Wollan and by Kappeler to the study of the Compton effect, the idea of causing the modified line progressively to shift across the critical absorption edge of a filter with variation of the scattering angle.

A paper by A. H. Compton[6] in the November, 1923 issue of the *Physical Review* communicated May 9, 1923 reported in a single paragraph that the modified line in his ionization spectrum seemed spectrally broader than could be explained by the inhomogeneity of the scattering angle and the rather low resolution employed to obtain intensity. *No explanation was offered.* On this important phenomenon, to the best of our knowledge, this author remained completely silent until the publication of his book, *X-Rays and Electrons*, in which the theory of Jauncey for the modified and unmodified scattering was presented.[7]

In the meanwhile many workers[8] including P. A. Ross, de Broglie and Dauvillier had published the conclusion that the broadening of the

[1] J. A. Gray, J. Frank. Inst., p. 633, Nov. (1920).
[2] A. H. Compton, Bull. Nat. Res. Council No. 20 (1922), p. 19.
[3] A. H. Compton, Phys. Rev. **21**, 483 (1923).
[4] P. P. Debye, Physik. Zeits. **24**, 161 (1923). A paper by A. H. Compton presented at the Chicago meeting of the American Physical Society, Dec. 1, 1922 correctly states the physical assumptions and the results of the analysis at an earlier date than Debye's paper, however.
[5] P. A. Ross, Proc. Nat. Acad. Sci. **9**, 246 (1923).
[6] A. H. Compton, Phys. Rev. **22**, 412 (1923).
[7] A. H. Compton, *X-Rays and Electrons* (Van Nostrand, May 24, 1926), p. 293 and Sec. 134. Even in this work the indecisive nature of the evidence then existing as to the magnitude and significance of the broadening of the shifted line is frankly admitted.
[8] P. A. Ross and D. L. Webster, Proc. Nat. Acad. Sci. **11**, 56 (1925). M. de Broglie and A. Dauvillier, J. de phys. **6**, 369 (1925). These opinions as to the spurious nature of the broadening of the modified line seem to have persisted as late as 1930 for the erroneous results in the three following papers would otherwise surely never have been published. B. Davis and H. Purks, Phys. Rev. **34**, 1 (1929); J. H. Bearden, Phys. Rev. **36**, 791 (1930); N. L. Gingrich, Phys. Rev. **36**, 1050 (1930). The last author reported very sharply pointed shifted lines, the K alpha-doublet of Mo being clearly resolved in the shifted position for scattering under a large angle from graphite!

modified line was a spurious effect of inhomogeneity of scattering angle, or some other cause.

In a series of ingenious papers[9] G. E. M. Jauncey presented the results of the application of the idea of Ross that the initial momenta of the scattering electrons play a part in the scattering process and influence the structure of the shifted line. Jauncey's theory of scattering by bound electrons assumed these electrons from the start to have the dynamics required by the original Bohr-Sommerfeld orbit theory and hence its results suffered from the defects of that theory. The simple nature of the broadening of the shifted line as *a Doppler effect of whatever statistical momentum distribution the scattering electrons may happen to have* was not clearly set forth. *Position* in its orbit was emphasized as the factor determining whether an electron should scatter with or without ejection from the atom, a particularly unfortunate emphasis since it is amply evident that this author was very close to the correct formulation of the problem. Indeed he deserves great credit for the following more precise formulation of Ross' germinal idea which he offers to explain the mechanism of modified and unmodified scattering: The interaction between photon and bound electron is conceived as an impulsive one (relative to the orbital period) and the momentum configuration of this collision (vector momenta of incident photon, scattered photon and orbital electron) is conceived as determining the energy imparted to the electron by the radiation exactly the same as though the electron under the same collision configuration were free. For all collisions where this imparted energy exceeds the binding energy of that particular electron, Jauncey assumes the electron will be ejected from the atom and the radiation will be scattered with change of wavelength. For all collisions where the imparted energy is *less* than the binding energy the electron will transfer the imparted momentum to the heavy nucleus of the atom which will thus as a whole acquire an entirely negligible recoil velocity and energy. A consequent entirely negligible shift of the scattered radiation (unmodified line, coherent scattering) will occur.

Jauncey's theory emphasizes the *energy* of the bound electron rather than its *momentum* as the factor important in the broadening of the shifted line, this broadening being expressed as proportional to the square root of the energy. Again, though correct (in first approximation), the emphasis is unfortunate since it befogs rather than clarifies the mechanism. The true nature of the mechanism as a Doppler broadening first clearly emphasized by one of us,[10] seems now to be generally conceded by European writers.[11]

Wentzel gave the first correct theoretical formulation of modified scattering by bound electrons according to modern quantum mechanics.[12] He recognizes the problem as a case of Smekal transition like the Raman effect save that while the initial state of the electron is quantized, in the final state the electron belongs to the continuum of unquantized energy states, the most probable of which is, to a first approximation, fixed by conditions identical to the conservation of energy and momentum for a free electron scattering radiation (provided the binding energy is small compared to the recoil energy).

The reality of the broadening of the modified line and the correctness of its interpretation as a Doppler broadening caused by the initial linear momentum distribution of the electrons in the scattering body was first clearly established by the work of the present authors. Clear cut experimental evidence for this second effect in the mechanism of modified scattering came only after most physicists[8] including Ross (who first reported the effect) had reversed their opinions and decided that the observed broadening of the modified line was a result of inhomogeneity of scattering angle, multiple scattering or

[9] G. E. M. Jauncey, Phys. Rev. **24**, 204 (1924); **25**, 314 (1925); **25**, 723 (1925).

[10] The importance of the Doppler effect of the initial velocities of the scattering electrons as an interpretation of modified line breadth first occurred to the senior author while reading a monograph by L. de Broglie (*Ondes et Mouvements* (Gautier-Villars, Feb. 1926), p. 95) though this idea is not therein explicitly stated. The Doppler interpretation of modified line breadth is first stated in a paper by J. W. M. DuMond, Phys. Rev. **33**, 643 (1929).

[11] For example G. Burkhardt, Ann. d. Physik **26**, 583 (1936), who states (author's translation), "The deciding factor for the form of the Compton line is the momentum distribution; the potential energy of the electron is only important insofar as it is implicitly contained in the momentum distribution."

[12] G. Wentzel, Zeits. f. Physik **43**, 1 (1927); **43**, 779 (1927); **58**, 348 (1929).

some other experimental impurity. The experimental requirements of high resolution and very homogeneous scattering angle necessary for the complete quantitative revelation of the behavior of the broadening of the modified line in accord with its Doppler effect interpretation, are antagonistic to the third requirement of sufficient intensity in the scattered beam to permit the study of its spectral distribution. This difficulty was first surmounted by the present authors in two ways for a discussion of which the reader is referred to their original papers.[13–17] An experiment done under Compton's direction by H. M. Sharp in 1925 as a precision measurement of the shift at a large scattering angle revealed a rather broad modified line but it occurred to neither of these workers to point out either the fact or its significance, an omission which we believe is significant as to the state of general uncertainty on these questions at that time.

In six spectrograms published by the present authors[13] the functional dependence of shifted line breadth on scattering angle and primary wave-length was for the first time firmly established as in accord with the behavior to be expected from a Doppler broadening. In view of the fact that the present authors were the first to demonstrate by an experimental study of its behavior the nature and significance as well as the reality of the shifted line breadth and structure, the claim in a paper by one of us as to our experiments "revealing a new physical effect" seems decidedly justified (although A. H. Compton in private correspondence[18] with one of us took exception to this).

The next advance was the experimental discovery by Ross and Kirkpatrick[19] of the defect in the shift and their correct half-classical interpretation of this phenomenon. The dragging effect of the nucleus upon the bound electron as it is being ejected by the imparted momentum of the incident and scattered radiation caused a slight reduction in shift of the order of one percent. They showed that this shift defect should and did vary as the square of the primary wave-length. This beautiful second order shift effect which previous work on the shift had been insufficiently precise to reveal[20] was established by the most ingenious method of the ring target tube utilizing in a very clever way the properties of radiation scattered forward and backward from the same scatterer so as to annul the effect of their rather large inhomogeneity of scattering

[13] J. W. DuMond and H. A. Kirkpatrick, Phys. Rev. **37**, 136 (1931); **38**, 1094 (1931). In the first of these two papers the functional dependence of shifted line breadth on the scattering angle is shown to be in accord with the Doppler interpretation of this breadth. In the second paper the same thing is proved for the functional dependence of shifted line breadth on primary wave-length. Thus we have shown that the broadening of the shifted line behaves in all respects like a Doppler broadening.

[14] J. W. DuMond, Phys. Rev. **33**, 643 (1929). This paper which actually preceded those mentioned in footnote 13 should logically follow them since its argument depends on the confirmations they furnished. It shows that the breadth and general form of the shifted line when beryllium is used as the scattering body is consistent only with the electron velocities required by the Fermi statistics as distinguished from Maxwell-Boltzmann statistics applied to two of the four Be electrons (the conduction electrons) regarded as a degenerate gas. This paper contains therefore the first direct experimental evidence for the applicability of the ideas of Fermi, Dirac, and Sommerfeld which have so successfully explained many of the difficulties in the theory of metallic thermal and electric conduction, as well as the first correct experimental estimate in the case of Be of the number of electrons (2) taking part in metallic conduction. Almost simultaneously Chandrasekhar published substantially the same theoretical result but without experimental confirmation.

[15] DuMond, Kirkpatrick and Alden, Phys. Rev. **40**, 165 (1932). This paper was an effort to explain the narrow sharply peaked modified line structures reported by Gingrich (see footnote 8). We thought it barely possible that the linear momenta of a large class of electrons in crystalline Ceylon graphite might not be isotropically directed in space and that a proper orientation of the crystals used as scatterers might yield a narrow shifted line. No such effect appeared and all other evidence up to the present indicates Gingrich's work as erroneous.

[16] DuMond and Hoyt, Phys. Rev. **37**, 1443 (1931). In this paper our results on the structure of the shifted line obtained with the two crystal spectrometer were found to agree with our previous results using the multicrystal spectrograph, a further refutation of Gingrich's work which has since been confirmed by others at Columbia and at Stanford.

[17] J. W. DuMond, Rev. Mod. Phys. **5**, 1 (1933). This summarizes all the preceding work of its author and his co-workers and gives some new results on the momentum distribution of electrons in carbon.

[18] Compton's objections were based chiefly on the early evidence presented in his paper, Phys. Rev. **22**, 412 (1923). That this evidence was too inconclusive to prevent serious errors both of omission and commission (such as those of Sharp and Gingrich) the literature, as we have already indicated, amply proves.

[19] Ross and Kirkpatrick, Phys. Rev. **45**, 223 (1934); **46**, 668 (1934).

[20] The paper of Gingrich (footnote 8) described by Compton as "perhaps the best experiment of this character" (*X-Rays in Theory and Experiment*, p. 210) *claimed* sufficient precision to have revealed the shift defect. In a footnote on the same page of Compton's chapter the reader might be misled into supposing that he implies that others including the present authors agreed in this very questionable verification of his early shift formula but we know of no other work, certainly not our own, where any such unjustified claims of precision in the measurement of shift were entertained or made.

angle as far as precise determination of shift was concerned. On the theoretical side F. Bloch[21] has carried the quantum-mechanical calculations of scattering by bound electrons in hydrogen-like orbits to a sufficient degree of approximation to discuss the defect in the shift observed by Ross and Kirkpatrick.

In all of the previous work the experimental verifications of theory have suffered from at least one defect and, save in the case of Kappeler,[22] indeed from two defects, namely, the substances used for scattering the radiation have been either *solids* so that the statistics of the electron momenta become difficult to compute with absolute certainty on account of the proximity of neighboring atoms or they have been gases such as neon in Kappeler's case whose momentum distribution requires some approximate method such as the Hartree method of self-consistent fields for its computation. Furthermore the investigation of the spectrum of modified scattering from gaseous scatterers has up to the present always been made by the indirect method of filters mentioned above as originally suggested by Ross.[5] For the application of this method the behavior of the breadth and structure of the shifted line as the scattering angle changes *must be assumed to be known* as well as the behavior of the shift and, while these *are* known in first approximation as the result of the work[13] of the authors of the present paper, uncertainties come in when one considers the varying degrees to which different electron shells will contribute to the modified line at different scattering angles so as possibly to produce rather complicated second order changes in the shape of the line with the variation of the scattering angle required by the experimental method itself.

One final verification with a helium scatterer still highly desirable

We have felt therefore that it would be highly desirable at least once to obtain a direct spectrum of radiation scattered from a monatomic gas of sufficiently simple electronic structure to permit the theoretical prediction with rigor of both the shape and absolute breadth of the modified line as well as its shift including the Ross and Kirkpatrick shift defect. Helium satisfies all the requirements.

Up to the present as Kirkpatrick, Ross and Ritland have emphasized in their recent article[23] while the *shapes* of modified lines have all been in more or less good agreement with theoretical predictions and while the variation of breadth with scattering angle, primary wave-length and atomic number of scatterer has been shown satisfactorily to follow our expectations, the *absolute breadth* has for solid scattering bodies been *invariably greater* than one computes for the free atom. This we have more or less lamely explained as a consequence of the higher momenta to be expected in a solid body than in a free atom as a result of the higher number density of electrons (per unit volume) in the solid. For according to the Pauli principle in any assemblage of electrons the presence of two of them (with opposite spins) in an element of space $dV=dxdydz$ and an element of momentum $dP=dp_xdp_ydp_z$ having the phase volume $dVdP=h^3$ excludes all other electrons of the assemblage from occupying that phase volume. Evidently if dV is compressed $dP=h^3/dV$ must expand and in a momentum space densely packed with such cells dP, as required by the degeneracy of the great majority of the electron states in a solid or in an atom, it is evident that the fastest electrons must move faster if they are compressed into smaller volume. Or from another point of view if the electron waves are conceived as natural modes of vibration of a box when the box is made smaller their wave-lengths diminish and hence according to the famous de Broglie formula $p=h/\lambda$ their momenta must increase.

The shift defect of Ross and Kirkpatrick, so beautifully verified by them as to its wave-length dependence, also suffers slightly from certain objections on the side of theoretical prediction of the absolute value for the solid scatters they used, as Bloch himself remarked.[21]

[21] F. Bloch, Phys. Rev. **46**, 674 (1934). Certain numerical errors have also been found in this paper. Until Bloch has corrected these a comparison of experimental results with his theory would be premature.

[22] Kappeler, Ann. d. Physik **27**, 129 (1936). This author does not obtain a direct spectrum of the radiation scattered by a gas but uses a refinement of the method of Ross in which by varying the angle of scattering and hence the shift the modified line is made to cross an absorption discontinuity defined by a filter.

[23] Kirkpatrick, Ross and Ritland, Phys. Rev. **50**, 928 (1936).

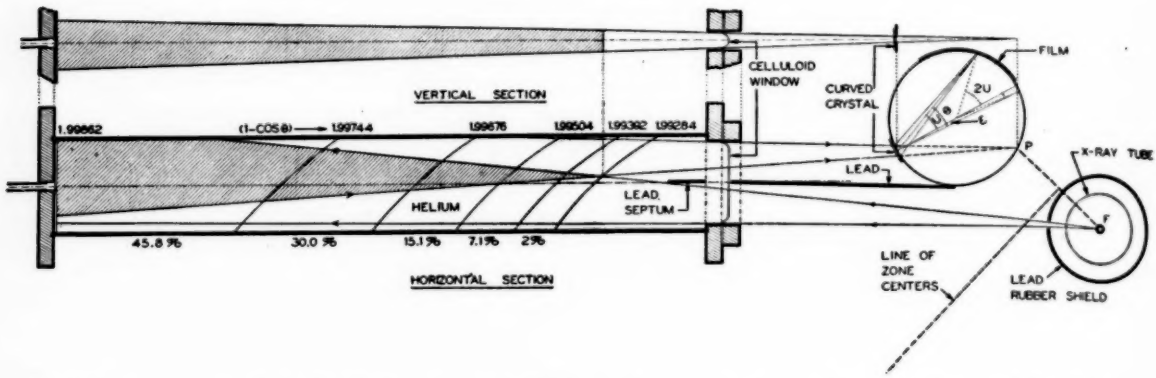

FIG. 1. The geometry of the incident and scattered beams of x-rays is shown. The radiation used by the curved quartz crystal spectrograph for the formation of the shifted band converges to a virtual focus at the point P shown. The shaded region inside the helium pressure chamber is the volume of gas effective in scattering. This appears both in elevation and plan above. Note the lead septum both outside and inside the helium chamber so disposed that no primary rays scattered from the celluloid window can reach the spectrograph. The faintness of the unmodified scattered line (relative to the modified band) on our spectra is convincing internal evidence that the modified scattering was exclusively from the helium. The effective scattering volume is shown divided into regions by the curved loci corresponding to approximately uniform steps of the function $(1-\cos\theta)$ whose exact values are shown.

If then a spectrum of modified x-radiation scattered from helium gas could be shown in respect to the breadth and structure of its modified line to have precisely the correct absolute values and shape and also the shift defect predicted by theory we feel that the subject of the modified scattering of radiation by bound electrons could be fairly considered to be rounded out to a successful termination. The excess breadth of modified lines from *solid* scatterers could then safely be interpreted as reflecting the higher momenta in solids and some hope of a precise measurement of h/mc from the Compton shift (by making appropriate corrections for shift defect) might be entertained. Further work on Compton line structures could then proceed sure-footedly as momentum distribution studies.

In the following pages we present precisely the above mentioned evidence.

II. EXPERIMENTAL PROCEDURE

Geometry of the experiment

Fig. 1 shows the general arrangement of the x-ray tube, the helium pressure chamber with its celluloid window, the geometry of incident and scattered x-ray beams and the curved crystal spectrograph, the latter in very schematic form. The precise geometry was carefully surveyed *in situ* by sighting and measuring accurately through the helium chamber with the rear end removed after the exposure was finished and a careful full size scale drawing was made as an aid to determining the effective scattering angle. Fig. 1 is a reproduction of this.

The scattered x-rays which the curved quartz crystal spectrograph uses to form the center of the modified line converge to a virtual focus at the point P shown. The finite breadth of the modified line and the finite size of the focal spot in the x-ray tube introduce an entirely negligible error in this geometry.

The scattering chamber

The division of the scattering chamber into various properly weighted domains of shift as shown and the determination of the effective scattering angle will be explained in the next section. The shaded areas show the active scattering volume of the gas. In order to reduce the modified scattering from everything but the helium to negligible proportions the rear end of the scattering chamber was provided with an eighth of an inch sheet of lead and the entire interior of the chamber was heavily coated with litharge. For molybdenum K line radiation scattered at 180° lead exhibits little scattering of any kind because the true (fluorescence) absorption so limits the depth of penetration of the x-rays (both incident and scattered) in the lead according to the Z^4 law that an insufficient number of electrons are illuminated to permit

appreciable scattering (the scattering being only proportional to Z). As we shall point out later more fully in such slight scattering as does come from the lead only a very small fraction is of the modified type in which we are here interested.

The celluloid window

Considerable experimentation was found necessary before a safe yet thin celluloid window was chosen to withstand the pressure of about fourteen atmospheres of helium. It was found unnecessary to design the window frame so as to impose an initial curvature on the celluloid as this material deforms under pressure so as to assume a shape favorable to strength. It is treacherous, however, in that it exhibits very little tendency to "cold harden" with deformation and below a critical thickness we found our windows might burst after several weeks of successful resistance. A valuable precaution which we advise others to adopt when testing windows behind which large volumes of gas are trapped is to place an otherwise tight metal partition perforated with a tiny hole close behind and inside the window to baffle the explosive energy stored in the compressed gas. Needless to say we used air for the preliminary tests. No eventual difficulty was encountered in making both the window and the other joints tight with properly designed rubber gaskets. On account of the failure of a first exposure and delays in the replacement of x-ray tubes the helium remained in the chamber for more than a year during which time there was no detectable change in the pressure as measured on a Bourdon gauge connected to the chamber through a Lunkenheimer steel needle valve. The pipe threads for connecting this valve were tinned with half and half solder and simply screwed together firmly without heat.

The x-ray tube

The water cooled molybdenum target x-ray tube was enclosed in a cylinder of Bakelite covered with three $\frac{1}{8}$-inch layers of leaded rubber. This electrically insulating flexible material used for protective aprons etc. in the medical applications of x-rays is equivalent in opacity to x-rays to about half its physical thickness of metallic lead and we have found it frequently of great utility for shielding. A properly dimensioned hole cut in this shield permitted an x-ray beam of the correct dimensions and direction to enter the window of the scattering chamber. The tube was run for 2059 hours at about 60 kv and 20 ma night and day with very few interruptions. Compressed air was blown through the shielding cylinder for cooling.

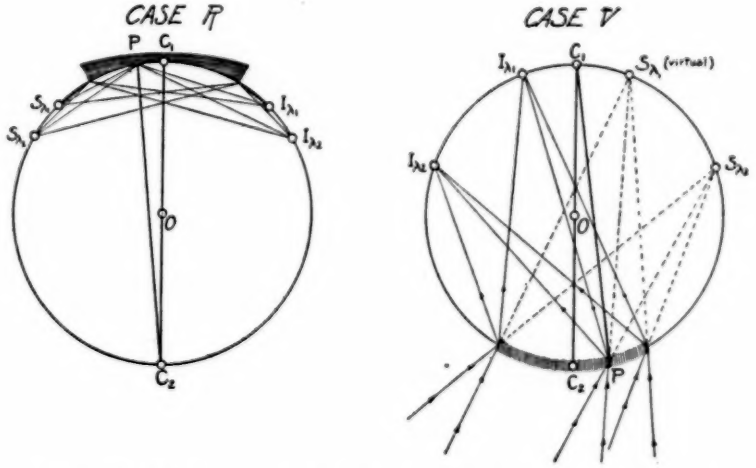

FIG. 2. The ideal geometry of the curved crystal focusing x-ray spectrograph first proposed by DuMond and Kirkpatrick is illustrated. In the reflection case, R, shown here both the source and image are real points. In the transmission case, V, the images of spectral lines are real but the source has a virtual image point. The incoming radiation of any given wave-length used by the spectrometer converges before being reflected by the crystal planes as though it were directed at this virtual source point. Reproduced from Rev. Sci. Inst. **1**, 90 (1930).

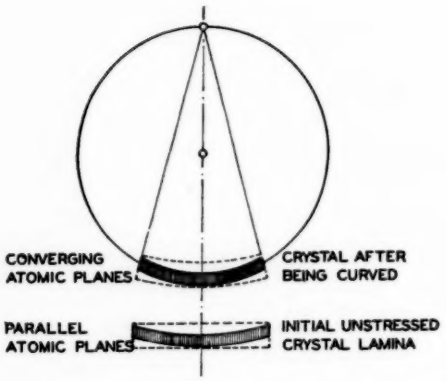

FIG. 3. It is shown how a crystal lamina such as the one shown in Fig. 2, case *V*, might be realized by cutting the unstressed crystal lamina to a curved shape and then bending this to make the crystal planes converge.

The curved quartz crystal spectrograph

The transmission type curved quartz crystal spectrograph which makes this experiment with a gaseous scatterer possible was recently described briefly by one of us in collaboration with Bernard B. Watson.[24] The design follows closely that of the transmission type curved crystal spectrograph of Y. Cauchois.[25]

To the best of our knowledge the authors of the present paper were the first to suggest the basic ideas which have led to the development of both the reflection and transmission types of curved crystal focusing spectrograph. Fig. 2 taken from our first article[26] on this subject shows how a source of x-rays either reflected from (case *R*) or transmitted through (case *V*) a crystal curved to the appropriate radius can be made to focus its different wave-lengths at different points on a cylindrical focal surface. As we showed at that time the crystal must be curved or sprung so that in the reflecting type the normals to the reflecting crystal planes converge in a point (the center of curvature) located on the periphery of the focal cylinder. In the transmission type the reflecting planes themselves (produced) must converge so as to intersect in an element of the focal cylinder. A second condition necessary for theoretically correct focusing which we pointed out[26] was that the crystal lamina must coincide with the focal cylinder. We suggested that this might be accomplished if the crystal lamina were properly cut to a curve as shown in our Fig. 3. The cut surface, even before bending or curving the crystal, would then itself have to be a curved one. The difficulties of cutting and imposing the proper curvature led us to modify the design and the result was the multicrystal spectrograph which served our purposes very effectively in the study of scattered x-radiation.

Johann[27] in the case of the reflection type and Cauchois for the transmission type of curved crystal focusing spectrograph perceived that our *second condition* for focusing mentioned in the last paragraph is not as exacting as the first condition. Thus Cauchois was led to start with a thin flat lamina (of mica) to which she gave a curvature of radius just twice that of the focal cylinder of the spectrograph by imprisoning it between two accurately shaped cylindrical metal surfaces provided with a window through which the x-rays might pass. In this way the first focusing condition is satisfied. This curved crystalline lamina was set so as to stand with its center accurately tangent to the focal cylinder. The second condition is then only truly fulfilled at the point of tangency. However, the aberration of focusing produced by reflection from those regions of the lamina that fail to coincide exactly with the focal cylinder can be kept sufficiently small to be negligible without restricting the aperture of the focusing crystal unduly and in this way Cauchois has achieved a highly luminous instrument which is at the same time not difficult to construct and adjust.

The transmission type curved crystal spectrograph used in the present research differing but little from Cauchois design is provided with reversible crystal mounting so that the slight but unavoidable constant angle between the reflecting planes and the radius of curvature of the lamina caused by inaccuracy in cutting the quartz could be accurately determined. The instrument also has a divided circle of high quality and with its help B. B. Watson made an accurate determination of the grating constant for the reflecting planes of the quartz lamina (basal planes). We have found quartz superior to

[24] DuMond and Watson, Phys. Rev. **46**, 316 (1934).
[25] Y. Cauchois, J. de phys. (July) (1932); Thesis (Masson & Cie, 1933); J. de phys. (Feb.) (1933); H. Hulubei, C. R., Dec. 19 (1932); H. Hulubei, Thesis (Masson & Cie, 1933).
[26] DuMond and Kirkpatrick, R. S. I. **1**, 88 (1930).
[27] H. Johann, Zeits. f. Physik **69**, 185 (1931).

any mica we have been able to obtain. We are also deeply indebted to him for the careful study of the aberrations of this instrument and the excellent calibration he has made of its constants.[28] For the present purpose this instrument is far superior to the multicrystal spectrograph previously used by the authors. It attains a luminosity superior to the latter instrument with an angle of aperture of the incoming beam of only about 5° 43′. This not only permits the use of a reasonably small chamber and window for the high pressure gaseous scatterer but also greatly facilitates in the present experiment the geometrical design which reduces the inhomogeneity of the Compton shift to a negligible value. On the other hand the transmission type curved crystal spectrograph in its present state of development still has certain disadvantages which would have disqualified it for some of the work we previously did with the multicrystal spectrograph. Our work,[13] for example, with scattered tungsten K radiation to exhibit the functional dependence of shifted line breadth on primary wave-length we have been quite unable to reproduce with our curved quartz crystal transmission spectrograph since the excellent luminosity of the instrument for wave-lengths of order 0.7A seems to disappear completely for the shorter wave-lengths of 0.2A. We are not yet in a position to say whether a transmission type focusing curved crystal spectrograph could be designed with a thicker crystal lamina so as to obviate this difficulty. A second inconvenience in the transmission type curved crystal spectrograph which was absent in our multicrystal instrument springs from the fact that there appear on the negative spectral lines reflected not only from the crystal planes which have been selected for use but also from a multitude of other planes having quite different Miller indices. Some of these undesired reflections are harmless since they focus sharply and stand vertically on the spectrum but others from reflecting planes not parallel to the axis of the cylinder of curvature form bands and triangular areas of blackening on the film whose presence in an interesting region of spectrum can be very objectionable. Fortunately for our present purpose none of these bands appear in the immediate region of the shifted Mo$K\alpha$ doublet although there is one not far removed from the short wave-length side of the shifted β band which would disqualify it for accurate measurements if its faintness did not prohibit its use. (See hump B on microphotometer trace Fig. 5.)

[28] Watson's work in developing this instrument, calibrating it and studying its aberrations formed the subject of a doctorate thesis at this Institute in 1935. Had time permitted he would also have continued his collaboration on the present study of scattering from helium. We are further indebted to him for the construction and testing of the pressure chamber and its window.

Shielding

The spectrograph was completely enclosed in a cylindrical box of lead $\frac{1}{8}''$ thick. This was reinforced on the side toward the primary radiation with five more sheets of the same thickness. Beside the thick lead septum shown in the drawing separating the primary from the scattered beam the latter was conducted from the scattering chamber to the lead spectrograph housing in a completely enclosed lead conduit to prevent entry of stray radiation scattered by the air. A lead septum was so placed inside the spectrograph as to separate the reflected and direct beams in the region where they do not overlap to prevent radiation scattered from the latter from fogging the photographic emulsion. For simplicity in Fig. 1 most of these shielding features are omitted.

Test films

Two extra strips of x-ray film somewhat narrower than the definitive film were inserted behind the latter in a small cavity provided in the back of the holder. As the 2059 hour exposure progressed these were withdrawn and developed to give some idea of the progress of the exposure.

Reference comparison spectrum

We expected the unmodified lines in our spectrum to be extremely faint (they are due almost entirely to scattering from the lead lining of the helium chamber) and we therefore took the precaution to make reference lines on the edges of our definitive film before removing it from the spectrograph. To avoid all danger of spoiling the valuable results of the 2059 hour exposure we placed a lead shield in front of the film so shaped and positioned that the reference lines could only be formed on its top and bottom edges while the

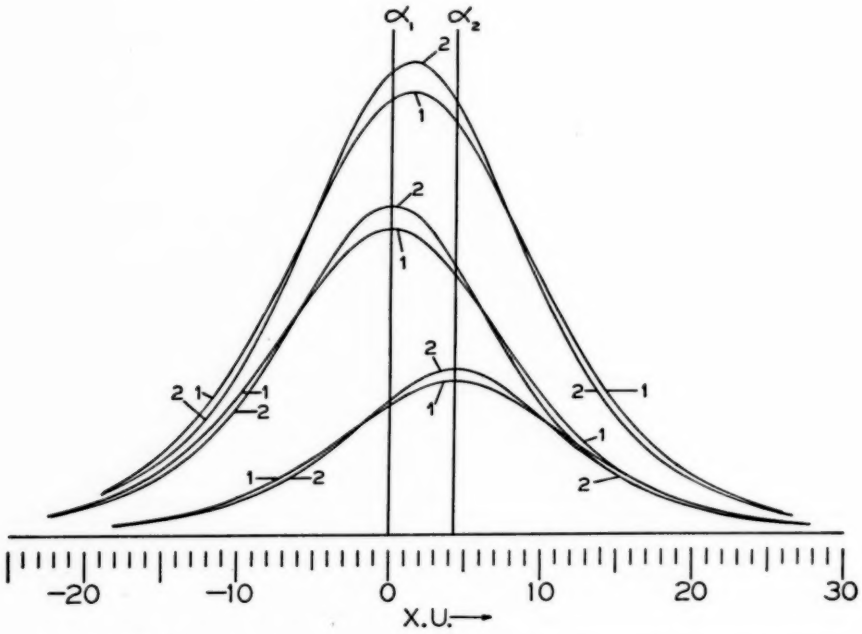

FIG. 4. Hicks' curves and their composition to form the computed composite shifted $\alpha_1\alpha_2$ "line" are shown. The ordinate scales of curves 1 and 2 are in all cases normalized so as to give the curves equal areas.

central region was completely cut off. The reference lines were made by fastening a sheet of metallic molybdenum of about the same size as the exit part of the celluloid window in the scattering chamber directly over that window. This sheet was then excited to fluoresce its characteristic K spectrum by radiation from the x-ray tube, a part of the lead septum being removed to facilitate this. An exposure of only 140 hours sufficed to give a strong K spectrum on the edges of the film. We call attention to the fact that this method of forming the reference spectrum utilizes the whole aperture of the curved crystal in as nearly as possible the same way as it was used to form the modified scattered spectrum and hence first-order corrections for shift of the lines caused by aberrations inherent in the geometry of the curved crystal instrument are unnecessary. Unfortunately the spectrum lines in our spectrograph are not quite vertical because of a very slight error in orientation of the quartz lamina in its cylindrical holder so that the reflecting planes are slightly tilted with respect to the axis of the focal cylinder. For this reason there appear on our microphotometer traces just barely perceptible minute differences in the position of the alpha-doublet reference peaks on the top edge of the film when compared with the position of those on the bottom edge. In measuring the shift therefore the *average* between top and bottom reference line positions was taken as representing the true position in the middle of the film where the modified line was microphotometered. These average positions so determined agree perfectly with the faint unmodified scattered lines.

III. RESULTS AND THEIR INTERPRETATION

Computation of predicted line profile

We are much indebted to Mr. Bruce Hicks[29] who has computed the distribution of linear momentum to be expected in helium by two methods: (1) On the approximate assumption that with appropriate choice of a screening constant the helium atom for this purpose can be simulated by a hydrogen-like atom and (2) by the more accurate method similar to that used by Hylleraas taking account of the interaction of the two electrons. From these results Hicks by the methods described in our previous papers[13, 14, 17] has computed the Doppler broadened line profiles to be expected from helium.

[29] See his article in this number of the *Physical Review*.

Because we have used the alpha-doublet of the molybdenum K spectrum as the primary radiation the modified line profiles of Hicks must be treated as shown in Fig. 4 to obtain composite profiles for comparison with the observed line shape obtained on the microphotometer. In Fig. 4 curve 1 is Hicks' profile computed by the first method mentioned above and curve 2 is the profile computed by the second method. Curve 2 is normalized to give the same area as curve 1. In this figure we have added two such curves to represent to correct wave-length scale the respective contributions of shifted α_1 and shifted α_2 to form the complete shifted alpha-doublet.[30]

In Fig. 5 we show four out of the total of twelve microphotometer records we have made of our film. Fifty uniformly spaced ordinates the first one coinciding with the position of the α_1 line were measured on each of the twelve microphotometer traces and the averages of these twelve sets was replotted for comparison with the theoretically predicted line shapes. In Fig. 6 this average curve is shown with dots to avoid confusion with the continuous curves representing the theoretically predicted shapes.

The backgrounds of the microphotometer traces are not quite level. Part of this on some of the traces is due to the gradual decline in the intensity of the light source as its storage battery supply voltage declines with discharge. The remainder probably represents the real shape of the scattered continuous spectrum. We have removed this sloping background in the averaged (dotted) values of Fig. 6 by subtracting from the ordinates an appropriate linear function of wave-length.

Comparison of predicted and observed line profiles

The two curves 1 and 2 (corresponding to Hicks' two methods of computation) we plot upon transparent paper to the same wave-length scale as our microphotometer traces. The vertical intensity scale of these curves is chosen so as to normalize their integrated areas to the same value as the area under the averaged microphotometer profile. We then superpose these curves so prepared on the averaged microphotometer profile and shift them bodily to left or right until a wave-length position is obtained which gives the best fit. Fig. 6 shows how surprisingly good this fit turns out to be. It is evident that we have here for the case of a gaseous scatterer no such discrepancies between observed and predicted modified line breadths as have been observed both by Ross and Kirkpatrick and by the present authors for the case of solid scatterers. In fact the fit is evidently as near perfection as the accidental fluctuations of the grain of the photographic emulsion permit us to verify. These results which accord so well with our theory constitute a decisive refutation of the sharply peaked modified line structures of N. Gingrich.[31]

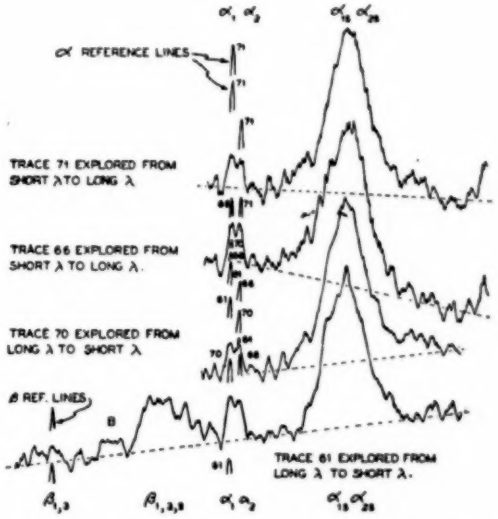
α REFERENCE LINES
TRACE 71 EXPLORED FROM SHORT λ TO LONG λ
TRACE 66 EXPLORED FROM SHORT λ TO LONG λ.
TRACE 70 EXPLORED FROM LONG λ TO SHORT λ
β REF. LINES
TRACE 61 EXPLORED FROM LONG λ TO SHORT λ.

FIG. 5. Four out of a total of twelve records made on our recording microphotometer of the blackening of our scattered spectrum. The small isolated peaks $\alpha_1\alpha_2$ are made by shifting the film vertically (the carriage on our microphotometer being designed to facilitate doing this without horizontal shift) so that the light beam explores across the reference lines on the edges of our film.

[30] It is evident that curves (representing shifted α_1 and α_2) as broad and smooth as those here required by our theory and with only about 4 X.U. separation could not possibly show the sharply resolved peaks reported by Gingrich.

[31] Compton's suggestion (on page 248) that our shifted line, so much broader than that reported by Gingrich, might have been spuriously broadened by inhomogeneity of scattering angle in our experiment is quite untenable. The results of Kirkpatrick, Ross and Ritland (Phys. Rev. **50**, 932 (1936)) support our previous line profiles from solid scatterers. It was the peculiar merit of our experiments by reason of the geometry we employed with the multicrystal spectrograph to have for the first time far less inhomogeneity of scattering angle at all angles investigated than had ever been present in any other previous work including that of Gingrich and it was this fact that made our evidence on the structure of the line for the first time so clear cut and convincing (See references in footnotes 13, 14, 17). We have made every effort to give the

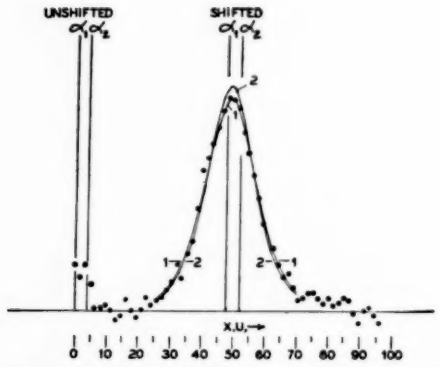

FIG. 6. Comparison of Hicks' computed profiles with our microphotometer traces of the modified line scattered by helium gas. The continuous curves are the theoretical curves of Hicks corrected for the composite nature of the primary radiation as shown in Fig. 4 and replotted to the abscissa scale required by the computed dispersion of the curved crystal spectrograph for the center of the shifted line. The ordinate scale used in these curves is chosen so as to normalize the areas under them to the same value as the area (obtained with a planimeter) under the averaged experimental curve. (In this process some uncertainty enters in the choice of the experimental background.) The theoretical curves have been bodily shifted to left or right until a best fit on the experimental (dotted) curve was obtained. The dots are the average of twelve microphotometer traces. The excellent fit obtained here for a gaseous scatterer is in striking contrast to the experimental breadths from solid scatterers which exceed the expectations for a free scattering atom in the case of carbon by 60 percent.

To the best of our knowledge this is the first *direct spectrum* of modified scattered x-rays ever made with a gaseous scatterer.

The abscissa scale of our microphotometer has been carefully checked with a transparent scale of high quality which we calibrated on a comparator. The instrument magnifies the wave-length scale on the original photographic spectrum by a factor 10.0024 ± 0.001 which is uniform to the indicated precision over the entire two centimeters travel of the carriage carrying the spectrum to be analyzed. By an over-all calibration with a rotating shutter described in a previous paper[32] we have shown that over the very restricted range of contrast involved in our photographs of modified lines the galvanometer deflections (ordinates) of our recording microphotometer are so closely linear with x-ray intensity that no correction of the ordinate scale is required.

Method used to determine dispersion of curved crystal spectrograph

A word or two is in order to explain how we determine the dispersion of our curved crystal spectrograph and thus establish the correct wave-length scale against which to plot Hicks' computed profiles for comparison with the microphotometer curves. The geometry of this curved crystal instrument is such that the dispersion varies from point to point along the wave-length scale (not very rapidly however). In Fig. 7 the spectrograph geometry is shown. O is the point where the reflecting planes of the curved crystal would converge if produced. A is the point of tangency between crystal and focal cylinder. AO is not necessarily exactly a diameter of the cylinder and in our instrument it stands at about three degrees to a diameter through A. The incoming and selectively reflected x-ray beams of wave-length λ will make equal angles θ with AO on either side satisfying the Bragg

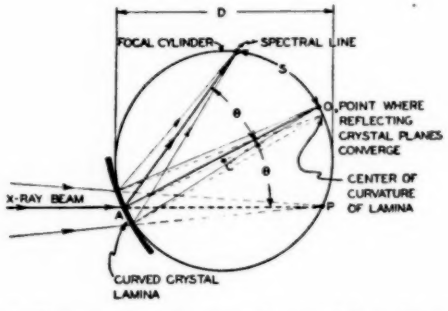

FIG. 7. Geometry of the curved crystal focusing spectrograph for the derivation of its dispersion. A is the point of tangency between crystal lamina and focal cylinder. O is the point where the reflecting planes of the curved crystal would converge if produced. AO is not necessarily a diameter of the focal cylinder.

results of Gingrich a fair explanation. One of us undertook a rather elaborate theoretical analysis of the effect of multiple scattering on our shifted spectrum (J. W. DuMond, Phys. Rev. **36**, 1685 (1930)) and we also made an elaborate experimental check as to the possible spurious broadening effect in our multicrystal spectrograph experiments from this cause. (See note added to proof in DuMond and Kirkpatrick, Phys. Rev. **37**, 136 (1931).) In footnote 15 we have already mentioned our effort to reveal some mechanism for obtaining shifted lines as narrow as Gingrich reported by the possible effect of preferential directions of electron momenta in Ceylon graphite. No such narrow lines could be found. Our present results with the helium scatterer showing a line structure in such good accord with our theory of its Doppler broadening could not possibly be explained if the modified line were indeed as sharp as Gingrich reported it to be. Our extremely small range of $(1-\cos\theta)$ is utterly inadequate to transform a line as sharp as Gingrich reported into the profile we obtain. We are forced to the conclusion that Gingrich's result is incorrect.

[32] J. W. DuMond, Rev. Mod. Phys. **5**, 27 (1933). See section 15.

equation between λ and θ. The linear distance on the focal cylinder from O to the spectral line of wave-length λ is S. If D is the diameter of the focal cylinder then evidently

$$n\lambda = 2d \sin (S/D) \tag{1}$$

and the dispersion $d\lambda/dS$ is given by

$$d\lambda/dS = (2d/nD) \cos S/D. \tag{2}$$

The point O is not of course marked on the photographic film, so that S cannot be directly measured thereon. We can write one convenient expression for the dispersion as a function of the wave-length λ as follows:

$$d\lambda/dS = \frac{2d}{nD}\left[1-\left(\frac{n\lambda}{2d}\right)^2\right]^{\frac{1}{2}}, \tag{3}$$

where the radical which accounts for the variation in the dispersion is simply cos θ. This formula requires that we know $2d/nD$ with the same order of precision as that desired for $d\lambda/dS$. It contains no corrections for the several aberrations of the instrument. If the spectrum has two reference lines of accurately known wave-lengths λ_1 and λ_2 appearing near the point where we wish to know $d\lambda/dS$ at positions S_1 and S_2 it is obviously better to compute the dispersion *using these lines* for then the slight aberrations of the instrument and any possible slight warping of the photographic film are to a large extent automatically corrected. The differences S_1-S_2 and $\lambda_1-\lambda_2$ will be of importance in the formula and hence the reference lines chosen should be far enough apart to give the required relative accuracy in these differences but save for this consideration they should both be as near as possible to the point where $d\lambda/dS$ is to be found in order to make the most of the advantages we have just stated. The quantity $2d/nD$ of formula (3) is computed from the separation S_1-S_2 of the reference lines on the film by means of the formula

$$\frac{2d}{nD} = \frac{\lambda_1-\lambda_2}{2D \sin \frac{1}{2}((S_1-S_2)/D) \cos \frac{1}{2}(\theta_1+\theta_2)}, \tag{4}$$

which can be improved for purposes of calculation by expanding $2D \sin \frac{1}{2}(S_1-S_2/D)$ so that the D only appears in a small correction term. This gives the approximate formula

$$\frac{2d}{nD} = \frac{\lambda_1-\lambda_2}{\left\{(S_1-S_2)-\frac{D}{24}\left(\frac{S_1-S_2}{D}\right)^3\right\} \cos \frac{1}{2}(\theta_1+\theta_2)}. \tag{5}$$

The relative error introduced by neglecting higher order terms in the expansion is $(1/1920) \times[(S_1-S_2)/D]^4$ so that even if the angle $(S_1-S_2)/D$ is as large as one radian the relative error involved is only about 0.05 percent while if as in the present case $(S_1-S_2)/D$ is less than 0.1 the relative error is less than half a part in ten million. In fact the correction term itself in equation (5) is usually so small as to be nearly negligible. Suppose now we wish to compute the wave-length interval on the film $\lambda_a-\lambda_b$ between two points (one of which λ_b, for example, may be a line of known wave-length say Mo $K\alpha_1$ and the other the shifted position of Mo $K\alpha_1$ of unknown wave-length as in our present experimental determination of the exact shift). We determine by means of Eqs. (5) and (2) a value $(d\lambda/dS)_m$ applicable to the mid-point of the interval on the film for which the wave-length interval $\lambda_a-\lambda_b$ is desired. This admittedly requires a fore knowledge (to a lesser degree of accuracy however) of the value of λ_a or its corresponding θ_a which can be computed from λ_a. Then to obtain the wave-length interval we have only to use this median value of $d\lambda/dS$ in the following approximate formula:

$$\lambda_a-\lambda_b = (d\lambda/dS)_m\left[S_a-S_b-\frac{1}{24}\frac{(S_a-S_b)^3}{D^2}\right]. \tag{6}$$

This formula again has limits of relative error depending on $(S_a-S_b)/D$ in the same way as formula (5).

In formulae (2), (3), (4), and (5) there appear factors of the form cos θ. These are computed from the value of λ corresponding to θ by means of the formula $\sin \theta = n\lambda/2d$ and for this purpose a value of the grating constant d of the reflecting planes used in the curved crystal is required. In the present work we have used the sixth-order spectrum for which the angle θ corresponding to the wave-length of the Mo $K\alpha_1$ line is 23° 11′. All of the cosine terms necessary for the computations are in excess of 0.9 and hence the consequent relative error in determining cos θ is only

about half the relative error with which d or λ are afflicted.

Determination of d for the curved crystal

In his original calibration of our instrument B. B. Watson made a very careful experimental determination of this value of d for the curved quartz crystal we have used which turned out to be in excellent accord with the best estimate of Wyckoff[33] from a comparison of the results of a number of observers. Watson's determination of d for the basal planes of the quartz crystal was made using three different orders of reflection, the 3rd, 6th and 9th. Spectra were taken on both sides of the point O, Fig. 6, the film being rotated through a certain angle precisely measured on the precision divided circle of the instrument between the two exposures so that the distance between lines to be measured on the film would be small. Careful corrections were made for all the aberrations of the instrument. Watson's final result was

$$d = 5.393 \pm 0.002\text{A}$$

in complete accord with Wyckoff's estimate and also with a recent determination of Harrington[34] who found

$$d = 5.393 \pm 0.006\text{A}.$$

The structure of quartz is such that for the basal planes which we use for our reflections the 3rd, 6th and 9th orders are, respectively, the 1st, 2nd and 3rd orders with which any intensity is associated. Watson's results after making the slight corrections for aberrations showed excellent agreement between these three orders.

Precise determination of shift

For the shift determinations we deemed it more accurate to measure the microphotometer records directly rather than the average curve. Theoretical composite shifted alpha lines like those in Figs. 4 and 6 but to which an appropriately chosen linear background slope had been added to fit the individual case of each microphotometer record were plotted to the same wave-length scale as the microphotometer records. It was then an easy matter to measure the displacement in centimeters between the unshifted or reference lines on the plate and the centers of the corresponding theoretical composite shifted lines after these had been located for a best fit. This was done for all the microphotometer plates, twelve in number, which made it possible to compute an average shift and its probable error from the consistency of the determinations. This shift in centimeters is (with sufficient precision) just ten times the shift on the original negative and from this by the application of formula (6) we can compute the wave-length shift for which we obtain 47.54 X.U. $\pm$0.05 X.U. (Probable error from internal consistency). (This is expressed on the Siegbahn wave-length scale, calcite $d_{18^\circ} = 3029.45$ X.U.)

In obtaining this value no correction has been made for the fact that although we have plotted our computed shifted line profiles to a uniform scale of dispersion the dispersion $(d\lambda/ds)$ on the actual spectrum is in fact slightly greater on the short wave-length side of the line than on the long wave-length side and the center of the line is very slightly shifted by this cause. Calculation shows this correction negligible. The breadth of line assumed in computing this correction is the breadth at half maximum.

Converting the above shift to the ruled grating scale of wave-lengths, which gives presumably the correct absolute value in cm, we obtain 47.63×10^{-10} cm $\pm 0.05 \times 10^{-10}$ cm.

It is evident that our method of fitting the computed and observed profiles lays far more emphasis on the steepest portions of the profile at the sides (points of inflection) than it does on the maximum point of the line. The latter is far too ill defined to be a dependable reference point because of the unavoidable accidental fluctuations of film grain. Roughly speaking the fit applies to the region of the line in the vicinity of half maximum height. The results of Felix Bloch before mentioned apply however to the shift of the maximum point itself and are therefore not quite comparable with our results because the refined calculations show that the line possesses a slight asymmetry.

Computation of the predicted shift

In order to see whether there exists a defect in the shift in our present spectra in accord with the results reported by Ross and Kirkpatrick we

[33] R. W. G. Wyckoff, *The Structure of Crystals*, 2nd edition.

[34] E. A. Harrington, Am. J. Sci. **13**, 467 (1927).

must compute the shift to be expected upon the simple Compton theory. This involves the determination of an effective scattering angle taking into account the geometry of the scattering chamber. Referring to Fig. 1 it will be seen how we have divided the volume of the helium gas effective in scattering the radiation (shaded region) into five zones corresponding to approximately equal steps of the function $(1-\cos\theta)$ to which the shift is proportional. The curved boundaries of these zones are circular arcs which if produced would pass through the points F and P (source of incident radiation and virtual image of the shifted spectral line) and which therefore have their centers situated on the dotted line marked "line of zone centers." These arcs are thus the loci of points in the scattering chamber corresponding to constant values of $(1-\cos\theta)$ and the value for each locus is shown in the drawing. It can be seen that the variation in $(1-\cos\theta)$ is all in the third decimal place the extreme difference between front and back being only 0.29 percent while the contribution of each zone differs in shift from that of its neighbor by only 0.06 percent. Each zone then may be thought of as contributing a modified line profile having an intensity and shift peculiar to it. The intensity from a zone will be directly proportional jointly to the squares of its distances from A and P. The determination of relative intensities for the scattering zones involved the evaluation then of integrals over their volumes. For simplicity here the curved loci were replaced by plane surfaces. The variation in height of the scattering volume was taken into account in these integrations. The mean of the two boundary values of $(1-\cos\theta)$ for each zone was taken as the value for the entire zone.

With the intensity and shift of each zone thus determined we could simply have plotted five shifted line profiles with the correct relative intensities and with the relative slight displacements on the wave-length scale required by their respective values of $(1-\cos\theta)$ and then we could have added these curves to obtain a composite curve. The displacements of the centers of these five curves from each other would be very small however in comparison to the half maximum widths of the curves and for this reason an easily proved theorem can be shown to hold very accurately which makes unnecessary the above mentioned laborious method. The said laborious method would indeed introduce more inaccuracy than it avoided.

On the line profile contributed by the ith zone in the scattering chamber consider a narrow horizontal strip at some convenient fractional height (say half maximum height). Let the wave-length value at the mid-point of this strip be λ_i and let the intensity associated with the ith zone be A_i. On the total line profile obtained by summing all such component profiles consider a narrow horizontal strip at the same fractional height (say half-maximum) as was taken for all the component profiles and let the wave-length value at the mid-point of this strip be λ. Then the theorem mentioned above asserts that if the differences between the values λ_i are small in comparison to the half-maximum breadth of the curves we shall have

$$\lambda=\sum_i A_i\lambda_i/\sum_i A_i.$$

The conditions for the applicability of this theorem are extremely well satisfied in the present case. We can thus compute an effective weighted mean value of $(1-\cos\theta)$ for the entire scattering volume by simply weighting the values for the individual zones with the intensity factor computed for that zone and dividing the sum by the sum of the intensity factors. The computed intensities of the zones are shown in Fig. 1 as percents. The resultant weighted mean we obtain is $(1-\cos\theta)=1.9970$. Taking as the best value of h/mc 24.15 X.U. we obtain for the predicted shift on the simple Compton theory 48.23 X.U.

Comparing this with our observed shift we see that there is indeed a shift defect of 0.60 X.U. or about 1.25 percent of the shift itself. This shift defect is not exactly comparable with that predicted by Bloch[21] for the *maximum* of the line profile.

Relativistic correction to the shift

As one of us has shown in a paper[35] published

[35] J. W. M. DuMond, Phys. Rev. **33**, 657, 658 (1929). See Eq. (22), page 657, which gives the range of the shifted line for an assemblage of scattering electrons all having the same momentum $m\beta c$ but with isotropically distributed directions in space for the *non-relativistic* case. On the next line just below is given the corresponding range for the

early in 1929 as well as more generally in later work, if relativity is taken into account then a slight shift of the modified line toward longer wave-lengths and a slight asymmetry of the line profile will occur. Following the method of DuMond if the modified line profile is broken up into horizontal bands superposed upon each other in descending order of width and each band is considered as the contribution of an assemblage of scattering electrons having one small characteristic range of the *absolute value* of linear momentum $mc\beta$ to $mc\beta+mcd\beta$ but an isotropic distribution over all possible spacial directions of this linear momentum then each such band will, when relativity is taken into account, have its center shifted toward longer wave-lengths by a slight amount $2\beta_1^2\lambda^* \sin \frac{1}{2}\theta$ more than in the non-relativistic case. Since the width of each band is itself proportional to β (equal in fact to $4\beta\lambda^*$) it is evident that at the peak of the line there will be no relativity shift at all and this shift will increase with increasing width as we proceed toward the base of the profile. The total effect will therefore be to confer a slight asymmetry on the line. Since our method of fitting observed and computed line profiles lays principal emphasis on the part of the profile near half-maximum height it suffices to compute the relativistic shift for half-maximum breadth. This turns out to have the very small value 0.0458 X.U. Burkhardt also refers to this slight relativistic correction to the shift.[36] It is far too small in the present case to be observable. With this correction included our experiment shows a shift defect from electron binding of 0.66 X.U. $\pm$0.05 X.U.

Internal evidence that our modified lines are due to scattering from helium only

The extreme faintness of the unmodified scattered line on our spectra relative to the modified line is conclusive evidence that the scattering from other materials than helium in our spectrum constitutes an entirely negligible fraction of the modified scattering. The only elements in the scattering chamber other than helium are the iron of the walls of the chamber, lead in the lining of the chamber, oxygen combined with the lead, carbon and hydrogen principally in the celluloid window. As for the window the geometry of the lead septum makes it impossible by any single scattering process for primary radiation scattered by the window to contribute to the scattered spectrum. (Multiple scattering in the window need not be considered because it would be too faint.) It is a well-known fact that the ratio of unmodified to modified scattered intensity decreases rapidly with decreasing atomic number. In one of our papers[37] we show a spectrogram of scattering from carbon under conditions otherwise substantially similar to those of the present experiment and it is evident that even for this case ($Z=6$) the height of each unmodified α line is about equal to the height of the corresponding analytically resolved component of the modified line. Even if the celluloid window could scatter directly to the spectrograph the hydrogen in it, since it is associated with carbon, need not be considered in the argument because the ratio of unmodified to modified scattered intensities for a celluloid scatterer will be essentially the same as for pure carbon. Every other element in the chamber is thus of equal or higher atomic number than carbon and the lead lining which without any doubt is principally responsible for our unmodified line has so high an atomic number that its modified scattering will be utterly negligible in comparison to its unmodified scattering. Thus the modified scattering from anything in the chamber but the helium must be very much less intense than our very faint unmodified scattered lines and therefore quite negligible compared to the modified line. Helium on the contrary should give very intense modified scattering and practically no unmodified scattering under the conditions of this experiment. The conclusion

relativistic case under 180° scattering angle. This range has the same width as the former but is bodily displaced by a slight amount which fact the author explicitly states in the last paragraph of the article, page 658. In a later article (Rev. Mod. Phys. **5**, 7 (1933)) DuMond gives in Eq. (16) the more general relativistic expression for the range of the modified line again for the same type of electron assemblage but for any scattering angle θ. The center of the shifted band is here shown to be shifted toward longer wave-lengths by an amount $2\beta_1^2\lambda^* \sin \frac{1}{2}\theta$.

[36] Von Gerd Burkhardt, Ann. d. Physik **26**, 581 (1936).

[37] J. W. M. DuMond, Rev. Mod. Phys. **5**, 27 (1933). In Fig. 24 the scattering of Mo$K\alpha$ radiation by carbon at 156 degree scattering angle is shown with the shifted band resolved into the two alpha-components by a method explained in section 16 of that article. Note that the height of these components is about equal to the height of the unshifted lines.

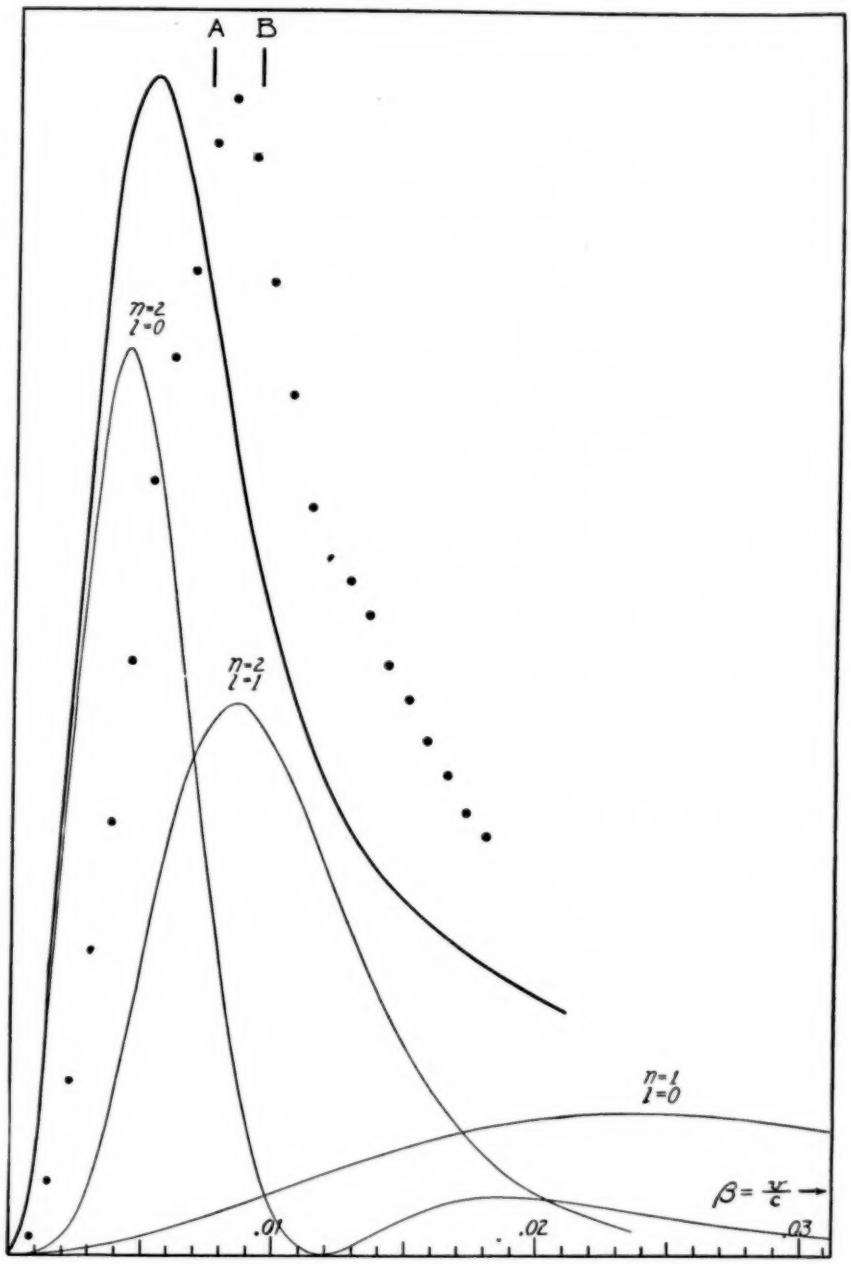

FIG. 8. The marked excess in the experimentally determined most probable momentum in the case of a solid scatterer (carbon) as compared with the theoretical predictions for a *free* carbon atom. The excess in this case is 60 percent of the theoretical value. This is reproduced from *Reviews of Modern Physics* **5**, 33 (1933).

therefore is clearly that our modified line is due to the helium only. These considerations render unnecessary a control experiment with vacuum in place of helium.

Huge difference between the electron velocities in the solid and vapor states

Before closing we wish to call especial attention to the enormous difference between the electron velocities in the solid state and those in the vapor state which the results of this paper, together with our previous work, clearly indicate must exist. In carbon, for example, the maximum of the electron velocity distribution curve is displaced to velocities 60 percent higher than in the free atom, an excess which our present results force us to take seriously as a real effect. See Fig. 8, reproduced from one of our papers.[17]

This speeding up of the electrons applying, let us say, to four electrons per atom as in carbon represents an enormous positive increase in electronic kinetic energy in the solid state as compared to the vapor state. For carbon we compute the increase to be in excess of 3×10^5 joules per gram. There is of course an even slightly greater *fall* in electron potential energy caused by the proximity of positive nuclei in the solid state so that the net energy of the solid state is lower than the vapor state by the familiar required amount. Thus this profound difference between the two states is entirely masked in all conceivable methods of observation save the broadening of the modified line which alone affords a direct measurement of the electron velocities in the scattering material independent of their potential energy.

Acknowledgments

We are indebted to Dr. B. B. Watson (now of Arizona State Teachers College) for his excellent preliminary work on the curved quartz crystal spectrograph and the scattering chamber, to Mr. Bruce Hicks for the laborious calculations of helium momentum distribution and to Dr. A. Goetz for lending his facilities to supply the helium.

The funds for this work were derived from the gift of Dr. Leon L. Watters of New York City to the California Institute of Technology, known as the Frances Hayes Watters Memorial Research Fund, and it is a pleasure to take this opportunity to express our thanks for this gift.

SEPTEMBER 1, 1937 PHYSICAL REVIEW VOLUME 52

The Shape of the Compton Line for Helium and Molecular Hydrogen

BRUCE HICKS
California Institute of Technology, Pasadena, California
(Received April 19, 1937)

By using variation functions which take into consideration the instantaneous interaction of the electrons, momentum distribution functions and intensity distributions in the Compton line are computed for helium and molecular hydrogen, neglecting small relativity and binding corrections. The half-value breadths are expressed in terms of $l/2\lambda^*$ where l is the wave-length displacement from the center of the shifted line and $2\lambda^*=(\lambda_1^2+\lambda_e^2-2\lambda_1\lambda_e\cos\chi)^{\frac{1}{2}}$. λ_1 and λ_e are the primary and scattered wave-lengths and χ the scattering angle. The absolute breadth of the line may therefore be computed for any λ_1 and χ. For helium and molecular hydrogen the values of $l/2\lambda^*$ at half-maximum are 10.8 and 8.5, respectively.

INTRODUCTION

THERE have been many theoretical investigations of the shape of the Compton line differing from one another both in the treatment of the scattering process itself and in the electronic configuration assumed to exist before scattering has occurred.[1, 2] However, in no

[1] J. W. M. DuMond, Rev. Mod. Phys. **5**, 1 (1933); Phys. Rev. **33**, 643 (1929).
[2] G. E. M. Jauncey, Phys. Rev. **25**, 314, 723 (1925); P. A. Ross and Paul Kirkpatrick, Phys. Rev. **45**, 223

calculation has the interaction of the electrons found suitable representation, for the Hartree functions or hydrogen-like wave functions with screening constants which have heretofore been used introduce only an average perturbing effect of the electrons upon one another. Since computations of the Compton line shape have been most successful for gases, it is natural when attempting a more rigorous investigation to turn to the simplest elementary gases containing two electrons, namely helium and molecular hydrogen. For these substances it is not necessary to depend upon the Hartree or screening-constant-type wave function since variation functions containing interaction terms explicitly have been developed, the most accurate of which lead to energy values for the ground state which are correct within experimental error. Line shapes for helium and molecular hydrogen are here computed from some of the less accurate of these variation functions which nevertheless approximate the true wave functions much more closely than do the Hartree or the hydrogen-like screening-constant type. By reason of the greater accuracy possible in these calculations as compared to calculations on other gases or solids, the line shapes for these two gases probably offer the best opportunity to compare in a quantitative fashion theory and experiment.[3]

General Method

The variation function chosen to describe the He or H_2 system is here represented by $\phi(r_1, \vartheta_1, r_2, \vartheta_2)$, where r_1, ϑ_1 are polar coordinates of the first electron, r_2, ϑ_2 of the second electron with respect to the same origin. Azimuthal angles do not appear in any of the variation functions used. $A(P_1, \Theta_1; r_2, \vartheta_2)$, the mixed wave function in the polar coordinates of the first electron in momentum space and the position coordinates of the second electron, can be obtained from this ϕ by the following Dirac transformation,

$$A(P_1, \Theta_1, r_2, \vartheta_2) = h^{-\frac{1}{2}}\int_{r_1=0}^{\infty}\int_{\vartheta_1=0}^{\pi}\int_{\varphi_1=0}^{2\pi} \exp\left[-(2\pi i/h)\mathbf{P}_1\cdot\mathbf{r}_1\right] \cdot\phi(r_1, \vartheta_1, r_2, \vartheta_2) r_1^2 \sin\vartheta_1 dr_1 d\vartheta_1 d\varphi_1 \quad (1)$$

(No azimuthal angle enters in A as none enters in ϕ.) Here, $\mathbf{P}_1$ and $\mathbf{r}_1$ are the vectors whose endpoints lie at (P_1, Θ_1), (r_1, ϑ_1), respectively. All the transformation integrals which must be evaluated may be written down immediately by using the general expression for the momentum wave functions of a hydrogenlike atom, Υ_{nlm}, given by Podolsky and Pauling.[4] Those functions which will be used here are:

$$\Upsilon_{100} = (1+\zeta_1^2)^{-2},$$
$$\Upsilon_{200} = 2(1+\zeta_1^2)^{-2}(\zeta_1^2-1)/(\zeta_1^2+1),$$
$$\Upsilon_{300} = (1+\zeta_1^2)^{-2}\left[4\left(\frac{\zeta_1^2-1}{\zeta_1^2+1}\right)-1\right], \quad (2)$$
$$\Upsilon_{210} = -4i\cos\theta\frac{\zeta_1}{(1+\zeta_1^2)^3},$$

where $\zeta_1 = 2\pi P_1 a_0/Z'h$, Z' = effective nuclear charge and a_0 = radius of first Bohr orbit in hydrogen, the subscripts in Υ_{nlm} referring to the quantum numbers, n, l, m. ζ_1 will be used in place of P_1, in the explicit functions of P_1 developed later for He and H_2. The momentum distribution function $B(P_1, \Theta_1)$ can now be found by integrating the modulus squared of $A(P_1, \Theta_1; r_2, \vartheta_2)$. Thus

$$B(P, \Theta) = 2\pi\int_{r_2=0}^{\infty}\int_{\vartheta_2=0}^{\pi} AA^* r_2^2 \sin\vartheta_2 dr_2 d\vartheta_2. \quad (3)$$

The subscripts have been dropped in $B(P, \Theta)$ for the electrons contribute equally to the momentum.

Since for this case of scattering by field-free gases, all orientations of the molecule are equally probable, the function $B(P, \Theta)$ must be averaged over the angle Θ to obtain the radial momentum distribution function, $C(P)$:

$$C(P) = \int_{\Theta=0}^{\pi} B(P, \Theta)\sin\Theta d\Theta. \quad (4)$$

(1934); F. Bloch, Phys. Rev. **46**, 674 (1934); F. Schnaidt, Ann. d. Physik **21**, 89 (1934); W. Franz, Zeits. f. Physik **90**, 623 (1934); **95**, 652 (1935); G. Burkhardt, Ann. d. Physik **26**, 567 (1936); Kirkpatrick, Ross, and Ritland, Phys. Rev. **50**, 928 (1936).

[3] The complete experimental results of DuMond and Kirkpatrick (Phys. Rev., this issue) on scattering in He demonstrate the feasibility of such a comparison and its importance in determining the position of the shifted line accurately.

[4] Boris Podolsky and Linus Pauling, Phys. Rev. **34**, 109 (1929).

TABLE I. *Variation functions for the normal He atom.*

	Z'	c_2	c_5	$E-$ (UNITS $R_{He}hc$)	% ERROR
1	1.6875	0	0	5.695	1.93
2	1.850	0	0.112	5.755	0.91
3	1.69	0.142	0	5.754	0.92
4	1.822	0.126	0.089	5.784	0.40

DuMond[1] has shown that the shape of the Compton line can be computed from such a momentum distribution function or *vice versa*, the formula for the intensity y as a function of wave-length displacement l from the center of the shifted line being

$$y=k\int_{l=l}^{\infty} l^{-1}C\left(\frac{l}{2\lambda^*}\right)dl, \tag{5}$$

in which $l=\lambda_2-\lambda_1-(h/mc)(1-\cos\chi)$, $2\lambda^*=(\lambda_c^2+\lambda_1^2-2\lambda_1\lambda_c\cos\chi_1)^{\frac{1}{2}}$, $\lambda_c=\lambda_2$ for $l=0$. λ_1 and λ_2 are initial and scattered wave-lengths and χ is the scattering angle. $C(P)$ has been replaced by $C(l/2\lambda^*)$ where

$$\frac{l}{2\lambda^*}=\beta=\frac{v}{c}=\frac{P}{mc} \qquad \zeta=\frac{l}{2\lambda^*}\cdot\frac{1}{\alpha Z'},$$

α being the fine structure constant. Since the constant of integration k is arbitrary, all constant factors multiplying ϕ, A, B, and C are omitted.

It should be mentioned that DuMond's formula for the intensity distribution in the modified line does not consider the generally small effect due to binding and relativistic corrections. However, for the case of scattering from helium and the hydrogen molecule, binding and relativistic corrections to the shape are less than the error in the calculations due to the use of a variation function as an approximation to the true wave function. The error produced in the half-width itself is negligible since the corrections to the intensity corresponding to a given absolute value of l are nearly equal, though of opposite sign, on either side of the maximum.

Scattering from helium

The variation functions developed by Hylleraas[5] for He are of the form

$$\phi=\sum_{nlm} c_{nlm}e^{-Z's}s^n t^l u^m \qquad (l \text{ even}) \tag{6}$$

in which $s=(r_1+r_2)/a_0$, $t=(r_1-r_2)/a_0$, $a_0u=r_{12}$ = interelectronic distance, a_0 = radius of first Bohr orbit. Since a ϕ which involves the first power of u cannot be transformed in finite terms to the mixed wave function, variation functions which may be represented by

$$\phi=e^{-Z's}(1+c_2t^2+c_5u^2)$$

are used here. In Table I appear the four variation functions of this type together with the energy values to which they lead and the percentage difference from the true value. $E=-78.605$ ev $=-5.8074\ R_{He}hc$. The first of these is due to Kellner[6] and is a hydrogen-like screening constant type function. The second is due to Hylleraas[7] and the third and fourth have been developed by the author using Hylleraas' formulae.[5] The terms in u^2 were included in an effort to compensate for the missing linear u term which is primarily responsible for the accuracy of Hylleraas' energy calculations. The third function describes the actual electronic system well since it represents a He atom with electrons in two different orbits with effective nuclear charges 2.15 and 1.19 corresponding to almost complete shielding of the outer one and slight negative shielding of the inner one. The second function, in comparison, although it now introduces the interelectronic interaction, represents this interaction as being much stronger than is actually the case. Consequently, of the two functions, the third probably corresponds more closely to the actual state of the system although the energy E calculated from the two functions is about the same. To check the effect of adding further integrable terms, values of E resulting from many different combinations of u^2, u^4, t^2, t^4, s, s^2 were computed. The most accurate value of the energy obtained in this way was only 0.1 percent better than the fourth variation function above. In view of the rapidly increasing complexity of the algebra entering into the evaluation of the integrals, it was not considered that the inclusion of further terms

[5] Egil A. Hylleraas, Skrifter det Norske Vid.-ak. Oslo, I Nat. Nuturw. Klasse 1932, p. 107.

[6] G. W. Kellner, Zeits. f. Physik **44**, 91 (1927).

[7] Egil A. Hylleraas, Zeits. f. Physik **54**, 347 (1929).

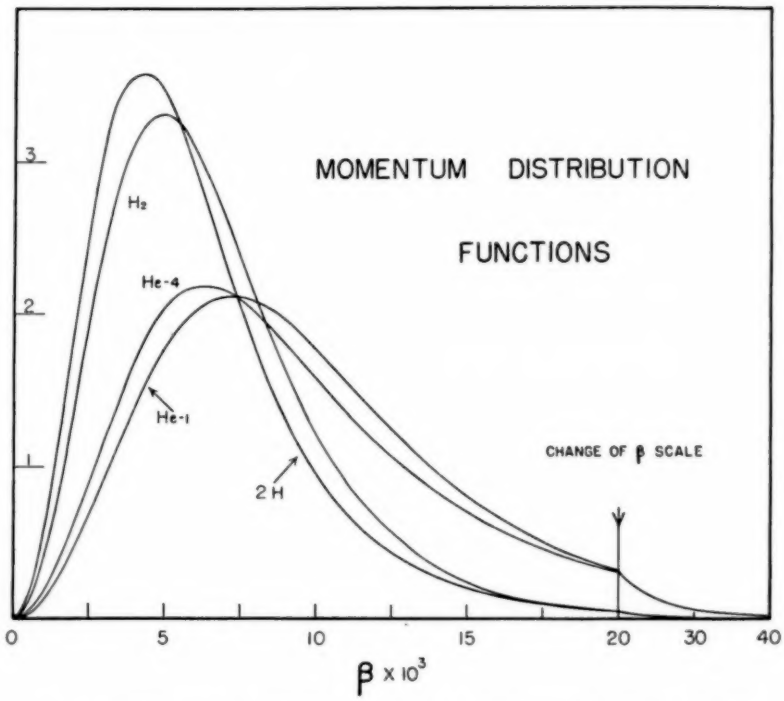

FIG. 1. Momentum distribution functions for helium and molecular hydrogen, normalized to the same area. The ordinates are in arbitrary units, the abscissae, in terms of $\beta=v/c$, the ratio of the velocity of an electron to that of light.

was justified. Furthermore, functions two and four lead to practically identical line shapes so that further terms would probably have little significance.

The necessary restriction of the exponents in the ϕ's to even powers of u and t makes it possible to express these as linear functions of hydrogen-like $1s$, $2s$, $2p$, and $3s$ wave functions:

$$\phi=a_1\psi_{100}(1Z')+a_2\psi_{200}(2Z') +a_2'\psi_{210}(2Z')+a_3\psi_{300}(3Z'). \quad (7)$$

Here a_1, a_2, a_2', a_3 are quantities involving r_2 which are constants for the first integration and ψ_{nlm} is a hydrogen-like wave function for the first electron around a nucleus with charge $1Z'$, $2Z'$, $\cdots$. From Eqs. (2) the mixed wave function then can be immediately written down as

$$A(\zeta_1,\Theta_1,r_2)=(1+\zeta_1^2)^{-2}\left[a_1+2a_2\cdot\frac{\zeta_1^2-1}{\zeta_1^2+1} +a_3\left\{4\left(\frac{\zeta_1^2-1}{\zeta_1^2+1}\right)^2-1\right\}-4i\cos\Theta_1\frac{\zeta_1\cdot a_2'}{1+\zeta_1^2}\right] \quad (8)$$

and it becomes after integration over r_2 and Θ

$$C(\zeta)=(1+\zeta^2)^{-4}\sum_{p=0}^{4}D_p\cdot\left(\frac{\zeta^2-1}{\zeta^2+1}\right)^p, \quad (9)$$

$$y=(1+\zeta^2)^{-3}\sum_{p=0}^{4}E_p(1+\zeta^2)^{-p}. \quad (10)$$

The coefficients D_p and E_p are polynomials in c_2/Z'^2 and c_5/Z'^2. (For the first variation function $y\propto(1+\zeta^2)^{-3}$ so that the polynomial in $(1+\zeta^2)^{-1}$ may be considered to be a correction factor in the other expressions.) Consequently there should be expected a simple relationship between the *half-value breadths*, $\beta_{\frac{1}{2}}$, and the energy values corresponding to the different variation functions. A rough calculation of the line breadths of different many-electron systems may be made from a knowledge of the total energy E of the system alone if this energy has been computed by minimizing with respect to the effective nuclear charge Z' appearing in a hydrogen-like wave function with screening constants. This minimizing insures that the virial theorem hold so that the root mean square momentum and the

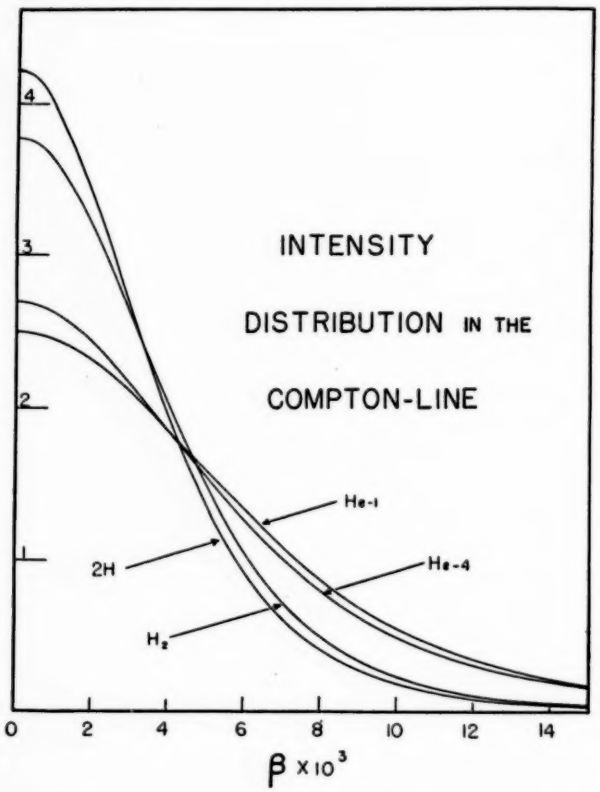

FIG. 2. Intensity distribution of the Compton line as a function of $\beta = l/2\lambda^*$ where l = displacement from the center of the shifted line, $2\lambda^* = (\lambda_1^2 + \lambda_c^2 - 2\lambda_1\lambda_c \cos\chi)^{\frac{1}{2}}$, λ_1 and λ_c being the initial and scattered wave-lengths and cos χ the scattering angle. Ordinates are in arbitrary units and the curves are normalized to the same area.

half-value breadth may be taken as proportional to $(-E)^{\frac{1}{2}}$. For systems which may be considered to be hydrogen-like with all electrons in the same shell, this method will be exact since in this case $E \propto Z'^2$ and $\beta_{\frac{1}{2}}$ should be proportional to Z', which is obviously true from a consideration of the simple form which y assumes for the hydrogen-like case.

A more accurate comparison may be made on the basis of the momentum distribution function, Fig. 1, for in general, $\beta_{\frac{1}{2}}$ corresponds closely in value to the most probable β. Thus, assuming that $\beta_{\frac{1}{2}}$ as calculated from the first variation function is correct and that the half widths are directly proportional to the most probable β's, approximate half widths are found which, with no attempt to adjust the constant of proportionality, fit to a few percent as is seen from the last column of Table II.

TABLE II. *Half-value breadths.*

$\beta_{\frac{1}{2}} \times 10^3$	Z'	$10^3 \times \beta_{\frac{1}{2}}/Z'$	$\beta_{\frac{1}{2}}$ calculated from most probable β
12.67	1.69	7.50	12.67
12.08	1.85	6.53	11.91
11.24	1.69	6.65	10.87
11.38	1.82	6.25	11.02

Since the variable is $\zeta = l/2\lambda^* Z'\alpha$ and the line shapes are plotted as functions of $l/2\lambda^* = \beta$, the half-value widths that should be compared are $\beta_{\frac{1}{2}}/Z'$. Values of $\beta_{\frac{1}{2}}$ (the half-value breadth) and $\beta_{\frac{1}{2}}/Z'$ are tabulated in Table II. If $(\beta_{\frac{1}{2}}/Z')$ is plotted as a function of the corresponding energy, it is seen to be an approximately linear function of the energy over a range which is long in comparison to the error in the energy computed from the fourth variation function and in consideration of the probable unreliability of the second variation function. Consequently, the extrapolated value of $(\beta_{\frac{1}{2}}/Z') = 5.99 \times 10^{-3}$ corresponding to $E = -5.8074\ R_{He}hc$ may be assumed. By using the value $Z' = 1.818$ which occurs in the most accurate of the Hylleraas functions, the value $\beta_{\frac{1}{2}} = 10.8 \times 10^{-3}$ is then found, which is the best value that can be calculated from these variation functions. This method would not be valid if the constants did not enter into the variation function linearly.

In Fig. 2, y as a function of $l/2\lambda^* = \beta = v/c$ is plotted. From such a curve, the line shape for any scattering angle and any incident wave-length can be computed by a proper choice of λ^* (Eq. (5)). [For example, the half-width in He at $\lambda_1 = 710$ X.U., $\chi = 180°$ is 15.8 X.U.] All curves are reduced to the same area since the total number of scattering electrons is constant. The two curves for He correspond to the first and fourth variation functions, and show clearly that

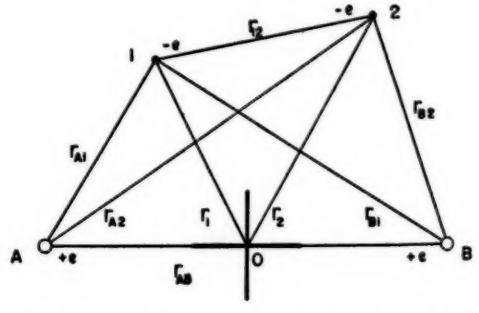

FIG. 3. Coordinates for the hydrogen molecule.

the line whose shape is computed from the more accurate function is narrower than the line derived from the simple hydrogen-like screening constant function.

Scattering from molecular hydrogen

A variation treatment for the hydrogen molecule has been carried out by James and Coolidge[8] using terms in u to introduce the electronic interaction as Hylleraas did for He. However, the exponential of $(r_{A1}+r_{B1}+r_{A2}+r_{B2})/r_{AB}$, occurs in all the variation functions making impossible the evaluation of the transformation integral in finite terms. (See Fig. 3 for coordinates.) Consequently, a function of the ionic-polarization type studied by Weinbaum[9] which permits the direct evaluation of all integrals but that for y has been chosen.

This variation function is

$$\phi=[u_{1sA}(1)+\sigma u_{2pA}(1)][u_{1sB}(2)+\sigma u_{2pB}(2)]+[u_{1sA}(2)+\sigma_{2pA}(2)][u_{1sB}(1)+\sigma u_{2pB}(1)]$$
$$+c\{[u_{1sA}(1)+\sigma u_{2pA}(1)][u_{1sA}(2)+\sigma u_{2pA}(2)]+[u_{1sB}(1)+\sigma u_{2pB}(1)][u_{1sB}(2)+\sigma u_{2pB}(2)]\}, \quad (11)$$

in which $\sigma=0.07$, $c=0.176$, and u_{1sA} (1) represents a hydrogen-like $1s$ wave function for electron (1) about nucleus A which carries a charge Z', etc. Thus

$$u_{1sA}(1)=\exp(-Z'r_{A1}/a_0), \quad u_{2pA}(1)=(r_{A1}Z'/a_0)\cos\vartheta_{A1}\cdot\exp(-Z'r_{A1}/a_0),$$
$$\vartheta_{A1}=\text{angle between } r_{AB} \text{ and } r_{A1}, \quad \text{measured from } r_{A1} \text{ to } r_{AB}.$$

The quantity r_{AB}, the internuclear distance, although not occurring in the variation function, enters in the calculation of the transformation integral. The experimental value, 0.7395A, of r_{AB} is taken instead of 0.77 which corresponds to Weinbaum's function. This reduces the dissociation energy by a few percent, but gives a more accurate representation of the actual structure of the molecule. Z' is taken to be 1.19 since most variation functions of this general type lead to this value. ϕ may be rewritten as

$$\phi=a_A[u_{1sA}(1)+u_{2pA}(1)]+a_B[u_{1sB}(1)+\sigma u_{2pB}(1)]$$

in which

$$a_A=u_{1sB}(2)+\sigma u_{2pB}(2)+cu_{1sA}(2)+c\sigma u_{2pA}(2),$$
$$a_B=u_{1sA}(2)+\sigma u_{2pA}(2)+cu_{1sB}(2)+c\sigma u_{2pB}(2),$$

and a_A and a_B are therefore functions of the second electron's position alone. Since the transformation integral, Eq. (1), was expressed in terms of coordinates with but one origin, it is necessary to change its form slightly. Noting that ϕ splits up into two parts containing position variables with A and B as origin, and taking (x_{A1}, y_{A1}, z_{A1}), (x_{B1}, y_{B1}, z_{B1}) to be rectangular Cartesian coordinates of the first electron with respect to A and B, the z-axis lying in the direction of the line AB, then the transformation integral becomes

$$A(P_{z_1}, P_{y_1}, P_{z_1}, x_{A2}, \cdots z_{B2})=h^{-1}\Big\{a_A\exp[(\pi i/h)r_{AB}P_{z_1}]\int_{x_{A1}=0}^{\infty}\int_{y_{A1}=0}^{\infty}\int_{z_{A1}=0}^{\infty}$$
$$\times\exp[-(2\pi i/h)\bar{P}_1\cdot\bar{r}_{A1}]\cdot[u_{1sA}(1)+u_{2pA}(1)]dx_{A1}\,dy_{A1}\,dz_{A1}+a_B\exp[-(\pi i/h)r_{AB}P_{z_1}]$$
$$\int_{x_{B1}=0}^{\infty}\int_{y_{B1}=0}^{\infty}\int_{z_{B1}=0}^{\infty}[u_{1sB}(1)+u_{2pB}(1)]\exp[-2\pi i/h)\bar{P}_1\cdot\bar{r}_{B1}]dx_{B1}dy_{B1}dz_{B1}\Big\}.$$

Since these integrals are exactly those for $1s$ and $2s$ hydrogen-like atoms, the mixed wave functions can at once be written out in polar coordinates by use of Eq. (2).

---

[8] H. M. James and A. S. Coolidge, J. Chem. Phys. **1**, 825 (1933).
[9] S. Weinbaum, J. Chem. Phys. **1**, 593 (1933).

$$A(P_1, \Theta_1, r_{A2}, \cdots \vartheta_{B2}) = [a_A \exp[(\pi i/h) r_{AB} P_1 \cos \Theta_1] + a_B \exp[-(\pi i/h) r_{AB} P_1 \cos \Theta_1]][(1+\zeta_1^2)^2 - 4i\sigma\zeta_1 \cos \Theta_1] \cdot (1+\zeta_1^2)^{-3}. \quad (12)$$

Here ϑ_{A1} = angle between r_{A2} and r_{AB}, etc., while Θ = polar angle in momentum space of the first electron. Integrating over $r_{A1} \cdots \vartheta_{B2}$ and Θ_1, it follows that $A(P_1 \cdots \vartheta_{B2})$ becomes

$$c(\zeta) = (1+\zeta^2)^{-6}\left[(1+\zeta^2)^2\left(1+\frac{\lambda}{f\zeta}\sin(f\zeta)\right)+\frac{16}{3}\sigma^2\zeta^2+\frac{32\lambda\sigma^2}{f^2}\cos(f\zeta)+\frac{16\lambda^2\sigma^2}{f^3\zeta}(f^2\zeta^2-2)\sin(f\zeta)\right], \quad (13)$$

in which $\zeta = 2\pi P a_0/Z'h$ as before, $f = Z' r_{AB}/a_0 = 1.67$, $\lambda = 2\mu(\mu c+1+c^2)/(4c/\mu+1+c^2) = 0.857$, where $\mu = 2(e^f/f^2)(1+\sigma^2)$ [polynomial in σ and f].

It is seen that in order to find y it is necessary to evaluate indefinite integrals of the form

$$\int_\zeta^\infty \frac{\sin(f\zeta)}{(1+\zeta^2)^n} d\zeta.$$

As a simplification, all integrals of this type were taken together and integrated graphically with an error of less than 1 percent. For purposes of comparison the resulting y curve was normalized to the same area as for two hydrogen atoms, or for a He atom and plotted with the He curves in Fig. 2.

Many other variation functions which it is possible to integrate have been studied by various investigators, but as each is of essentially different character from every other, and since the difference between any two is not merely a term in a polynomial as in the case of the helium, and the change in λ is consequently of a complicated nature, they would not provide basis for an extrapolation such as was carried out for helium. Accordingly it has not seemed worth while to calculate line shapes for these functions.

Interpolating on the y curve (Fig. 2), the value $8.50\times10^{-3} = \beta_{\frac{1}{2}}$ is found for the half-value breadth of the line in H_2. Since the half-width in atomic hydrogen is only 7.50×10^{-3}, the more accurate calculation leads to a broader line. This is not surprising in view of the change in the electronic configuration which occurs when two hydrogen atoms are brought together to form a molecule. The most important change which affects the momentum distribution is in the effective nuclear charge Z'. Because of the finite separation of the atoms and the interaction of the electrons with each other, Z' does not approach the value 2 as it would for independent electrons but increases to 1.19, according to the variation functions used. This Z' is near to the value 1.13 of the ratio of the two half-widths calculated above and would probably agree more closely if the assumption of the experimental value of r_{AB} had not invalidated the virial theorem in this case. It is interesting to note that the ratio of the most probable β's calculated as in the case of helium is 1.12, checking closely the actual ratio of the half-widths.

The author is indebted to Dr. Linus Pauling for valuable criticisms during the course of this investigation.

Experiments on the Variation of the Atomic Structure Factor of Nickel with X-Ray Wave-Length

WILLIAM P. JESSE
University of Chicago, Chicago, Illinois
(Received July 10, 1937)

X-ray measurements have been made with a vacuum ionization spectrometer on powdered nickel to determine the variation of the atomic structure factor in the region of the K absorption edge, $\lambda = 1.4839$A, and as far out as possible on the long wave-length side. Powdered NaCl and LiF have been used as comparison substances. Extensive measurements over a range of wave-lengths from 0.560 to 2.74A have been made. *Conclusions:* The experimentally determined dispersion curve for the atomic structure factor of nickel, based upon the difference between measured structure factor values on the long and short wave-length side of the K absorption edge, does not agree in shape with the theoretical curve of Hönl. The experimental curve rises more rapidly from the absorption edge and is then flatter than the theoretical curve. The two curves come into closer agreement at longer wave-lengths. The maximum discrepancy between theory and experiment is about 0.9 electron at $\lambda/\lambda_K = 1.11$. The predicted invariance of the structure factor decrement due to K electrons with $(\sin\theta)/\lambda$ is again confirmed.

INTRODUCTION

IN a previous paper,[1] experiments have been described in which the crystal structure factor in powdered KF was measured for wave-lengths in the neighborhood of the potassium K absorption edge. Such experiments showed the expected decrease in the crystal structure factor near the absorption edge on the short wave-length side and the change with wave-length was very closely in accord with the wave mechanical theory of Hönl. On the long wave-length side, however, the experimental values rose in a curve both steeper and higher than the theoretical curve and the *differences* in experimental values between the short and long wave-length sides were considerably less than the theory demands. Since it was impossible because of the limitations of the apparatus to carry the measurements as far as was desirable on the long wave-length side and thus determine the final shape of the experimental curve, it has seemed worth while to carry out further measurements on an element having a K critical absorption frequency within the range of convenient wave-lengths. For such measurements metallic nickel seemed well suited.

EXPERIMENTAL TECHNIQUE

The apparatus used in these experiments was the vacuum ionization spectrometer designed by Professor Allison and used by us in our previous measurements. Since the apparatus and the technique of measurement have been fully described in our previous paper,[1] any detailed account would seem unnecessary here. The powdered nickel used was chemically prepared by the reduction of nickel formate in hydrogen. The standard comparison substance was sodium chloride which was precipitated in a very fine powder by the addition of excess ethyl alcohol to a saturated aqueous solution of the salt. The resulting powder was dried, heated to 200°C, cooled and sifted through a bolting cloth having 275 meshes per inch. For the longer wave-lengths the standard substance was lithium fluoride. This was obtained from a chemical supply house and, according to the special analysis given on the container, showed negligible quantities of impurities. The LiF was also sifted through the bolting cloth. Throughout the experiment, the NaCl(200) plane was used as a standard comparison plane and for the longer wave-lengths the LiF(111) plane was used as a secondary standard. The latter was calibrated against NaCl(200) for the wave-lengths Cu $K\alpha$ and Fe $K\alpha$ so that the whole experiment is fundamentally based upon the value of the crystal structure factor for NaCl(200). Three separate briquets of powdered nickel and three briquets of NaCl were used during the course of the experi-

[1] S. K. Allison and W. P. Jesse, Phys. Rev. **49**, 483 (1936).

ment. The results from the different samples were very consistent.

The comparison of the relative power diffracted in the Debye-Scherrer ring from any given nickel plane to that diffracted from the standard plane was made by the second experimental method given in our paper. In this method the ionization chamber was moved in small steps, 5 or 10 minutes of arc, through the region of the diffracted beam and adjacent to it, until a level background was obtained. With Pliotron readings as ordinates and angles as abscissae, a smooth curve was drawn through the points obtained. The area under the peak and above the base-line is proportional to the diffracted power whose measurement is desired.

Experimental Results

From the measurement of the relative diffracted power from two planes either in the same crystal or in two different crystals the relative values of the crystal structure factor may be computed from the expression[2]

$$\frac{F_1}{F_2}=\frac{M_2}{M_1}\left\{\frac{j_2\mu_1 \sin\theta_1}{j_1\mu_2 \sin\theta_2}\left(\frac{1+\cos^2 2\theta_1}{\sin 2\theta_1}\right)^{-1} \times\left(\frac{1+\cos^2 2\theta_2}{\sin 2\theta_2}\right)\frac{[P_d]_1}{[P_d]_2}\right\}^{\frac{1}{2}},$$

where the subscripts refer to the individual planes.

F is the crystal structure factor.
M is the number of unit cells per unit volume.
j is the factor giving the number of possible orientations of the cell contributing to the diffraction halo in question.
μ is the linear absorption coefficient of the particles composing the briquet.
2θ is the angle between the forward directions of the incident and diffracted beams.

[2] Compton and Allison, *X-Rays in Theory and Experiment* (D. Van Nostrand), p. 419.

Table I. *Observed crystal structure factors, uncorrected for temperature. Based on* $\frac{1}{4}F[NaCl(220)]=15.62$ *for* $\lambda=0.709A$.

Powders	λ (A)	Line	Orders	θ's	Φ (θ)	j's	μ's	$P_{d_1}:P_{d_2}$	Value for Basic Plane	Result
Ni : NaCl	0.5598	Ag $K\alpha$	220 : 220	13°-00′ : 8°-05′	36.7 : 98.2	12 : 12	220 : 9.20	0.170	15.58	$f_{Ni220}=12.85$
"	0.7092	Mo $K\alpha$	220 : 220	16°-34′ : 10°-16′	21.8 : 60.1	12 : 12	428 : 18.05	0.168	15.62	$f_{Ni220}=12.75$
"	0.7092	Mo $K\alpha$	111 : 220	10°-03′ : 10°-16′	62.8 : 60.1	8 : 12	428 : 18.05	0.656	15.62	$f_{Ni111}=18.02$
"	0.7092	Mo $K\alpha$	200 : 220	11°-38′ : 10°-16′	46.3 : 60.1	6 : 12	428 : 18.05	0.333	15.62	$f_{Ni200}=17.24$
"	0.7857	Zr $K\alpha$	111 : 220	11°-09′ : 11°-23′	50.6 : 48.3	8 : 12	548 : 23.8	0.669	15.62	$f_{Ni111}=17.93$
"	1.497	Ni $K\beta$	111 : 220	21°-37′ : 22°-06′	12.13 : 11.55	8 : 12	361 : 150	3.17	15.84	$f_{Ni111}=12.66$
"	1.538	Cu $K\alpha$	200 : 220	25°-57′ : 22°-45′	8.02 : 10.81	6 : 12	427 : 163	1.69	15.84	$f_{Ni200}=13.35$
"	1.656	Ni $K\alpha$	200 : 220	28°-05′ : 24°-35′	6.70 : 9.07	6 : 12	522 : 200	2.05	15.84	$f_{Ni200}=14.71$
"	1.656	Ni $K\alpha$	111 : 220	24°-03′ : 24°-35′	9.54 : 9.07	8 : 12	522 : 200	4.80	15.84	$f_{Ni111}=16.36$
"	1.656	Ni $K\alpha$	220 : 220	41°-44′ : 24°-35′	3.06 : 9.07	12 : 12	522 : 200	1.098	15.84	$f_{Ni220}=11.26$
"	1.934	Fe $K\alpha$	220 : 220	51°-02′ : 29°-05′	2.75 : 6.19	12 : 12	795 : 312	1.47	15.91	$f_{Ni220}=11.27$
LiF : NaCl	1.934	Fe $K\alpha$	111 : 220	24°-41′ : 29°-05′	8.99 : 6.19	8 : 12	69.4 : 312	2.69	15.91	$\frac{1}{4}F[LiF(111)]=4.53$
"	1.538	Cu $K\alpha$	111 : 220	19°-25′ : 22°-45′	15.41 : 10.81	8 : 12	33.8 : 162.6	2.97	15.84	$\frac{1}{4}F[LiF(111)]=4.62$
"	1.538	Cu $K\alpha$	200 : 220	22°-34′ : 22°-45′	11.01 : 10.81	6 : 12	33.8 : 162.6	3.52	15.84	$\frac{1}{4}F[LiF(200)]=6.86$
Ni : LiF	2.744	Ti $K\alpha$	200 : 111	51°-15′ : 36°-21′	2.75 : 3.85	6 : 8	2054 : 187.3	1.07	4.65	$f_{Ni200}=14.70$
"	3.353	Ca $K\alpha$	111 : 111	55°-38′ : 46°-24′	2.94 : 2.77	8 : 8	3445 : 339	2.56	4.69	$f_{Ni111}=15.69$
							$(\sin\theta)/\lambda$			
Ni	0.7857	Zr $K\alpha$	200 : 111	12°-54′ : 11°-09′	37.25 : 50.61	6 : 8	.284 : .246	0.494	17.93	$f_{Ni200}=16.97$
"	1.497	Ni $K\beta$	200 : 111	25°-11′ : 21°-37′	8.584 : 12.13	6 : 8	.284 : .246	0.437	12.66	$f_{Ni200}=11.49$
"	1.497	Ni $K\beta$	220 : 111	37°-00′ : 21°-37′	3.719 : 12.13	12 : 8	.402 : .246	0.186	12.66	$f_{Ni220}=8.05$
"	1.538	Cu $K\alpha$	111 : 200	22°-16′ : 25°-57′	11.38 : 8.02	8 : 6	.246 : .284	2.25	13.35	$f_{Ni111}=14.57$
"	1.538	Cu $K\alpha$	220 : 200	38°-13′ : 25°-57′	3.51 : 8.02	12 : 6	.402 : .284	0.478	13.35	$f_{Ni220}=9.87$
"	1.656	Ni $K\alpha$	111 : 200	24°-03′ : 28°-05′	9.54 : 6.70	8 : 6	.246 : .284	2.31	14.71	$f_{Ni111}=16.26$
"	1.656	Ni $K\alpha$	220 : 200	41°-44′ : 28°-05′	3.06 : 6.70	12 : 6	.402 : .284	0.508	14.71	$f_{Ni220}=10.98$
"	1.656	Ni $K\alpha$	220 : 111	41°-44′ : 24°-03′	3.06 : 9.54	12 : 8	.402 : .246	0.232	16.25	$f_{Ni220}=11.24$
"	1.934	Fe $K\alpha$	200 : 220	33°-21′ : 51°-02′	4.58 : 2.75	6 : 12	.284 : .402	1.52	11.27	$f_{Ni200}=15.21$
"	1.934	Fe $K\alpha$	111 : 220	28°-26′ : 51°-02′	6.51 : 2.75	8 : 12	.246 : .402	3.29	11.27	$f_{Ni111}=16.25$
"	2.744	Ti $K\alpha$	111 : 200	42°-29′ : 51°-15′	3.00 : 2.75	8 : 6	.246 : .284	1.78	14.70	$f_{Ni111}=16.27$
LiF	1.538	Cu $K\alpha$	111 : 200	19°-25′ : 22°-34′	15.41 : 11.01	8 : 6	.216 : .249	0.826	6.86	$\frac{1}{4}F[LiF(111)]=4.56$

P_d is the power in the arc of the diffraction halo entering the ionization chamber window.

The experimental results are given in some detail in Table I, and in the various columns are found the quantities which appear in the above equation. The symbol $\Phi(\theta)$ represents a grouping of the trigonometric factors and is given by

$$\Phi(\theta)=(1+\cos^2 2\theta)/\sin^2\theta\cos\theta.$$

Since cubic crystals were used throughout, the values of M_2/M_1 were computed from the ratios of the cubes of the lengths of the sides of the unit cells. The cube edge of nickel was taken as $3.518A$ in this and other such computations.

As was stated before, the NaCl(220) plane was used throughout as a standard plane and the basic value for the crystal structure factor for $\frac{1}{4}F[\text{NaCl}(220)]=f_{\text{Na}}+f_{\text{Cl}}$ was taken as 15.62, a value determined by James and Firth[3] for the wave-length $0.709A$. Even though the wave-lengths used in the experiment are far removed from the K critical absorption wave-lengths of both sodium and chlorine, nevertheless the value for the structure factor for NaCl(220) is not entirely invariant and small corrections for dispersion must be made especially at the longer wave-lengths. These corrections, as before, were calculated from the theory of Hönl.[4] Tables of dispersion corrections for the atoms Na and F have been given in our previous paper. Since the chlorine atom is very close in atomic number to potassium, our previous calculations for the latter, with some extensions to the shorter wave-lengths, were considered a close enough approximation for the small corrections in question here. The values of $\frac{1}{4}F[\text{NaCl}(220)]=15.62$ for $\lambda=0.709A$ plus the dispersion correction are found in vertical column 10 in the table. In this column are also found the values of $\frac{1}{4}F[\text{LiF}(111)]$ based upon a value 4.56 for $\lambda=1.539$ and similarly corrected for dispersion whenever used as a secondary standard. In the latter part of Table I where comparisons between two nickel planes are given, the comparison value given in column 10 always by convention refers to the plane indexed in the denominator of the ratio in column 4. The last vertical column gives the final result for the atomic structure factors at room temperature derived from the comparisons indicated. This final value may often be the mean of from six to eight separate runs.

It is believed that the random error of measurement for lines Cu $K\alpha$, Ni $K\alpha$, and Fe $K\alpha$ represents a deviation from the above structure factor values of not more than 1 percent. The measurements with Ti $K\alpha$ are almost as good. On the short wave-length side the experimental conditions are not so favorable, and the error may be two or three times the above value. Systematic errors, which are by far the more important, will be discussed later. A difficulty was found in the measurement of Ni(200) with Mo $K\alpha$ in that the Ni(111) and Ni(200) peaks just failed to be resolved and a very small extrapolation at the foot of each curve was necessary. Different methods of making this extrapolation showed a negligible difference for the larger peak Ni(111) but did affect the smaller Ni(200) by several percent. The value of Ni(200) for Mo $K\alpha$ is, therefore, probably not quite so reliable as the other values obtained but is has been included for the sake of completeness. It gives throughout the experiment uniformly higher results than the others.

It should perhaps be noted at this point that the value here determined of $\frac{1}{4}F[\text{LiF}(111)]=4.56$ for $\lambda=1.538A$ is about 10 percent lower than the one previously determined by us where a value 5.00 was obtained from a comparison of LiF(111) and NaCl(200) with wave-length $1.934A$. The reason for this discrepancy is not entirely clear since the same LiF powder was used in both cases. The most probable reason would seem to be that for the NaCl(200) plane in the ground sodium chloride briquet formerly used a certain extinction error[5] was present, which has been here avoided by the use of finely precipitated powder and by taking a higher order plane as the standard plane. The present value of 4.56 for $\frac{1}{4}[\text{LiF}(111)]$ is in good agreement with the experimental value 4.61 for $\lambda=0.709A$ of Havighurst,[6] and the value for $\frac{1}{4}F[\text{LiF}(200)]$ of 6.86 agrees with his value of 6.72. The dispersion correction

[3] James and Firth, Proc. Roy. Soc. **A117**, 62 (1927).
[4] Hönl, Zeits. f. Physik **84**, 1 (1933), Ann. d. Physik **18**, 625 (1933).

[5] As will be shown later, a systematic error of this type and magnitude in the standard NaCl (200) plane would cause but a very small change in the results previously obtained in potassium fluoride for the structure factor decrement, probably not more than the random experimental error.
[6] R. J. Havighurst, Phys. Rev. **28**, 869 (1926).

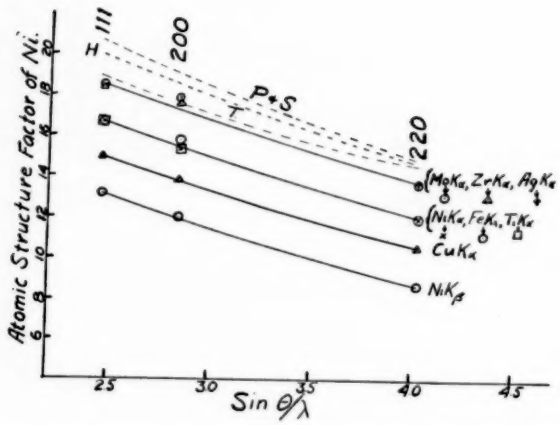

FIG. 1. Variation of the observed structure factor decrements with sin θ/λ.

is here negligible. Further when the present value for $\frac{1}{4}F[\text{LiF}(200)]$ is reduced to that corresponding to atoms at rest in the crystal by multiplication by a temperature factor $e^M=1.048$ for LiF(200) and a dispersion correction of 0.06 is subtracted, the final result 7.13 is comparable with and is but slightly lower than the sum of the theoretical Hartree values for f_{Li} and f_{F}; i.e., 7.30 for the corresponding value of $(\sin\theta)/\lambda$.

The final structure factor values in Table I, which are for nickel at room temperature, were reduced to corresponding values for atoms at rest in the lattice by means of the relation $f_0=fe^M$ where f_0 is the corrected structure factor and f is the factor observed at absolute temperature T. The value of M was determined by Waller's[7] formula

$$M=\frac{6h^2}{m_a k\Theta}\left(\frac{\Phi(x)}{x}+\frac{1}{4}\right)\frac{(\sin^2\theta)}{\lambda^2},$$

where h is Planck's constant,

m_a is the mass of the atom considered,
k is Boltzmann's constant,
x is the ratio Θ/T, where Θ is the characteristic temperature of the crystal.

The function $\Phi(x)$ is the result of the evaluation of a definite integral and is taken from a table of values given by Debye.[8] For nickel the characteristic temperature has been determined from thermal measurements by Lapp[9] who gives a value $\Theta=380°$. A check on this value was obtained by deriving the characteristic temperature for nickel from the known characteristic temperature for copper by comparison of the two crystals by the Lindemann[10] melting point formula. The value thus obtained was in excellent agreement with the value given above. In the first column of Table II are given final mean values of the structure factors derived from the comparisons indicated in Table I. The second vertical column shows the corresponding values of e^M and the third column gives the final values for the atomic structure factors corresponding to atoms at rest in the lattice. These values have been plotted against $(\sin\theta)/\lambda$ in Fig. 1. The legend to the right of the figure identifies the experimental points lying on each curve.

STATEMENT OF THEORY

The atomic structure factor is defined as the ratio of the amplitude of the wave scattered to a distant observing point P by an atom at 0 to the amplitude of the wave scattered to the same point P by a single electron replacing the atom, it being assumed that the electron scatters in the

TABLE II. *Temperature corrections applied to values of* f_{Ni} *of Table I.*

fNi Table I	e^M	$f_0=fe^M$	INDICES	λ (A)	LINE
18.02	1.025	18.47	(111)	0.7092	Mo $K\alpha$
17.93	"	18.38	(111)	0.7857	Zr $K\alpha$
12.66	"	12.98	(111)	1.497	Ni $K\beta$
14.57	"	14.93	(111)	1.538	Cu $K\alpha$
16.27	"	16.67	(111)	1.656	Ni $K\alpha$
16.25	"	16.65	(111)	1.934	Fe $K\alpha$
16.27	"	16.67	(111)	2.744	Ti $K\alpha$
15.69	"	16.08	(111)	3.353	Ca $K\alpha$
17.24	1.034	17.83	(200)	0.7092	Mo $K\alpha$
16.97	"	17.55	(200)	0.7857	Zr $K\alpha$
11.49	"	11.88	(200)	1.497	Ni $K\beta$
13.35	"	13.81	"	1.538	Cu $K\alpha$
14.81	"	15.32	"	1.656	Ni $K\alpha$
15.23	"	15.75	"	1.934	Fe $K\alpha$
14.70	"	15.22	"	2.744	Ti $K\alpha$
12.85	1.068	13.73	(220)	0.5598	Ag $K\alpha$
12.75	"	13.62	"	0.7092	Mo $K\alpha$
8.05	"	8.60	"	1.497	Ni $K\beta$
9.87	"	10.54	"	1.538	Cu $K\alpha$
11.19	"	11.95	"	1.656	Ni $K\alpha$
11.27	"	12.04	"	1.934	Fe $K\alpha$

[7] I. Waller, Zeits. f. Physik **17**, 398 (1923); Diss. Uppsala (1925).
[8] P. Debye, see Compton and Allison, reference 2, p. 437.
[9] E. Lapp, Ann. de physique **12**, p. 442 (1929).
[10] Lindemann, Zeits. f. Electrochem. **17**, 817 (1911).

J. J. Thomson manner. So long as the frequency of the wave which is scattered remains far removed from any critical absorption frequency in the atom itself, the value of the structure factor changes but little with wave-length. When, however, frequencies only slightly higher than the K critical absorption frequency are used, then the amplitude of the two K electrons in the atom is greatly increased by resonance and a phase change also results. As a consequence, destructive interference is obtained between the radiation scattered by the K electrons and that scattered by the other electrons in the atom, and for frequencies very close to the critical absorption frequency the atomic structure factor may be greatly reduced. On the long wave-length side of the absorption edge the atomic structure factor rises again as we pass out of the region of resonance but never attains the full value experienced on the short wave-length side since the K electrons no longer share in the scattering process. The shape of the curves for the variation of the atomic structure factor with wave-length depends in a large measure upon the distribution with wave-length assumed for the virtual oscillators in the atom. The net difference between the values of the structure factor for $\lambda \to 0$ and $\lambda \to \infty$ gives the so called "oscillator strength"; i.e., the normal contribution of the electrons in the K shell to the scattering. Using the wave mechanics, Hönl[4] has been able to compute both the oscillator strength and the distribution of oscillators with wave-length from purely theoretical grounds. His equation for the expected change in the structure factor with wave-length is given by

$$\Delta f = -\frac{2^7 e^{-4}}{9}\left[\frac{4x^2 \ln |1-x^{-2}|}{(1-\Delta)^2} - \frac{1}{(1-\Delta)^3}\left\{x^3 \ln \left|\frac{1-x}{1+x}\right| + 2x^2\right\}\right]. \quad (1)$$

Here Δf, the so-called "structure factor decrement," is defined as $\Delta f = f_{\lambda \to 0} - f_\lambda$ where f_λ is the value of the structure factor for a wave-length λ and $f_{\lambda \to 0}$ the value for wave-lengths so short that all dispersion effects are negligible.

x represents the ratio λ/λ_K where λ_K is the wave-length value at the K critical absorption edge.

Δ is an atomic screening correction which in the case of nickel has the value 0.209.

e is the natural logarithm base.

For large values of x approaching infinity the above expression gives a value of $\Delta f = 1.32$ which is the oscillator strength of the K electrons of nickel. Hönl has further shown that the Δf values are independent of $(\sin\theta)/\lambda$, or rather that the variations are so small as to be undetectable experimentally except possibly for very heavy atoms.

TABLE III. *Determination of decrement Δf from corrected values in Table II.*

	λ(A)	Ni(111)	Ni(200)	Ni(220)	Ni(111)	Ni(200)	Ni(220)	MEAN Δf (Exp)	Δf HÖNL THEORY
$f_{\lambda \to 0}$		$f_{Mo\ K\alpha} - .28 = 18.19$	$f_{Mo\ K\alpha} - .28 = 17.55$	$f_{Mo\ K\alpha} - .28 = 13.34$	$f_{Zr\ K\alpha} - .24 = 18.14$	$f_{Zr\ K\alpha} - .24 = 17.31$	$f_{Ag\ K\alpha} - .30 = 13.43$		
$\Delta f_{Ni\ K\beta}$	1.497	5.21	5.67	4.74	5.16	5.43	4.83	5.17	5.00
$\Delta f_{Cu\ K\alpha}$	1.538	3.26	3.74	2.80	3.21	3.50	2.89	3.23	3.56
$\Delta f_{Ni\ K\alpha}$	1.656	1.52	2.23	1.39	1.47	1.99	1.49	1.68	2.55
$\Delta f_{Fe\ K\alpha}$	1.934	1.54	1.80	1.30	1.49	1.56	1.39	1.51	1.94
Exp. values below relative to mean $\Delta f_{Ni\ K\alpha} = 1.68$.									
$\Delta f_{Ti\ K\alpha}$	2.744	1.68	1.78					1.73	1.58
$\Delta f_{Ca\ K\alpha}$	3.353	2.27						2.27	1.45

Comparison of Theory and Experiment

In Table II the third column gives the values of the atomic structure factors for nickel corrected for temperature. Fig. 1 gives a plot of these values against $(\sin\theta)/\lambda$ for the various wave-lengths used. The invariance predicted by the Hönl theory of the structure factor decrement with $(\sin\theta)/\lambda$ is clearly shown by the fact that the curves representing experimental results are all parallel. This has previously been shown to be the case by ourselves[1] and others. To determine values of Δf, which is defined as $f_{\lambda\to 0}-f_\lambda$, entirely by experiment would be quite impractical since it would involve the use of infinitely short waves with their attendant difficulties, both theoretical and practical. It is therefore assumed that the theoretical equation of Hönl gives the correct value of Δf for the wave-lengths corresponding to Ag $K\alpha$, Mo $K\alpha$ and Zr $K\alpha$. It is further assumed that such Δf values are included in the values for the atomic structure factors experimentally determined for all planes with these wave-lengths. Our former paper has shown excellent relative agreement over a wide range of wave-lengths between the Hönl theory and experiment on the short wave-length side of the absorption edge of the potassium atom and there seems to be no reason to believe that the small Δf's here assumed are greatly in error. Their values are -0.30, -0.28 and -0.24 electrons for wave-lengths corresponding to Ag $K\alpha$, Mo $K\alpha$ and Zr $K\alpha$, respectively. If such negative decrements are added respectively to the values in Table II of the structure factors for the various planes determined with these three wave-lengths, we obtain values of $f_{\lambda\to 0}(111)$, $f_{\lambda\to 0}(200)$, $f_{\lambda\to 0}(220)$, corresponding to each set of measurements. The values thus obtained are tabulated in the top horizontal row of Table III. By definition, therefore, we may compute the decrement Δf for any wave-length λ by subtracting the structure factor derived at such a wave-length from the corresponding $f_{\lambda\to 0}$. This subtraction has been carried out in the next four horizontal rows of Table III, the values from Table II being subtracted from the values in the top row. Each horizontal row thus tabulates for the given wave-length at the left the values of the decrement derived from different combinations of experimental values. The mean

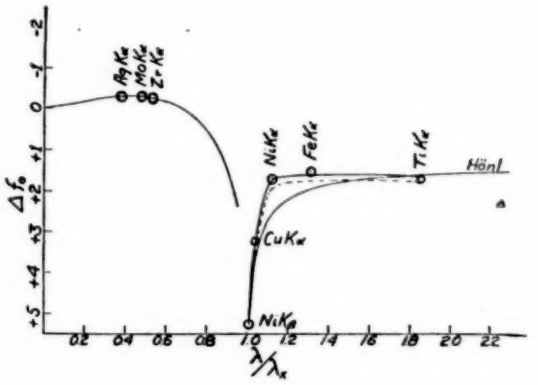

Fig. 2. The variation of the mean experimental decrement as a function of relative wave-length and comparison with Hönl theory. The point △ represents a determination for a single plane with line Ca $K\alpha$.

of these is given in the column next to the last, while the last column gives the theoretical value of Hönl derived from Eq. (1). For the values of the structure factors obtained with Ti $K\alpha$ and Ca $K\alpha$ a slightly different procedure was followed. Because of the longer wave-length involved, measurements of only two planes with Ti $K\alpha$ and one with Ca $K\alpha$ were possible. The structure factors (Table II) for such planes were compared with the corresponding values for Ni $K\alpha$ and the mean $\Delta f_{\text{Ni } K\alpha}=1.68$ was raised or lowered correspondingly. The values for the last two wave-lengths are thus relative to the value determined for Ni $K\alpha$. Because the value $\Delta f_{\text{Ca } K\alpha}$ rests upon measurements of a single plane, Ni(111), as compared with measurements of three planes for most of the wave-lengths used, very little relative weight should be given to this single measurement. There may also be some uncertainty here as to the effect of the very high absorption coefficient, which is almost double that encountered in any previous work. No anomalous results, however, traceable to such a source have so far been observed.

A comparison of the last two vertical columns of Table III and a reference to Fig. 2 where the results are plotted shows definite discrepancies between theory and experiment. The experimental curve rises much more rapidly than the theoretical curve on the long wave-length side and for the wave-length corresponding to Ni $K\alpha$ is almost 0.9 of an electron higher than the theoretical curve. Such an error, it is believed, is distinctly beyond the error of experiment. Since

because of our method of fitting the curve on the short wave-length side, we are dealing only in differences between structure factors on the long and short wave-length sides of the absorption edge, the discrepancy could, of course, lie in incorrect predictions of the theory for the short wave-length values of Δf. Two arguments can be advanced against such a supposition. In our former paper we found that the shape of the theoretical curve on the short wave-length side was in excellent agreement with the actual experimental curve although a similar discrepancy was found for the differences between the two sides. Also here for nickel the different shapes of the experimental and theoretical curves on the long wave-length side preclude any possibility of bringing the curves into coincidence even though they are fitted to each other at any one given point on the long wave-length side. Fig. 1 shows that the structure factor values for Ni $K\alpha$, Fe $K\alpha$ and Ti $K\alpha$ are very nearly the same. Theory, however, demands a difference of almost 1 full electron between the values for Ni $K\alpha$ and Ti $K\alpha$ and 0.6 electron between the values for Ni $K\alpha$ and Fe $K\alpha$. Since these wave-lengths were especially favorable to accurate measurement, it is difficult to believe that such differences are attributable to experimental error. If we neglect the inconclusive point for Ca $K\alpha$ it would seem that theory and experiment are in better accord as we go to longer wave-lengths from the point for Ni $K\alpha$. Thus one would suspect that any inadequacy in the theory results from an improper estimate of the distribution of virtual oscillators with frequency rather than an erroneous determination of the oscillator strength.

Discussion of Results

Before comparing the above results with those of other experiments it might be well to emphasize the manner in which the experimental Δf is determined in this case. Here experimental values of f_0 have been determined for any given plane for wave-lengths on the long wave-length side of the limit and also for a standardizing wave-length on the short wave-length side. The experimental values are then fitted to the Hönl dispersion curve at the origin λ_{-0} by applying to the value f_0 for the standardizing wave-length the dispersion value Δf calculated from Hönl's theory for this wave-length. The values of Δf obtained thereafter from the data are as nearly as possible the result of pure experiment and do not rely, as in some experiments, upon subtracting experimental values of f_0 determined on the long wave-length side from values of f_0 computed from theory. The advantage of the method here used is a very real one. Should the experimental values of f_0 contain errors which are not a function of wave-length, then the values of f_0 would be raised or lowered by the same percent on both sides of the limit and the Δf decrement determined would suffer the same percent error as the values of f_0. The method would thus minimize the effect of erroneous temperature corrections, incorrect values of M, the number of unit cells per unit volume, and primary extinction which, according to Darwin,[11] is a function of the order of the reflection rather than of the wave-length. On the other hand, the compensation would not be so good for systematic errors which are a function of wave-length. Thus errors in the linear absorption coefficient, for example, would not be well compensated for except in so far as they might result from erroneous densities. As an example of the above discussion, in Fig. 2 there is shown the resultant change in the experimental Δf's of assuming the determined structure factors to be uniformly 10 percent too low. If every experimental structure factor is raised then 10 percent, and hence every value of Δf by the same amount, the dotted curve in the figure shows the final result. As may be seen, such a curve differs from the original curve by hardly more than the random experimental error. If, on the other hand, the values on the long wave-length side had been formerly subtracted from an invariant value on the short wave-length side, let us say a theoretically derived value, then the ten percent increase might have introduced changes in Δf in some cases as large as the original values of Δf.

A resumé of previous work done on this problem has already been given[1] and a repetition of this would, therefore, seem unnecessary here. A mention, however, of the more recently determined values of Brindley and Spiers[12] seems de-

[11] C. G. Darwin, Phil. Mag. **43**, 800 (1922).
[12] G. W. Brindley and F. W. Spiers, Phil. Mag. **20**, 865 (1935).

sirable and their values are given in Table IV for comparison with the present values. Brindley and Spiers made a comparison between powdered nickel and powdered KCl for the line Cu $K\alpha$, the standard values of the structure factors for KCl being those determined by James and Brindley[13] through comparison of single crystals of KCl and NaCl. It will be seen that the values for four planes for nickel are in excellent agreement with those of the present paper given in column 2. Later, however, in the light of comparisons with powdered aluminum as a standard substance, Brindley[14] has concluded that the James and Brindley values of KCl are incorrect and must be raised just 10 percent. The fourth column of Table IV gives his revised values for nickel based upon aluminum powder as a standdard. The values used by Brindley for the atomic structure factors for aluminum were the theoretically derived ones of Hartree. The Hartree curve, atomic structure factor against $(\sin\theta)/\lambda$, was corrected to room temperature and a dispersion correction was added. To this was fitted at one point the similar experimental relative curve, i.e., atomic structure factor against $\sin\theta/\lambda$, through the multiplication of the latter by an arbitrary factor.

Although but little indication is given in the paper in regard to the difficulties with KCl, Brindley seems to assume that the differences obtained between his two comparison substances are the result of the fact that KCl is a poor standard substance. The comparison in Table IV might possibly indicate that the basic difficulty lies in an incorrect absolute value of the atomic structure factors for NaCl. As is shown in the table, the same result is apparently obtained for nickel powder whether we use powdered NaCl directly as a standard or KCl powder with structure factors determined through an original comparison with a single NaCl crystal. No value is given by James and Brindley[13] for the absolute value of the structure factor for the plane of NaCl in their paper on the comparison of KCl and NaCl but it is undoubtedly a value consistent with the value of NaCl by James and Firth used throughout the present work. A further interesting comparison may be made with the results shown in Table IV. If the values derived in the present paper are reduced to equivalent values referred to aluminum powder, then all values should be raised by 10 percent including the average values for $f_{\lambda\to 0}$. The mean values derived from the top row of Table III are re-tabulated in column 5 of Table IV. Column 6 shows them raised by 10 percent. Column 7 shows approximate Hartree $f_{\lambda\to 0}$ values for nickel which are given in Brindley's paper. In the absence of directly computed Hartree values for nickel an approximate curve is interpolated between the Thomas and the Pauling and Sherman curves, Fig. 1, in the same manner that the computed curve of Hartree for copper divides the interval between the corresponding two curves for copper. The Hartree curve, marked *H* in Fig. 1, while only approximate, is probably not greatly different from what would be computed directly by the Hartree method. The agreement between columns 6 and 7 would indicate a certain internal consistency in the results based on aluminum powder using theoretical Hartree values.

[13] R. W. James and G. W. Brindley, Proc. Roy. Soc. **A121**, 154 (1928).
[14] G W. Brindley, Phil. Mag. **21**, 778 (1936).

TABLE IV. *Comparison of present results with results of other experiments.*

PLANE	f_0 VALUES FOR Cu $K\alpha$ W.P.J.	f_0 VALUES Cu $K\alpha$ KCl STAND. B&S	f_0 VALUES AL. STAND. BRINDLEY COL. 3+10%	$f_{\lambda\to 0}$ MEAN VALUES W.P.J.	$f_{\lambda\to 0}$ W.P.J. AL. STAND. COL. 5+10%	$f_{\lambda\to 0}$ APPROX. HARTREE VALUES	Δf BRINDLEY COL. 7 −COL. 4	Δf W.P.J. COL. 5 −COL. 2
Ni(111)	14.93	15.3	16.83	18.17	20.00	19.9	3.07	3.24
Ni(200)	13.81	13.55	14.88	17.43	19.17	18.5	3.62	3.62
Ni(220)	10.54	10.45	11.49	13.38	14.72	14.7	3.21	2.84
Ni(311)	8.75	8.7	9.56			12.7	3.33	
Ni(331)			6.06			10.4	4.34	
					Mean		3.51	3.23

In this connection reference might be made to a table in a paper by Renninger[15] in which he compares the various experimental absolute determinations made for structure factors for the planes NaCl(200), NaCl(400), NaCl(600) and shows that differences amounting to more than 10 percent exist between the various determinations. His own determination obtained with a double crystal spectrometer for the line Cu $K\alpha$ is about 7 percent higher than the James and Firth value for NaCl(400) and Renninger's determination is more than 10 percent higher for NaCl(600). Thus there would seem to be possible grounds for questioning the correctness of the value 15.62 for $\frac{1}{4}F$[NaCl(220)] as determined by James and Firth. However, it must be noted that the experimental value of $\frac{1}{4}F$[LiF(200)] here obtained which is based upon the above value for NaCl(220) is quite consistent with the theoretical value of Hartree and the same applies to a lesser degree to the value of $\frac{1}{4}F$[LiF(111)].

In the light of the above discussion it is possible that later work may show that the absolute value here used for $\frac{1}{4}F$[NaCl(220)] is not correct but should be raised by 10 percent as might be indicated by Brindley's results with an aluminum standard. Even in such an event the final experimental values of Δf here given would be altered but little provided we assume that *any existing error is not a function of wave-length* as would very probably be the case. The Δf values in column 9, Table III, would then be increased by 10 percent. The dispersion curve resulting under these conditions is that given by the dotted line in Fig. 2 instead of the full line. As can be seen, the difference between the curves is very small. The experimental Δf is still definitely higher than the Hönl curve in the vicinity of the point for Ni $K\alpha$ The point corresponding to the line Cu $K\alpha$ is, however, now in almost exact agreement with the theory.

Brindley[14] has also determined in the same manner as for nickel the decrement Δf for metallic copper for the line Cu $K\alpha$ ($\lambda = 1.539$) and finds a value in very close agreement with the theoretical value of Hönl. Since in Eq. (1) the shielding constant Δ is a very slowly changing function of the atomic number, the predicted value of Δf varies but little for elements of adjacent atomic number for the same value $x = \lambda/\lambda_K$. The value determined by Brindley for metallic copper for Cu $K\alpha$ should thus be directly comparable with the present value for metallic nickel for Ni $K\alpha$ since the value of x is practically the same in the two cases. Here the two experiments are definitely in disagreement, his value of $\Delta f = 2.61$ being definitely lower than the value found here. On the other hand, Lameris and Prins[16] using the method of total reflection of the general x-radiation from a mirror of metallic nickel have obtained a dispersion curve which shows a steeper rise for the structure factor than the theory predicts on the long wave-length side of the limit, just as is indicated in the present experiments

Finally, the present experiments are in qualitative agreement with our previous results[1] for the potassium atom in KF in that in both cases the rise in the value of the atomic structure factor on the long wave-length side of the limit is more rapid and higher than the theory predicts. Quantitatively, however, the agreement is not so good since the differences between theoretical and experimental values of Δf are relatively less in the present experiments on nickel. The former results for potassium would indicate an erroneous value of the total oscillator strength for the K electrons of potassium from the Hönl theory as well as an erroneous distribution of virtual oscillators. The present results for nickel indicate a correct total oscillator strength but an incorrect distribution of virtual oscillators.

In conclusion, the author wishes to extend his thanks to the chairman of the department of physics, Dean Henry G. Gale, for the excellent facilities provided for this work. He wishes also to thank especially Professor S. K. Allison, who designed the vacuum ionization spectrometer used, and to whom he is indebted for many suggestions and for discussions of the present problem.

[15] M. Renninger, Zeits. f. Krist. **89**, 373 (1934).

[16] A. J. Lameris and J. A. Prins, Physica **1**, 881 (1934).

An Attempt to Observe the Spectrum of Doubly Excited Helium

F. P. BUNDY
Mendenhall Laboratory of Physics, Ohio State University, Columbus, Ohio
(Received July 1, 1937)

In this paper is described an electron-impact discharge tube which was designed to give excitation conditions favorable to the production of doubly excited helium. The tube furnished a concentrated 1000 ma beam of 300 to 500 volt electrons which passed through purified helium gas at a pressure of approximately 0.01 mm Hg. The comparatively feeble glow produced was photographed with a high speed two-prism glass spectrograph. Long exposures yielded only very much over-exposed He_I lines and rather strong He_{II} lines. This result is consistent with certain approximate theoretical calculations of Kreisler which show that the lifetimes of the doubly excited states of helium are limited by autoionization to approximately 10^{-14} sec., so that any spectral "lines" would be far too broad to be observable. This result tends to weaken the argument that the far ultraviolet helium lines, λλ320.4 and 357.5A, found by Kruger, and by Compton and Boyce, are due to transitions from doubly excited states to singly excited ones; and that the 60-volt energy losses of electrons passing through helium, observed by Whiddington, are due to a transition from the ground state to a doubly excited state.

INTRODUCTION

ATTEMPTS have been made by Rosenthal,[1] by Kiang, Ma, and Wu,[2] and by others to observe the visible spectrum of doubly excited helium. In this paper is described a discharge tube which is of the same general type as that used by Kiang, Ma, and Wu, but twenty-five times more powerful in regard to the magnitude of the electron current available for excitation. This experiment, which was near completion when Kiang, Ma, and Wu reported their work, merely strengthens their conclusion that in such a tube no visible spectrum attributable to doubly excited helium is observable. We do not give a detailed discussion of the general problem since an ample treatment has been given by Kiang, Ma, and Wu in their report.

It has been suggested by several people[3, 4] that the bright lines of the solar corona may be due to doubly excited helium. This suggestion was strengthened by the fact that Kruger,[5] and Compton and Boyce,[6] had observed two lines, λλ320.4 and 357.5A, in the far ultraviolet spectrum of helium which were attributed to transitions from doubly excited states to singly excited ones; and by the fact that Whiddington[7–9] and collaborators found energy losses in beams of electrons through helium gas which corresponded well with calculated energies[10–13] of the doubly excited states of helium. These, and other considerations, pointed out that the most favorable conditions for exciting the spectrum of doubly excited helium would be to have a heavy stream of 300 to 500 volt electrons[14] pass through the gas at very low pressure.

EXPERIMENTAL

The essentials of the discharge tube are shown in Fig. 1. The hollow cylinder bearing the grids, *G*, is 45 mm in diameter and 65 mm in length. Electrons from the flat spiral filaments, *F*, are accelerated by the grids, *G*, and stream through the region, *R*, exciting the gas to a glow. The grids were held at potentials of 300 to 500 volts positive to the filaments. Electron currents up to 1200 ma could be maintained for many hours. The gas pressure was kept at about 0.01 mm Hg in all the experiments. The entire tube was sub-

[1] Rosenthal, Zeits. f. Physik **84**, 794 (1933).
[2] Kiang, Ma and Wu, Phys. Rev. **50**, 673 (1936) and Chinese J. Phys. **2**, 117 (1936).
[3] Rosenthal, Zeits. f. Astrophys. **1**, 115 (1930).
[4] Goudsmit and Wu, Astrophys. J. **80**, 154 (1934).
[5] Kruger, Phys. Rev. **36**, 855 (1930).
[6] Compton and Boyce, J. Frank. Inst. **205**, 497 (1928).
[7] Whiddington and Priestley, Proc. Roy. Soc. **A145**, 462 (1934).
[8] Whiddington and Priestley, Proc. Leeds Phil. Soc. **3**, 81 (1935).
[9] Whiddington and Swift, Leeds Phil. and Lit. Soc., Proc. **3**, 262 (1937).
[10] Fender and Vinti, Phys. Rev. **46**, 77 (1934).
[11] Wu, Phys. Rev. **46**, 239 (1934).
[12] Wu and Ma, Phys. Rev. **48**, 917 (1935).
[13] Wilson, Phys. Rev. **48**, 536 (1935).
[14] Massey and Mohr, Proc. Camb. Phil. Soc. **31**, 604 (1935).

merged in a water bath for cooling. The feeble glow in the region, *R*, was observed through the window *W*, against the dark background afforded by the blackened absorption horn, *H*. This horn was required in order to absorb the brilliant filament light, which if scattered into the spectrograph would fog the plate with continuous spectrum.

Tank helium, 96 percent pure, was purified by passing it very slowly through a hot tube containing successively, copper pellets, magnesium ribbon, and black copper oxide; then over P_2O_5; then through activated charcoal at liquid-air temperature. The purified gas was stored in a 12 liter reservoir flask. During operation of the discharge tube, fresh helium from the reservoir was continuously pumped through the tube. It was necessary to operate the tube for a few hours in order to "clean it up." The tube was considered "clean" when the bands of CO and NO no longer appeared in the spectrum.

A high speed two-prism glass spectrograph was employed. Long exposures of 15 hours revealed only over-exposed He_I lines, fairly strong He_{II} lines, and very faintly the auroral bands of N_2^+ at λλ3914 and 4278A. There were no indications of lines at λλ5303 and 4231A (the positions of the strongest solar corona lines suggested to be due to doubly excited helium). The lines reported by Rosenthal,[1] λλ5058.9, 5028.8, 4958.9, 4269.5 and 4258.5A, were not present.

Discussion

The results of this experiment and that of Kiang, Ma and Wu may be interpreted in two ways. First, that helium cannot give a spectrum from its doubly excited states due to the nature

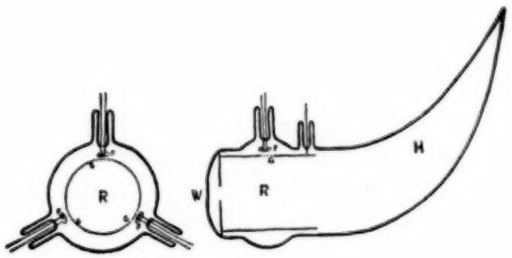

FIG. 1. Discharge tube.

of these states or, second, that the proper discharge conditions and technique have not yet been attained.

The first alternative would be consistent with the approximate theoretical calculations of Kreisler[15] which show the lifetimes of these states to be limited by autoionization to about 10^{-14} sec. Under these conditions all spectral "lines" would be far too broad to observe. This would not, however, be consistent with the experimental observations of Whiddington, and Kruger, and Compton and Boyce, because the line in Whiddington's electron spectrum is comparatively sharp and the far ultraviolet lines, λλ320.4 and 357.5A, are very sharp.

The second alternative is not consistent with the calculations of Kreisler but stands in accord with the electron energy loss experiments and the sharp far ultraviolet lines, λλ320.4 and 357.5A, of helium, as well as the tentative explanation of the solar corona bright lines.

In conclusion, the author wishes to express his most sincere appreciation for the valuable discussions and suggestions of Dr. M. L. Pool, Dr. H. A. Robinson, and Dr. G. H. Shortley during the progress of this experiment.

[15] Kreisler, Physica Acta Polonica **4**, 15 (1935).

The Absorption Spectrum of $Tm_2(SO_4)_3 \cdot 8H_2O$

H. A. BETHE AND F. H. SPEDDING*
Department of Physics and Chemistry, Cornell University, Ithaca, New York
(Received June 12, 1937)

THE absorption spectra of the salts of the rare earths have been attributed by some authors[1] exclusively to transitions within the $4f$ shell; others, including one of the present authors,[2] considered transitions of a $4f$ electron to one of the outer shells, e.g., $5d$, as an alternative possibility. This note is to present evidence for the first assumption and to show that at least semiquantitative agreement may be obtained for Tm salts.

Two theoretical arguments may be given *a priori* for the transitions within the $4f$ shell: First, the sharpness of the absorption lines would be immediately evident in the case of a transition within an inner shell and second, the intensity of the absorption lines is extremely small (about $10^{-8}-10^{-7}$ dispersion electrons for the stronger lines). This indicates that they are due to a "forbidden" transition which would be true for a rearrangement within the $4f$ shell.

Thulium was selected as the rare earth most favorable for a comparison between theory and experiment. Tm IV has its $4f$ shell filled except for two "holes" so that the energy levels are comparatively simple. It is preferable to Pr IV which contains two *electrons* in the $4f$ shell because the spectra of Pr salts (and salts of other "light" rare earths) possess a large number of lines many of which are probably due to coupling with crystal vibrations. The smaller $4f$ shell in Tm will have smaller coupling with vibrations so that we obtain a simpler spectrum representing, probably, only transitions between electronic states. Yb would have an even simpler spectrum than Tm because it has only one hole in the $4f$ shell: But this reduces the spectrum to a single line $^2F_{7/2}-{}^2F_{5/2}$ which lies in the infrared.

The levels of the free ion Tm IV were calculated as follows: For the electrostatic interaction between the electrons, the empirical spectrum of La II (which is analogous to Tm IV) was taken as basis. It was assumed that the spacing between the energy levels without spin-orbit interaction is simply multiplied by a constant factor when we go over from La II to Tm IV which arises (a) from the higher degree of ionization and (b) from the greater "internal" nuclear charge. The effect (a) was estimated from a comparison of the spectra of La II and Pr IV,[4] to introduce a factor of about 2.4. Because of (b), the electrostatic interaction is directly proportional to the effective nuclear charge; taking a screening constant of 34 for the $4f$ shell of all rare earths, this gives for the ratio Tm IV/Pr IV $=(69-34)/(59-34)=1.4$, and therefore Tm IV/La II $=3.3$.

The constant ζ (cf. Condon and Shortley) characteristic of the spin-orbit interaction was found to be about 170 cm^{-1} for La II, from the splitting of the *II* levels which have most nearly Russell-Saunders coupling. We assume that ζ increases again by a factor of 2.4 from La II to Pr IV (probably underestimated) and is proportional to Z_{eff}^3 for ions of the same degree of ionization. This gives another factor $1.4^4=3.8$ from Pr IV to Tm IV, giving $\zeta=1500$ cm^{-1} for Tm IV. In order to get a better value, we calculated the levels of Tm IV including spin-orbit interaction, assuming for ζ values in the neighborhood of 1500 cm^{-1}. Very satisfactory agreement with the position of the line groups in the absorption spectrum of thulium sulfate[4] was obtained for $\zeta=1400$ cm^{-1}. With this value for ζ, the coupling is very far from the Russell-Saunders case. Table I gives the calculated and observed positions of the levels in cm^{-1} above the ground state. For each level, we give the spectroscopic designation of the Russell-Saunders level to which it is connected by an adiabatic change of ζ.

The splitting of the levels in the crystalline field was calculated by using essentially the

* Baker Fellow in Chemistry.
[1] S. Freed, J. Chem. Phys. **5**, 22 (1937); J. H. Van Vleck, J. Phys. Chem. Jan. (1937).
[2] F. H. Spedding, J. Chem. Phys. **5**, 416 (1937).
[3] C. B. Ellis, Phys. Rev. to be published.
[4] Brandtl and Scheiner, Zeits. f. anorg. allgem. Chemie **220**, 107 (1934). Nutting and Meehan, unpublished work. Spedding and Keller, unpublished work.

TABLE I. *Absorption multiplets of* $Tm_2(SO_4)_3 \cdot 8H_2O$.

TERM	CALCULATED 1400 CM^{-1}	OBSERVED CM^{-1}
$^3H_6$	0	0
$^3H_4$	5565	infrared
$^3H_5$	8490	"
$^3F_2$	10740	"
$^3F_4$	13270	14600
$^3F_3$	14560	15150
$^1G_4$	22580	21500
$^1D_2$	23730	21100
$^1I_6$	27680	28000
$^3P_0$	32155	—
$^3P_2$	35020	
$^3P_1$	35290	—
$^1S_0$	57425	—

TABLE II. *Crystalline states of Tm IV in a cubic field.*

	$^3H_6$	CM^{-1} $^1I_6$		
Γ_1	0	183		
Γ_4	14	162		
$\Gamma_{5\alpha}$	31	137		
Γ_2	97	37		
$\Gamma_{5\beta}$	116	9		
Γ_3	122	0		
	$^3H_4$	$^3F_4$		$^1G_4$
Γ_5	0	0		0
Γ_3	64	47		120
Γ_4	85	62.5		160
Γ_1	115	84		216
		$^3F_2$	$^1D_2$	
	Γ_2	0	3	0
	Γ_5	7	5	25
	Γ_4	13		

method of Penney and Schlapp[5] but taking into account the large deviation from Russell-Saunders coupling. The field was assumed to be cubic on the strength of the experimental evidence obtained with erbium.[6] From the experimental data on erbium we also deduced the strength of the cubic field. Table II gives the crystalline states of Tm IV calculated in this way.

The intensity of the absorption lines was calculated on the basis of the following considerations: Direct dipole transitions within the $4f$ shell are forbidden as long as the $4f$ electrons are subject to an electric field symmetrical with respect to inversion at the atomic nucleus. There are therefore three possible types of transitions:

(a) Ordinary quadrupole transitions. Selection rule $\Delta J=0, \pm 1$ or ± 2.

(b) Dipole transitions caused by a *natural* lack of symmetry of the crystalline field. This symmetry may correspond to a term in the potential energy which is either linear or cubic (or of higher order) in the coordinates with respect to the nucleus. The linear term will in general be absent because of the equilibrium condition; moreover, it will give the same selection rules which hold for the ordinary quadrupole radiation. The cubic term will therefore be the most important, and was considered in our calculations. J may change by any amount up to 4.

(c) Dipole transitions caused by coupling with crystal vibrations. In general, only the term of first order in the vibrational amplitude will be important. In this case, the selection rule will be the same as in (a).

The J selection rules should hold rather strictly since the crystal splitting is small compared to the spacing between levels of different J. A simple estimate shows that the quadrupole transitions should, for Tm, be about 10 times as strong as the dipole transitions (b), (c). Since the ground state is $^3H_6$, we expect therefore particularly strong transitions to states with $J=6$ ($^1I_6$), $J=5$ ($^3H_5$, in the infrared) and $J=4$ ($^3H_4$, $^1G_4$, $^3F_4$) which agrees with experiment.

The intensities of the individual lines were calculated, assuming quadrupole transitions in all cases where J changes by 2 or less, and type (b) dipole transitions for larger changes of J. Good agreement was obtained for the transition $^3H_6-{}^3F_4$, and reasonable agreement for the other line groups. A more extensive account of this work will appear in the *Journal of Chemical Physics*.

[5] Penney and Schlapp, Phys. Rev. **41**, 194 (1932).
[6] F. H. Spedding, J. Chem. Phys. **5**, 316 (1937).

The Third Spectrum of Cerium (Ce III)

HENRY NORRIS RUSSELL, *Princeton University, Princeton, New Jersey*
ROBERT B. KING, *Massachusetts Institute of Technology, Cambridge, Massachusetts*
AND
R. J. LANG, *University of Alberta, Edmonton, Alberta, Canada*

(Received June 24, 1937)

Thirty-three triplet and singlet terms of Ce III have been recognized, and account for 294 lines, including almost all of wave-length exceeding 2000A. The *electron configurations* $4f5d$, $4f6p$, $(5d)^2$, $4f6s$, $4f6d$, and $5d6s$, have been almost completely identified. The last three show evidence of JJ coupling. *Zeeman data* by de Bruin and King confirm the classification. The *lowest known level* is $4f5d\ {}^1G_4$ and the *ionization potential* from this to $4f\ {}^2F_{2\frac{1}{2}}$ of Ce IV is 19.5 volts. *The* $(4f)^2$ *configuration may be lower*, but has not been discovered, as its combinations lie in the infrared and the far ultraviolet. *The ultimate lines must be in the infrared*, as is probably the case for the third spectrum of most of the rare earths.

MANY strong lines of cerium in the ultraviolet evidently arise from doubly ionized atoms. A list of these was published by A. S. and R. B. King in 1932.[1] The first attempt to analyze the spectrum was made by Kalia,[2] who found a considerable array of energy levels. Almost all these are real, although their interpretation by means of electron configurations and terms requires change.

Recently de Bruin[3] has published observations of the Zeeman effect, which he employs to correct Kalia's term designations (while confirming his energy levels). The g values, though somewhat perturbed, suffice for unequivocal identification of the term components.

The present work was begun more than three years ago. It is based upon the observations of the Kings at Mount Wilson and on measures with the vacuum spectrograph at Edmonton by Lang, and has resulted in the classification of all but a few weak lines with wave-lengths greater than 2100A, and many beyond this.

In the region of longer wave-length the lines fall into two classes, one sharp, the other diffuse. From general experience it was certain in advance[4] that the former arise from transitions between low and middle energy-levels, and the latter from transitions between these and higher levels. It was soon found that the sharp and diffuse lines corresponded to transitions from Kalia's "low" levels to other groups lying on opposite sides of them, showing that these were really the middle levels and that Kalia's energy scheme was upside down.

The same correction has been made by de Bruin without, however, identifying the high levels or all the lower ones.

An extensive scheme of levels was thus developed. They should form a system of triplets and singlets. To group these into terms was not easy. As might be expected for so heavy an atom, the separations of the components are very wide; the interval rules are not even roughly obeyed; the various terms overlap extensively, and intersystem combinations are strong. Some tentative multiplets were picked out and confirmed by Zeeman observations. These measures [obtained by one of us (R.B.K.) in Pasadena] did not completely resolve any patterns and hardly permitted the calculation of exact g values; but they settled without doubt which levels had the larger inner quantum numbers and showed that the arrangement of the components was "normal" —as might have been assumed in advance, since Ce III is a two-electron system. It was not, however, till the analysis was far advanced that the actual J values could be determined.

It finally became clear that the lowest levels represented a group of triplet and singlet $P\ D\ F\ G\ H$ terms, of which the lowest is the ${}^1G$

[1] A. S. and R. B. King, Astrophys. J. **75**, 40 (1932); Mt. Wilson Contribution No. 441.
[2] Kalia, Ind. J. Phys. **8**, 137 (1933).
[3] de Bruin, Proc. Kon. Akad. Wet. Amsterdam **40**, 334 (1937).
[4] Astrophys. J. **75**, 44 (1932); Mt. Wilson Contribution No. 441, p. 5.

term. Above these and conspicuously isolated were a ^3F and ^1F. The lowest of the middle terms was ^3F, followed by ^3P, ^3G ^3F ^3D, ^1F and two ^1D and ^1G terms.

This unprecedented arrangement can be completely explained if the electron configuration of lowest energy is $4f5d$, followed by $4f6s$. The middle levels are then $5d^2$ and $4f6p$, which account for everything, except one ^1S term predicted and not found (as usually happens). This analysis was completed long before the publication of de Bruin's work, which agrees completely in the assignment of the configurations $4f6s$ and $4f6p$. His unclassified term X_4 is our $d^2\,{}^1G_4$.

A considerable portion of the array $4f5d-4f6p$

TABLE I. *Relative Terms in the Ce III Spectrum.*

Electron Configuration	Term	Level	Level Separations	g Obs.	Electron Configuration	Term	Level	Level Separations	g Obs.
$4f5d$	$^1G_4^0$	*0.00*			$4f6p$	$^1F_3$	47097.24		1.16
$4f5d$	$^3F_2^0$	*545.06*	1680.54		$4f6p$	$^3D_1$	48654.50	−291.63	0.40
	$^3F_3^0$	*2225.60*	1647.95			$^3D_2$	48362.87	1975.48	0.99
	$^3F_4^0$	*3873.55*				$^3D_3$	50338.35		1.24
$4f5d$	$^3H_4^0$	*1850.80*	1233.70		$4f6p$	$^1G_4$	51271.60		1.05
	$^3H_5^0$	*3084.50*	1989.17						
	$^3H_6^0$	*5073.67*			$4f6p$	$^1D_2$	51278.60		1.08
$4f5d$	$^3G_3^0$	*2988.50*	1571.53		$5d6s$	$^3D_1$	60056.73	675.52	
	$^3G_4^0$	*4560.03*	1488.83			$^3D_2$	60732.25	1540.12	
	$^3G_5^0$	*6048.86*				$^3D_3$	62272.37		
$4f5d$	$^1D_2^0$	*3294.49*			$5d6s$	$^1D_2$	62556.2		
$4f5d$	$^3D_1^0$	*5645.27*	978.37		$4f6d$	$^3F_2^0$	*86070.10*	312.26	
	$^3D_2^0$	*6623.64*	226.09			$^3F_3^0$	*86382.36*	2177.36	
	$^3D_3^0$	*6849.73*				$^3F_4^0$	*88559.72*		
$4f5d$	$^3P_0^0$	*8300.30*	35.47		$4f6d$	$^3D_1^0$	*86315.47*	628.07	
	$^3P_1^0$	*8335.77*	1028.89			$^3D_2^0$	*86943.54*	1857.15	
	$^3P_2^0$	*9364.66*				$^3D_3^0$	*88800.69*		
$4f5d$	$^1F_3^0$	*9223.85*			$4f6d$	$^3G_3^0$	*86463.55*	343.27	
						$^3G_4^0$	*86806.82?*	2093.58	
$4f5d$	$^1H_5^0$	*12875.22*				$^3G_5^0$	*88900.40*		
$4f5d$	$^1P_1^0$	*15166.50*			$4f6d$	$^3H_4^0$	*86765.35*	613.72	
						$^3H_5^0$	*87379.07*	1867.48	
$4f6s$	$^3F_2^0$	*15958.27*	228.25	0.665		$^3H_6^0$	*89246.55*		
	$^3F_3^0$	*16186.52*	2012.08	1.07					
	$^3F_4^0$	*18198.60*		1.27	$4f6d$	$^3P_0^0$	—		
						$^3P_1^0$	*87598.66*	1826.69	
$4f6s$	$^1F_3^0$	*18571.47*		1.035		$^3P_2^0$	*89425.35*		
$(5d)^2$	$^3F_2$	37163.31	1498.32		$4f6d$	$^1F_3^0$	*88642.27*		
	$^3F_3$	38661.63	1578.82						
	$^3F_4$	40240.45			$4f6d$	$^1G_4^0$	*88480.12*		
$(5d)^2$	$^1D_2$	43612.74			$4f6d$	$^1D_2^0$	*88738.90*		
$(5d)^2$	$^3P_0$	44798.84	598.09		$4f6d$	$^1H_5^0$	*89946.60*		
	$^3P_1$	45396.93	1369.59						
	$^3P_2$	46766.52				1_0^0	*88455.93*		
						2_3^0	*88674.42*		
$4f6p$	$^3G_3$	44989.30	4173.93	0.87	$5d6p?$	3_1^0	*92288.61*		
	$^3G_4$	49163.23	1752.88	1.135		4_2^0	*92548.41*		
	$^3G_5$	50916.11		1.21		5_3^0	*92744.25*		
						6_2^0	*93097.15*		
$4f6p$	$^3F_2$	45127.12	2857.23	0.85		7_3^0	*94686.28*		
	$^3F_3$	47984.35	27.43	0.29		8_4^0	*95890.54*		
	$^3F_4$	48011.78		1.90		9_2^0	*97689.62*		
						10_1^0	*98967.75*		
$(5d)^2$	$^1G_4$	46780.19		1.06					

TABLE II. *Intensities in multiplets of Ce III.*

		$(5d)^2$								$4f6p$											
		^3F			^3P			^1G	^1D	^3G			^3F			^3D			^1G	^1F	^1D
$4f5d$	J	4	3	2	2	1	0	4	2	5	4	3	4	3	2	3	2	1	4	3	2
$^3H^0$	6									*100*											
	5							*12*		*9*	*75*		*40*						*4*		
	4	4								*5*	*2*	*20*	*5*	*100*		*15*			*10*	*12*	
$^3G^0$	5	100†						*15*		[*135*]	*30*		*12*						*15*		
	4	10	100					*15*		*2*	*15*	[*15*]	*20*	*25*		*15*			*3*	*35*	
	3		10	80					[*8*]		*2*	*30*			*35*	*5**	*20*		*2*		
$^3F^0$	4	50	25					*6*		*15**	*20*		*20*	*2*		*30*			*25*	*7*	
	3	4	60	15				*4*				*12*	*12*	*15*	*6*	m	*20*			*20*	*18*
	2		4	60	*2d*							*18*		*3*	*25*		*8*	*15*			
$^3D^0$	3		2		6			10	60		40	15	*10*	*15*	[*2*]	*10*	*12*			*20*	*3*
	2				3	30								*10d**	[*2*]		*25*	*10*		*20*	*15*
	1					4	12								*18*			*15*			[*3*]
$^3P^0$	2		4		10	8						1		2		*30*	*6*	[*8*]		50	15
	1				4		5		8						10		*20*	15*			3
	0					6												*12*			
$^1H^0$	5							15			80		10						400		
$^1G^0$	4	5						*30*			*25*	*40*	*7*	*35**		*15*			*30*	*12*	
$^1F^0$	3				30				30			8		6		*35*	[*3*]		*18*	4	*18*
$^1D^0$	2								50*			3		*10*		*15**	*20*	*12*		8	*35*
$^1P^0$	1				2										1		8				150
$4f6s$																					
$^3F^0$	4							60		600	400		150	m		200			200	200	
	3				2			4			500	300	250	200	150	10	200		80	7	
	2				3							150		400	125		200	100		3	
$^1F^0$	3				3			80	m		*6h*		50	20		300			200	100	125
$4f6d$																					
$^3H^0$	6									150*h*											
	5									m	60*h*		20*h*								
	4									[2]	3*h*	2*h*		80*h*							
$^3G^0$	5							6*h*		30*h*	4*h*		10*h*						[*12*]		
	4										20*h**	1*		20*h*			20*h*§			1*h*	
	3											30*h*			10*h*		4*h*		1*h*		
$^3F^0$	4									20*h**	2*h*		4*h*						2*h*	6*h*	
	3										10*h*		2*h*		10*h*				3*h*		
	2													3	20*h*			1			
$^3D^0$	3										4*h*					30*h*			10*h*		
	2													2*h*	1		15*h*	4*h*			
	1																4*h*	6*h*			
$^3P^0$	2															30*h*					2*h*
	1																5*h*	4*h*			
	0																				
$^1H^0$	5							8											70*h*		
$^1G^0$	4																		10*h*	60*h*	
$^1F^0$	3																		4*h*	20*h*	2*h*
$^1D^0$	2																			10*h*	8*h*

† Blend with Ce II. * Blend. *m* Masked. § May be accidental.

extends into the vacuum region, as far as 1950A. Lang's measures complete it, and leave very few lines of the super-multiplet missing.

The high levels, like the low, are odd. They can be matched in a fairly satisfactory way with the configuration $4f6d$. The intensities are irregular (which is not surprising) and the assignments of some levels (such as that here called $^3G_4^0$) are uncertain, but the general scheme appears to be reliable. Later study revealed higher middle terms ^3D, ^1D evidently from $5d6s$, giving good multiplets, and combining with still higher levels (about 95,000) which probably belong to $5d6p$—though they are not completely enough known to group into terms.

The scheme thus developed accounts for 294 lines including all those of any strength in wavelength exceeding 2000A. Under ordinary circumstances, it might be concluded that the spectrum was almost completely analyzed. But no evidence at all has been found of the $(4f)^2$ configuration. This might be expected to be very low—as $4f$ is nearly 50,000 cm^{-1} below $5d$ in Ce IV. Failure to find it can be explained only by assuming that it is so nearly at the same level as $4f5d$ that the transitions between the two give lines lying exclusively in the infrared. In this case the $(4f)^2$ terms could be detected only by their combinations with $4f6d$, which would have wave numbers of the order of 90,000. The $4f5f$ configuration should then be almost superposed upon $4f6d$, and be observable only by the combinations with $4f5d$—also far in the Schumann region. The spectrum of the cerium hot-spark in this region is very rich, but it has not yet been practicable to disentangle such combinations from it.

The lowest observed level, $df\ ^1G^0$, may therefore not be the ground level, although all known strong lines of easy excitation have been accounted for. A similar situation exists in La III, where the $4f\ ^2F$ term has not yet been found, and may be lower than $5d\ ^2D$; and the same may happen in the third spectra of other rare earths. As the analysis of Ce III stands, it affords the first exception to Hund's rule that the lowest level of the ground configuration is that of highest L value among the terms of greatest multiplicity.

The term values finally adopted are given in Table I. The terms are grouped separately, in order of the lowest level in each—though the high odd levels, for which the term assignments are not always certain, might as well have been arranged in the order of the individual energy levels.

The usual custom of denoting the terms by letters has been deliberately avoided, since it is not certain whether the $4f5d$ group is the lowest

TABLE III. *Levels in each configuration measured from lowest level within it.*

$4f5d$			$4f6p$			$4f6s$			$(5d)^2$			$5d6s$		
Term	Ce III	La II	Term	Ce III	La II	Term	Ce III	La II	Term	Ce III	La II	Term	Ce III	La II
$^1G_4^0$	0	0	$^3G_3$	0	0	$^3F_2^0$	0	0	$^3F_2$	0	0	$^3D_1$	0	501
$^3F_2^0$	545	612	$^3F_2$	138	335	$^3F_3^0$	228	227	$^3F_3$	1498	1016	$^3D_2$	675	1197
$^3H_4^0$	1850	1226	$^1F_3$	2408	1757	$^3F_4^0$	2240	1551	$^3F_4$	3077	1971	$^3D_3$	2216	1856
$^3F_3^0$	2225	1636	$^3F_3$	2995	1502	$^1F_3^0$	2613	1626	$^1D_2$	6449	10095	$^1D_2$	2500	0
$^3G_3^0$	2988	3803	$^3F_4$	3022	2338				$^3P_0$	7636	5249			
$^3H_5^0$	3084	1981	$^3D_2$	3373	2769				$^3P_1$	8234	5718			
$^1D_2^0$	3294	2296	$^3D_1$	3665	3081				$^3P_2$	9603	6227			
$^3F_4^0$	3873	2615	$^3G_4$	4174	1720				$^1G_4$	9617	7473			
$^3G_4^0$	4560	4732	$^3D_3$	5349	3950				$^1S_0$	—	—			
$^3H_6^0$	5073	3150	$^3G_5$	5927	3565									
$^3D_1^0$	5645	4842	$^1G_4$	6283	3769									
$^3G_5^0$	6048	5683	$^1D_2$	6289	5005									
$^3D_2^0$	6623	5507												
$^3D_3^0$	6849	5938												
$^3P_0^0$	8300	6084												
$^3P_1^0$	8335	6106												
$^1F_3^0$	9223	7923												
$^3P_2^0$	9364	6647												
$^1H_5^0$	12875	11926												
$^1P_1^0$	15166	10824												

—in which case the rules assign to its terms the letters a, b, c,—or next to the lowest when they get the letters z, y, x. The electron configurations —which are securely known in this relatively simple spectrum—are used instead. In the abbreviated form $fs = 4f6s$, $fp = 4f6p$, $fd = 4f5d$, $d^2 = (5d)^2$, and $f \cdot d = 4f6d$.

The g values derived by de Bruin are added for completeness.

The intensities of the combinations between the terms of the configurations d^2, fp, and fd, fs, $f \cdot d$ are given in Table II. King's estimates are in Roman figures, Lang's in italics. As the two are on different scales, all the lines in a given multiplet have been recorded (when possible) on the same system.

The relative arrangement of the levels belonging to the same configuration is strikingly similar in La II and Ce III. Table III gives the levels in each configuration, measured from the lowest level within it, in the order in which they appear in Ce III. The order in La II is very nearly the same. The discordance for $d^2\,{}^1D$, $ds\,{}^1D$ arises from a well-known perturbation in La II—where there is also a perturbation between $fd\,{}^3F_4$, $fd\,{}^3G_4$. The $(4f)^2$ configuration in La II extends from $e\,{}^3H_4$ at 55107 to $f\,{}^3P_2$ (62506) and $g\,{}^1S_0$ (69505). The corresponding terms in Ce III should be more widely spaced, and range over about 12,000 units (not counting the ${}^1S_0$). If their median were more than about 10,000 units away from that of $4f5d$, some of the combinations should be observable in the deep red.

The general arrangement of the terms in the fd, fp, and d^2 configurations indicates an approximation to LS coupling, as Condon and Shortley[5] have shown to be the case for La II. The fs and ds groups, however, approach JJ coupling, and the same is true for $4f6d$. Here the singlets, and the component of highest J in the triplets, lie between 88480 and 89946, while the other components of the triplets are all between 86070 and 87598. The means for the groups, 88971 and 86747, differ by 2224, while the separation of the parent $4f^2F$ term in Ce IV is 2253.[6] For $4f6s$ the corresponding difference is 2193.

The application of a Rydberg formula to the corresponding components of the $4f5d$ and $4f6d$ terms gives values for the upper limit ranging from 173800 to 170400, with mean 172500, and for the lower limit 171900 to 168800, mean 170500. This corresponds to an ionization potential of 21.0 volts from $fd\,{}^1G_4$ of Ce III to $f^2F_{2\frac{1}{2}}$ of Ce IV.

It is however certain that the Rydberg denominator n^* increases considerably from $5d$ to $6d$. The increase Δn^* in the comparable case of La II has been estimated as 0.15,[7] though it may be as great as 0.20. Taking the mean of the nine levels with limit ${}^2F_{3\frac{1}{2}}$, and of the nine with limit ${}^2F_{2\frac{1}{2}}$, we find easily with the aid of the Rydberg tables[8]

Limit	${}^2F_{3\frac{1}{2}}$		${}^2F_{2\frac{1}{2}}$
mean for $5d$	6289		3984
mean for $6d$	88971		86747
n^*	2.5142		2.5133
	3.6642		2.6633
Terms	156240		156357
	73557		73593
Limit	162529		160341
Level in Ce IV	2253		0
I.P.	160276		160341
Mean	160308	=	19.77 volts

If Δn is assumed to be 0.20, the I.P. is 157450 or 19.42 volts. The f^2 configuration may be as much as a volt lower than fd, but not two volts. The approximate value 20 ± 1 volts may therefore be adopted. This is lower than any other third ionization potential except that of La III (19.1).

The isoelectronic sequence Ba I, La II, Ce III, is of unusual interest. In Ba I the lowest configurations are $(6s)^2$ and $6s5d$; in La II, $(5d)^2$ and $5d6s$; in Ce III, so far as known, $4f5d$ and $4f6s$. These three spectra, though similar in nature, are all very different in detail. The next member of the sequence, Pr IV, will have $(4f)^2$ as the low configuration, and again be quite different.

A list of all the classified lines of Ce III is given in Table IV. The first column gives the wave-length according to King and King; the second, the decimal part from Lang's unpublished measures; the third, King's intensity in the spark in air; the fourth, Lang's intensity in the vacuum spark, or, in a few cases, in the spark in nitrogen (denoted by parentheses) or in air (by brackets). Next follows the wave number

[5] Shortley, Phys. Rev. **37**, 1025 (1931).
[6] Lang, Can. J. Res. **A14**, 127 (1936).
[7] Russell and Meggers, Nat. Bur. Stand. J. Research **9**, 664 (1932).
[8] Princeton, 1934.

TABLE IV. *Classified lines of Ce III.*

λ King	λ Lang	Intensity King	Intensity Lang	Wave Number Vac.	Wave Number o−c King	Wave Number o−c Lang	Multiplet Designation
3543.999		80		28208.68	−0.04		$fs^1F_3^0 - d^2\,{}^1G_4$
3504.596		100		28525.83	+0.06		$fs^1F_3^0 - fp^1F_3$
3497.755		60		28581.62	+0.03		$fs^3F_4^0 - d^2\,{}^3G_4$
3470.894		300		28802.80	+0.02		$fs^3F_3^0 - fp^3G_3$
3459.374		200		28898.71	+0.07		$fs^3F_4^0 - fp^1F_3$
3454.368		150		28940.59	−0.01		$fs^3F_3^0 - fp^3F_2$
3443.609		150		29031.01	−0.02		$fs^3F_2^0 - fp^3G_3$
3427.332		125		29168.88	+0.03		$fs^3F_2^0 - fp^3F_2$
3412.334		4		29297.08	+0.11		$fd^3P_2^0 - d^2\,{}^3F_3$
3398.910		20		29412.79	−0.09		$fs^1F_3^0 - fp^3F_3$
3395.735		50		29440.28	−0.03		$fs^1F_3^0 - fp^3F_4$
3356.410[1, 2]		6		29785.21	−0.54		$(fs^3F_4^0 - fp^3F_3)$
3353.262		150		29813.17	−0.01		$fs^3F_4^0 - fp^3F_4$
3336.742		1		29960.77	+0.15		$fd^1P_1^0 - fp^3F_2$
3280.78		2		30471.81	−0.07		$ds^3D_3 - 5_3^0$
3269.129		2		30580.40	+0.40		$fs^3F_3^0 - d^2\,{}^3P_2$?
3267.92		6*h*		30591.72	−0.04		$fs^1F_3^0 - fp^3G_4$
3267.72		4		30593.59	−0.08		$fs^3F_3^0 - d^2\,{}^1G_4$
3244.950		3		30808.26	+0.01		$fs^3F_2^0 - d^2\,{}^3P_2$
3234.161[3]		7		30911.03	+0.31		$fs^3F_3^0 - fp^1F_3$?
3228.564		400		30964.61	−0.02		$fs^3F_4^0 - fp^3G_4$
3210.48		3		31139.02	+0.05		$fs^3F_2^0 - fp^1F_3$
3168.02		25*h*		31556.36	0.00		$ds^3D_2 - 3_1^0$
3163.644		2		31600.00	−0.02		$fd^1P_1^0 - d^2\,{}^3P_2$
3147.05		300		31766.62	−0.26		$fs^1F_3^0 - fp^3D_3$
3143.956		200		31797.88	+0.05		$fs^3F_2^0 - fp^3F_3$
3142.551		2		31812.09	+0.19		$fd^3D_3^0 - d^2\,{}^3F_2$
3141.247		250		31825.30	+0.04		$fs^3F_2^0 - fp^3F_4$
3122.93		4*h*		32011.96	−0.04		$ds^3D_2 - 5_3^0$
3121.548		400		32026.13	+0.05		$fs^3F_2^0 - fp^3F_2$
3110.516		200		32139.71	−0.04		$fs^3F_4^0 - fp^3D_3$
3106.974		200		32176.35	0.00		$fs^3F_3^0 - fp^3D_2$
3088.86		5*h*		32365.04	+0.14		$ds^3D_2 - 6_2^0$
3085.089		200		32404.60	0.00		$fs^3F_2^0 - fp^3D_2$
3076.82		6*h*		32491.68	0.00		$ds^3D_1 - 4_2^0$
3057.575		100		32696.18	−0.05		$fs^3F_2^0 - fp^3D_1$
3057.214		200		32700.04	−0.09		$fs^1F_3^0 - fp^1G_4$
3056.556		125		32707.08	−0.05		$fs^1F_3^0 - fp^1D_2$
3055.585		600		32717.47	−0.04		$fs^3F_4^0 - fp^3G_5$
3031.559		500		32976.76	+0.05		$fs^3F_3^0 - fp^3G_4$
3025.73		8		33040.28	−0.14		$ds^3D_1 - 6_2^0$
3022.736		200		33073.01	+0.01		$fs^3F_4^0 - fp^1G_4$
3011.493		8		33196.48	+0.11		$fd^1P_1^0 - fp^3D_2$
2973.716		50		33618.17	0.00		$ds^3D_3 - 8_4^0$
2948.564		15		33904.93	−0.04		$fd^1H_5^0 - d^2\,{}^1G_4$
2944.3		15		33954.0	0.0		$ds^3D_2 - 7_3^0$
2931.558		100		34101.60	0.00		$fd^3G_4^0 - d^2\,{}^3F_3$
2927.258		10		34151.70	−0.13		$fs^3F_3^0 - fp^3D_3$
2925.283		80		34174.75	−0.06		$fd^3G_3^0 - d^2\,{}^3F_2$
2923.84		100		34191.62	+0.03		$fd^3G_5^0 - d^2\,{}^3F_4$
2907.064		30		34388.92	+0.03		$fd^1F_3^0 - d^2\,{}^1D_2$
2873.722		25		34787.89	−0.19		$fd^3F_4^0 - d^2\,{}^3F_3$
2861.416		15		34937.50	−0.21		$fd^3F_3^0 - d^2\,{}^3F_2$
2849.372		80		35085.17	+0.09		$fs^3F_3^0 - fp^1G_4$
2847.3		3*h*		35110.7	−0.1		$fp^1G_4 - f\cdot d^3F_3^0$
2845.19		10		35136.73	+0.17		$fd^1H_5^0 - fp^3F_4$
2840.7		1*h*		35192.3	+0.3		$fp^1G_4 - f\cdot d^3G_3^0$
2833.868		8		35277.11	+0.14		$fd^3P_1^0 - d^2\,{}^1D_2$
2822.648		8		35417.33	+0.08		$ds^3D_3 - 9_3^0$
2806.3		1		35623.6	−1.0		$fd^3P_2^0 - fp^3G_3$
2802.408		10*s*		35673.11	−0.02		$fd^3G_3^0 - d^2\,{}^3F_3$
2801.824		10*s*		35680.54	+0.12		$fd^3G_4^0 - d^2\,{}^3F_4$
2795.158		8		35765.63	+0.18		$fd^1F_3^0 - fp^3G_3$

[1] This line is due to Ce II and masks the expected line of Ce III.
[2] Parentheses in last column denote that line is masked.
[3] Near strong line of Ce II.

TABLE IV—(*Continued*).

λ King	λ Lang	Intensity		Wave Number Vac.	Wave Number $o-c$		Multiplet Designation
		King	Lang		King	Lang	
2788	66		2	35849.0		[−0.2]	$fp^3G_5 - f\cdot d^3H_4^0$
2774.473		8*s*		36032.26	−0.01		$fd^3P_2^0 - d^2\,{}^3P_1$
2768.339		150		36112.10	0.00		$fd^1P_1^0 - fp^1D_2$
2754.912		80		36288.10	+0.09		$fd^1H_5^0 - fp^3G_4$
2748.936		50*s*		36366.98	+0.08		$fd^3F_4^0 - d^2\,{}^3F_4$
2743.736		60*s*		36435.90	−0.13		$fd^3F_3^0 - d^2\,{}^3F_3$
2741.688		5		36463.11	+0.04 +0.15		$fd^3P_1^0 - d^2\,{}^3P_0$ $(fp^3G_5 - f\cdot d^3H_5^0)$
2730.069		60*s*		36618.29	+0.04		$fd^3F_2^0 - d^2\,{}^3F_2$
2719.329		60*s*		36762.90	−0.11		$fd^3D_3^0 - d^2\,{}^1D_2$
2717.22		10		36791.44	+0.09		$fd^3P_1^0 - fp^3F_2$
2705.026		2		36957.28	−0.09		$ds^3D_2 - 9_2^0$
2694.857		6*s*		37096.73	+0.10		$fd^3P_0^0 - d^2\,{}^3P_1$
2686.74		10*h*		37208.80	+0.28		$fp^1G_4 - f\cdot d^1G_4^0$
2685.99		10*h*		37219.18	+0.05		$fp^3G_4 - f\cdot d^3F_3^0$
2681.03		2*h*		37288.04	−0.08		$fp^1G_4 - f\cdot d^3F_4^0$
2675.6		2*h*		37363.7	0.0		$fp^1D_2 - f\cdot d^1F_3^0$
2675.08		4*h*		37370.97	+0.30		$fp^1G_4 - f\cdot d^1F_3^0$
2673.3		4*h*		37395.8	0.0		$fp^1D_2 - 2_3^0$
2672.857		10*s*		37402.05	+0.19		$fd^3P_2^0 - d^2\,{}^3P_2$
2671.9		1		37415.4	−0.2		$fp^3D_1 - f\cdot d^3F_2^0$
2668.69		8*h*		37460.45	+0.15		$fp^1D_2 - f\cdot d^1D_2^0$
2663.80		10*h*		37529.21	+0.12		$fp^1G_4 - f\cdot d^3D_3^0$
2662.836		30*s*		37542.79	+0.12		$fd^1F_3^0 - d^2\,{}^3P_2$
2658.6		3*h*		37602.6	+0.5		$fp^3G_4 - f\cdot d^3H_4^0$
2656	77		[12]	37628.5		−0.3	$fp^1G_4 - f\cdot d^3G_5^0$
2655.71		20*h*		37643.53	−0.08 −0.06		$fp^3G_5 - f\cdot d^3F_4^0$ $fp^3G_4 - f\cdot d^3G_4^0$?
2654.48		6*h*		37660.97	0.00		$fp^3D_1 - f\cdot d^3D_1^0$
2649.418		50		37732.92	+0.34		$fd^3P_2^0 - fp^1F_3$
2639.57		4		37873.69	+0.30		$fd^1F_3^0 - fp^1F_3$
2634.08		4*h*		37952.62	+0.02		$fp^3D_2 - f\cdot d^3D_1^0$
2631.88		30*h*		37984.34	+0.05		$fp^3G_5 - f\cdot d^3G_5^0$
2629.773		4		38014.77	−0.08		$fd^3F_3^0 - d^2\,{}^3F_4$
2624.86		3		38085.92	+0.17		$fp^3F_3 - f\cdot d^3F_2^0$
2623.83		4*h*		38100.87	+0.19		$fp^3D_2 - f\cdot d^3G_3^0$
2622.753		4*s*		38116.52	−0.05		$fd^3F_2^0 - d^2\,{}^3F_3$
2621.151		15		38139.81	+0.24		$fd^3D_3^0 - fp^3G_3$
2620.68		2*h*		38146.66	−0.09		$fp^1D_2 - f\cdot d^3P_2^0$
2615.93		60*h*		38215.93	+0.09		$fp^3G_4 - f\cdot d^3H_5^0$
2614.58		3*h*		38235.66	+0.16		$ds^3D_2 - 10_1^0$
2611	78		[2]	38276.6		−0.8	$fd^3D_3^0 - fp^3F_2$?
2610.91		4*h*		38289.40	+0.36		$fp^3D_1 - f\cdot d^3D_2^0$
2608.114		150*h*		38330.44	0.00		$fp^3G_5 - f\cdot d^3H_6^0$
2605.3		2*h*		38371.8	+1.2		$fp^3F_4 - f\cdot d^3F_3^0$?
2604.078		4*s*		38389.85	+0.20		$fd^3H_4^0 - d^2\,{}^3F_4$
2603.646		400		38396.22	−0.16		$fd^1H_5^0 - fp^1G_4$
2601.32		4*s*		38430.55	−0.20		$fd^3P_1^0 - d^2\,{}^3P_2$
2600.408		20*h*		38444.02	+0.07		$fp^3D_2 - f\cdot d^3G_4^0$ [4]
2599.18		30*h*		38462.19	−0.15		$fp^3D_3 - f\cdot d^3D_3^0$
2596	42		2	38503.1		−0.4	$fd^3D_2^0 - fp^3F_2$
2591.19		15*h*		38580.78	+0.11		$fp^3D_2 - f\cdot d^3D_2^0$
2588.58		2		38619.68	−0.01		$fd^3P_2^0 - fp^3F_3$
2584.87		70*h*		38675.10	+0.10		$fp^1G_4 - f\cdot d^1H_5^0$
2579.17		6		38760.57	+0.07		$fd^1F_3^0 - fp^3F_3$
2578.34		30*s*		38773.04	−0.25		$fd^3D_2^0 - d^2\,{}^3P_1$
2577.828		80*h*		38780.75	−0.25		$fp^3F_3 - f\cdot d^3H_4^0$
2575.06		20*h*		38822.43	−0.04		$fp^3F_3 - f\cdot d^3G_4^0$
2569.21		4		38910.82	−0.20		$ds^3D_1 - 10_1^0$
2567.02		4*h*		38944.02	−0.14		$fp^3D_1 - f\cdot d^3P_1^0$
2566.02		2*h*		38959.19	0.00		$fp^3F_3 - f\cdot d^3D_2^0$
2563.450		6		38998.24	+0.03		$fd^3P_2^0 - fp^3D_2$
2557.628	76	30*h*	12	39087.01	+0.01	−2.0	$fp^3D_3 - f\cdot d^3P_2^0$
2554.3	22	1	[3]	39137.9	−1.1	+0.2	$fd^1F_3^0 - fp^3D_2$
2553.28	28	12*s*	3	39153.57	0.00	0.0	$fd^3D_1^0 - d^2\,{}^3P_0$

[4] Either this is a coincidence or the level $f\cdot d^3G_4^0$ is wrongly identified.

TABLE IV—(*Continued*).

λ KING	λ LANG	INTENSITY		WAVE NUMBER VAC.	WAVE NUMBER $o-c$		MULTIPLET DESIGNATION
		King	Lang		King	Lang	
2547.92	90	5*h*	1	39235.93	+0.14	+0.4	$fp^3D_2 - f\cdot d^3P_1^0$
2544.39	37	3*h*	[8]	39290.36	+0.52	+0.9	$fd^3P_2^0 - fp^3D_1$
2539.43	42	20*h*	10	39367.10	−0.19	−0.1	$fp^3F_4 - f\cdot d^3H_5^0$
2537.6	70	2*h*	[3]	39395.5	−1.0	−2.6	$fp^3G_4 - f\cdot d^3F_4^0$
2532.040	02	100	18	39481.98	+0.13	+0.5	$fd^3D_1^0 - fp^3F_2$
2522.11	06	4*h*	0	39637.42	−0.04	+0.7	$fp^3G_4 - f\cdot d^3D_3^0$
2517.6		1*h*		39708.4	−1.2		$fp^1F_3 - f\cdot d^3G_4^0$
2515.77	72	4*h*	[5]	39737.30	+0.13	+0.9	$fp^3G_4 - f\cdot d^3G_5^0$
2514.864	85	4*s*	[12]	39751.62	−0.04	+0.1	$fd^3D_1^0 - d^2\,{}^3P_1$
2504.454	45	6*s*	4	39916.84	+0.05	+0.1	$fd^3D_3^0 - d^2\,{}^3P_2$
2503.605	60	10	5	39930.37	−0.09	0.0	$fd^3D_3^0 - d^2\,{}^1G_4$
2497.56	53	60	20	40027.01	−0.09	+0.4	$fd^3P_1^0 - fp^3D_2$
2490.35	32	3*s*		40142.89	+0.01	+0.5	$fd^3D_2^0 - d^2\,{}^3P_2$
2484.31	30	5*s*	0	40240.48	+0.03	+0.2	$fd^1G_4^0 - d^2\,{}^3F_4$
2483.88	85	60	20	40247.44	−0.07	+0.4	$fd^3D_3^0 - fp^1F_3$
2479.50	50	50	15	40318.53	+0.28 −0.20	+0.3 −0.2	$fd^1D_2^0 - d^2\,{}^1D_2$ $fd^3P_1^0 - fp^3D_1$
2477.31	30	40	12	40354.17	0.00	+0.1	$fd^3P_0^0 - fp^3D_1$
2472.71	68	4	[15]	40429.24	−0.03	+0.4	$fd^3G_4^0 - fp^3G_3$
2471.81	85	15*h*	5	40443.96	−0.19	−0.9	$fp^3F_4 - 1^0$
2470.00	96	150	20	40473.59	−0.01	+0.6	$fd^3D_2^0 - fp^1F_3$
2465.49		4*h*		40547.62	−0.32		$fp^3F_4 - f\cdot d^3F_4^0$
2460.86	83	2*s*	[8]	40623.91	−0.33	+0.2	$fd^3G_3^0 - d^2\,{}^1D_2$
2454.37	35	50*s*	15	40731.32	−0.01	+0.3	$fd^3G_5^0 - d^2\,{}^1G_4$
2444.93	88	10*h*	5	40888.57	−0.05	+0.8	$fp^3F_4 - f\cdot d^3G_5^0$
2441.69	62	20*h*	7	40942.82	−0.16	+1.0	$fp^3F_2 - f\cdot d^3F_2^0$
2439.87	82	250	30	40973.36	−0.33	+0.5	$fd^3P_2^0 - fp^3D_3$
2431.51	45	300	35	41114.22	−0.28	+0.7	$fd^1F_3^0 - fp^3D_3$
2430.31	25	60	15	41134.52	−0.10	+0.9	$fd^3D_3^0 - fp^3F_3$
2428.68	63	15*s*	10	41162.13	+0.08	+1.0	$fd^3D_3^0 - fp^3F_4$
2423.20	10	10*h*	12	41255.21	−0.03	+1.6	$fp^3F_2 - f\cdot d^3F_2^0$
2418.44	37	10*h*	9	41336.40	−0.03	+1.2	$fp^3F_2 - f\cdot d^3G_3^0$
2417.11	09	30*h*	10*d*	41359.14	+0.45 −1.57	+0.8 −1.2	$fp^1F_3 - 1^0$ $fd^3D_2^0 - fp^3F_2$
2415.74	67	60*h*	15	41382.60	−0.28	+0.9	$fp^1F_3 - f\cdot d^1G_4^0$
2411.06	00	6*h*	10	41462.92	+0.44	+1.4	$fp^1F_3 - f\cdot d^3F_4^0$
2410.41	32	30*h*	12	41474.10	−0.15	+1.4	$fp^3G_3 - f\cdot d^3G_3^0$
2408.15	05	30*s*	12	41513.02	−0.12	+1.6	$fd^3D_3^0 - fp^3D_2$
2406.31	32	20*h*	10	41544.76	−0.27	−0.4	$fp^1F_3 - f\cdot d^1F_3^0$
2404.44	40	6*h*	7	41577.06	−0.12	+0.6	$fp^1F_3 - 2_3^0$
2400.72	71	10*h*	8	41641.48	−0.18	0.0	$fp^1F_3 - f\cdot d^1D_2^0$
2398.76	79	8*h*	8	41675.51	−0.23	−0.7	$d^2\,{}^1G_4 - 1^0$
2397.66		3*s*		41694.62	−0.19		$fd^1D_2^0 - fp^3G_3$
2395.10	06	60	25	41739.18	−0.05	+0.7	$fd^3D_2^0 - fp^3D_2$
2393.00	88	2*h*	3	41775.81	−0.24	+1.9	$fp^3G_3 - f\cdot d^3H_4^0$
2390.7	51	1	2	41816.0	−1.5 −0.4	+1.8 +2.9	$fp^3G_3 - f\cdot d^3G_4^0$? $fp^3F_2 - f\cdot d^3D_2^0$
2386.23	11	3*h*	5	41894.32	+0.09	+2.2	$d^2\,{}^1G_4 - 2_3^0$
2385.11	08	15	10	41913.99	+0.05	+0.6	$fd^3P_2^0 - fp^1D_2$
2382.33	30	30	12	41962.90	−0.02	+0.5	$fd^3G_5^0 - fp^3F_4$
2380.18	14	200	30	42000.80	0.00	+0.7	$fd^3G_3^0 - fp^3G_3$
2378.48	43	6	10	42030.82	−0.04	+0.7	$fd^3D_2^0 - fp^3D_1$
2377.53	48	40	18	42047.61	−0.14	+0.7	$fd^1F_3^0 - fp^1G_4$
2377.13	06	50	18	42054.68	−0.07	+1.1	$fd^1F_3^0 - fp^1D_2$
2373.44	29	6*h*	7	42120.06	−0.15	+2.5	$d^2\,{}^1G_4 - f\cdot d^3G_5^0$
2372.39	35	300	35	42138.70	+0.08	+0.8	$fd^3G_3^0 - fp^3F_2$
2371.15	13	4*s*	[3]	42160.74	−0.04	+0.3	$fs^1F_3^0 - ds^3D_2$
2367.81	79	30*s*	15	42220.20	+0.04	+0.4	$fd^3G_4^0 - d^2\,{}^1G_4$
2362.58	52	40	20	42313.66	+0.16	+1.2	$fd^3D_3^0 - fp^3G_4$
2350.16	10	200	35	42537.26	+0.05	+1.1	$fd^3G_4^0 - fp^1F_3$
2337.71	66	25	12	42763.77	+0.07	+1.0	$fd^3F_3^0 - fp^3G_3$
2330.19	15	4	6	42901.77	+0.25	+1.0	$fd^3F_3^0 - fp^3F_2$
2329.92	87	6*s*	6	42906.74	+0.10	+1.1	$fd^3F_4^0 - d^2\,{}^1G_4$
2327.95	91	3	4	42943.05	+0.20	+1.0	$fd^3P_1^0 - fp^1D_2$
2324.37	32	50	15	43009.18	−0.05	+0.9	$fd^3D_1^0 - fp^3D_1$
2318.70	68	200	30	43114.34	−0.03	+0.3	$fd^3G_5^0 - fp^3G_4$

TABLE IV—(*Continued*).

λ King	λ Lang	Intensity King	Intensity Lang	Wave Number Vac.	Wave Number o−c King	Wave Number o−c Lang	Multiplet Designation
2317.40	33	100	20	43138.53	+0.03	+1.3	$fd^3H_4^0 - fp^3G_3$
2315.91	73	8	7	43166.28	−0.13	+3.2	$d^2\,{}^1G_4 - f\cdot d^1H_5^0$
2312.83	73	8	7	43223.76	+0.07	+1.9	$fd^3F_4^0 - fp^1F_3$
2302.14	06	100	25	43424.45	+0.13	+1.7	$fd^3G_4^0 - fp^3F_3$
2300.70	61	80	20	43451.62	−0.13	+1.6	$fd^3G_4^0 - fp^3F_4$
2298.75	66	20	10	43488.48	−0.14	+1.6	$fd^3D_3^0 - fp^3D_3$
2287.85	77	30*s*	12	43695.65	−0.04	+1.5	$fd^3H_5^0 - d^2\,{}^1G_4$
2282.25	18	6	8	43802.86	+0.11	+1.4	$fd^1D_2^0 - fp^1F_3$
2277	52		3	43893.8		−0.1	$fp^3D_1 - 4_2^0$
2272	81		2	43984.8		+0.1	$fs^1F_3^0 - ds^1D_2$
2268.22	15	25	20	44073.77	0.00	+1.3	$fs^3F_4^0 - ds^3D_3$
2266.95	87	10*s*	15	44098.46	0.00	+1.5	$fs^3F_2^0 - ds^3D_1$
2266	22		2	44112.7		+1.9	$fd^3F_4^0 - fp^3F_3$
2264.91	80	50	20	44138.18	−0.05	+2.1	$fd^3F_4^0 - fp^3F_4$
2250	02		3	44430.2		+1.3	$fd^3D_3^0 - fp^1D_2$
2249.31	20	15*s*	18	44444.26	+0.02	+2.2	$fd^3F_2^0 - fp^3G_3$
2244.18	11	8*s*	15	44545.85	+0.12	+1.5	$fs^3F_3^0 - ds^3D_2$
2243	67		4	44556.0		+1.4	$fd^3F_2^0 - d^2\,{}^1G_4$
2242.35	25	80	25	44582.20	+0.14	+2.1	$fd^3F_2^0 - fp^3F_2$
2241.30	18	10	15	44603.08	−0.12	+2.3	$fd^3G_4^0 - fp^3G_4$
2238.69	58	8	15	44655.08	+0.12	+2.3	$fd^3D_2^0 - fp^1D_2$
2236.95	84	4	10	44689.81	−0.05	+2.1	$fd^1D_2^0 - fp^3F_3$
2234	74		3	44734.0		+1.5	$fp^3F_4 - 5_3^0$
2232	69		4	44775.1		+1.1	$fs^3F_2^0 - ds^3D_2$
2228.10	05	50	[135]	44867.30	+0.05	+1.1	$fd^3G_5^0 - fp^3G_5$
2227.88	76	40	20	44871.73	+0.09	+2.5	$fd^3F_3^0 - fp^1F_3$
2225.12	00	125	40	44927.38	+0.10	+2.5	$fd^3H_5^0 - fp^3F_4$
2222.06	97	100	40	44989.24	−0.06	+1.8	$fd^1G_4^0 - fp^3G_3$
2218.16	07	12*s*	20	45068.34	−0.04	+1.8	$fd^1D_2^0 - fp^3D_2$
2215	91		1	45114.1		+1.3	$fp^3F_3 - 6_2^0$
2210.7	50	2	15	45220.4	−2.3	+1.8	$fd^3G_5^0 - fp^1G_4$
2209	34		12	45248.2		+1.8	$fd^3H_4^0 - fp^1F_3$
2207.30	22	8	20	45290.05	+0.37	+2.0	$fd^3F_4^0 - fp^3G_4$
2203	82		12	45361.6		+1.6	$fd^1D_2^0 - fp^3D_1$
2203.22	10	6	20	45373.91	−0.46	+2.0	$fd^3G_3^0 - fp^3D_2$
2199	40		4	45452.7		+1.5	$fp^1F_3 - 4_2^0$
2195	98		4	45523.5		+1.4	$d^2\,{}^3P_2 - 3_1^0$
2190	56		[3]	45636.1		+2.8	$fd^3D_1^0 - fp^1D_2$
2184	61		15	45760.4		+1.6	$fd^3F_2^0 - fp^3F_2$
2183.8	70	1	15	45777.4	−0.9	+1.2	$fd^3G_4^0 - fp^3D_3$
2183	32		12	45787.4		+1.2	$fd^3F_3^0 - fp^3F_4$
2180.70	60	100	100	45842.43	−0.01	+2.1	$fd^3H_6^0 - fp^3G_5$
2169.55	44	6	75	46078.00	−0.73	+1.6	$fd^3H_5^0 - fp^3G_4$
2166.95	85	20	100	46133.28	−0.27	+1.8	$fd^3H_4^0 - fp^3F_3$
2166	71		20	46138.4		+1.1	$fd^3F_3^0 - fp^3D_2$
2165	59		5	46162.3		+1.3	$fd^3H_4^0 - fp^3F_4$
2164	94		2	46176.1		+1.4	$fd^3G_3^0 - fp^3G_4$
2162	83		2*d*	46221.2		−0.3	$fd^3F_2^0 - d^2\,{}^3P_2$
2156	46		2	46357.7		+1.6	$fd^3G_4^0 - fp^3G_5$
2151	43		30	46466.0		+1.2	$fd^3F_4^0 - fp^3D_3$
2145	34		2	46597.9		0.0	$fs^3F_2^0 - ds^1D_2$
2140	09		3	46712.2		+0.6	$fd^3G_4^0 - fp^3G_4$
2136	94		30	46781.1		+0.9	$fd^1G_4^0 - d^2\,{}^1G_4$
2124	98		15	47044.3		{+1.7 +0.4	$fd^3F_4^0 - fp^3G_5$ $fd^1D_2^0 - fp^3D_3$
2122	55		12	47098.2		+1.0	$fd^1G_4^0 - fp^1F_3$
2112	89		2	47313.5		+1.1	$fd^3H_4^0 - fp^3G_4$
2111	19		5	47351.6		{+1.8 +0.3	$fd^3G_3^0 - fp^3D_3$ $fp^3D_3 - 9_2^0$
2109	49		2	47389.7		0.0	$fd^1P_1^0 - ds^1D_2$
2109	08		25	47398.9		+0.9	$fd^3F_4^0 - fp^1G_4$
2107	25		3	47440.1		+0.8	$fd^3F_2^0 - fp^3F_3$
2095	73		1	47700.9		+0.7	$d^2\,{}^3P_1 - 6_2^0$
2090	54		8	47819.3		+1.5	$fd^3F_2^0 - fp^3D_2$
2089	99		9	47831.8		+0.2	$fd^3H_5^0 - fp^3G_5$
2086	16		2	47919.6		−0.2	$d^2\,{}^3P_2 - 7_3^0$

TABLE IV—(*Continued*).

λ King	λ Lang	Intensity		Wave Number Vac.	Wave Number $o-c$		Multiplet Designation
		King	Lang		King	Lang	
2083	34		35	47984.5		+0.1 +0.4	$fd^1G_4^0 - fp^3F_3$ $fd^1D_2^0 - fp^1D_2$
2082	16		7	48011.7		−0.1	$fd^1G_4^0 - fp^3F_4$
2077	89		15	48110.3		+0.9	$fd^3F_2^0 - fp^3D_1$
2074	59		4	48186.9		−0.2	$fd^3H_5^0 - fp^1G_4$
2070	41		2	48284.1		+1.0	$fd^3G_3^0 - fp^1G_4$
2061	71		15	48487.8		+0.2	$fd^3H_4^0 - fp^3D_3$
2042	82		18	48936.2		+0.5	$d^2\,{}^1D_2 - 4_2^0$
2037	96		18	49052.8		−0.2	$fd^3F_3^0 - fp^1D_2$
2037	43		5	49065.6		+0.3	$fd^3H_4^0 - fp^3G_4$
2033	39		25	49163.1		−0.1	$fd^1G_4^0 - fp^3G_4$
2022	77		10	49421.2		+0.4	$fd^3H_4^0 - fp^1G_4$
λ Vac							
1986	55		15	50338.5		+0.1	$fd^1G_4^0 - fp^3D_3$
1963	74		14	50923.2		+0.1	$d^2\,{}^3P_2 - 9_2^0$
1950	39		30	51271.8		+0.2	$fd^1G_4^0 - fp^1G_4$
1946	72		2	51368.5		+0.9	$fd^3P_2^0 - ds^3D_2$
1933	41		3	51722.1		+1.1	$fd^3P_1^0 - ds^3D_1$
1932	08		6	51757.7		+1.3	$fd^3P_0^0 - ds^3D_1$
1912	30		5	52293.1		+0.4	$d^2\,{}^3P_1 - 9_2^0$
1908	48		10	52397.7		+1.2	$fd^3P_1^0 - ds^3D_2$
1904	60		1	52504.5		+0.7	$d^2\,{}^3F_4 - 5_3^0$
1890	04		10	52908.9		+1.2	$fd^3P_2^0 - ds^3D_3$
1885	01		8	53050.1		+1.6	$fd^1F_3^0 - ds^3D_3$
1875	03		1	53332.5		+0.1	$fd^1F_3^0 - ds^1D_2$
1871	46		5	53434.2		+1.1	$fd^3D_2^0 - ds^3D_1$
1855	81		3	53884.8		+2.3	$fd^3D_3^0 - ds^3D_2$
1855	68		1	53888.6		+1.8	$d^2\,{}^3F_3 - 4_2^0$
1848	97		18	54084.2		+1.6	$d^2\,{}^3F_3 - 5_3^0$
1848	07		9	54110.5		+1.9	$fd^3D_2^0 - ds^3D_2$
1844	30		(6)	54221.1		+0.7	$fd^3P_1^0 - ds^1D_2$
1837	78		8	54413.5		+2.0	$fd^3D_1^0 - ds^3D_1$
1836	99		20	54436.9		+1.4	$d^2\,{}^3F_3 - 6_3^0$
1836	64		20	54447.3		+1.5	$d^2\,{}^3F_4 - 7_3^0$
1815	18		7*d*	55091.0		+4.0	$fd^3D_1^0 - ds^3D_2$?
1813	98		4	55127.4		+2.1	$d^2\,{}^3F_2 - 3_1^0$
1805	46		9	55387.6		+2.5	$d^2\,{}^3F_2 - 4_2^0$
1804	25		10	55424.7		+2.1	$fd^3D_3^0 - ds^3D_3$
1799	11		2	55583.0		+2.1	$d^2\,{}^3F_2 - 5_3^0$
1796	89		18	55651.7		+1.6 +3.0	$d^2\,{}^3F_4 - 8_4^0$ $fd^3D_2^0 - ds^3D_3$
1747	31		3	57230.9		+2.0	$d^2\,{}^3F_3 - 8_4^0$
1712	32		8	58400.3		+1.5	$fd^3F_4^0 - ds^3D_3$
1709	17		8	58507.9		+1.3	$fd^3F_3^0 - ds^3D_2$
1680	30		4	59513.2		+1.5	$fd^3F_2^0 - ds^3D_1$

from King's data when available, otherwise from Lang's; then the residual $o-c$ from the value computed from the terms of Table I; and finally the multiplet designation.

There is a small systematic difference between King's and Lang's wave-lengths. For convenience King's have been adopted as a standard for the present purpose, and the term values derived from these when possible (for all levels except ds^1D_2).

The differences in wave number are summarized in Table V in the sense Lang *minus*

TABLE V. *Summary of wave number differences.*

Wave Number	No.	Mean cm^{-1}	Av. Resid.
39000–40000	13	+0.1	±0.6
40000–41000	14	+0.4	0.3
41000–42000	20	+1.0	0.5
42000–43000	14	+1.0	0.4
43000–44000	11	+1.4	0.6
44000–45000	18	+1.8	0.4
45000–46000	14	+1.7	0.3
46000–48000	17	+1.1	0.4
48000–50000	10	+0.3	0.4
50000–54000	14	+1.0	0.5
54000–59000	13	+1.8	0.3

TABLE VI. *Zeeman effects in Ce III.*

λ	OBS. Z E	CALC. Z E	λ	OBS. Z E	CALC. Z E
3543	(0) 1.11	(0) 1.10	2927	(w_2) 0.98w_2	(0.44) 1.16
3504	(0.34) 1.15w_2	(0.32) 1.10	2925	(w_3) 0.98	(0) 0.83*
3497	(0.70) 1.31w_4	(0.70) 1.16	2923	(0) 1.17	(0) 1.10*
3470	(0.55) 0.99w_3	(0.51) 0.97	2907	(w_1) 1.18	(0) 1.00*
3459	(w_1) 1.50	(0) 1.44	2873	(w_2) 1.31w_2	(0) 1.50*
3454	(w_2) 1.47w_2	(0) 1.32	2861	(w_4?) 1.27w_2	(0) 1.50*
3443	(w_2) 1.19w_1	(0) 1.07	2849	(0) 1.17w_1	(0) 1.02
3427	(w_3) 0.76w_1	(0.28) 0.74	2802	(?) 1.23w_2	(0.86) 0.92*
3398	(0) 1.04w_1	(0.22) 0.99	2801	(?) 1.41w_2	(0.67) 1.15*
3395	(0) 1.27w_2	(0) 1.17	2774	(?) 1.54	(0) 1.50*
3353	(0.57) 1.15w_2	(0.60) 1.18	2768	(w_2) 1.16	(0) 1.12†
3228	(0.44) 1.23w_2	(0.45) 1.20	2754	(w_1) 0.83w_1	(0) 0.73†
3147	(0.48) 1.16w_3	(0.53) 1.14	2748	(0) 1.35	(0) 1.25*
3143	(0.27) 1.07w_1	(0.31) 1.01	2743	(0) 1.18	(0) 1.08*
3141	(0) 1.18	(0) 1.12	2730	(w_1) 0.79	(0) 0.67*
3121	(w_2) 1.35w_2	(0) 1.24	2719	(0) 1.50	(0) 1.68*
3110	(0) 1.36	(0) 1.32	2672	(?) 1.43	(0) 1.50*
3106	(0) 1.20	(0) 1.15	2662	(w_2) 0.75w_4	(0) 0.50*
3085	(0.62) 0.88w_4	(0.58) 0.82	2649	(w_2) 0.86w_4	(0) 0.82†
3057.5	(0) 0.80	(0) 0.80	2603	(w_2) 1.06	(0) 0.90†
3057.2	(0) 1.18	(0) 1.07	2578	(w_2) 1.24w_2	(0) 1.00*
3056	(0) 1.06	(0) 0.94	2532	(w_1) 1.09w_2	(0) 0.98†
3055	(0) 1.16	(0) 1.09	2483	(?) 1.25w_1	(0.44) 1.25†
3031	(0) 1.31	(0) 1.23	2470	(?) 1.13w_3	(0) 1.15†
3022	(?) 1.35	(0.73) 1.16	2454	(?) 1.67	(0) 1.48†
2931	(0) 1.08	(0) 1.00*	2431	(?) 1.69w_4	(0.62) 1.12†

* Theoretical blended pattern.
† Theoretical value used for one g; other g observed.

King. The values computed from the adopted terms (being on King's scale) have been used to extend the comparison into the vacuum region. The maximum difference corresponds to 0.09A near λ2300. The last column gives the average deviation, without regard to sign, of an individual difference from the group mean. The general average of these residuals is ± 0.44 cm^{-1}, which corresponds to ± 0.027A at λ2500, and ± 0.014A at λ1800.

A considerable series of measures of the Zeeman effect, made at Pasadena by one of us (R.B.K.), is summarized in Table VI. The first column gives the wave-length (for identification in Table IV); the second, the observed Zeeman pattern; and the third, the computed patterns for blends, according to the formulae of Shenstone and Blair.[9, 10] These have been derived from de Bruin's g values when available. For many other lines the data do not suffice to determine separate g values for both the terms involved, and the theoretical positions derived from Lande's formulae are tabulated (and marked with an asterisk). These suffice to show that no very serious deviations from normal g values occur.

We are indebted to Miss Moore for valuable aid in preparing and checking the tables.

[9] Shenstone and Blair, Phil. Mag. **8**, 765 (1929).
[10] Russell, Phys. Rev. **36**, 1590 (1930).

On the Cameron Bands ($^3\Pi - {}^1\Sigma$) of Carbon Monoxide

L. GERÖ,
Royal Hungarian University for Technical and Economical Sciences, Budapest, Hungary
G. HERZBERG,
University of Saskatchewan, Saskatoon, Saskatchewan, Canada
and R. SCHMID,
Royal Hungarian University for Technical and Economical Sciences, Budapest, Hungary

(Received June 28, 1937)

The 0−0 and 1−0 Cameron bands of CO are investigated in absorption with high dispersion. Three P, three Q and three R branches are observed for each band. New accurate values for the rotational constants of the ground state of CO are derived: $B_e = 1.9310$ cm^{-1}, $\alpha = 0.01744$ cm^{-1} and, using Bearden's values for e, h and N, we obtain the moment of inertia $I_e = 14.456 \cdot 10^{-40}$ g cm^2, $I_0 = 14.521 \cdot 10^{-40}$ g cm^2, the nuclear distance $r_e = 1.127$A, $r_0 = 1.129$A. From the way in which the Λ doublets of the $a^3\Pi$ state combine with the $^1\Sigma^+$ ground state it can be definitely shown that the upper state of the third positive group of CO (whose lower state is $a^3\Pi$) is $^3\Sigma^+$ not $^3\Sigma^-$. For the electronic excitation energy of the $a^3\Pi$ level a value 48473.7 cm^{-1} is obtained which differs to some extent from the values at present used in the literature.

A. INTRODUCTION

THE Cameron bands of CO have been discovered by Cameron[1] in emission in a discharge through Ne with traces of CO, and have subsequently been observed in absorption by Hopfield.[2] As was first concluded by Johnson[3] they constitute the transition from the lower state of the third positive group $a^3\Pi$ to the ground state $X^1\Sigma$ of the CO molecule. As a singlet-triplet inter-combination the bands are very weak in absorption compared to the 4th positive group $^1\Pi - {}^1\Sigma$.

Since thus far no example of the fine structure of $^3\Pi - {}^1\Sigma$ bands has been analyzed, and since an analysis would also supply better values than now available, for the rotational constants of the ground state and the electronic energy of the triplet levels it seemed to us worth while to study the Cameron bands under high dispersion in absorption.

B. EXPERIMENTAL

With an absorbing layer of 1 m and 6 m respectively of CO, spectrograms were independently taken at Budapest and at Darmstadt. At Budapest the first order of a 6 m grating with 30,000 lines per inch was used (dispersion 1.15A/mm); at Darmstadt the third order of a 3 m grating with 15,000 lines per inch (dispersion 1.7A/mm). After finding out that both at Budapest and at Darmstadt the same spectrograms had been taken we decided to evaluate the plates and publish the results together.

A hydrogen discharge tube was used to supply the continuous background.[4] Only the 0−0 and the 1−0 bands lie in the region accessible without the use of a vacuum spectrograph. The 1−0 band could not be measured on the Budapest plates because of over-lapping by the oxygen absorption bands which of course in a 6 m spectrograph appear much stronger than in a 3 m spectrograph. The 0−0 band was measured only on the Budapest plates except for the weakest lines which appeared more intense on the Darmstadt plates because of the longer absorbing layer.

In Budapest Fe lines of the first order were used as comparison spectrum; in Darmstadt, Fe lines of the second order, and some silicon lines of the H_2 discharge tube in the third order. The lines of the 0−0 band measured both on the Budapest and on the Darmstadt plates showed a constant difference of 0.094A corresponding to 2.2 cm^{-1}. Consequently half this shift (in wavelength) was added to all measurements of the Budapest plates and subtracted from those of the Darmstadt plates. The absolute values of the

[1] W. H. B. Cameron, Phil. Mag. **1**, 405 (1926).
[2] J. J. Hopfield, Phys. Rev. **29**, 356 (1927).
[3] R. C. Johnson, Nature **117**, 376 (1926).

[4] At Darmstadt in order to cut out the strong second order continuous spectrum that over-laps the third order, the method given by Curry and Herzberg (Ann. d. Physik **19**, 800 (1934)) was used.

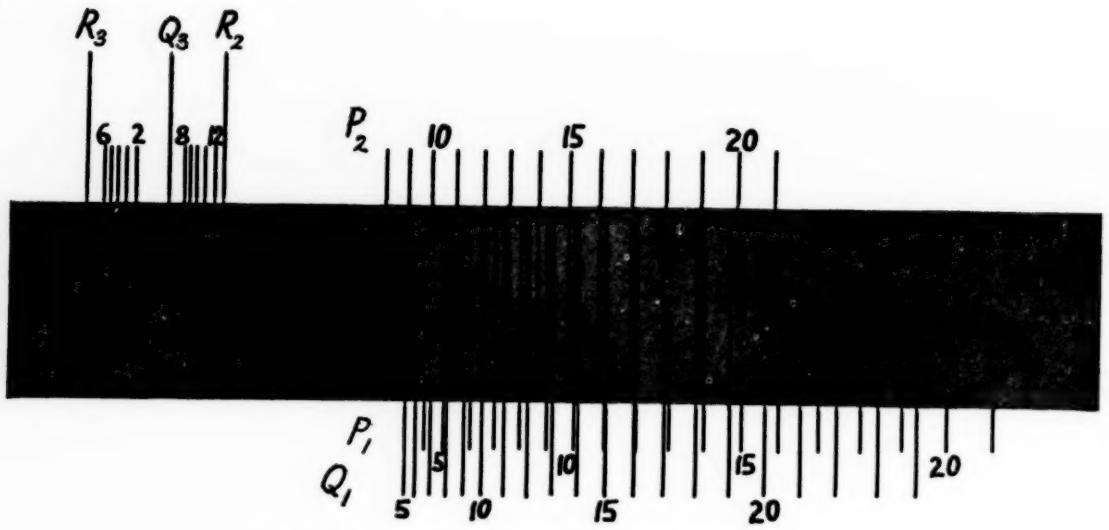

FIG. 1. The 0−0 band of the Cameron system in absorption.

wave numbers given may therefore be in error by 1–2 cm^{-1} but the relative accuracy is of course better (a few tenths of a cm^{-1}).

Figure 1 is a reproduction of the 0−0 band from a Budapest plate.

C. Rotational Analysis

According to the selection rule $\Delta J=0, \pm1$ nine branches are to be expected for a $^3\Pi-{}^1\Sigma$ transition: a P, Q and R branch for each component $^3\Pi_0-{}^1\Sigma$, $^3\Pi_1-{}^1\Sigma$ and $^3\Pi_2-{}^1\Sigma$. Some lines of these branches are indicated in Fig. 2. The branches are designated as P_1, Q_1, R_1; P_2, Q_2, R_2; P_3, Q_3, R_3. Since the $^3\Pi$ state is, at least for larger J values, near to case b the quantum number K has a meaning for the rotational levels of both the upper and lower states. For the above mentioned branches ΔK takes the values ±2, ±1, 0. Therefore the branches have, at least for larger K, the form of O, P, Q, R, and S branches. According to Mulliken[5] they may also be designated by

P_1	Q_1	R_1	P_2	Q_2	R_2	P_3	Q_3	R_3
^OP	^PQ	^QR	^PP	^QQ	^RR	^QP	^RQ	^SR

Table I gives the wave numbers of the branches of the 0−0 and 1−0 bands. Unresolved lines used in two or even three different places are indicated by an asterisk in Table I. Their accuracy is of course less than that of the unblended lines.

[5] R. S. Mulliken, Phys. Rev. **36**, 611 (1930).

In Table II the combination differences

$$R_i(K-1)-P_i(K+1)=\Delta_2F''(K)$$

are given which should coincide for the two bands. The last column contains the average $\Delta_2F''(K)$. In forming the average values the Δ_2F'' values obtained from blended lines (marked by *) have been given half the weight of the unblended Δ_2F'' values. From the average Δ_2F''

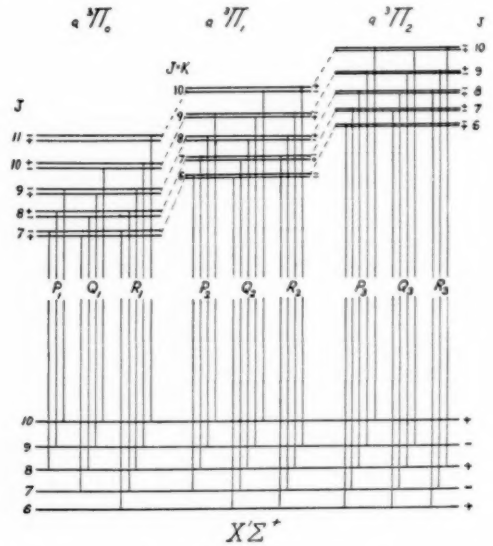

FIG. 2. Energy level diagram for the Cameron bands showing the nine branches. The J values on the right for $a^3\Pi_2$ should be lowered by one unit. In order to represent the relations as actually found by the following analysis the designations + and − in the upper state should be interchanged and the end points of the lines representing the transitions should be changed correspondingly.

TABLE I. *Wave numbers of the lines in the 0−0 and 1−0 Cameron bands.*

0−0 BAND
$\lambda_H = 2059.6$A $\quad \nu_0 = 48473.7$

K	P_1	Q_1	R_1	P_2	Q_2	R_2	P_3	Q_3	R_3
0	—	—	—	—	—	48479.42*	—	—	48511.13
1	—	—	—	—	—	482.28*	—	—	516.23
2	—	—	—	48467.55	—	484.56*	—	—	520.42
3	—	—	—	463.01*	—	486.16*	—	48509.33*	524.21
4	48415.98*	48428.59*	48442.51*	457.70*	—	487.01*	48494.06	509.33*	526.99
5	408.32*	424.18*	441.50	451.34	—	—	489.24*	507.99	529.49
6	400.24*	419.21*	440.09	444.62	48465.17*	488.44	484.56*	506.77	531.75
7	390.52	414.22*	438.10*	438.10*	461.44	—	479.42*	504.84	533.78
8	382.21	408.33*	435.17	430.57	457.70*	487.01*	474.20	503.03	535.45
9	372.51	402.25	432.70	422.80	453.08	486.16*	468.56	500.67	536.65
10	362.03	394.64	428.59*	414.22*	448.17	484.56*	463.01*	498.60	537.97
11	351.57*	387.71	424.18*	405.42	442.51*	482.28*	455.94	495.55	538.77
12	340.56	379.40	419.21*	395.88	436.52	479.42*	449.48	492.30	539.29*
13	328.41	370.45		386.35	430.57*	476.95	442.51*	489.24*	539.29*
14	315.68	361.28		376.02	424.18*	472.88			
15	302.86	351.57*		365.21	415.98*	469.41			
16	288.94	341.45		353.87	408.33*	465.17*			
17	275.09	330.21*		342.41	400.24*				
18	259.90	318.90		330.21*					
19	244.57	306.86		317.08					
20	229.30	294.35		304.34					
21	212.74	281.55		290.62					
22	196.56	267.68							
23	178.66	253.23							
24	160.01	238.80							
25	142.55	223.46							
26	124.13	208.60							
27		192.24							
28		175.55							

1−0 BAND
$\lambda_H = 1989.4$A $\quad \nu_0 = 50188.3$

K	P_1	Q_1	R_1	P_2	Q_2	R_2	P_3	Q_3	R_3
0	—	—	—	—	—	—	—	—	—
1	—	—	—	—	—	—	—	—	50229.30
2	—	—	—	—	—	50198.67*	—	—	233.21
3	—	—	—	—	—	—	—	—	237.40
4	—	—	—	—	—	—	—	—	240.40
5	—	50138.13	—	—	—	—	50202.35	—	242.88
6	50113.58	133.88	—	—	50178.18	—	198.67*	50220.09	244.90
7	105.07	126.82*	—	—	174.83	—	193.74*	218.13	246.66
8	097.59	122.10	—	—	171.16	—	187.45*	216.01	—
9	086.85*	115.69	—	50136.27	165.74	198.67*	—	213.41	—
10	075.94	108.38	50141.57*	126.82*	160.84	196.41	174.83*	210.76	—
11	064.49	100.08*	—	118.23	154.62	193.74*	167.93*	207.31	—
12	052.91	091.77	131.39*	108.38	148.54	189.97*	160.84*	204.06	—
13	040.61	082.44	—	097.59	141.57*	187.45*		198.67*	—
14	027.62*	072.63	118.23	086.85*	133.88	182.71		193.74*	246.66
15	014.48	062.23	111.65	075.94*	126.82*	178.18*		189.97*	244.90
16	49999.75	051.73	103.74	064.49	118.23*	—		184.80	242.88
17	984.95	039.66	095.98	—	108.38*	167.93		178.18*	240.40
18	969.64	027.62*	086.85*	039.66*	100.08*	—		171.16*	
19	952.89	014.48*	077.77		089.36	154.62*		164.72	
20	937.25	001.51	067.72		079.05	148.54*			
21	919.25	49988.42	056.84		067.72*	140.04			
22	903.21	974.16	045.54		056.84*	131.39*			
23		958.86	034.03		045.54*				
24		944.31			034.03*				
25		—			019.51				
26		910.11			005.11				

λ_H is the wave-length in air of the most refrangible head formed by the R_3 branch.

TABLE II. $\Delta_2F''(K)=R_i(K-1)-P_i(K+1)$.

K	$R_1(K-1)$ $-P_1(K+1)$		$R_2(K-1)$ $-P_2(K+1)$		$R_3(K-1)$ $-P_3(K+1)$		Weighted Average
	0–0	1–0	0–0	1–0	0–0	1–0	
1	—	—	11.87*	—	—	—	11.87
2	—	—	19.27*	—	—	—	19.27
3	—	—	26.86*	—	26.36	—	26.53
4	—	—	34.82*	—	34.97*	35.05	34.97
5	42.27*	—	42.39*	—	42.43*	41.73*	42.21
6	50.98	—	—	—	50.07*	49.14*	50.29
7	57.88	—	57.87*	—	57.55	57.45*	57.70
8	65.59*	—	—	—	65.22		65.34
9	73.14	—	72.79*	—	72.44*		72.88
10	81.13*	—	80.74*	80.44*	80.71		80.75
11	88.03*	88.66*	88.68*	88.03	88.49		88.34
12	95.77*	—	95.93*	96.15*	96.26*		96.03
13	103.53*	103.77*	103.40*	103.12*			103.46
14		—	111.74	111.51*			111.66
15		118.48	119.01	118.22*			118.64
16		126.70	127.00	—			126.85
17		134.10	134.96*	—			134.39
18		143.09					143.09
19		149.60*					149.60
20		158.52					158.52
21		164.51					164.51

values the rotational constant B_0'' for the vibrationless ground state can be obtained in the usual way. Taking $D''=6\cdot10^{-6}$ cm^{-1} (see Schmid and Gerö)[6] a value

$$B_0''=1.9228\pm0.0010 \text{ cm}^{-1}$$

was obtained. The only other direct determination of B_0 for the ground state of CO was obtained by Amaldi[7] from the Raman effect. He obtained 1.925 ± 0.020 cm^{-1} which agrees with our value within the accuracy given by Amaldi. Our value however is much more accurate. Schmid and Gerö, by an extrapolation of the higher B_v values derived from an analysis of the 4th positive group have obtained the value of $B_0''=1.9213$ which, considering the uncertainty of the extrapolation, agrees very well with the above value.

The new B_0'', with Schmid and Gerö's B_v values, leads to the following slightly altered B_v formula for the ground state of CO

$$B_v=1.9310-0.01744(v+\tfrac{1}{2}).$$

That is $B_e=1.9310$ and $\alpha=0.01744$. There seems to be a very slight curvature in the B_v curve but the data are too scarce to evaluate a quadratic term for B_v.

The values of the moments of inertia I_0 and I_e and the nuclear distances r_0 and r_e of the CO molecule in its ground state following from the above B_0 and B_e are (depending on the choice of

[6] R. Schmid and L. Gerö, Zeits. f. Physik **101**, 343 (1936).

[7] E. Amaldi, Zeits. f. Physik **79**, 492 (1932).

TABLE III. $\Delta_1F_1(K)=F_1(K+1)-F_1(K)$ *for* $^3\Pi_0$.

K	$v=0$				$v=1$			
	Cameron Bands		3. Positive Group		Cameron Bands		3. Positive Group	
	$R_1(K+1)$ $-Q_1(K+1)$	$Q_1(K+2)$ $-P_1(K+2)$	$R_1(K)$ $-Q_1(K+1)$	$Q_1(K)$ $-P_1(K+1)$	$R_1(K+1)$ $-Q_1(K+1)$	$Q_1(K+2)$ $-P_1(K+2)$	$R_1(K)$ $-Q_1(K+1)$	$Q_1(K)$ $-P_1(K+1)$
1	—	—	—	—	—	—	—	—
2	—	12.61*	—	—	—	—	—	—
3	13.92*	15.86*	—	—	—	—	—	—
4	17.32*	18.97*	17.11	20.06	—	20.30	16.82	—
5	20.86*	23.70*	20.43	23.28	—	21.75	20.12	23.23
6	23.88*	26.12*	23.60	26.28	—	24.51	23.47	26.15
7	26.84*	29.74	26.91	29.55	—	28.84*	26.59	29.11
8	30.45	32.61	30.34	32.72	—	32.44	29.74	32.54
9	33.95*	36.14*	33.38	36.14	33.19*	35.59*	32.94	35.29
10	36.47*	38.84	36.64	38.96	—	38.86	36.13	38.67
11	39.81	42.04	39.97	42.52	39.62*	41.83	39.46	42.00
12		45.60		45.43	—	45.01*	42.77	45.10
13		48.71*		48.74	45.60	47.75	46.09	48.41
14		52.51		51.99	49.42	51.98	49.40	51.47
15		55.12*		55.31	52.01	54.71	52.62	54.78
16		59.00		58.70	56.32	57.98*	56.05	57.93
17		62.29		61.76	59.23*	61.59*	59.26	61.13
18		65.05		65.13	63.29*	64.26	62.62	64.35
19		68.81		68.21	66.21	69.17	65.95	67.57
20		71.12		71.58	68.42	70.95	69.33	70.85
21		74.57		74.80	71.38		72.51	
22		78.79		78.05	75.17		75.74	
23		80.91		81.36				
24		84.47		84.78				

the old Birge or the new Bearden values for the atomic constants e, h and N):

$I_0 = 14.383$ or $14.521 \cdot 10^{-40}$ g cm^2 resp.,
$I_e = 14.318$ or $14.456 \cdot 10^{-40}$ g cm^2 resp.,
$r_0 = 1.128$ or 1.129A resp.,
$r_e = 1.125$ or 1.127A resp.

In Table III the combination differences

$$\Delta_1 F_1 = F_1(K+1) - F_1(K)$$

for the $^3\Pi_0$ component of the upper state are given, calculated from the differences $R_1(K+1) - Q_1(K+1)$ and $Q_1(K+2) - P_1(K+2)$ in the Cameron bands for both $v=0$ and $v=1$. Table III shows that $R_1(K+1) - Q_1(K+1)$ and $Q_1(K+2) - P_1(K+2)$ do not exactly coincide. As can be seen from Fig. 2 this is to be expected because of the Λ type doubling which is particularly strong for the $^3\Pi_0$ component of $a^3\Pi$. In Table III are also given the $\Delta_1 F_1$ values as calculated from the data of Dieke and Mauchley[8] and Gerö[9] for the third positive group of CO which has the same $a^3\Pi$ state as lower state. The differences $R_1(K) - Q_1(K+1)$ and $Q_1(K) - P_1(K+1)$ in the third positive group give $\Delta_1 F_1$, apart from Λ-type doubling.

It can be seen from Table III that $R_1(K) - Q_1(K+1)$ of the third positive group coincides very well with $R_1(K+1) - Q_1(K+1)$ of the Cameron bands, and $Q_1(K) - P_1(K+1)$ of the third positive group with $Q_1(K+2) - P_1(K+2)$ of the Cameron bands for both $v=0$ and $v=1$. This agreement is definite proof that the lower state of the third positive group is identical with the upper state of the Cameron bands.

The upper state of the third positive group is a $^3\Sigma$ state.[8] From the analysis of the third positive group ($b^3\Sigma - a^3\Pi$) alone it cannot be decided whether the upper state is $^3\Sigma^+$ or $^3\Sigma^-$. However, this can now be decided from Table III if the assumption is made that the ground state of CO is $^1\Sigma^+$ (not $^1\Sigma^-$). The correctness of this assumption follows from the fact that the ground state has closed electron shells only.[10] In the ground state therefore the even rotational levels are positive, the odd negative, as indicated in Fig. 2. If in the $b^3\Sigma$ state the odd rotational levels were positive and the even negative, that is, if it were a $^3\Sigma^-$ level, $Q_1(K) - P_1(K+1)$ of the third positive group should coincide with $R_1(K+1) - Q(K+1)$ of the Cameron bands, and not with $Q_1(K+2) - P_1(K+2)$ as it actually does. It therefore follows that the upper state of the third positive group is a $^3\Sigma^+$ level. This is in agreement with the fact that the ground state $^1\Sigma^+$ combines, though very weakly, with the $b^3\Sigma^+$ state.[11] A $^3\Sigma^- - {}^1\Sigma^+$ combination would be expected to be much weaker still.

To save space the data for the combination differences $\Delta_1 F$ for the $^3\Pi_1$ and $^3\Pi_2$ components are not given here. The agreement with the corresponding values from the third positive group is about as good as for $^3\Pi_0$, and the conclusions as to the symmetry are the same. By a mistake in drawing Fig. 2 (noticed only in the proof) the + and − characters of the rotational levels of the $^3\Pi$ state indicated there are just opposite to the correct ones.

The *zero lines* ν_0 of the two Cameron bands, given in Table I, were obtained by extrapolating $\frac{1}{3}(Q_1 + Q_2 + Q_3)$ to $J=0$. It can be easily seen from a paper by Budó[12] that this procedure supplies the correct zero lines apart from Λ-doubling. The difference of the two zero lines 1714.6 is the $\Delta G_{\frac{1}{2}}$ value of the $a^3\Pi$ state. Due to the fact that hitherto only the heads of the Cameron bands have been measured the values for the electronic excitation energy of the $a^3\Pi$ states given in recent tables deviate appreciably from the above ν_0 value 48473.7 cm^{-1} for the 0−0 band. The values for the electronic energies of the other triplet states of CO have to be changed correspondingly.

[8] G. H. Dieke and J. W. Mauchley, Phys. Rev. **43**, 12 (1933).
[9] L. Gerö, Zeits. f. Physik **101**, 311 (1936).
[10] Quite generally the + and − character of the Σ states of a molecule can be determined only relatively from a band analysis alone. To determine it absolutely the + and − character of one state has to be known from other evidence, such as electron configurations.
[11] J. J. Hopfield and R. T. Birge, Phys. Rev. **29**, 922 (1927).
[12] A. Budó, Zeits. f. Physik **98**, 437 (1936).

The Abundance Ratio of the Isotopes in Natural or Isotopically Separated Carbon

A. R. Brosi and William D. Harkins
George Herbert Jones Chemical Laboratory, University of Chicago, Chicago, Illinois
(Received June 19, 1937)

The relative intensity of the 1,0 band heads of the $C_{12}C_{12}$ and $C_{12}C_{13}$ molecules in the Swan system of the C_2 spectrum has been measured by a photographic spectrophotometric method and found to be 0.0217 ± 0.0009. This yields a value of 92.2 ± 3.7 for the C_{12}/C_{13} abundance ratio of the carbon isotopes in good agreement with the value reported by Vaughan, Williams and Tate (91.6 ± 2.2), from mass-spectrographic data. This work was done in connection with the development of a simple method suited to the determination of the abundance ratio in the small samples obtained in the separation of natural carbon into isotopes. This method is described.

I. Introduction

THE purpose of the work reported here was to obtain a simple method to be used in following the extent of separation of carbon into isotopes. By the use of this modified and improved form of the spectroscopic method used by Jenkins and Ornstein[1] the abundance ratio of C^{12} and C^{13} in natural carbon has been determined. This method is extremely easy and simple if the band spectra employed are obtained by the use in the discharge tube of an unsaturated hydrocarbon. Thus acetylene, which contains one atom of hydrogen to one of carbon gives excellent results and is easily prepared. However, if the oxides of carbon or saturated hydrocarbons are used in an isotopic separation, it is difficult to convert the small quantity obtained in some of the fractions into acetylene or even ethylene. On this account methane, a saturated hydrocarbon, which may be easily prepared from any carbon compound, was used, and the spectroscopic difficulties due to an excess of hydrogen were overcome by the method described later.

Values for the abundance ratio of the carbon isotopes and for the chemical atomic weight of carbon which have been reported recently show variations which are larger than would be expected to result from isotopic separation during the preparation and purification of carbon compounds. Jenkins and Ornstein[1] in a study of the relative intensity of the 1,0 band heads of $C_{12}C_{13}$ and $C_{12}C_{12}$ in the Swan system of C_2 concluded that this intensity ratio (0.019 ± 0.002) was independent of the method of excitation and proportional within two or three percent[2] to the abundance ratio of the isotopes. They gave 106 for the ratio C_{12}/C_{13}. In a mass-spectrographic study of the abundance ratios of the isotopes of the lighter elements Aston[3] reported 140 ± 14 for the C_{12}/C_{13} ratio. Vaughan, Williams and Tate,[4] gave 91.6 ± 2.2 for this ratio.

II. Apparatus and Procedure

As in the work of Jenkins and Ornstein[1] the relative intensity of the 1,0 band heads of the Swan systems of $C_{12}C_{12}$ and $C_{12}C_{13}$ at $\lambda4737$ and $\lambda4744$, respectively, was measured by a photographic spectrophotometric method. The apparatus used in the excitation of the Swan system of the C_2 spectrum is shown in Fig. 1. The discharge tube *D* was made of Pyrex glass with a capillary restriction 1.5 mm in diameter and 5 cm in length. The cylindrical electrodes were made of 16 gauge (B & S) nickel wire wound into a tight coil 15 mm long and 15 mm in diameter. They were 12 cm apart and were connected to the external electrical circuit through Pyrex-tungsten seals. The discharge was maintained by a 0.44 kva Thordarson transformer *H* which supplied 15,000 volts maximum, a 0.04 mf condenser *I* and an adjustable spark gap *J*.

The Swan system of the C_2 spectrum was obtained with great intensity when the discharge tube contained methane at a pressure of about 0.25 mm of mercury and helium at a pressure of 16 mm. Helium was used to lower the effective temperature of the C_2 bands thereby increasing

[1] Jenkins and Ornstein, Proc. Amst. Acad. Sci. **35**, 1212 (1932).

[2] Dunham, Phys. Rev. **36**, 1553 (1930).

[3] Aston, Proc. Roy. Soc. (London) **A149**, 400 (1935).

[4] Vaughan, Williams and Tate, Phys. Rev. **46**, 327 (1934).

the intensity of the 1,0 band head relative to the background intensity and at the same time suppressing the overlapping tails of the bands of the zero sequence. With helium pressures below 12 mm or methane pressures above 0.5 mm reliable intensity measurements could not be made because of overlapping of the zero sequence. With helium pressures above 20 mm or methane pressures much below 0.1 mm the intensity of the Swan system was greatly reduced.

Harkins and Jackson[5] in work done in this laboratory found that in the glow discharge through methane the C_2 bands disappeared altogether and the molecular spectrum of hydrogen became very strong. In this work the intensity of the C_2 spectrum was maintained by removing H_2 through the palladium valve *C* (Fig. 1). This was made from a palladium tube 3 mm in diameter and 4 cm long connected to the discharge tube through Pd-Pt and Pt soft glass seals and a soft glass Pyrex ground glass joint. It was heated by a tungsten filament insulated from the Pd by a thin sheet of mica. Hydrogen was pumped continuously from the bulb surrounding the valve with a mercury vapor pump and a Cenco Hyvac fore pump. The hydrogen molecular spectrum was further suppressed by introducing sulfuric acid[6] into the bulb *E*.

During an exposure the discharge was observed through a small spectrometer. When the decomposition of methane progressed to the stage where the intensity of the C_2 spectrum began to decrease methane was admitted from the reservoir *G* to the chamber of known volume *F* and from there to give a known pressure in the discharge tube.

A charcoal trap *B* immersed in liquid nitrogen was used to purify helium and to outgas the electrodes. This was done by running the discharge for three hours through 20 mm of helium with the charcoal trap in communication with the discharge tube.

When an unsaturated hydrocarbon with a low hydrogen to carbon ratio was used as a source of carbon it was no longer necessary to remove hydrogen through the palladium valve. It was found, however, that the introduction of sulfuric

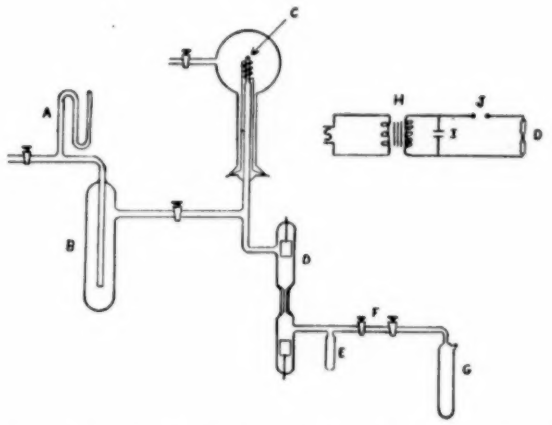

FIG. 1. Apparatus used to obtain the 1,0 band heads of the $C_{12}C_{12}$ and $C_{12}C_{13}$ spectrum.

acid into the bulb *E* greatly enhanced the C_2 spectrum in this case. An unsaturated hydrocarbon was not used in this work because of the difficulty in converting small amounts of methane or the oxides of carbon, which are most usually obtained as final products in isotopic separations, into an unsaturated hydrocarbon.

The oxides of carbon could not be used as a source of C_2 because it was found impossible to suppress the overlapping λ4835 band of carbon monoxide sufficiently.

The methane used in all of the experiments reported in this paper was made by reducing tank carbon dioxide with hydrogen over a nickel catalyst.[7] It was purified by repeated fractional distillation.

The C_2 spectrum was photographed through the side of the capillary of the discharge tube with a Hilger E1 spectrograph. In order to obtain sufficient definition it was necessary to keep the temperature of the instrument constant within ±0.5°C for at least an hour before and during the exposure which usually lasted about one hour. A photographic step weakener was placed immediately before the slit to obtain density marks for the calibration[8] of the plates.

The step weakener was made from an Eastman lantern slide plate exposed to give densities with transmissions decreasing in an approximately geometric ratio. A protective glass cover was

[5] Harkins and Jackson, J. Chem. Phys. **1**, 37 (1933).
[6] Smallwood, J. Am. Chem. Soc. **56**, 1542 (1934).
[7] Hightower and White, Ind. and Eng. Chem. **20**, 10 (1928).
[8] Harrison, J. Opt. Soc. Am. **19**, 267 (1929); **24**, 59 (1934).

TABLE I. *Intensity ratio of band heads.*

PLATE	INTENSITY RATIO λ4744/λ4737	DEVIATION FROM MEAN
11	0.0222	0.0005
14	0.0237	0.0020
15	0.0220	0.0003
17	0.0207	0.0010
18	0.0217	0.0000
19	0.0202	0.0015
Average	0.0217	0.0009

cemented to the emulsion side of the plate with Canada balsam. The weakener had six steps 2 mm wide and 3 cm long with clear portions at each end which made it possible to detect and correct for any intensity gradient which might exist along the slit.

The transmissions of the weakener steps at λ4740 were measured by three different methods: (1) By placing the weakener behind a slit in a parallel beam in the photoelectric spectrophotometer described by Hogness, Zscheile and Sidwell.[9] A narrow band 10A on each side of λ4740 was used in comparing the transmissions of the separate steps with the clear portions of the weakener. (2) By placing the weakener immediately before the slit in a photoelectric photometer of the type described by Dershem.[10] A combination of Jena glass filters BG7 and GG5 was placed between the source and the weakener. (3) The spectrum of a constant and continuous source was photographed with equal periods of exposure through the weakener and through a step sector rotating at 1800 r.p.m. on the same plate. From the densities produced through the sector a calibration curve was drawn for the plate at λ4740. The transmissions of the weakener steps were then obtained by reading the intensities corresponding to the densities produced through the weakener from the calibration curve. The transmissions obtained by the three methods agreed within two percent.

[9] Hogness, Zscheile and Sidwell, J. Phys. Chem. **41**, 379 (1937).
[10] Dershem, Rev. Sci. Inst. **3**, 43 (1932).

TABLE II. *Values of C_{12}/C_{13} ratio recently reported.*

REFERENCE	METHOD	C_{12}/C_{13}
1	Band Spectrum Intensities	106 ±11
3	Mass-Spectrographic Data	140 ±14
4	Mass-Spectrographic Data	91.6± 2.2
This work	Band Spectrum Intensities	92.2± 3.7

The Eastman 33 plates used in this work were developed in Rodinal one part water twenty parts for five minutes at 18°C using rocked tray technique. They were thoroughly fixed, washed and dried in a dust free atmosphere.

The plates were photometered on a photoelectric photometer of the type described by Dershem.[10] A separate calibration curve was constructed for each plate from the densities of the λ4737 band head in the weakened portions and the relative intensities of the λ4744 isotopic band head and background in the unweakened portion were read from the calibration curve. The data given in Table I involve the assumptions that the background intensity is constant over the region from λ4750 to λ4737 and that fogging from the $C_{12}C_{12}$ band head at λ4737 in the unweakened portion does not extend to λ4744.

III. RESULTS

The average intensity ratio λ4744/λ4737 from six plates (0.0217±0.0009) gives 92.2±3.7 for the C_{12}/C_{13} abundance ratio. This is in good agreement with the ratio obtained by Vaughan, Williams and Tate from mass-spectrographic data. Recently reported values for this ratio are tabulated in Table II.

With values for the physical atomic weights of C_{12} and C_{13} as determined from mass-spectrographic[11] and nuclear disintegration[12] data and 1.00025 for the conversion factor[13] from the chemical to the physical system gives 12.011_2 ±0.0005 for the chemical atomic weight of carbon.

[11] Aston, Nature **137**, 357 (1936); **139**, 922 (1937).
[12] Oliphant, Nature **137**, 396 (1936).
[13] Smyth, Phys. Rev. **45**, 299 (1934).

A Determination of e/m for an Electron by a New Deflection Method. II

FRANK G. DUNNINGTON*
Norman Bridge Laboratory of Physics, California Institute of Technology, Pasadena, California
(Received June 17, 1937)

A final report is here made of a deflection determination using a new method described in a preliminary report (Part I). There are two fundamental advantages of this method over other free electron methods: (1) the accelerating voltage is not measured. In its place, the determination of the frequency of a radiofrequency oscillator is made, and this can be done with far greater precision. (2) Errors from *all* contact potentials are either entirely eliminated or made negligibly small, as is shown in detail. The ever prevalent error arising from surface changes in all free electron determinations was at least greatly reduced by the use of evaporated gold surfaces throughout the deflecting chamber, said surfaces being frequently renewed to cover over the insulating layers formed. The error remaining was eliminated by extrapolation of results to infinite electron energy. The magnetic field was most carefully calibrated in terms of a specially designed standard solenoid. The frequency calibration was based on government standards through the cooperation of the Federal Radio Commission. Standards of voltage, resistance and lengths were calibrated at the National Bureau of Standards. The object throughout the work has been to produce a value as free as possible from errors both experimental and subjective. The result obtained is

$$e/m_0 = (1.7597 \pm 0.0004) \times 10^7 \text{ e.m.u.}$$

The stated probable error is based on allowances for unknown constant errors, the observational probable errors being negligible. This value of e/m_0 is about 1.25 parts in 10^3 higher than that found in recent spectroscopic determinations, a definite discrepancy being indicated. With the inclusion of the final values obtained in the last ten years by nine experimenters using both free electron and spectroscopic methods, the present most probable value is found to be

$$e/m_0 = (1.7584 \pm 0.0003) \times 10^7 \text{ e.m.u.}$$

but in view of the discrepancy this is at best only a tentative value.

INTRODUCTION

IN an earlier paper[1] a preliminary report was made on the determination of e/m by a new deflection method. Work has been in progress since then on the perfection of the method and on the establishment of the necessary standards. The object throughout this work has been to produce a result as free as possible from errors, both experimental and subjective, so that the result would be good as near as possible to one part in 10,000. As a consequence many sources of error were discovered, the existence of some of which was not even suspected at the end of the year's preliminary work. Insofar as possible such errors have been corrected. The precision of observation in all the factors entering into e/m has been refined until the observational probable errors are negligible, leaving only basic uncertainties in the method and in the interpretation of the physical phenomena observed.

No free electron determinations of e/m have appeared since the preliminary paper[1] (hereafter called Part I) in which the value of $e/m_0 = (1.7571 \pm 0.0015) \times 10^7$ e.m.u. was tentatively set. Three new spectroscopic determinations[2–4] have given consistent values ranging from 1.7570 to 1.7579. The currently accepted figure has therefore been about 1.7576. The present work indicates an appreciably higher value.

METHOD

The method used has been described in Part I. Reference should be made to the section "Simplified Description of Action in the Tube" on pages 406–7. To summarize in brief: electrons from the filament F, Fig. 1, are accelerated across the gap A during half of each cycle of the radio frequency voltage impressed on the lead-in L. The velocity attained by an electron depends on the part of the cycle during which it crosses A.

* Work from January, 1933 to February, 1935 done under a National Research Council Fellowship. Remainder of the work was made possible by grants from the Penrose Fund of the American Philosophical Society and from the Carnegie Corporation of New York.

[1] F. G. Dunnington, Phys. Rev. **43**, 404 (1933).

[2] L. E. Kinsler and W. V. Houston, Phys. Rev. **45**, 104 (1934); **46**, 533 (1934).

[3] C. D. Shane and F. H. Spedding, Phys. Rev. **47**, 33 (1935).

[4] R. C. Gibbs and R. C. Williams, Phys. Rev. **48**, 971 (1935).

A magnetic field perpendicular to the figure bends the electrons in circles with radii proportional to their velocity. With the frequency constant, any given magnetic field allows electrons of one velocity to pass around through the slits and arrive at the gap D. If the magnetic field passes a velocity such that the electrons require exactly one cycle to travel from A to D, then the electrons are completely stopped by the retarding field at D and do not reach the shielded collector at C. For any other magnetic field half the electrons reach the collector. Observations then consist in noting the magnetic field H_r at which this current minimum or "resonance" condition occurs, together with the frequency ν of the impressed voltage and the angle θ in radians subtended by the electron path. e/m is then given by (Eq. (3), Part I)

$$e/m = \theta\nu/H_r \cdots \text{e.m.u.}, \qquad (1)$$

in which m is the relativistic mass.

It should be noted particularly that, in contrast to Part I, no d.c. voltage was applied between the filament and the first slit. This results in considerable simplification of the phenomena involved and makes unnecessary the extra d.c. retarding field in front of the collector for which it has been found impossible to calculate the proper correction.

There are two fundamental advantages of the present method over other free electron methods: (1) the electron accelerating voltage is not measured. In its place, the determination of the frequency of a radiofrequency oscillator is made, and this determination can be done with far greater precision. (2) Errors from *all* contact potentials are either entirely eliminated or made negligibly small. This is shown in detail in the next section. (Errors from surface charges[5, 6, 6a] in the supposedly field free regions 1, 2 and 3, Fig. 1, are not eliminated but are minimized by the technique used.) (3) A third advantage of the method is the high observational precision possible. Thus a series of ten readings have an observational probable error of the order of 3 parts in a million.

[5] R. Lariviere Stewart, Phys. Rev. **45**, 488 (1934).
[6] A. E. Shaw, Phys. Rev. **44**, 1009 (1933).
[6a] Bainbridge and Jordan, Phys. Rev. **50**, 290 (1936).

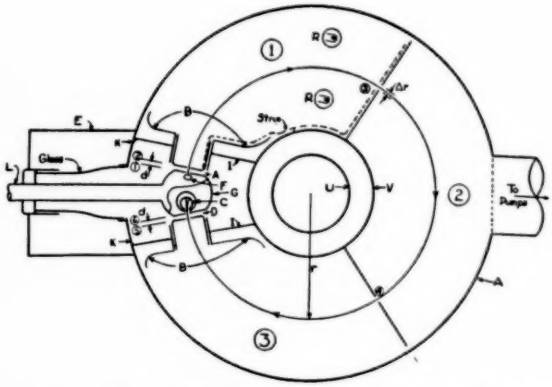

FIG. 1. Schematic diagram of measuring chamber, approximately to scale. Chamber diameter = 32 cm. Electron radius = 9.9 cm. The "strip" indicated by the dotted line was inserted only in a test experiment.

EFFECTIVE ANGLE θ

In Eq. (1) above, the quantities ν and H_r are determined by direct measurement, but θ does not correspond exactly to the angle between any physical points. By definition in the derivative of Eq. (1), θ is defined as "the angle which would be subtended by the path of an electron if an electron traveled for one cycle at the constant velocity v_f which it has in the electric field free space" (regions 1, 2 and e, Fig. 1). Since finite times are required for acceleration and deceleration, an electron does not travel for quite a full cycle at its maximum speed. An accurate expression for θ in terms of measurable quantities is needed.[7]

The obtaining of an expression for θ is complicated by the penetration of the radiofrequency field through the slits at A and D, Fig. 1, since this alters the distance over which acceleration and deceleration occurs. With the geometry necessary the penetration was large. Thus with a gap $d = 1.6$ mm and a slit width $\Delta r = 0.25$ mm the field at $1/10d$ either way from the slits still amounts to 10 percent of the maximum. An attempt was made to obtain the expression for θ, but even rough approximations could not be handled due to the fact that with the slit width not zero the acceleration is a function of both time and position. It was found, however, that the function giving θ could be obtained if Δr were assumed to be zero. To utilize this, experimental

[7] The expression obtained in Part I was based on such an oversimplified picture of conditions that it is considerably in error.

observations were taken as follows: The value of the magnetic field H_r at "resonance" was observed for several values of slit width. A curve was then plotted of H_r against Δr and the extrapolated value at $\Delta r=0$ was used with the θ computed for the same condition to obtain e/m.

Derivation of expression for θ with $\Delta r=0$

The path of an electron is conveniently divided into three parts: (1) an acceleration distance of length d between slits 1 and 2 (see Fig. 1); a distance d_f of constant speed between slits 2 to 5; and a decelerating distance, also equal to d, between slits 5 and 6. Since an angle is equal to its arc divided by the radius Eq. (1) may be rewritten as

$$e/m=[d_f+f(d)](\nu/rH_r), \tag{2}$$

where the function of d, namely $f(d)$, is the expression to be found.

Five simplifying assumptions are necessary besides the condition that $\Delta r=0$: (1) there exists a uniform electric field in both gaps A and D, but the field is zero elsewhere. The extent and symmetry of the slits on either side of the region crossed by the electron beam assures uniformity. Its absence elsewhere was assured insofar as it is possible by completely coating regions 1, 2 and 3, Fig. 1, with gold (evaporated on). Surface charges will be discussed in the section "Results." (2) The electric field E between the slits varies linearly with time during the acceleration or deceleration of an electron (i.e., curvature of the sine wave neglected); that is:

$$E=E_i+st \text{ (e.m.u.)}, \tag{3}$$

where $s=dE/dt$, t is time measured from entrance of electron into the field and E_i is the field at $t=0$. Since the time spent by an electron in crossing either gap is about 1/200 of a period and since E_i is about 80 percent of the maximum field, it is easily found that the deviation from linearity amounts to only about 1.2 parts in 10,000 so that the assumption is well justified. (3) The mass m of the electron is constant and equal to that at its maximum velocity, as determined by the radiofrequency ν (see straight line $m=m_\nu$, Fig. 2). The actual variation (of the order of 0.3 to 0.6 percent) is indicated by the dotted curve. To test the assumption, a solution B was also obtained with the other extreme of mass in the gaps 1–2 and 5–6, namely $m=m_0$. This changed the calculated e/m_0 by the utterly negligible amount of 6 parts in 10^{10}. (4) The initial velocity (at slit (1)) is zero. This neglects thermal velocities as well as contact potentials between the filament and slit (1). (As previously stated no d.c. potential was applied.) (5) No contact potentials exist around the path between slits (1) and (6). Assumptions (4) and (5) are tested by special solutions given after the main derivation and are shown not to effect appreciably the results.

The method of solution can be most easily understood by referring to Fig. 3 in which two segments of the sine wave of field variation are shown, and here drawn as straight lines of slope s in view of assumption (2). Equal ordinates of the two segments are, of course, separated by a time interval equal to one period or $1/\nu$. E_a and E_d are the fields at the beginning of acceleration and deceleration respectively, while t_a and t_d are the total times of acceleration and deceleration. The constant velocity v_f of an electron between slits (2) and (5) is directly obtained from the radial force equation in terms of the magnetic field H_r as

$$v_f=H_rre/m \text{ (e.m.u.)}. \tag{4}$$

Hence the time spent between slits (2) and (5) is simply the distance divided by the velocity as given in Fig. 3. In view of the periodicity of E we can write

$$E_d=E_a+s\left(t_a+\frac{d_f}{H_rre/m}-\frac{1}{\nu}\right). \tag{5}$$

The tangential force equation for acceleration (tangential motion being taken as the y direction) is

$$d^2y/dt^2=(e/m)(E_a+st). \tag{6}$$

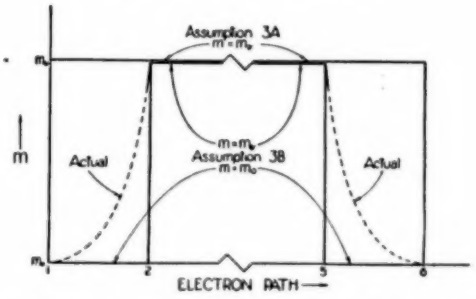

FIG. 2. Assumed and actual variation of electron mass.

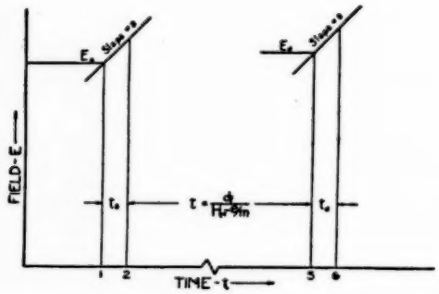

FIG. 3. Field and time terminology in motion of electron from slits (1) to (6). Lines with slope s are segments of successive sine waves.

The value of E_a can be obtained from this upon integration once and setting equal to Eq. (4) with $t=t_a$, giving

$$E_a=(H_r r/t_a)-(st_a/2). \tag{7}$$

Eq. (7) substituted in a second integration of (6), again with $t=t_a$, yields a cubic in t_a. The correct root after lengthy algebraic manipulation gives a power series expression for t_a

$$t_a=\frac{2d}{H_r r(e/m)}\left[1+\frac{2}{3}\left(\frac{d^2s}{H_r^3r^3(e/m)^2}\right)+\frac{4}{3}\left(\frac{d^2s}{H_r^3r^3(e/m)^2}\right)^2\right]. \tag{8}$$

In a similar manner E_d is found identical with Eq. (7) when the subscripts are changed from a to d, and t_d is identical with Eq. (8) except for a negative second term in the bracket.

These results placed in Eq. (5) give

$$\frac{e}{m}=\left\{d_f+d\left[\frac{4}{3}+\frac{8}{3}\left(\frac{d^2s}{H_r^3r^3(e/m)^2}\right)^2\right]\right\}\frac{v}{rH_r}\text{ e.m.u.} \tag{9}$$

The last term in the bracket [ ] affects e/m only to the extent of two parts in 10^7 and so is quite negligible. With sufficient accuracy we therefore have

$$e/m=\{d_f+(4/3)d\}v/rH_r\text{ e.m.u.} \tag{10}$$

Comparison with Eq. (2) shows that $f(d)$ is simply $4/3d$ and the effective angle θ is then

$$\theta=(d_f+(4/3)d)1/r=\theta_f+(4/3)\theta_d. \tag{11}$$

We have so far considered only the group R electrons (see Part I, page 407) accelerated and decelerated on the rising or positive slope part of the voltage wave. A similar treatment of the group F on the falling or negative slope of the voltage wave yields the same relation as Eq. (9), and hence the two groups behave identically in spite of the asymmetry in acceleration.

Test of assumption (4)

The initial and final velocities in the above deviation were assumed zero (assumptions 4 and 5). Let us now assume the initial velocity is not zero but say equal to v_0 due to thermal velocities and a contact potential between filament and slit (1). Then if no further contact potentials exists (assumption 5) the final velocity will also be v_0. If a new solution is made with these limits, the result can be put into the form of Eq. (10) but with an added factor multiplying d, *viz.*

$$e/m=\left\{d_f+\frac{4}{3}d\left[\frac{1+2(v_0/v_f)+\frac{3}{4}(1+v_0/v_f)(8/3)K}{1+2(v_0/v_f)+(v_0/v_f)^2}\right]\right\}\frac{v}{rH_r}\text{ (e.m.u.)}, \tag{12}$$

in which $(8/3)K$ is the negligible term in Eq. (9), and v_f is defined in Eq. (4). Since v_f involves e/m the equation is not completely solved for e/m, but due to the smallness of the [ ] term, this is immaterial. The effect of v on the calculated e/m can be determined by substituting in Eq. (12) the following typical values of the quantities in the bracket { }: $d_f=58.4$ cm, $d=0.1594$ cm, $(8/3)K=7.9\times10^{-5}$, $v_0=$velocity of a one volt electron, $v_f=$velocity of a 2000 volt electron. The change in the calculated e/m is found to be only -1.5 parts in 10^6. For an initial velocity corresponding to two volts, it is -3.2 parts in 10^6. Thus no reasonable assumption for the initial velocity results in an appreciable change in the calculated e/m. In passing, it should be noted that if the direction of the contact potential is such as to oppose the electron motion from filament to slit (1) then no error results from the contact potential as long as it is constant during a series of measurements.

Test of assumption (5)

In all of the foregoing, it has been assumed there were no contact potentials between slits

(1) and (6) (assumption 5). This is equivalent to saying that the initial fields E_a and E_d (see Fig. 3) are produced entirely by the impressed radiofrequency voltage. If a contact potential V_a exists between slits (1) and (2) and a potential V_d between slits (5) and (6), then the following substitutions must be made in place of the initial fields:

$$E_a \rightarrow E_a + V_a/d, \quad E_d \rightarrow E_d + V_d/d. \qquad (13)$$

The potentials are taken as positive when they produce a field in the same direction as E_a or E_d. If with these substitutions a new solution is made for each electron group there results in place of Eq. (10)

$$e/m = \frac{d_f + (4/3)d}{rH_r((1/\nu) \pm (V_a - V_d)/sd)} \text{(e.m.u.)}, \qquad (14)$$

where the (+) sign is for the (R) group and the (−) sign for the (F) group of electrons. This result shows that if $V_a \neq V_d$ the two groups are not in resonance (i.e., will not be stopped) at the same values of the magnetic field. Since the shift for the two groups is equal and opposite, the effect (see Fig. 4) is to make the collector current minimum at resonance shallow if the potential difference is positive and broad if negative. Thus contact potentials in the two gaps can cause poor experimental conditions but *do not produce any shift of the observed* e/m. The existence of any contact potentials in the region between slits (2) and (5) is highly improbable since all the surfaces there were coated with gold by evaporation. Surface charges[5, 6] will be considered in "Results."

Evaluated for typical conditions, the magnitude of the shift indicated in Eq. (14) can be seen from the expression

$$\frac{(V_a - V_d)/sd}{1/\nu} \doteq \pm 8 \times 10^{-4}(V_a - V_d), \qquad (15)$$

where the potentials are now expressed in volts. Thus a *net* contact potential difference of one volt results in a shift in the magnetic field H of ±8 parts in 10,000. Judging from the depth and sharpness of the minimum existing during the recording of all final data of this work, and making allowance for the actual slit width used, it is probable that $(V_a - V_d) \leq 0.05$ volt.

To summarize this section: an accurate expression giving θ in terms of measurable quantities has been found in Eq. (11), and contact potentials as well as initial thermal velocities have been shown to produce a negligible effect on the result. Eq. (1) when multiplied by m/m_0 gives the formula used in all computations, namely

$$e/m_0 = (m/m_0)(\theta\nu/H_r) \text{ (e.m.u.)}, \qquad (16)$$

where we now have

$$\theta = \theta_f + (4/3)\theta_d \text{ (radians)}. \qquad (11)$$

θ_f is the angle subtended by the path from slit (2) to (5) and θ_d is the angle subtended by the path from slit (1) to (2) (equal to that from (5) to (6)). The mass ratio is

$$m/m_0 = [1 - (r\theta\nu/c)^2]^{-\frac{1}{2}} \qquad (18)$$

since $v_f = r\theta\nu$ (i.e., distance ÷ time). c is the velocity of light, H_r is the magnetic field at resonance and ν is the radiofrequency.

Apparatus and Standards

The apparatus for the present work was largely new and was built subsequent to the work of Part I. Particular care was taken on the numerous details of the equipment, much of which cannot be mentioned here. Some general precautions taken included: continuous thermostating of the whole room as well as the more precise thermostating of the standard cells and the Helmholtz coils; complete radiofrequency shielding of all electrical apparatus; a high speed pumping system (oil diffusion pumps because of the gold coated measuring chamber) which gave a pressure under working conditions of 1 to 2×10^{-6} mm/Hg; the keeping of liquid air on

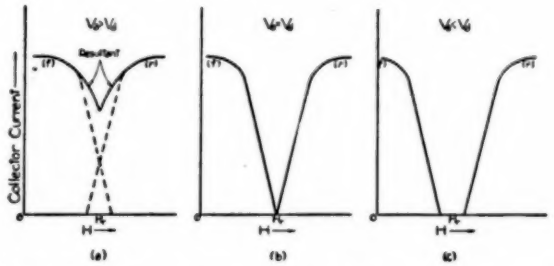

FIG. 4. Effect of contact potentials in gaps. V_a = potential between slits (1) and (2). V_d = potential between slits (5) and (6).

the trap between pumps and chamber at *all* times when the chamber was sealed and evacuated to prevent, as far as possible, the contamination of the gold surfaces with oil vapor; the careful reduction of stray magnetic fields from various parts of the equipment and from elsewhere in the building until the total of such d.c. fields was about 1.5×10^{-4} oersteds (effect on e/m negligible as the axial component of this is measured as a part of the earth's field) and of the a.c. fields to about one-quarter of this; the placing of all apparatus containing iron as far away as possible with a minimum distance of 1.5 meters from the chamber.

(A) Measuring chamber

A new chamber was constructed having many refinements in mechanical precision and accuracy. Some idea of the care put into its construction can be gained from the fact that ten months time of a skilled mechanic was required for its construction. (Auxiliary equipment made by the machine shops, which included the angle and radius measuring device, the form for the standard solenoid, etc., required another five months.)

A schematic diagram of the whole chamber has been given in Fig. 1. A detail of the region of the electron gun and collector is shown in Fig. 5 (same lettering of parts in both). A heavy brass can A with a removable cover has a heavy tube U passing through its center. A spider V consisting of a cylinder with four arms carrying slits (2), (3), (4), and (5) is accurately centered, aligned and *entirely* supported by a cone on U. The purpose of this design is to avoid any motion of the slit system due to compression of the chamber when evacuated. All four of these slits have conical joints, as at J, by means of which the edges of the slits could be adjusted to parallelism with the axis of U. All slits were adjustable also in a radial direction through the rotation of eccentric pins (not shown) and were held tightly in their adjusted positions by concealed leaf springs. The axial length of opening of all slits was stepped down to 2 mm by thimbles as at T. The spacing of slits (2) and (5) relative to (1) and (6) respectively (i.e., the distance d) could be varied by sliding the cylinders N in the cylinders O. Keys prevented rotation.

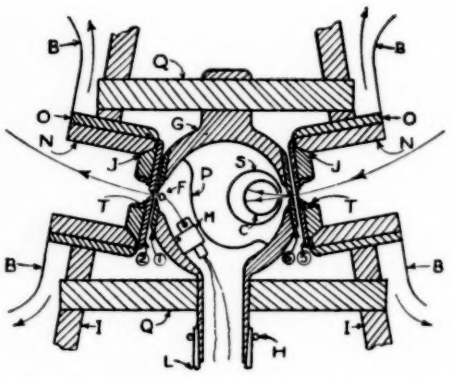

FIG. 5. Cross section of chamber in vicinity of electron gun G and collector C.

The electron gun mounting G (a cylinder perpendicular to the plane of figure) was supported on two ground quartz rods Q, the lead-in L to it being in part flexible braided copper tubing. A water cooling coil at H (supplied through flexible leads along L) kept the gun at the same temperature as the rest of the chamber. The gun subtended an angle of about 20° on the axis. The unipotential oxide coated filament at F was 5 mm long and indirectly heated by a hairpin heater which produced a negligible external magnetic field. The geometry connected with this filament and slit (1) is most important. The primary requirement is that, as the slit width Δr is reduced towards zero, the extent of the radiofrequency field approach in the limit the accurately measurable outer face of the slit (1). Other requirements are that sufficient emission be attained through the penetration of the radiofrequency field and that the distance from the face of F to the outer face of slit (1) be a minimum to avoid curling inward of the electron paths by the magnetic field before the electrons attain appreciable speeds. These requirements were satisfied by reducing the thickness of the slits (1) to 0.005 inch at their edges and by placing the filament by means of a microscope 0.005 ± 0.001 inch back of them. The filament was supported at M and enclosed in a "box" by a partition P with end caps above and below. Leads to it came through L and *through* the inductance plugged into the end of it.

The radiofrequency was fed to the electron gun through L and to the chamber through the concentric copper tube E (the chamber being

grounded). Brushes K along the outer edge, top and bottom of the arms I provided a direct path from E to the slits (2) and (5). Pumping around the gun was accomplished through a large number of holes in the arms I and thence around the baffles B. The holes were covered with screen to further improve the radiofrequency shielding.

The collector at C was shielded by a shield S extending up from the bottom of the chamber. The outer edges of S and C were on the same radius as the outer slits, but the inner edges were on successively shorter radii to allow for curling of the electrons at lower velocities. The spacing between S and the back of slit (6) was about 1.5 mm.

To reduce the effect of surface charges on insulating films formed under electrom bombardment[5, 6] all of the surfaces of regions (1), (2) and (3), Fig. 1, were coated with gold. This was applied by evaporation from helical filaments after thorough cleaning, followed by the running of a discharge under a partial vacuum. In regions (2) and (3) the filaments were introduced temporarily through holes in the cover. In region (1) two filaments surrounded by gold grids were permanently mounted at R. This region frequently required recoating since the electron current bombarded a large fraction of the walls over a central strip about 5 mm wide. An electrode for running a discharge could be lowered (under vacuum) from the cover, after which it was withdrawn leaving no insulating surfaces visible to the beam.

The Helmholtz coils which produced the magnetic field were accurately aligned and spaced by mounting them on extensions of tube U above and below the vacuum chamber. To avoid the long time (3 or 4 hours) required for temperature, and hence for current equilibrium, the coils were equipped with water jackets supplied with thermostated water by a constant gravity flow system. The whole chamber was mounted on three legs and its axis kept parallel with the earth's field by use of the amplifier arrangement described in Part I, page 409.

(B) Radius and angle measurement

The value of e/m found is directly dependent on the angle θ given by Eq. (11). The electron radius r must be known only approximately for calculating the mass ratio, Eq. (18), but enters more precisely through the magnetic field H_r since the field constant of the Helmholtz coils is a function of the radius of the electron orbit.

A device to measure both angles and radius was designed as follows: a long internal cone was turned in the upper end of the tube U, Fig. 1. A male cone inserted in this carried a heavy plate in a plane perpendicular to the axis. The plate had a (silver) angle scale ruled along its outer periphery for some 35° and also carried a microscope with micrometer eyepiece located with axis parallel to the main axis and passing through the electron orbit. A second microscope with micrometer eyepiece was mounted on the outer (turned) face of the chamber C, Fig. 1.

If cross hairs in the rotating microscope are turned radially and made successively coincident with faces of slits (2), (1), (6) and (5) and the readings on the angle scale noted through the fixed microscope, the angles θ_f and θ_d are readily obtained. Since a complete circle was not ruled, errors of eccentricity could not be directly checked. Through the cone construction used in centering and pivoting, through the avoidance of dust particles on the cone, and through the most careful centering of the plate on the divided circle when the scale was ruled, it is believed the maximum possible eccentricity was 0.0003 inch, which would cause an error in θ of only 3 parts in 10^6. Through the courtesy of the Mount Wilson Observatory the scale was ruled on its large (approximately 4 foot) divided circle. The two microscope system was used in ruling, and lines were ruled every 5′ of arc. Measurements were always made using several pairs of lines on the angle scale but the results never differed by more than a few seconds of arc. To insure accuracy of setting, both micrometer eyepieces had cross hairs consisting of a *pair* of closely ruled lines, the object sighted on being centered between them. In spite of this there is a subjective error possible when sighting on the face (or end) of a slit due to the light and dark contrast. To check this the contrast was reversed in direction by sighting on the edges of the polished steel spacers used in setting the gap d. Agreement to one second of arc (probably this small only by chance) was obtained from the

average of several sets of readings. Furthermore, the measured angle θ_d checked within 2″ arc that computed from the length d and radius r.

The observational probable error in measuring an angle, based on the external consistency of five determinations taken over a period of a year, was $\pm 3''$ arc. In spite of the apparent sum in Eq. (11), analysis shows that the observational error in θ is the same as for one angle. The probable error in θ was then estimated in seconds of arc as follows: observational $\pm 3''$; instrumental $\pm 3''$; indefiniteness of a slit edge due to rounding, etc. $\pm 4''$; total probable error $= \pm 6''$. An additive allowance of 4″ for constant errors brings the final p.e. in the angle θ to $\pm 10''$ arc in 340° or ± 8 parts in 10^6.

For the radial setting of the slits, the micrometer eyepiece of the rotating microscope was provided with both a fixed and a moving pair of cross hairs. One slit was then set to bisect the inner, the other to bisect the outer cross hair. This was done successively at all six slits and resulted in an accurately constant slit width Δr and slit radius r (mean). The actual values of r and Δr were obtained from a specially ruled glass scale. This scale (which had a large hole through its center) was placed on a table with a vertical column and cone (duplicate of that in U, Fig. 1), and centered on the axis of the cone. By placing the arm with microscope in this cone the radius of both the fixed and movable cross hairs could be determined from the closely spaced lines on the scale. The table was adjustable in height (for focus) and *both* the table and arm could be rotated to detect errors of eccentricity. The table moved about cylindrical surfaces so carefully ground that no error from play could be detected. Errors from illumination of the lines at different angles were eliminated by a device through which the light source was centered on the optical axis. The scale was calibrated in terms of a newly calibrated (N.B.S.) decimeter scale.

The probable error in the radius measurement was estimated as follows: since a motion of a slit of 2×10^{-4} cm was easily apparent, the p.e. in setting is taken as $\pm 1\times10^{-4}$ cm; error from rounded edges $\pm 2\times10^{-4}$ cm; lack of exact parallelism of edges with axis of U (Fig. 1) $\pm 0.5\times10^{-4}$ cm; calibration of scale $\pm 2\times10^{-4}$ cm; total p.e. $= \pm 3\times10^{-4}$ cm. An additive allowance of 2×10^{-4} cm was made for constant errors, giving a final p.e. in the radius of $\pm 5\times10^{-4}$ cm, or about ± 5 parts in 10^5. The resulting error in the magnetic field H_r happens to be one seventh of this or $\pm 7\times10^{-6}$ parts. Temperature corrections were made to the standard temperature used, namely 23.6°C.

The validity of taking the effective radius as the average of the inner and outer slit radii must be considered. It is well known, particularly in connection with 180° velocity filters,[8] that the divergence of the beam from the source causes a spread of the focal point into a short line extending radially inward. In the present case slits (5) and (6) are somewhat in front of the second focus (at which point the error would be zero). This, combined with the relatively small slit width used ($\Delta r/r \doteq 2.5\times10^{-3}$) makes the effect small. An order of magnitude computation indicates that the shift of the center of gravity of the beam was probably not more than one part in a million of the radius, and hence is negligible.

(C) Collector current measurement

The electron current to the collector C, Fig. 5, was measured by an FP 54 electrometer tube used in a DuBridge and Brown circuit.[9] The maximum sensitivity with a leak of 8×10^{10} ohms was 1.4×10^{-16} amp./mm. Originally a large zero shift was observed with changing magnetic field due to a magnetron effect of the magnetic field (order of 15 oersteds) on the FP 54. This was eliminated by so placing and orienting the FP 54 that this shift was substantially zero over the range of magnetic fields used.

Since the collector was situated near the center of a source of radiofrequency radiation of the order of one-third of a kilowatt, shielding would not prevent blocking of the tube. The trouble was avoided by the insertion of a resistance of 10^8 ohms between the control grid and the collector side of the leak. At the high frequencies used (of the order of 5×10^7 cycles) this resistor removes most of the radiofrequency voltage from the grid to itself. Even at maximum sensitivity the switching on of full radiofrequency power

[8] W. A. Wooster, Proc. Roy. Soc. **A114**, 729 (1927).
[9] DuBridge and Brown, Phys. Rev. **4**, 532 (1933).

did not produce a detectable deflection of the galvanometer.

The collector and shield S (Fig. 5) were mounted eccentrically on a ground joint so that a small rotation of the system produced in effect a radial motion of the collector slit. The proper location of the collector slit (1 mm wide) was therefore easily found. Quantitative measurements showed that over a large "central" region no shift in the position of the current minimum could be detected.

No retarding potential was put on the collector to draw back secondaries since it was found that such a potential, for reasons not evident, caused a slight irregularity and asymmetry in the current minimum.[10]

(D) Frequency source and measurement

The general requirements in the radiofrequency source were the following: (1) it must furnish a continuous range of frequencies between 40 and 60 megacycles (7.5 to 5 meters); and (2) peak voltages up to 4000 volts; (3) the frequency must be constant and known to at least one part in 10^5.

The continuous range of frequency with good constancy was sufficiently well satisfied by using a low power electron coupled[11] master oscillator. The output of the oscillator was tuned to the second harmonic. This was followed by four stages of class C power amplification to yield the power of about one-half kilowatt necessary to produce the 4000 volt peak. This is shown schematically in the lower part of Fig. 6, the lower numbers in each block indicating the number and type of tubes used. The last amplifier fed through a concentric tube transmission line T_3 into a shielded box (adjacent to the e/m chamber) and was coupled to the inductance L. The capacity of this tank circuit consisted primarily of that of the electron gun to the adjacent slits. A *small* trimmer was added at C in order to be able to tune this circuit over a small frequency range. The use of two tuned tank circuits connected by a matched impedance transmission line undoubtedly produced a much more nearly sinusoidal voltage on the electron gun than the arrangement in Part I, and also greatly reduced in the e/m chamber dc magnetic fields from the plate current flowing through the inductances. To aid in this latter the r.f. chokes in the last two stages were made in the form of space wound toroids.

Leads to the electron gun filament, as mentioned earlier, pass *through* the tubing of which L is made and are taken out in a shielded cable at the point F (r.f. ground). At V is indicated a wire acting as an antenna which picked up a constant fraction of the electron gun voltage and impressed it on the grid of a tube voltmeter immediately adjacent. The latter was used to adjust the peak voltage to the desired value, as a monitor to check constancy, and as an aid in exact tuning of the amplifier. The voltmeter was calibrated by finding the maximum value of the magnetic field for a given r.f. voltage at which electrons can be sent around the e/m chamber (the inner slit radius was used for the voltage computation). The voltage (in volts) is given by

$$V=\frac{c^2}{(e/m_0)\times 10^8}\left(\frac{m}{m_0}-1\right).$$

Using Eq. (18) the voltage is obtained as a function of the frequency ν:

$$V=\frac{c^2}{(e/m_0)\times 10^8}\left[\left\{1-\left(\frac{r\theta\nu}{c}\right)^2\right\}^{-\frac{1}{2}}-1\right]. \quad (19)$$

Frequencies were obtained in terms of a government standard, using the carrier wave of one of the larger broadcast stations as an intermediary. Through arrangements made with the Federal Radio Commission, the San Pedro Monitoring Station made checks on the carrier frequency at times during which measurements were being made. In addition the management of KFI (the station whose carrier was used) made available the record of their checks taken at half-hour intervals in terms of their own standard. The latter was calibrated weekly by the crystal-clock system of RCA Communications Laboratory at Point Reyes. These two checks were in substantial agreement and indicated that the carrier frequency seldom deviated from its nominal value (640 kc) by more than one part in 10^5 and was usually within 4 cycles or 6 parts in 10^6.

No attempt was made to demodulate the carrier and to produce harmonics directly be-

[10] The use of a retarding potential did not cause any change in the location of the minimum.

[11] J. B. Dow, Proc. I. R. E. **19**, 2095 (1931) and Q. S. T. **16**, No. 1, 23 (1932).

cause it was felt that enough frequency modulation would be left to be troublesome. Instead a local oscillator (electron coupled) was set to within a fraction of a cycle of KFI's frequency through use of a broadcast receiver and a zero beat indicator (upper part Fig. 6). High harmonics of this (11th to 87th) were selected by a tuned output circuit and fed into a detector with tuned output. A small fraction of the output of the master oscillator was also fed into the detector by the transmission line T_1. Thus the nth harmonic of KFI's fundamental could be heard from the speaker beating with the mth harmonic of the master oscillator. Since the frequency of the master oscillator was doubled, the output frequency is given by

$$\nu = 2(m/m)\nu_0. \tag{20}$$

In some of the earlier results the multiplying factor was 6 instead of 2.

The probable error in the frequency ν was estimated as follows: variation of carrier from nominal value ± 4 parts in 10^6; operational, in setting and maintaining the zero beats ± 2 parts in 10^6; total p.e. $= \pm 3.5$ parts in 10^6. An additive allowance of 2.5 parts in 10^6 was made for constant errors giving a final p.e. in the frequency of ± 6 parts in 10^6.

The question was raised during the course of the work as to the exactness of the integral relationship of harmonics at these frequencies (order of 50 megacycles) where the size of a tank circuit is beginning to become an appreciable (though small) fraction of a quarter wave-length. A test was made to see if results were consistent

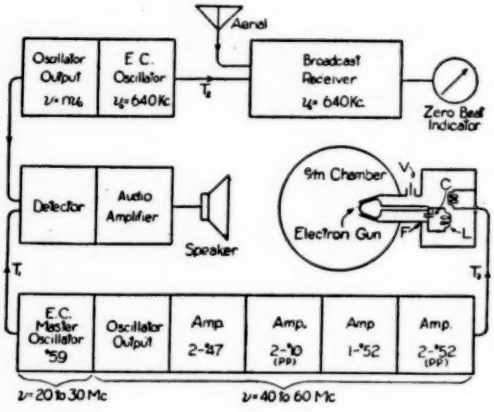

FIG. 6. Source of radiofrequency and scheme for frequency measurement.

when different harmonic combinations giving little change in frequency were used. The combinations[12] used were 6(54/5) and 6(11/1) with a frequency difference of only 1.8 percent. Measurements, made with a minimum possible lapse of time between to eliminate other possible variations, gave results differing in e/m_0 by only 1 part in 10^6, which is less than the observational probable error.

(E) Magnetic field determination

The magnetic field is made up of two parts: that produced by the current i_H in the Helmholtz coils and that due to the earth's field (about 4 percent of the former). The first involves knowledge of the Helmholtz constant k_R on the central plane at a radius R equal to that of the electron orbit; the latter requires the value of the Helmholtz constant k_0 on the axis at the central plane, since the earth's field was measured by reversing the Helmholtz current and determining the current i_e necessary to balance the Helmholtz field on the axis against the earth's field. The expression for the magnetic field at the electron radius R is then:

$$H_R = k_R i_H + k_0 i_e. \tag{21}$$

Instead of using a flip coil and ballistic galvanometer to determine the balance with the earth's field, a much more sensitive and rapid arrangement was used consisting of a continuously rotating coil (40 r.p.s.) connected to a high gain amplifier (up to 10^6 voltage gain). The output was indicated by a sensitive detector circuit with a long time constant to smooth out transients. Ten readings spread out over ten minutes (to give a better time average) gave a result with an observational probable error of only ± 2.5 parts in 10^5, which effects H_R by ± 1 part in 10^6. The earth's field was measured before and after each run, small differences being linearly interpolated with time.

Both i_H and i_e were measured by the usual potentiometer method. A careful calibration of the Wolf potentiometer used was made and the small ohmic corrections applied to each reading. The currents could be read directly to one microampere (about 1 part in 10^6 of i_H). The standard of voltage consisted of three standard

[12] See Eq. (20).

cells kept in a thermostat with a temperature constancy better than 0.01°C. Two of the cells had new N.B.S. certificates shortly after the beginning of the present work (1933). The absolute value of the voltage standard was reestablished late in 1936 by a new cell with an N.B.S. calibration. Spurious errors of more than a few microvolts were eliminated by careful construction of the circuit and switching plugs.

(1) *Helmholtz coils.*—The same coils were used as in the work of Part I. Each consisted of 399 turns (19 layers, 21 turns/layer) wound in the channel of a cast aluminum wheel with stiff fiber insulation between layers. The mean radius was about 20 cm. The coils were hermetically sealed with beeswax to prevent moisture absorption.

The magnetic field constants were calculated directly from the geometry in Part I. Although the absolute values obtained were not used in the present work it was necessary in the process of comparison with a standard to know the manner of variation of the field over a region in the vicinity of the electron orbit. The method used to determine this variation took into account the cross section of the coils and was based on a direct adaptation to the present problem of Lyle's method[13] for the computation of mutual inductance between coaxial coils. Since his method is based on finding an approximately equivalent single filament which will give the same magnetic potential at all points, it is equally applicable to magnetic field computations. By computing the field constant for a series of radii centered about the electron orbit of radius $R(\doteq 9.9$ cm) and spaced at equal intervals, an expression of the following form (valid over interval $r=9.5$ to 10.3 cm) was obtained by central differences:

$$k_r = k_R[1 - B(r-R) - C(r-R)^2 - D(r-R)^3 - E(r-R)^4]. \quad (22)$$

(2) *Standard solenoid.*—The absolute values of the Helmholtz field constants were determined by comparison with a carefully constructed solenoid. In choosing the general dimensions of the latter the choice had to be made between the usual long solenoid involving in this case certain difficult mechanical features, and a short solenoid without the mechanical difficulties and crowding. The latter was chosen. Although it is now felt the former would have been better, the only essential difference has been the increased work required to measure the short solenoid geometry.

The standard solenoid consisted of 100 turns of about No. 21 B & S gauge copper wire wound with a spacing of 36 turns/inch and having a radius of about 5.6 cm. In precise work the form used has generally been of marble but more recently[14] of quartz, glass or porcelain. The surfacing of these materials requires considerable technique. To avoid the troubles associated with such materials a form was evolved after some experimentation which consisted of a heavy copper cylinder threaded with rather flat grooves (120°). On this were thoroughly baked two coats of Bakelite varnish. Grooves were turned in the Bakelite matching those in the copper and leaving a uniform film of Bakelite 0.010 cm in thickness. The wire wound in these grooves was made especially for the purpose[15] (commercial wire not being sufficiently round) and deviated from uniformity in diameter by only 0.00005 inch (maximum to minimum). The advantages of this design are: the Bakelite provides an easily machinable surface which has sufficient insulation and which, due to its negligible thickness, cannot appreciably change the coil dimensions by moisture absorption; the coefficients of expansion of wire and form are the same; and (of the greatest importance) the thermal conductivity between wire and form is so high that no appreciable temperature difference can exist with a reasonable current (only 0.12°C with one ampere). A disadvantage is that a period of six months or more after winding must elapse before the diameter is measured in order to allow for flow of the Bakelite under the wire tension. With an initial wire tension of 1.1 kg, the observed diameter decrease was 0.002 cm or 1.8 parts in 10^4. The form was turned with an internal cone to fit over that on the tube U, Fig. 1, so as to make the solenoid coaxial and centered relative to the Helmholtz coils.

The wire was specially treated to remove kinks

[13] See page 38, Sc. Papers of N.B.S., No. 169.

[14] See for example "An Absolute Determination of the Ohm," Curtis, Moon and Sparks, N.B.S. J. Research **16**, 5 (1936).

[15] Acknowledgment is made to the Cleveland Wire Works of the General Electric Company for making and donating the special wire used.

and wound on the solenoid under constant tension. During the winding, the wire diameter was measured in a radial direction every half turn using a micrometer reading directly to 0.00001 inch so that errors from the small wire ellipticity were eliminated. The calibration of this micrometer was later checked on the comparator.

The over-all solenoid diameter was measured at 45° intervals on every turn (i.e., four measurements per turn). This was accomplished by a special apparatus built to fit on the carriage of a Pratt-Whitney precision lathe. The apparatus consisted of two anvils sliding in grooves on a vertical base plate and each carrying a small piece of glass with a diamond ruled line. The anvil ends, lapped flat, and wide enough to cover only one turn of wire were situated on opposite ends of a solenoid diameter. The carriage was attached to the screw so that the anvils followed the turns as the coil was rotated. The pressure against the wire (37 grams or 1.3 oz.) was the minimum required to avoid sticking. Doubling the pressure gave no appreciable difference. By the use of a microscope and a calibrated micrometer eyepiece, small displacements of the anvils could be measured relative to two fixed lines on a sheet of plate glass mounted on the back of the base plate and in the same focal plane as the moving lines. The distance between those fixed lines was determined by the National Bureau of Standards. The distance between the anvil lines when their faces were in contact was measured in terms of a decimeter also calibrated at the N.B.S.

Several readings on a given diameter usually had a spread less than 2×10^{-5} cm. The average eccentricity (maximum less minimum diameter) was 2.5×10^{-4} cm and the diameter increased fairly uniformly from one end to the other by 9.1×10^{-4} cm. To determine the effect of this diameter change, the field at the solenoid center was computed by dividing the solenoid into ten equal sections and obtaining the contribution from each. The analysis showed that the field was greater than the value obtained from the average diameter by 3.6 parts in 10^6.

The observational probable error in the mean diameter of the whole coil was obtained from the four diameter measurements by separating them into two groups each consisting of a 90° pair. This avoids eccentricity errors in the comparison. The two groups differed by 1.7×10^{-5} cm, which indicates a probable error of $\pm0.6\times10^{-5}$ cm, but to be conservative the observational p.e. will be taken as $\pm1\times10^{-5}$ cm. This and the other estimated probable errors r entering into the diameter are listed in Table I. Five lengths were required to convert micrometer eyepiece readings to diameters, and the five corresponding probable errors are listed in addition to the above observational p.e. All but the first of these involves the accuracy of the decimeter standard and the calibration of the Gaertner comparator, which are also listed. In addition, an additive allowance of two microns is made for constant errors, giving a final p.e. in radius equivalent to ±2.7 parts in 10^5.

The measurement of the pitch of the solenoid was made by placing the coil directly on the carriage of the comparator. Here again four transits were made the length of the coil but spaced at 90° intervals. To determine the effect of variations in pitch on the magnetic field, data were taken for a ten section analysis. The mean pitch of a ten turn section was taken as the mean spacing of five turns at the beginning and five at the end; for example the pitch of the third section (from the 20th to the 30th turns) was taken as one-tenth the distance from the mean coordinate of turns 18, 19, 20, 21 and 22 to that of turns 28, 29, 30, 31 and 32. The coordinate for a single turn was taken as the mean of the readings on each side. This eliminates errors from varying wire diameter. The ten section analysis showed that the effect of the pitch variation (caused by an unbalanced rotating member of the lathe carriage) was such as to lower the magnetic field at the center by 1.55 parts in 10^5. A twenty section analysis would probably not change this figure more than 1 or 2 parts in 10^6.

A list of probable errors r is given in Table II. The observational probable error was computed from the consistency of the four transits. The maximum deviation from the mean was about 1×10^{-6} cm (in about 0.07 cm) and the p.e. $=\pm2.6\times10^{-7}$ cm. The probable errors in the decimeter standard and in the comparator calibration were the same as in the diameter measurements (see Table I) for a length equal to that of the coil. Hence for *one* pitch the values are 0.01 of these. An additive allowance for constant errors was

again made, giving a final p.e. in pitch equivalent to ± 1.4 parts in 10^5.

The mean radius and pitch of the winding on the solenoid can then be used to compute the magnetic field at the center, or as was actually done the mutual inductance with the flip coil. However, the result should be corrected by ± 3.6 parts in 10^6 for the radius variation, by -15.5 parts in 10^6 for the pitch variation, and by ± 4.2 parts in 10^6 due to the effective current radius being less than the radius of the geometric center of the wire, or a net correction of -7.7 parts in 10^6. The result so found had a probable error R given by the equation

$$R=[r_a^2(\partial H/\partial a)^2+r_p^2(\partial H/\partial p)^2]^{\frac{1}{2}}, \qquad (23)$$

where r_a and r_p are the probable errors in the mean radius and pitch, found above to be, respectively, $\pm 15\times 10^{-5}$ cm and $\pm 1.0\times 10^{-6}$ cm; and $(\partial H/\partial a)$ and $(\partial H/\partial p)$ are the rates of change of field with radius and pitch, equal respectively to 1.211 and 38.11 oersteds/amp. R, the p.e. in the field of the standard solenoid, was found from these to be $\pm 1.86\times 10^{-4}$ oersteds/amp., or $+2.0$ parts in 10^5.

(3) *Calibration of Helmholtz field on the axis.*—The Helmholtz field at the axis was directly determined in terms of the standard solenoid by the usual method of opposing the two and measuring the balance point with a flip coil and ballistic galvanometer.[16] The axes of the coils were made accurately parallel to the earth's field, and the earth's field linkages had to be added to those of one field, namely the Helmholtz.

This comparison method makes the flux linkages of the flip coil with the standard solenoid equal to the sum of those from the Helmholtz field and the earth's field, that is

$$M_s i_s = M_H i_H + M_H i_e,$$

where M is a mutual inductance and i is a coil current. By straightforward reasoning it can be shown that the Helmholtz field constant k_0 on the axis is given by

$$k_0=(M_s'/m_H')(i_s/i_H+i_e), \qquad (24)$$

where i_s and i_H are the standard solenoid and Helmholtz currents at balance, i_e is the Helmholtz current sufficient to produce a field equal to that of the earth, M_s' is the *calculated* value of the mutual inductance between flip coil and solenoid, M_H' is the same with the Helmholtz coils, and m_H' is defined by $M_H'=m_H'k_0'$, in which k_0' is the *calculated* Helmholtz field constant. Thus m_H' is the flux linkage with the flip coil from the Helmholtz field when the latter is equal to unity on the axis. It depends only on the manner of variation of the Helmholtz field in the flip coil region and not at all on the absolute value of the field.

The value of M_s', the mutual inductance of the solenoid with the flip coil, was calculated by the formula of Searle and Airey,[17] and as a check by the formula of Roiti,[17] the results agreeing to 1 part in 10^7 and giving the value 519,989.9 e.m.u. after the necessary correction of -7.7 parts in 10^6 (see preceding section). Since this is about $\frac{1}{3}$ percent less than would exist with a uniform solenoid field, it was necessary to calculate the uncertainty introduced into the result by uncertainties in the flip coil geometry. This was done in detail, together with some supplementary experimental measurements, and it was found that the probable error due to the flip coil geometry was not greater than ± 7 parts in 10^6. In passing it is to be noted that if *uniform* fields are being compared, this error is zero due to the ratio M_s'/m_H' in Eq. (24).

The value of m_H', the flux linkages from the Helmholtz coils per unit central field, was also calculated by the formula of Searle and Airey,[17] and as a check by the assumption of a uniform Helmholtz field, the latter approximation giving a value only 1.0 parts in 10^6 less. The result was 5507.131 e.m.u.

The value of i_s, the solenoid current at balance, was obtained by least squares from a plot of the galvanometer throws against i_s for values near balance, i_H being held constant. i_e was similarly obtained. Determinations were made on four days between 1 and 5 A.M. so as to avoid errors from the much larger earth's field (or local field) fluctuations in day time. Complete temperature corrections were computed but were negligibly small, due primarily to the design of the standard solenoid which kept the rise in temperature of the

[16] The continuously rotating coil and amplifier arrangement is not suitable for the comparison of fields, one or both of which vary appreciably in the volume occupied by the flip coil.

[17] Sc. Papers of the N.B.S., No. 169, pp. 61 and 57.

winding above that of the form to 0.12°C (with $i_s'=1$ amp.), and due to the thermostating of the room.

In the derivation of Eq. (24) it has been tacitly assumed that all surrounding space has a permeability equal to unity. The obvious deviation from this assumption requires investigation. During construction of the measuring chamber samples were prepared of every piece of brass used. Samples were also cut from one of the Helmholtz coil forms and from the standard solenoid. The susceptibility of each was measured and the results, expressed as the deviation from unity of the permeability, varied from -1×10^{-5} to $+1\times10^{-5}$. Since these materials occupied only a part of the space in the immediate vicinity, it is felt that the probable error from them is not more than ±5 parts in 10^6. As to material somewhat more removed: the placing of apparatus containing iron and the fields from all apparatus including circuits has been discussed earlier. There remains the effect of the iron reinforcing in the concrete floor at a distance of about 1.25 meters. A good estimate can be obtained from work[18] done at the National Bureau of Standards in the absolute determination of the ohm. Their glass form standard of inductance has approximately the same ratio of length to diameter as both the present standard solenoid and Helmholtz coils. Making allowances for the relative sizes, the iron in the floor probably increased the fields, and therefore the mutual inductance, of the Helmholtz coils by 5 parts in 10^6, and of the solenoid by less than 1 part in 10^6. The first increase would appear in the *measured* value of k_0 and the second is negligible. Hence no uncertainty results.

The value of k_0, the Helmholtz constant on the axis, was found by Eq. (24) to be

$$k_0=17.92116 \text{ oersteds/amp.},$$

a value 2.68 parts in 10^4 less than that calculated directly from the Helmholtz geometry.

A list of probable errors r is given in Table III.[19] The observational error given is the internal p.e. based on the p.e. (from least squares) of each of the four determinations. The external p.e. based on consistency of the four results was 1.1 parts in 10^5, a value slightly smaller than the internal p.e. An additive allowance for constant error brings the total p.e. in the Helmholtz field constant on the axis to ±4.0 parts in 10^5.

(4) *Ratio of Helmholtz field on axis to that on electron orbit.*—This ratio was determined through the use of two small flat coils placed in the plane of the electron orbit, one centered on the orbit (radius R) and one on the axis. These ratio coils were connected in series-opposing to a ballistic galvanometer so that the resulting deflection D_1 when the Helmholtz field was suddenly reversed was proportional to the *difference* of the two

TABLE I. *Probable errors in measurement of standard solenoid diameter (wire centers).*

Length	Origin of Error	Probable Error $r\times10^5$ cm
	Obs. p.e. in direct diameter measurement	1
1	P.e. in glass scale (taken as ½ limit of error given by N.B.S.)	5
2	Meas. of anvil distance	3
3	Calibration of micrometer eyepiece (one side)	1
4	Calibration of micrometer eyepiece (other side)	1
5	Measurement of wire diameter	5
2–3–4–5	Decimeter standard (taken as ½ limit of error given by N.B.S.)	5
2–3–4–5	Calibration of comparator in terms of decimeter	3

For diameter $(\Sigma r^2)^{\frac{1}{2}}$ $= 10\times10^{-5}$ cm
Allowance for constant errors $= 20\times10^{-5}$ cm
Final p.e. in diameter $=\pm30\times10^{-5}$ cm ($=\pm2.7$ parts in 10^5)
Final p.e. in radius $r_a=\pm15\times10^{-5}$ cm ($=\pm2.7$ parts in 10^5)

TABLE II. *Probable errors in measurement of standard solenoid pitch.*

Source of Error	Probable Error $\times10^7$ cm
Observational p.e.	2.6
Decimeter standard (taken as 0.5×0.01 limit of error given by N.B.S.)	5
Calibration of comparator ($=0.01$ p.e. in a 7 cm length)	3

$(\Sigma r^2)^{\frac{1}{2}}$ $= 6.4\times10^{-7}$ cm
Allowance for constant errors $= 3.6\times10^{-7}$ cm
Total p.e.: $r_p=\pm1.0\times10^{-6}$ cm ($=\pm1.4$ parts in 10^5)

[18] Curtis, Moon and Sparks, N.B.S. J. Research **16**, 32 (1936).

[19] The solenoid, Helmholtz coils and flip coil were so accurately centered and aligned that no appreciable errors could occur from this cause.

mutual inductances and to the Helmholtz current i_1, i.e.:

$$D_1 = c(M_0 - M_R)i_1.$$

The constant c can be eliminated if only one coil is used, for instance the one on the axis. The other is left in the circuit but removed to some distance. In this case the deflection is:

$$D_2 = cM_0 i_2.$$

By straightforward reasoning it can then be shown that the ratio of the Helmholtz field constant on the axis k_0 to that on the electron radius k_R is

$$k_0/k_R = [1 - (D_1 i_2/D_2 i_1)]^{-1} \cdot (m_R/m_0). \quad (25)$$

If the single coil used is the one on the electron orbit, the deflection then being D_3 and the Helmholtz current i_3, the ratio becomes

$$k_0/k_R = [1 + (D_1 i_3/D_3 i_1)](m_R/m_0), \quad (26)$$

in which m_R is defined by $M_R = m_R k_R$ and m_0 by $M_0 = m_0 k_0$. Here M_R and M_0 are the mutual inductances with the ratio coils on the electron orbit and axis respectively. m_R and m_0 are therefore the flux linkages per unit field at the center of the coil and depend on the manner of variation of the Helmholtz field (not on its absolute value) and on the geometry of the ratio coils.

In the above it has been assumed that the ratio coils are identical. The error resulting from their dissimilarity can be reduced to a negligible amount by interchanging them and taking the average of the two resulting ratios. The presence of a large amount of brass in the field causes a delay in the reversal because of the eddy currents induced, but the final change in flux linkages is unaltered. It is required only that the ballistic galvanometer period be long enough and that the rates of change of flux through the ratio coils be substantially the same. This last was accomplished by adjusting the relative amounts of brass around the two coils.

The ratio coils were very carefully made and each consisted of 594 turns, layer wound. The coil length was about 0.5 cm and the outer diameter about 2.6 cm. The diameter of each layer was measured at six points. Although such care is of some value for the ratio problem, it was taken primarily so that these coils might be used to check the geometry of the flip coil employed in the axis determination of the preceding section.

The value of m_0, the flux linkage with a ratio coil on the axis per unit axial field, is rigorously given by the formula

$$m_0 = \pi \sum_{n=1}^{n=NL} a_n^2 N_T, \quad (27)$$

where a_n = radius of the nth layer, $N_T = 18$ = number of turns per layer, $N_L = 33$, the number of layers. This was computed for both coils, and the coils were found to differ by 2.13 parts in 10^3, although they had exactly equal inner and outer diameters.

The value of m_R, the flux linkage with the ratio coil on the electron orbit per unit field at radius R, can be most conveniently calculated from a development (exact on the central plane) of the following form:

$$m_R = m_0 - 2N_T \sum_{n=1}^{n=NL} \int_{R-a_n}^{R+a_n} [B(r-R) + C(r-R)^2 + D(r-R)^3 + E(r-R)^4] r \cos^{-1}\left(\frac{r^2+R^2-a^2}{2rR}\right) dr, \quad (28)$$

where a is simply the radius a_n treated as a continuous variable in the integrand, and the bracket term is the fractional variation of the field from the value at R as given in Eq. (22). The integral was evaluated graphically. Sufficient precision is easily attainable since the whole negative term is less than 0.1 percent of m_0. The summation was evaluated for both ratio coils. These results were later checked by expressing the integrand in an approximate form which could be integrated, the result differing only 8 parts in a million from the graphical value (average) of m_R. These results from Eq. (28) were increased by 6.72 parts in 10^5 to allow for the small variation of the Helmholtz field off the central plane (i.e., along the 0.25 cm half-length of the ratio coils). This correction also was graphically determined. For comparison, m_R was of the order of 8 parts in 10^4 less than m_0.

In the taking of the data for Eqs. (25) and (26), two further precautions were observed: (1) all deflections were made closely the same in order

to avoid any ballistic galvanometer error from nonlinearity; (2) besides taking data with the coils interchanged, additional data were taken for D_1 with the outer ratio coil rotated through 180° in order to average out eccentricity errors. The results: Eqs. (25) and (26) give ratios the average of which at the electron radius was $k_0/k_R=1.033152$. From this and the value of k_0 given in the preceding section, the magnetic field constant at the electron radius (9.89810 cm) is

$$k_R=17.34610 \text{ oersteds/amp.}$$

which is 10.02 parts in 10^4 less than that calculated directly from Helmholtz geometry.

A list of the probable errors r entering into k_R is given in Table IV. The observational probable error was calculated from the consistency of the ratios found by Eqs. (25) and (26), using completely independent sets of data and was ±1.3 parts in 10^5. From the check on m_R mentioned it is believed that the p.e. in the calculation of m_R/m_0 is certainly not more than ±0.3 part in 10^5. The effect of uncertainties in the geometry and location of the ratio coils was studied. The only dimension of importance was found to be the radius R of the center of the outer ratio coil. The fractional change in k_R is one-seventh that in R. Due to the care exercised in the precise mechanical construction of coils and holder, and in the measurement and checks of R, it is believed that the p.e. in R can be taken as ±0.001 cm. This makes the fractional p.e. in $k_R=\pm1.4$ parts in 10^5. Small temperature corrections were made in R and in all other contributing factors. The uncertainty in k_0 must be included in k_R. An allowance for constant errors (in addition to that in k_0) brings the total p.e. in the Helmholtz field constant on the electron orbit to ±6.0 parts in 10^5.

(5) *Discussion of calibration results for the Helmholtz coils.*—The foregoing results of the calibration in terms of the standard solenoid gave measured values lower than those calculated directly from the Helmholtz geometry by 2.68 parts in 10^4 on the axis and 10.02 parts in 10^4 on the electron orbit. The reasonableness of this result should be examined. Since with the Helmholtz coils used, the rate of change of magnetic field on the electron orbit with changing Helmholtz radius was practically zero (a most useful property), there is one and only one solution to the necessary changes in the Helmholtz radius and spacing which will account for the results. It is that the radius is 0.0042 cm less and the total spacing 0.012 cm greater than the measured amounts. The first change is quite likely as a result of compression of the fiber interlayer insulation, as the radius was measured four years previous to calibration. Since the spacing between the Helmholtz forms was measured shortly before calibration, the mean centers of the windings must deviate this much from the geometrical centers of the forms. This deviation is quite possible. It is therefore concluded that the measured magnetic field constants are in reasonable agreement with the earlier calculated values.

TABLE III. *Probable errors in the Helmholtz field constant k_0 on the axis.*

SOURCE OF ERROR	PROBABLE ERROR $r\times10^5$ PARTS
Observational p.e. (internal)	1.4
Standard solenoid	2.0
Flip coil geometry	0.7
Permeability of surroundings not unity	0.5
$(\Sigma r^2)^{\frac{1}{2}}$	2.6
Allowance for constant errors	1.4
Total p.e.	±4.0

(6) *Earth's magnetic field nonuniformity and its compensation.*—The uniformity of the earth's field, or more precisely the net field in the room, was measured by placing the rotating coil used in the measurement of the earth's field on an arm at the electron orbit radius. This could be rotated to any point on the orbit. The field was found to vary (maximum to minimum) around the orbit by practically one percent. The cause was undoubtedly a group of vertical iron pipes in a wall about 5 meters away. Since this amounts to 4 parts in 10^4 of the total field, a compensation device was necessary.

The arrangement used was suggested by Professor Barnett and consisted of two compact coils placed on the axis of the chamber, one a half meter above, the other a half meter below the plane of the electron orbit. The two coils were oriented with axes parallel to the electron plane and in the direction of the field maximum-minimum. With opposite polarities there results

on the electron plane only an axial component (i.e., no radial component) which varies as cos ϕ, where ϕ is the azimuth angle. Thus correction is made for linear variation (in the maximum-minimum direction) of the room field. Since the room field did not vary quite linearly, it was possible to reduce the variation only from one percent to 0.25 percent. This, however, means that the deviation from the mean was only 5 parts in 10^5 of the total field, and since the direction of maximum-minimum happened to be symmetrically oriented with respect to the slit system, no appreciable error should result.

The mean value of the field around the orbit is higher than that at the center, and this requires a small correction of -6 parts in 10^6 in the value of e/m_0.

Results

In obtaining the data for the computation of e/m_0 by Eq. (16), the general procedure was to vary the magnetic field (i.e., vary the Helmholtz current i_H) and observe its value at the resonance minimum, with frequency held constant. Other experimental conditions held constant through all observations included: (1) The emission current to slit (1) was held at 10 μa; (2) the ratio of the peak of the radiofrequency voltage to that at which the electrons were accelerated was kept at the arbitrary value of 1.24; (3) the room was thermostated to a temperature at, or as near as possible to, 23.6°C; (4) the temperature of the Helmholtz coils also was maintained at about 23.6°C by adjustment of the temperature of the thermostated cooling water.

Helmholtz currents were recorded to a precision of 1 μa (they were of the order of one ampere) and all known corrections including temperature and ohmic errors in the potentiometer were applied to the same precision. These temperature corrections included standard resistance (kept in an oil bath), electron radius and Helmholtz spacing (the Helmholtz radius correction was negligible). These corrections were applied to the observed i_H so as to give the value which would have been obtained at 23.6°C (the temperature of all standardization). To facilitate comparison of runs at the same frequency the total magnetic field current i_T was defined as

$$i_T = i_H + (k_0/k_R)i_e, \tag{29}$$

so that the total magnetic field (see Eq. (21)) is then simply

$$H_R = k_R i_T = 17.34610 i_T. \tag{30}$$

H_R is now used with the added significance of the field *at resonance* and is therefore identical with H_r of Eq. (1).

(A) Shape of resonance minimum

A typical plot of current to the collector C, Fig. 1, as a function of the Helmholtz current is given in Fig. 7 for the region of resonance and on to the cut-off point. An enlarged detail of the lower quarter of the minimum is given in Fig. 8 in which a very narrow appendix is seen at the bottom. This tip of the minimum is further magnified in Fig. 9.

The shape of the resonance minimum is important since disturbing factors affecting it could cause the apparent minimum to differ in location from the true minimum. A small anti-clockwise tilting is evident in Fig. 7. However, if the large sloping background is subtracted most, though not quite all, of this tilting is removed. The deep, narrow tip of Fig. 8 is due to the fact that electrons in the vicinity of slit (6), when slowed down below a certain minimum velocity, suffer such an inward change of direction as to entirely miss the slit in the collector shield. The slowing down occurs, of course, *equally* on both sides of resonance. The correctness of this explanation was demonstrated by doubling the distance from slit (6) to the collector shield. The tip was then observed to triple in width. (In making this test a sleeve was inserted inside the gun to keep constant the capacity from shield to gun.) Part of the width of the tip was at times due to contact potentials in the gaps (see Fig. 4c). In two-thirds of the final essential data (upper two curves of Fig. 15) the tip was only 40 to 50 percent as wide as in Fig. 9.

In studying Fig. 8, it is noticed that the point P determined by extrapolation of the straight sides is to the left of the center of the tip by about 2.5 parts in 10^4. One reason the value of the field at the center of the tip has been taken as representing resonance and not P is that the location of P is not constant over a period of weeks and further can be shifted at will (over a small range) *without moving the tip* by applying,

for example, a small retarding potential between collector and shield (collector positive). Another most important property of the tip of the minimum is that along the lower three-quarters its center, as shown in Fig. 9 by the line of mean abscissas, is absolutely vertical to 1 or 2 parts in 10^6.

(B) Slit correction data

As explained in the section on the "Effective Angle," observations on the current minimum must be taken for a series of slit widths Δr and the extrapolated value of the magnetic field used in Eq. (16) to get e/m_0. In addition, it was desired to check experimentally the validity of Eq. (11) by varying the slit spacing d and observing the constancy of the results. The data for these objectives are given in the first quarter of Table V and are plotted in Fig. 10. Curves drawn through the points must have zero slope at $\Delta r=0$ because the slit penetration by the field approached zero asymptotically as $\Delta r/d \rightarrow 0$. First, the solid curves were drawn graphically. Later, dotted curves were obtained by least squares *assuming* a function of the form $y=a+bx^2$. With separate plots it is apparent that the graphical fit is better for the upper curve and poorer for the lower. Because of this and because of the arbitrariness of the assumed function (limited by the small number of points) an average of graphical and least squares results is probably as reliable a value as can be obtained.

In all of the work that follows the slit width was held at 0.250 mm and the larger d used. The slit correction to the observed magnetic field current is then (see Fig. 10) $i_s=-0.000049$ ampere when the frequency is 4.14720×10^7 cycles. Similar data at a higher frequency of 5.18400×10^7 cycles gave $i_s=-0.000052$. The magnetic field current in the remainder of Table V has been corrected in proportion to these values.

The values of e/m from the two slit spacings differed by only 1.5 parts in 10^5, which is within the sum of the probable errors of extrapolation and is therefore considered a good check on the validity of Eq. (11).

(C) Observed e/m_0 as a function of electron energy

The most important check in any free electron determination is the constancy of results with varying electron energy. The initial data for this are found in the middle of Table V,[20] points 1 to 9, and are plotted as the lower curve in Fig. 11. An increase of about 2 parts in 10^4 in e/m_0 was found with a 57 percent energy increase (of the same order and sign as in the preliminary results, Part I).

A possible cause of this increase might be a phase difference in the radiofrequency voltage between the accelerating and decelerating gaps as a result of the greater capacity on the decelerating side of the electron gun due to the collector shield S (Fig. 5). To check this, an added variable capacity was provided for the accelerating gap in the form of a disk placed parallel to the face of slit (2) and held by a sleeve in contact all around with the cylinder θ, Fig. 5. A strip the width and length of the slits (2) was cut out of the middle of the disk so as not to change the slit spacing d. Quantitative analysis seemed impossible but rough estimates indicated 0.5 $\mu\mu$f should provide an effective balance.

Observations were made with an added capacity of 2.1 $\mu\mu$f (points 10 to 14 of Table V and dotted curve, Fig. 11). The results were essentially the same below 2100 volts, though the resonance minimum was shallow. But towards the higher energies the minimum became so very shallow and broad that its apparent location was appreciably shifted by the sloping background,

TABLE IV. *Probable errors in the Helmholtz field constant k_R at the electron radius.*

Source of Error	Probable Error $r\times10^5$ Parts
Observational p.e.	1.3
Ratio of m_R/m_0	0.3
Effect on k_R of uncertainty in radius R	1.4
Field constant on axis, k_0	4.0
$(\Sigma r^2)^{\frac{1}{2}}$	4.4
Allowance for constant errors additional to that in k_0	1.6
Total p.e.	±6.0

[20] The calculated values in this table were computed by formula as follows: electron voltage by Eq. (19); the external probable error R_e by least squares from the values for the associated runs; the mass ratio by Eq. (18); the apparent e/m_0 by Eq. (16) with θ (calculated by Eq. (11)) equal to 5.922561 radians for $d=1.308$ mm, and $\theta=5.920636$ radians for $d=1.594$ mm, and with H_R as obtained from Eq. (30).

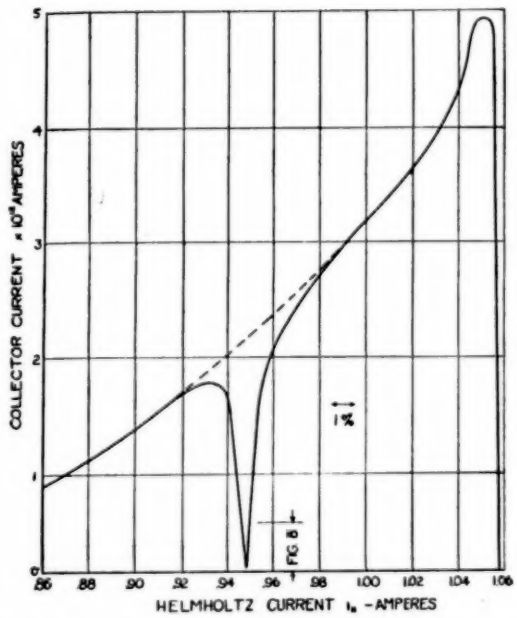

FIG. 7. Collector current in general region of resonance minimum. Frequency $\nu = 4.9920 \times 10^7$ cycles, slit width $\Delta r = 0.250$ mm, slit spacing $d = 1.594$ mm.

and rapidly increasing values of e/m_0 were found. The effect of unbalance due to considerable *over* correction having thus been shown, the correct estimated value of 0.5 $\mu\mu$f was tried (points 15 to 17). The minimum was now found to have returned to its normal depth but it was narrower by a factor of two than that shown in Fig. 9. This narrowing was probably not due to the change in capacity from 0 to 0.5 $\mu\mu$f but to a change in some other factor such as contact potentials (see Fig. 4c). No significant change from the $\Delta C = 0$ results was found using 0.5 $\mu\mu$f. The apparent e/m_0 averaged 7 parts in 10^5 higher but the curve was tilted slightly to the horizontal (see Fig. 11) so as to suggest an approach to the same value at high energies.

It was now apparent that the condition of the gold surface in the deflecting chamber was influencing the results. To obtain quantitative data, a complete new coat of gold was evaporated on the deflecting chamber and new data immediately obtained with the same capacity of 0.5 $\mu\mu$f (points 18 to 21). The apparent e/m_0 shifted about 1 part in 10^4 higher and the curve was tilted still more to the horizontal. Another example of this shift is point (10) taken with $\Delta C = 2.1$ $\mu\mu$f and all new gold. Due to experi-

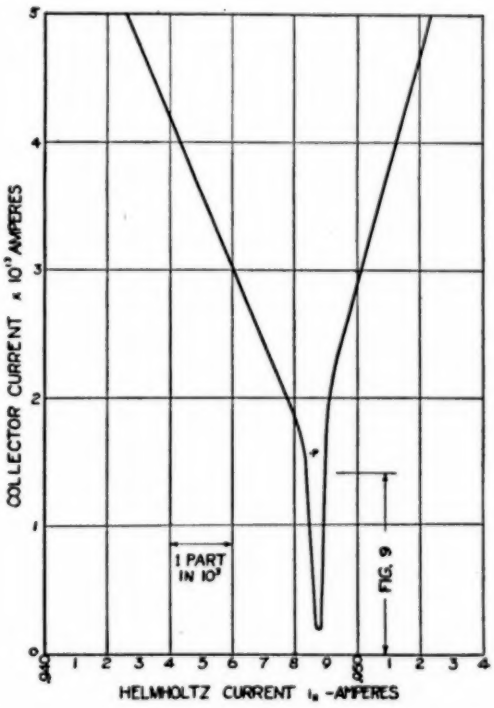

FIG. 8. A magnified section of Fig. 7 showing the bottom of the resonance minimum.

mental troubles a week's time and perhaps 15 hours of electron bombardment elapsed before

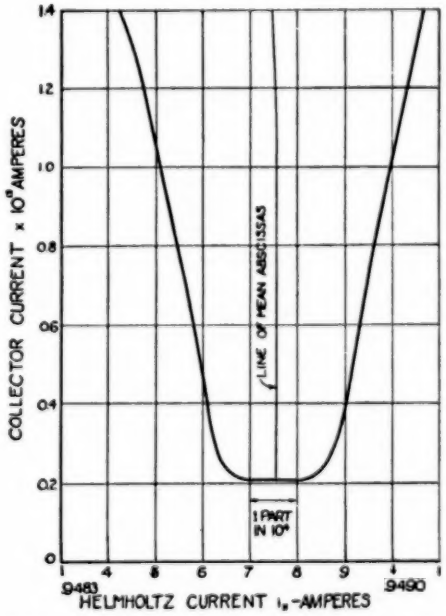

FIG. 9. A section of Figs. (7) and (8) with still greater magnification showing the bottom of the resonance minimum. During the taking of two-thirds of the final data the width was 40 to 50 percent of that shown here.

the taking of point (11), which was 1.4 parts in 10^4 lower. Still another example is the average value of the results, taken with new gold, of Fig. 10, namely $(\Delta e/m_0)/(e/m_0) = -5.45$ parts in 10^4 (on Fig. 11, would be near point (18) just below the curve), which is 2.42 parts in 10^4 higher than the average of points 1, 2, 3 and 4 taken with an old surface. From those examples and a study of earlier data it is evident that *if the gold surfaces of the deflecting chamber were a few days old and had suffered electron bombardment for perhaps fifteen hours, a reduction occurs in the apparent e/m_0 results of the order of 1 or 2 parts in 10^4, the curves becoming steeper the greater the reduction.*

(D) Surface potential study

It is believed that in spite of good vacuum conditions, small electron currents and the use of gold surfaces, the foregoing effect was due to the formation of an insulating film as described by Shaw[6] and Stewart.[5] Most of the electron bombardment occurs in compartment (1), Fig. 1. It therefore seemed of value to check this explanation roughly by inserting an insulated metal strip in compartment (1) (see dotted line, Fig. 1). This strip approximately covered the area bombarded by electrons and hence a positive potential applied to it should cancel the assumed negative charge on the insulating film (the latter of course would now be considered to have reformed on the strip). Qualitatively the results,

TABLE V. *Main data: first 7 points for slit correction (see Fig. 10); last 21 points show variation in e/m_0 with electron energy (see Fig. 11), taken with various capacities added to one side of electron gun to test possibility of phase error. A "run" consists of 10 consecutive observations, a "point" of two or more runs taken at different times.*

Curve	Point	Number of Runs	Slit Width Δr (mm)	Frequency ($\times 10^5$ Cycles)	Electron Voltage V (Volts)	Total Magnetic Field Current iT (Amperes)	Probable Error, R_e ($\times 10^{-6}$ e.m.u.)	Mass Ratio m/m_0	Apparent e/m_0 ($\times 10^7$ e.m.u.)	$\frac{1.760 - e/m_0}{1.760}$ ($\times 10^{-4}$ Parts)
Slit correction:	1	4	0.250	4.14720	1689	0.807 724	6	1.003 303		
	2	4	.300	"	"	.807 757	9	"		
$d = 1.308$ mm	3	4	.400	"	"	.807 832	4	"	1.759 029	−5.52
	4	3	.550	"	"	.807 979	5	"		
	5	3	.250	"	"	.807 423	4	"		
$d = 1.594$ mm	6	5	.400	"	"	.807 491	2	"	1.759 055	−5.37
	7	2	.550	"	"	.807 590	4	"		
	1	4	.250	"	"	.807 585	5	"	1.758 593	−7.99
	2	3	"	"	"	.807 579	2	"	1.758 606	−7.92
Variation with	3	4	"	"	"	.807 591	3	"	1.758 580	−8.07
energy:	4	4	"	4.16000	1700	.810 067	4	1.003 324	1.758 653	−7.65
	5	2	"	4.53120	2018	.882 809	3	1.003 947	1.758 829	−6.65
$C = 0$ μμf	6	2	"	4.54400	2030	.885 344	1	1.003 969	1.758 786	−6.89
	7	2	"	4.60800	2087	.897 905	5	1.004 082	1.758 806	−6.78
	8	6	"	4.99200	2452	.973 386	2	1.004 796	1.758 871	−6.41
	9	6	"	5.18400	2646	1.011 149	3	1.005 175	1.758 968	−5.86
	10	8	"	4.14720	1689	.807 453	4	1.003 303	1.758 880	−6.36
	11	2	"	4.16000	1700	.810 073	5	1.003 324	1.758 640	−7.73
	12	2	"	4.60800	2087	.897 917	3	1.004 082	1.758 782	−6.92
$C = 2.1$ μμf	13	2	"	4.99200	2452	.973 328	2	1.004 796	1.758 975	−5.82
	14	2	"	5.18400	2646	1.011 014	5	1.005 175	1.759 203	−4.53
	15	2	"	4.16000	1700	.810 013	1	1.003 324	1.758 771	−6.98
$C = 0.5$ μμf	16	2	"	4.60800	2087	.897 846	2	1.004 082	1.758 921	−6.13
(Old gold)	17	3	"	5.18400	2646	1.011 087	4	1.005 175	1.759 076	−5.25
	18	4	"	4.16000	1700	.809 876	5	1.003 324	1.759 068	−5.30
$C = 0.5$ μμf	19	3	"	4.60800	2087	.897 749	3	1.004 082	1.759 111	−5.05
(New gold)	20	2	"	5.18400	2646	1.010 997	0	1.005 175	1.759 233	−4.36
	21	2	"	5.56800	3056	1.086 727	3	1.005 977	1.759 274	−4.13

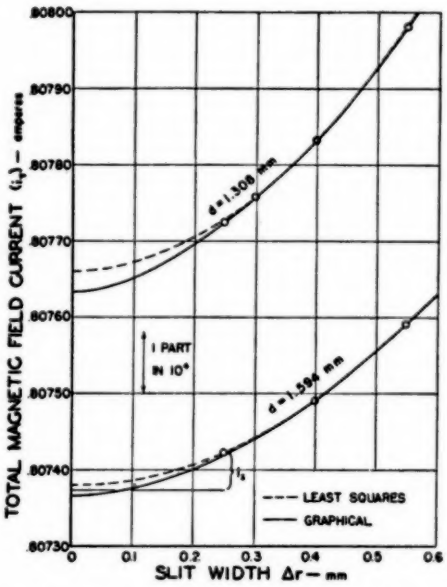

FIG. 10. Effect of slit width on location of resonance minimum. $\nu = 4.14720 \times 10^7$ cycles.

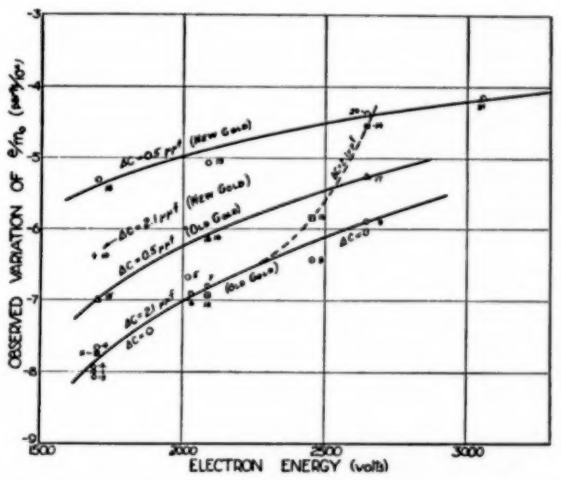

FIG. 11. Variation of observed e/m_0 with electron energy. Slit width $\Delta r = 0.250$ mm, slit spacing $d = 1.594$ mm. At zero variation $e/m_0 = 1.7600 \times 10^7$ e.m.u. ΔC is the extra capacity added at the accelerating gap. The curves were determined by least squares assuming the form $y = a - b/x$.

Fig. 12, check the surface charge explanation: the observed values of e/m_0 are *raised* and by amounts greater for lower electron voltages than higher, thus giving a more nearly constant value of e/m_0 with varying electron energy.

Quantitatively the points (18) and (20), on which the variation is based, require a *difference* in the two curves of Fig. 12 of 0.94 part in 10^4 to make the results independent of energy. This (by extrapolation) requires a strip potential of roughly +9.4 volts to neutralize the surface potential on a new gold surface. Similarly for an old gold surface the $\Delta C = 0$ curve indicates a surface potential of approximately 19 volts. The existence of surface potentials of this magnitude on metals such as gold, or even brass, has apparently not been previously reported. Even with positive ions under conditions of high current density and poor vacuum conditions, one volt is about the maximum reported.[6a] Shaw[6] has given some data for a transient phenomenon he terms "surface polarization" (electron beams moving parallel to metal surface). For gold under the present conditions, his work would indicate potentials of the order of 0.01 to 0.25 volt. He gives no data for the permanent films formed by electron impact with which we are mainly concerned here. Stewart[5] states that these films have minimum resistances of 10^6 ohms (over an area of perhaps (?) 10 mm²) and rupturing voltages of 4–14 volts. Nevertheless the positive experimental evidence that a reduction in the observed value of e/m_0 does occur with aging of the gold surfaces, the initial value being again found with a new surface, seems to indicate definitely such large surface potentials[21] as the cause of the variation of the observed e/m_0 with energy.

(E) Study of effect of space charge in front of filament

Two other factors have been found which change the observed e/m_0 values. Both of these are associated with the space charge in front of the filament. Fig. 13 is an instantaneous plot of the potential from the face of the filament to the deflecting chamber, when the slit width Δr is not zero. The effective accelerating distance is then not d but AB, and the location of A is a function of the space charge existing at that instant. A change in A[22] alters the observed e/m_0 through the change of the effective angle θ.

(1) *Effect of varying the filament emission.*—Increase of electron emission through raising the

[21] Since the strip test is an approximation to actual conditions the potentials found are also to be taken as approximate, but should be correct within a factor of two.

[22] The location of point A would also be changed if the filament were not replaced at the same distance from slit (1) after recoating. In practice it was found that results never differed after recoating by more than 1 part in 10^4 and averaged much closer than this.

filament temperature always caused a decrease in the observed e/m_0, as is shown in Fig. 14. The point A would be pushed outward from the filament by increased space charge. This would decrease θ and hence increase the observed e/m_0 since it is computed with constant θ. Since the observed shift is negative it is thus evident that increased negative surface potentials due to the increased density of current incident on the films is a more important factor resulting in a reduction of the observed e/m_0.

(2) *Variation of the peak radiofrequency voltage.*—If the frequency and emission were held constant and the peak radiofrequency voltage V_m increased from a value near the resonant electron voltage V_0, the observed e/m_0 was found to increase slightly: 0.6 part in 10^5 at $V_m/V_e = 1.24$, 1.2 parts in 10^5 at 1.35, 2.3 parts in 10^5 at 1.47. The space charge and field in front of the filament are not static but continually changing in step with the radiofrequency. During the half of each cycle in which slit (2) is negative no current flows and the space charge grows, probably spreading out even in front of slit (1). Then as the potential reverses, current again flows and the space charge is gradually reduced. But the time elapsing between zero potential and a potential of V_e volts is less the greater the peak V_m, and hence with more of the space charge left, the point A is farther from the filament and the observed e/m_0 is greater since it is computed with constant rather than with decreasing angle.

This applies to the electrons accelerated on the rising part of the cycle (see Part I, page 407). Those accelerated on the falling part of the cycle might experience no change in angle or possibly a smaller increase. Thus, increasingly higher peak voltages should also cause increasingly divergent effective angles for the two groups of electrons, the sense of the changes being such as to make the minimum more shallow. This effect was observed though it was small.

The essential point in consideration of both these space charge effects is that no net error results in e/m_0 with the procedure adopted: i.e., all results taken with the same emission current (10 μa to the first slit), the same ratio of peak to electron voltage ($V_m/V_e = 1.24$) and with the slit correction determined at various frequencies. In fact, it makes no difference where the point A occurs as long as it is fixed for all observations at a given frequency, since the method of extrapolating results to zero slit width Δr always moves it in the limit (through the i_s correction) to the face of slit (1).

The effect of surface changes remains after the slit correction. If, however, the surface charge is constant (constant emission current and small lapse of time) and the results are extrapolated to infinite electron energy, this error also should be removed.

(F) The value of e/m_0

The experimental situation is then briefly this: no indication of an error due to a phase difference between accelerating and decelerating slits was

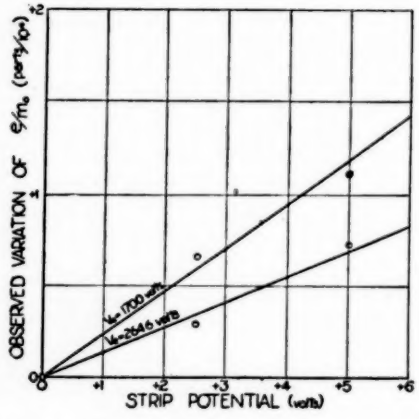

FIG. 12. Effect on e/m_0 of potential on an auxiliary strip placed to simulate the negative surface charges but used with a positive potential so as to cancel them. Data taken at two electron energies.

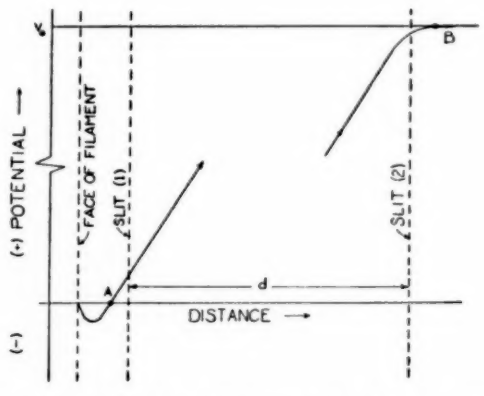

FIG. 13. Qualitative picture of potential in region of filament and accelerating gap at the time the electrons dealt with are accelerated, showing effect of space charge on accelerating distance $A-B$.

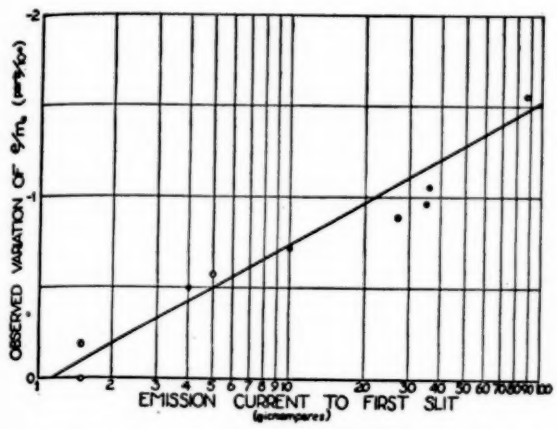

FIG. 14. Effect of varying filament emission on e/m_0. Taken at an electron energy of 2087 volts by varying the heater current of the oxide coated cathode. All other data in this paper were taken at about 10 μa.

found (quantitative data presently); error from the space charge in front of the filament changing the effective angle θ was eliminated by constant experimental conditions and by the method of extrapolating results to zero slit width; error from surface charges on the walls of the deflecting chamber remains but can be eliminated by extrapolating the e/m_0 observations to infinite electron energy.

To make this extrapolation with the limited number of points available it is necessary to assume a function to represent the curves of Fig. 11. (The $\Delta c = 2.1$ $\mu\mu$f curve was taken under obvious out-of-phase conditions and hence has been disregarded.) The function assumed was $y = a + b/x$. To check this, the data have been replotted in Fig. 15 against the reciprocal of the electron energy, and it is seen that, within the accuracy of the data, a linear variation occurs. The straight lines of Fig. 15 and the curves of Fig. 11 (equivalent) were determined by least squares.[23] The resulting values of the zero intercepts together with their observational probable errors, also determined by least squares,[24] are given in Table VI. The observational probable error in the average is indeed small, that determined by external consistency being $R_e = \pm 9.0$ parts in 10^6 and by internal consistency $R_i = \pm 9.4$ parts in 10^6. The close agreement between R_e and R_i indicates[25] not only the consistency of the data in the value of e/m_0 found under varied experimental conditions (with new and old surfaces and with appreciable variation of the capacity on the acceleration side of the electron gun) but is also a rather good check on the validity of the functional relation to which the points have been fitted. This last is particularly true in view of the variation in the slope of the three curves by a factor of two.

The mean value of e/m_0 given in Table VI must be changed by several small corrections as follows (expressed as parts in 10^5): $+7.2$ from international to absolute amperes;[26] -0.6 from the nonuniformity of the room magnetic field resulting in the mean value around the electron orbit averaging slightly higher than that measured at the center; -1.3 from a small error found in the Helmholtz magnetic field ratio calculations; total correction $+5.3$ parts in 10^5. This gives the final value[27] of e/m_0 as

$$e/m_0 = 1.7597.$$

The experimental data of this section constitute a determination of the total magnetic field current i_T of Eqs. (29) and (30). The estimated probable errors in this determination are listed in Table VII. The observational error is that of the mean zero intercept as given in Table VI. The uncertainty in i_T involves the p.e. in the slit correction i_s and in the ratio k_0/k_R (see Eq. (29)). The p.e. in the latter is that part of the determination of k_R which is not common to that of k_0 (to obtain, omit p.e. in k_0 from

[23] In making this computation each point was given unit weight, rather than being weighted according to the external probable errors R_e given in Table V, because it was felt that the *variation* in the probable errors so computed from the consistency of two or more runs did not really represent the relative accuracy of the points. In fact, frequently the p.e. (internal) of a single run was *less* than the external p.e. of the mean of two or more runs simply because the precision of a single observation was so high and because there were uncontrollable systematic variations between runs (such as aging of the gold surface). The actual p.e. of most of the points in Table V can probably be taken as 4 or 5×10^{-6} amp. (estimated by taking a large number of runs for a single point over a period of several days with gold surface and filament renewed when necessary).

[24] R. T. Birge, Phys. Rev. **40**, 224–227 (1932).

[25] R. T. Birge, Phys. Rev. **40**, 213–223 (1932), particularly page 219.

[26] H. L. Curtis and R. W. Curtis, N.B.S. J. Research **12**, 665 (1934).

[27] The preliminary result (reference 1) differs from this due primarily to the inaccuracy of the formula there used for the effective angle (Eq. (4)) and also probably to the difference between the actual magnetic field and that calculated from the Helmholtz geometry. Due to the impossibility of calculating either of these errors the preliminary result cannot be recomputed and compared with the final result.

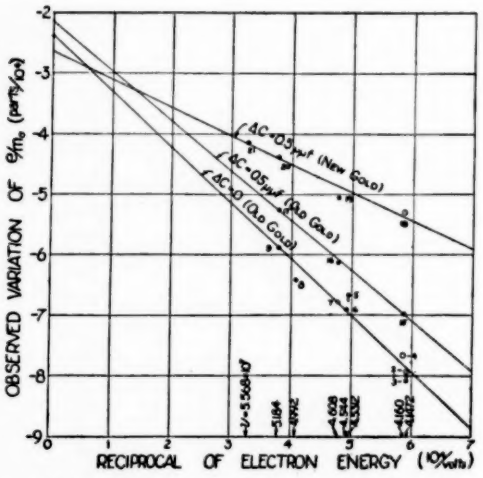
OBSERVED VARIATION OF e/m₀ (parts/10⁴)
RECIPROCAL OF ELECTRON ENERGY (10⁻⁷/e.m.u.)
(ΔC=.05 μμf (New Gold)
(ΔC=.05 μμf (Old Gold)
(ΔC=0 (Old Gold)

FIG. 15. Variation of observed e/m_0 with electron energy. Same data as Fig. 11 replotted against the reciprocal of electron energy. The radiofrequencies at which the observations were taken are also indicated along the abscissa scale. At zero variation $e/m_0=1.7600\times10^7$ e.m.u. The straight lines were determined by least squares, the zero intercepts giving the indicated values of e/m_0.

Table IV). The uncertainty introduced into i_T from this uncertainty in the ratio k_0/k_R (see Eq. (29)) is only about 4 percent of the latter because i_e is only about 4 percent of i_T. These probable errors, together with the standard voltage resistance and potentiometer errors, give a total p.e. of ±5.8 parts in 10^5. In addition, a generous allowance has been made for constant errors of 14.2 parts in 10^5 (almost one and a half squares in Fig. 15). This covers possible errors in extrapolation (including the assumed function), errors in phase of the radiofrequency voltage, and errors from penetration of the radiofrequency field into the deflecting chamber (felt to be negligible because of shielding precautions). The final p.e. in the total magnetic field current i_T is then ±20 parts in 10^5.

Estimated probable error

The probable error in each factor entering into Eq. (16) for the computation of e/m_0 has been evaluated in detail at the point in the article where the factor has been discussed. It is to be recalled that each of these components has already had added to it an allowance for constant errors, these allowances amounting on the average to more than a 100 percent increase. It should also be mentioned that the probable errors used for N.B.S. calibrated standards have been taken as one-half of the limit of error given by the Bureau. This is equivalent to saying that there is about one chance in five of their limit of error being exceeded.

In Table VIII the probable errors for each of the main factors have been listed together. In addition to the uncertainty in the Helmholtz constant k_R at any given radius there is a small additional probable error due to uncertainty in the actual radius used (i.e., in the radius of the electron orbit) which is one-seventh as great as the latter. The final probable error based on these components is ±2.09 parts in 10^4 or $(\pm0.00037)\times10^7$ e.m.u. The latter figure will be rounded off so that there results

adopted probable error in

$$e/m_0=(\pm0.0004)\times10^7 \text{ e.m.u.}$$

This is equivalent to ±2.3 parts in 10^4 or 1 part in 4400.

It is evident that the probable error is made up almost entirely of the allowance for constant errors in i_T since the magnetic field calibration enters but slightly and the other factors are negligible. In fact, if the error is calculated without the allowance for constant errors a value only one-fourth as large is obtained, namely ±0.0001.

DISCUSSION

The value of e/m_0 found in the present work is

$$e/m_0=(1.7597\pm0.0004)\times10^7 \text{ e.m.u.}$$

This is higher by 1.2 parts in 10^3 than the recent value of $(1.7576\pm0.0003)\times10^7$ as given by Birge,[28] a value determined primarily by the two recent spectroscopic determinations (fine structure of H^1-H^2) of Shane and Spedding[3] and of Gibbs and Williams[4] because the estimated

TABLE VI. *Results (from Fig. 15) of three determinations of e/m_0, the intercepts representing the fractional variation from an arbitrary value of $e/m_0=1.7600$. All data determined by least squares.*

CURVE	ZERO INTERCEPT $\times10^4$ PARTS	OBS. PROBABLE ERROR $\times10^5$ PARTS	WEIGHTED MEAN AND OBSERVATIONAL PROBABLE ERROR
$C=0$ (old gold)	-2.39	±2.87	-2.26 parts in 10^4 or $e/m_0=1.759602\pm0.000016$ $R_e/R_i=0.96$
$C=0.5$ " "	-2.15	±1.11	
$C=0.5$ (new gold)	-2.63	±2.20	

[28] R. T. Birge, Nature **137**, 187 (1936).

probable errors are appreciably smaller than those of all other determinations made previously. The other recent spectroscopic determination of Kinsler and Houston,[2] using the Zeeman effect, has a consistent but slightly lower value. The weighted mean of these three is $(1.75774 \pm 0.00023) \times 10^7$ e.m.u. and this may be taken as the most recent "spectroscopic" value. The author's value is higher than this by 1.1 parts in 10^3, or to put it differently, the values differ by 3.0 times the sum of the probable errors. Computing the weighted mean of the spectroscopic and author's values, the ratio of the external to the internal probable errors[25] R_e/R_i is found to be large compared with unity, namely 2.87. The chance of this occurring by purely statistical fluctuation[29] is about 1 in 120. The author's result then apparently reintroduces the question of the disagreement between spectroscopic and free electron values of e/m_0. By this there is implied not any real difference in e/m_0 but rather an error in the experimental work of either method or in the theory involved in the spectroscopic method.

There is, however, some new spectroscopic work which, when it has been carried beyond the present preliminary stage, may help to clear up the difficulty. Houston[30] has recently developed a new method of obtaining the fine structure separation from the microphotometer patterns. The method is essentially a Fourier analysis and should yield values much less subject to error. The value of e/m_0 he obtains in his fine structure study of H^1-H^2 is $(1.7601 \pm 0.0015) \times 10^7$ (the probable error was given to the author by Houston), a value very close to the author's result. No conclusions can be drawn until this probabler error is reduced, but the fact that Houston's result is considerably higher than the other two fine structure determinations at least raises the question as to what changes would result if the fine structure data of the others had been analyzed by this method. In addition there is the possibility that the fine structure theory itself is in need of revision, particularly in view of the fact that the observed separations of the two main components of $H\alpha$ and of $D\alpha$ are 2 percent less than the values predicted by the theory. If upward revision of the fine structure e/m_0 should result from either of these two possibilities (method of analysis or theory) there would still remain a discrepancy with the careful Zeeman effect work.[2]

During the writing of this discussion word has been received[31] of the final results of a deflection determination using crossed fields by A. E. Shaw of Chicago. The value found is 1.7571 ± 0.0013. This result is 1.5 parts in 10^3 lower than the author's, the two differing by 1.5 times the sum of their probable errors. In this case, however, Shaw's probable error is large enough to give a ratio of R_e/R_i much nearer unity, namely $R_e/R_i = 1.19$. The deviation of this from unity is less than half the probable error in the ratio, so that no real discrepancy is indicated. That is to say, the probable errors of the two measurements are sufficiently large that the difference in

TABLE VII. *Probable errors in the determination of the total magnetic field current i_T at resonance.*

SOURCE	PROBABLE ERROR $r \times 10^6$ PARTS
Observational error in determination of i_T	0.9
Uncertainty in the slit width correction i_s	1.2
Effect on i_T of p.e. of 3.5×10^{-5} parts in (k_0/k_R)	0.1
Standard of voltage (taken as $\frac{1}{2}$ of N.B.S. limit of error)	5.0
Standard resistance (taken as $\frac{1}{2}$ of N.B.S. limit of error)	2.5
Potentiometer (ohmic errors and thermal e.m.f.'s)	0.5
$(\Sigma r^2)^{\frac{1}{2}}$	5.8
Allowance for constant errors including extrapolation, etc.	14.2
Total p.e.	20.0

[29] Throughout this discussion the chance of a discrepancy occurring by statistical fluctuations has been based on the formula for the proportional p.e. in the estimated p.e. as given by Deming and Birge (Rev. Mod. Phys. **6**, 149 (1934), *viz.*: $u = 0.4769/(n-1)^{\frac{1}{2}}$ where n is the number of observations.

[30] W. V. Houston, Phys. Rev. **51**, 446 (1937).

TABLE VIII. *Probable error in e/m_0 estimated from the various main components entering into its determination.*

SOURCE	PROBABLE ERROR $r \times 10^6$ PARTS
Angle θ	0.8
Frequency ν	0.6
Helmholtz constant k_R	6.0
Additional uncertainty in k_R from p.e. of 5 parts in 10^5 in electron radius	0.7
Total magnetic field current i_T	20.0
Final p.e. in e/m_0	20.9

[31] Result communicated to the author in a letter from Dr. Shaw.

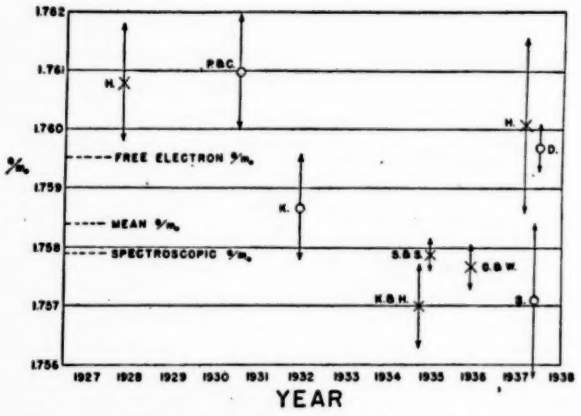

FIG. 16. Chronological plot of e/m_0 values used in estimating the present probable value of e/m_0. (×) are spectroscopic values, ⊙ are free electron values. Arrows show probable errors.

the e/m_0 values is well within the statistical fluctuation to be expected.

The preceding comparisons have been limited entirely to quite recent work (1934 and later). There is, however, some earlier work which should be included in making comparisons and estimating the present probable value of e/m_0. The results which are felt to be significant are listed in Table IX and are chronologically plotted in Fig. 16.[32] Houston's work[33] on H^1-He is included and though made with older methods of analysis is of interest since it is quite possible that an error in the fine structure theory would effect the results less with helium than with deuterium. Perry and Chaffee's[34] and Kirchner's[35] linear acceleration values have also been included. In all cases only the final results of an individual or group at a given institution have been retained.

If the data are treated as a *whole* to obtain the present probable value of e/m there results the value: $e/m_0=1.75842\pm0.00026$. For this the probable error ratio R_e/R_i is 1.42. While the chance of this occurring by statistical fluctuation is only 1 in 10, one cannot attach much weight to this alone as proving a discrepancy.[36]

If, however, the data are divided into the two groups indicated in Table IX, namely spectroscopic and free electron, the discrepancy is again evident since the inclusion of these additional e/m_0 results produces only small shifts in the weighted means as follows: in the spectroscopic value a shift of $+0.00020$, giving 1.75794 ± 0.00026; in the free electron value a shift of -0.00016 from the author's result giving 1.75954 ± 0.00033. The weighted mean of these has a ratio $R_e/R_i=2.55$, again differing considerably

[32] Kretschman's work (Phys. Rev. **43**, 417 (1933)) has not been included since it yields a value of $(e/m)(e/h)$ if the x-ray wave-lengths are assumed correct. It is of interest to note that, as shown by Birge (Nature **133**, 648 (1934)), if the x-ray value of $e=4.803\times10^{-10}$ e.s.u. is assumed and also the validity of the Rydberg formula, Kretschman's results give a value of $e/m_0=1.760$. Robinson's work (Phil. Mag. **18**, 1086 (1934)) has been omitted for the same reason.

[33] W. V. Houston, Phys. Rev. **30**, 608 (1927). Corrected by Birge, Rev. Mod. Phys. **1**, 1 (1929), but probable error used as given by Houston to author.

[34] C. T. Perry and E. L. Chaffee, Phys. Rev. **36**, 904 (1930).

[35] F. Kirchner, Ann. d. Physik **8**, 975 (1931) and **12**, 503 (1932).

[36] It is only when the chance becomes quite small, say of the order of 1 in 50 or 1 in 100, that a discrepancy can definitely be assumed. See reference 25, in particular page 223.

TABLE IX. *Summary of e/m_0 determinations used in estimating the present probable value of e/m_0 and in showing the discrepancy which has again appeared between the spectroscopic and free electron determinations.*

EXPERIMENTERS	DATE	METHOD	e/m_0 $\times10^{-7}$ e.m.u.	PROBABLE ERROR $r\times10^4$	WEIGHT $=225/r^2$	e/m_0 $\times10^{-7}$ e.m.u.	e/m_0 $\times10^{-7}$ e.m.u.
Houston[33]	1927	Fine structure H^1-He	1.7608	10	2.3		
Kinsler and Houston[2]	1934	Zeeman effect	1.7570	7	4.6		
Shane and Spedding[3]	1935	Fine structure H^1-H^2	1.7579	3	25.0	$1.7579\pm3-$ $(R_e/R_i=1.19)$	
Gibbs and Williams[4]	1935	"	1.7577	4	14.1		$1.7584\pm3-$ (From the whole: $R_e/R_i=1.42$ From the two groups: $R_e/R_i=2.55$)
Houston[30]	1937	"	1.7601	15	1.0		
Perry and Chaffee[34]	1930	Linear acceleration	1.761	10	2.3		
Kirchner[35]	1932	" "	1.7587	9	2.8	$1.7595\pm3+$ $(R/R=1.01)$	
Shaw[39]	1937	Deflection	1.7571	13	1.3		
Dunnington	1937	"	1.7597	4	14.1		

[39] A. E. Shaw, Phys. Rev. **51** (L), 887 (1937).

from unity. The chance of this occurring by purely statistical fluctuation is about 1 in 35. Although not as great a discrepancy is indicated with the inclusion of these additional data, the discrepancy is still very apparent, and amounts to 1 part in 1100 in the value of e/m_0.

The situation then is briefly this: both the author's value and the free electron value (mean of four determinations) are in definite disagreement with the spectroscopic value (mean of five determinations). The possibility that this disagreement is not real as far as the fine structure results are concerned but is due to the method of analysis is suggested by Houston's recent work.[30] This work, along with other earlier work,[37] also suggests the need of a refinement of the fine structure theory. That the trouble may be in the author's work is certainly also to be considered.

It should be mentioned that the increase in e/m_0 indicated by the author's results does not remove the present puzzling discrepancy in the fundamental physical constants,[28, 38] for this increase amounts to only about one-fifth of that necessary to bring agreement.

In conclusion it is desired to emphasize two points in connection with the author's value: (1) the probable error adopted is not simply an observation probable error. Rather, the precision of all the measurements was refined until the observational probable errors were negligible, leaving only basic uncertainties in the method and in the interpretation of the physical phenomena observed. (2) All of the final measurements were completed and the apparatus dismanteled before any computations were made of the value obtained. *During the taking of these measurements there was absolutely no knowledge whatever as to whether the results were coming out "high" or "low."* The author feels that this is a most essential precaution in precision measurement since, no matter how earnestly the experimenter endeavors to avoid bias, it seems impossible for him to make the many judgments necessary without being influenced to some extent by a knowledge of whether the results are coming out high or low.

It is again a pleasure to thank Professor E. O. Lawrence for suggesting the method used and for his encouragement. My appreciation is expressed to Professors W. R. Smythe, W. V. Houston and I. S. Bowen for many helpful discussions, to Professor R. A. Millikan for his interest in the work and his efforts in making possible its completion, and to Professor R. T. Birge for his interest in the problem and his criticism of the manuscript. Acknowledgment is made to the physics department of the University of California for their kindness and cooperation in making a loan of a considerable amount of special equipment built there for the preliminary work (Part I). My sincere thanks are given to G. H. Worrall whose skill as an instrument maker and understanding of the problem made possible the unusual degree of precision attained in the measuring chamber, and to B. E. Merkel who made most of the other machined parts. Many students assisted in the work. In particular the work of Herbert Ribner and Charles Perrine, Jr. should be mentioned. Grateful acknowledgment is made to the American Philosophical Society and to the Carnegie Corporation for grants which made possible the latter part of the work.

Note added after manuscript was finished: As stated near the beginning of *Section E* in *Apparatus and Standards* the standard voltage was reestablished late in 1936 with a new cell. Since a standard established with a single cell is always subject to question, a further check in terms of two additional new cells has just been completed. The standard determined by the mean of the three new cells is 0.000009 volt lower than that from the first cell alone. This increases the value of e/m_0 by 9 parts in 10^6 (i.e., by less than two units in the fifth decimal), a quite negligible change. The author wishes to express his appreciation to Dr. B. H. Sage for the loan of the two new standard cells.

By an oversight, correction was not made to the magnetic field constant k_R of Eqs. (29) and (30) to allow for its variation off the central plane. The integrated average over the extent of a slit length (2 mm) is 1.0 part in 10^5 greater than the value on the central plane. The value of e/m_0 should then be reduced by essentially this same amount.

These two corrections (standard cell and magnetic field) practically cancel each other leaving no net change in the value of e/m.

[37] See references given in Houston's paper, reference 30.
[38] J. DuMond and V. Bollman, Phys. Rev. **51**, 400 (1937) (in particular, Part IV).

Velocity Analysis by Means of the Stern-Gerlach Effect

V. W. COHEN AND A. ELLETT
State University of Iowa, Iowa City, Iowa

(Received June 11, 1937)

A Stern-Gerlach experiment furnishes a convenient method of studying the velocity distribution in a molecular beam. In addition it is possible to obtain some information concerning the behavior of the field gradient as a function of position. This method has been applied to a beam of alkali atoms and shows that with low vapor pressure in the oven the Maxwell distribution law is fulfilled whereas at oven pressures such that the mean free path is much less than the width of the oven slit a departure sets in. It is found that the field gradient is quite uniform over almost half the trough height for deflections inside the trough. Toward the wedge the gradient varies rapidly.

COMPARATIVELY little accurate work has been done on the analysis of the distribution in velocity of the molecules in a molecular beam. Although several methods are available for dispersing the molecules according to velocity there are certain serious difficulties associated with each. Use of rotating slits or sectored disks, the method used by several investigators[1] involves the attainment of very high and constant peripheral speeds of the rotating parts. In addition there is considerable loss of intensity in the beam. Such work has yielded only qualitative agreement with the Maxwell distribution law. Experiments on deflection by inhomogeneous electric fields[2] have yielded a dispersion insufficient for accurate velocity analysis. In order to secure appreciable resolving power with this method it would be necessary to use potentials and gradients considerably greater than those used in the past. The well-known method of deflection by an inhomogeneous magnetic field has been successfully applied to the measurement of atomic and nuclear magnetic moments as well as to secure a beam of single-velocity atoms.[3] However, no accurate extensive study has been made for the purpose of determining the velocity distribution in the beam. Particularly well adapted to this work are the alkali metals for whose detection we have the Taylor-Langmuir gauge[4] by far the most sensitive, accurate, and convenient molecular beam detector available.

A simple and rugged velocity analyzer of fair resolving power, even though limited to the alkalis will enable one to investigate several rather interesting problems. One question which almost every investigator in the molecular beam field must have asked himself is whether the distribution in velocity in the beam is that of Maxwell. It has been assumed that if the oven pressure is low enough so that the mean free path in the oven is large compared to the width of the slit, this will be true. If it were not for the need of greater oven pressures in many experiments this would be a sufficient answer. When high beam intensities are required the experimenter is immediately faced with the question of just how large the mean free path must be in order to preserve, approximately, the Maxwell distribution. This can be answered only by a velocity analysis of the beam.

THEORY OF THE ANALYZER

An essential condition for the satisfactory operation of a velocity analyzer of the magnetic type is that the gradient of the magnetic field be very nearly constant over the height of the beam, otherwise atoms of the same velocity may suffer quite different deflections depending upon how far they are from the center of the beam. Taylor[5] has shown by direct measurement, that in the so-called "Hamburg set-up" in which the beam is sent through the field just at the edge of the trough, this condition is very well realized, provided the beam height is not much more than one quarter of the height of the trough. We find

[1] Stern, Zeits. f. Physik **2**, 49 (1920); Eldridge, Phys. Rev. **30**, 931 (1927).
[2] Estermann, Zeits. f. physik. Chemie **B1**, 161 (1928); Scheffers and Stark, Physik. Zeits. **25**, 452 (1934).
[3] Rabi and Cohen, Phys. Rev. **46**, 707 (1934).
[4] Taylor, Zeits. f. Physik **57**, 242 (1929).
[5] Fraser, *Molecular Rays* (Cambridge, 1931), p. 120.

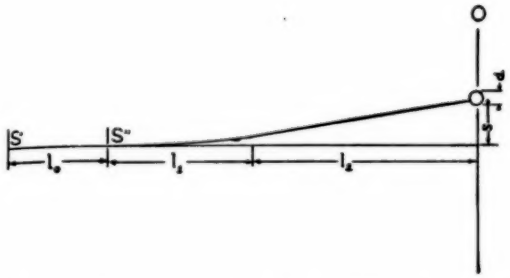

FIG. 1. Arrangement of the analyzer; S', effective source slit; S'', defining slit; l_1 beam path in the field; l_2, beam path after traversing field; d, width of detector wire; s, distance from center of detector wire to center of undeflected beam.

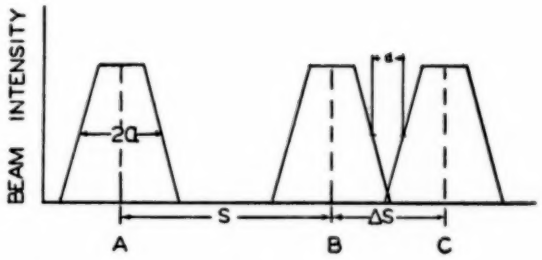

FIG. 2. Distribution of intensity in (A) undeflected beam; (B) deflection pattern of atoms with velocity v; (C) deflection pattern of atoms with velocities $v+\Delta v$.

no observable difference in the form of the intensity curve for beam heights of 1.6 and 3.25 mm. The total trough height is 8 mm. We take this to indicate a constant gradient over this distance.

Let us consider the resolving power which may be realized with a velocity analyzer of this type. Fig. 1 represents the schematic arrangement of the system. The beam is defined by slits S' and S'', separated by a distance l_0, and is detected by a wire of diameter d free to move laterally in the plane 0. In the region l_1 the atoms are accelerated in a direction normal to that of their original motion by an inhomogeneous magnetic field, while the region l_2 is field free. In the absence of an applied field the curve representing the number of atoms crossing the plane 0 per unit time between s and $s+\Delta s$ will if the slits be correctly aligned, be a trapezoid whose width at one-half its maximum height is

$$2a=((l_0+l_1+l_2)/l_0)w'', \qquad (1)$$

where w'' is the width of slit S'' (Fig. 2).

In the presence of a field, atoms having a velocity v will give rise to a precisely similar distribution but shifted bodily by an amount

$$s=(1/2mv^2)\mu(\partial H/\partial S)(l_1^2+2l_1l_2). \qquad (2)$$

Atoms of velocities v and $v+\Delta v$ will then give rise to a distribution represented by the superposition of two such trapezoids, the separation of their centers being

$$\Delta s=(2s/v)\Delta v. \qquad (3)$$

If a detector of width d is now run across this pattern its response will measure the total intensity in the pattern between the limits $s+\frac{1}{2}d$ and $s-\frac{1}{2}d$, where s is the position of the center of the wire. A sufficient condition for resolution, if d is less than $2a$, is that Δs be greater than $(2a+d)$. In this case

$$V/\Delta V=2s/(2a+d). \qquad (4)$$

With the apparatus to be described, the resolving power obtained for a typical curve is about 13 in the region of the most probable velocity of the Maxwell distribution characteristic of 450°K. Clearly the resolution increases as the velocities decrease. As the dispersion increases the intensity decreases correspondingly. We see from (2) that the gradient is the most easily adjusted parameter, so that in order to study any particular velocity range one may choose a value of the gradient to compromise between convenient intensity and sufficient resolving power.

Inspection of (1) and (2) shows that to design the instrument for high resolving power one must use narrow slits, as long a path in the field as is possible, and reduce the constant a by making l_0 comparible to l_1+l_2. Very little will be gained by increasing l_2 much above l_1 since a gain in deflection will be offset by an increase in a.

In order to obtain a calibration curve for the instrument (velocity *vs.* deflection) we have used as a source an oven operating at a vapor pressure so low that the Maxwell velocity distribution is certainly realized. The form of the intensity distribution curve to be expected may be calculated if the displacement of the beam by the field is so small that the gradient of the field may be assumed to be constant. If, by suitable choice of parameters, a curve of the computed form may be fitted to the data, it appears to be a reasonable inference that the gradient is essentially constant.

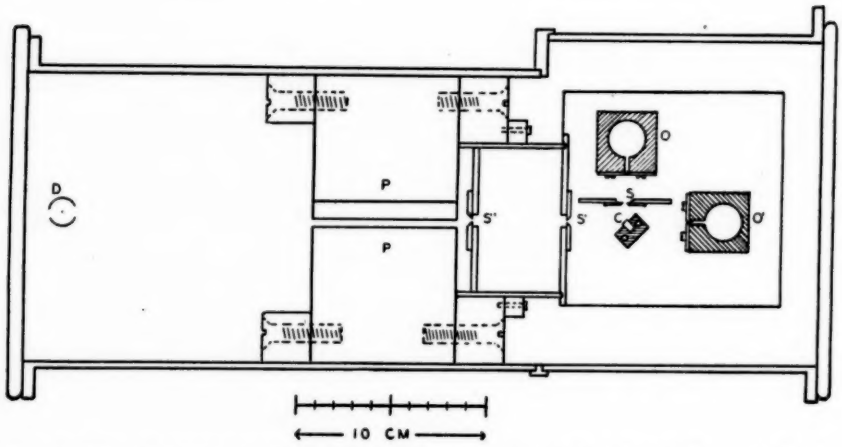

FIG. 3. Plan of apparatus. Oven position O and parts marked S and C are used only in connection with work described in the following paper.

However it seems desirable to see to just what extent a small variation in the gradient may be concealed by a suitable choice of parameters, i.e., of the effective or apparent gradient and of the constants introduced by finite width of slits and detector wire.

Consider the form of the distribution to be expected if we assume, not a constant gradient but merely that atoms of velocity v passing through the field suffer a deflection η and write

$$v=f(\eta). \tag{5}$$

For the number of atoms which, in the absence of field, pass through the plane of the detector within a region of width $d\xi$ at ξ and which have velocities within dv at v let us write

$$N(v)P(\xi)d\xi dv.$$

$P(\xi)$ gives the form of the undeviated beam. For the present we will assume merely that it is symmetrical about $\xi=0$. Both $N(v)$ and $P(\xi)$ are normalized to unity. In the presence of a field these atoms will be deflected a distance η given by (5) and the number of atoms crossing the plane of the detector in ds at s will be given by

$$I'(s)=\int_{\xi=0}^{\xi=+\infty} F(s+\xi)P(\xi)d\xi ds, \tag{6}$$

where $F(s+\xi)=N(v)dv$ in which v has been expressed explicitly in terms $\eta=s+\xi$ by means of (5).

Expanding $F(s+\xi)$ about $\xi=0$ by Taylor's series and remembering that because of the symmetry of $P(\xi)$ all odd moments vanish, we obtain

$$I'(s)=\sum_{n=0}^{n=\infty}\frac{F^{2n}(s)}{(2n)!}M(2n), \tag{7}$$

where $$M(2n)=\int_{-\infty}^{+\infty}\xi^{2n}p(\xi)d\xi$$

is the $2n$th moment of the field free distribution.

The detector wire of width $2b$ with its center at s measures

$$I''(s)=\int_{s-b}^{s+b} I(s)ds, \tag{8}$$

which may be written

$$I''(s)=\sum_{n=0}^{n=\infty}\sum_{r=0}^{r=\infty}\frac{M(2n)}{(2n)!}\frac{b^{2r+1}}{(2r+1)!}F^{2n+2r}(s), \tag{9}$$

in which the term $bM(0)F(s)$ gives the form of the distribution curve for infinitesimal widths of slit and detector. In any region in which the remaining terms are small we may evaluate them using for the function (5) that form appropriate for the case of a rigorously constant gradient. Now fortunately these terms do become small as s becomes large, and it is only for large s that the question of constancy of gradient becomes serious.

Writing (9) in the form

$$bM(0)F(s)=I''(s)$$
$$-\sum_{n=1}^{n=\infty}\sum_{r=1}^{r=\infty}\frac{M(2n)}{2n!}\frac{b^{2r+1}}{(2r+1)!}F^{2n+2r}(s) \tag{10}$$

and integrating, we have

$$bM(0)\int_0^s F(s)ds=\int_0^s I''(s)ds-\Delta I'', \quad (11)$$

where the integral on the left-hand side represents the integrated intensity which would be observed in an apparatus with infinitesimal width of slits and detector. Consequently those values of s and v for which

$$\frac{bM(0)\int_0^s F(s)ds}{bM(0)\int_0^\infty F(s)ds}=\frac{\int_\infty^v N(v)dv}{\int_\infty^0 N(v)dv} \quad (12)$$

must satisfy the equation $v=f(s)$.

If we assume the atoms in the beam to have the Maxwell distribution of velocities

$$N(v)dv=N_0\exp[-mv^2/2KT]v^2dv=N_1e^{-x}xdx,$$

where $x=mv^2/2KT=v^2/v_a^2$,

the integral on the right side of (12) is merely $e^{-x}(x+1)$ while the quantity on the left may be obtained by graphical integration of the observed intensity distribution curves. $\Delta I''$ can be calculated only approximately, however its value proves to be of the order of one-half to two percent of $\int I''(s)ds$ over the useful range of the intensity curve, so that an approximate evaluation is sufficient. The series for $\Delta I''$ converges so rapidly for large s that only the first term is appreciable.

Apparatus

The apparatus is illustrated schematically in Fig. 3. The chamber walls are of brass tubing closed on the ends with brass disks sealed with wax. The system is divided into two parts, an oven chamber and a beam chamber, which are pumped independently. Communication between the two is through slit S'. During runs the pressure in the beam chamber is "flat" as recorded on a McLeod gauge with a constant of 3.6×10^{-7} while in the oven chamber the gauge may read from 2 to 6×10^{-7} mm Hg. The oven is similar in design to that used in other experiments with alkali beams.[3] The oven slit jaws are of rectangular cross section, 2 mm thick.

The beam is effectively defined by slits S' and S'', the oven slit being considerably wider than either of them. By defining the beam in this manner scattering which occurs in the beam itself as well as by foreign gases in the oven chamber does not cause appreciable broadening of the beam with consequent loss in resolving power.

The magnetic field is produced by an electromagnet with Stern-Gerlach type pole pieces made of Armco iron. These pole pieces are held in position inside the vacuum system by a pair of bronze rings to which they are bolted. The slit-holders are carried on a brass tube which slides into one of the bronze rings in such a way that it may be removed for cleaning and be replaced without disturbing the alignment. The oven supports are attached rigidly to the slit unit. In this way the beam always traverses the same region of the magnetic field. Fig. 4 illustrates a side view of the pole piece unit with the slit unit in place.

The slit widths used were 0.15 mm for the oven, 0.022 mm for S', and 0.024 mm for S''. Slits S' and S'' are each formed by a pair of knife edged jaws. A pair of brass stops set into the trough pole piece limits the height of the beam to 3.25 mm. The distance between S' and S'' is 5 cm, the length of pole pieces 7.5 cm, and the path from the end of the pole pieces to the detector 13 cm. The angle of the wedge pole piece is 77°, the trough height, 8 mm; the distance of the vertex of the wedge from the plane of the trough 4 mm.

The detector wire is pure tungsten 0.002″ diameter, maintained at 45 volts above ground potential. The atoms after ionization are collected by a nickel plate connected to the grid of

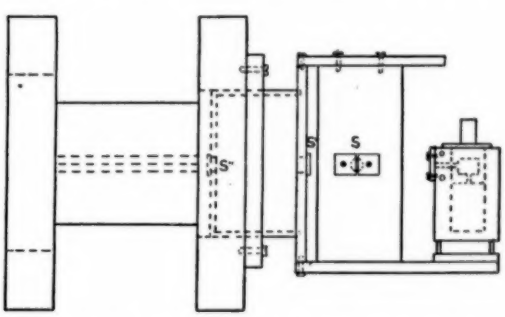

FIG. 4. Side view of slit and pole piece units.

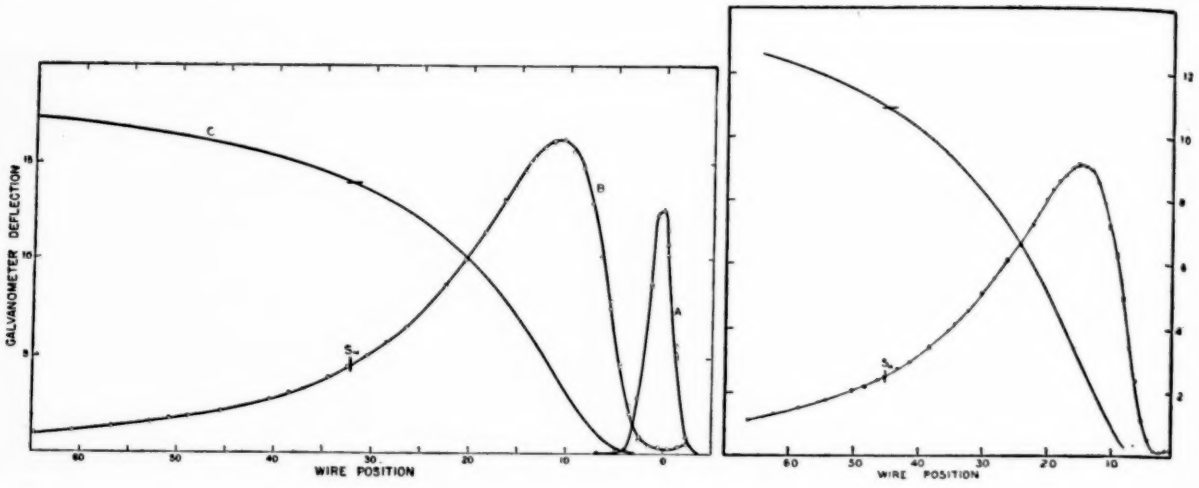

(a) (b)

FIG. 5. (a) *A*. Intensity distribution in typical undeviated beam. *B*. Intensity distribution in deflection pattern, magnet current 6 amp. *C*. Graphical integral of *B* as a function of *s*. (b) Same as (a) but for magnet current 9 amp.

an F. P. 54 vacuum tube amplifier. As beam intensities vary over a factor of 500, the amplifier sensitivity is varied by using several grid leaks whose resistances range from 10^8 to $2\times10^{10}\sim$ so that in any single run only potentials less than 0.05 volt are applied to the grid. In this region the response of the amplifier is quite linear. The detector wire is carried eccentrically on a conical spindle bearing which can be rotated externally by means of a ground glass joint. A telemicroscope with an ocular micrometer magnifying 80 times is used to measure the position of the detector wire. The observed galvanometer deflections are corrected for amplifier drift and residual ion emission of the wire by cutting off the beam after every few readings with a magnetically operated shutter.

CALIBRATION OF THE ANALYZER

Figures 5(*a*) and (*b*) represent two typical experimental curves taken with magnet currents of 6 and 9 amperes. The small triangles are points of the undeviated beam, the circles those of the velocity spectra, while the solid curves marked *C* represent the results of graphical integration. If corresponding to any value of x we calculate the value of $e^{-x}(x+1)$ we may pick the corresponding value of s from the curve. This procedure may be used to obtain values of s as a function of x. The short horizontal dashes represent the ordinates for $x=1$ namely, 0.7359. The corresponding values of s are the abscissas of the intersections, or the s_a's. For a constant gradient (5) takes the form (2), from which it is evident that the product sx should be constant. A plot of sx against s is given in Fig. 6. Curves *A* and *A'* are for the beam defined vertically by stops 3.25 mm high and deflected toward the trough. These curves show the gradient to be constant to within one percent. Curve *A''* represents sx under the same conditions (oven pressure 0.004 mm Hg, 9 amperes magnet current) but deflected toward the wedge. The field gradient is evidently not constant on this side. As constancy of the gradient greatly simplifies the interpretation of the results we have used the beam deflected toward the trough exclusively. Curve *D* shows the result of a run made with the beam limited to a height of 6 mm. Clearly the gradient at the upper and lower extremes varies rapidly, the average being roughly represented by curve *D*. Curves *B* and *C* show the effect of increasing the oven vapor pressure until the mean free path becomes smaller than the width of the oven slit. *B* was taken with an oven pressure of 0.13 mm Hg, (m.f.p. $\sim$0.04 mm) while *C* was taken at 1.4 mm Hg (m.f.p. $\sim$0.003 mm) while in both the beam stops were the same as in case *A*. The difference is no doubt due to a departure from the Maxwell distribution. This point will be discussed in more detail later.

It has frequently been assumed that the intensity distribution in the observed deflection pattern may be represented by the well-known formula of Stern.[6]

$$I_0''(s)=\frac{I_0}{2a'}\left[e^{-y}(y+1)\right]_{s_a/(s-a')}^{s_a/(s+a')}. \qquad (14)$$

One may readily show that for s large enough so that only the first term in $\Delta I''$ is appreciable this equation should be valid. It gives the density of atoms incident upon the plane of the detector if the intensity in the undeviated beam is constant over a breadth $2a'$ and zero outside this region. It is merely (6) with $P(\xi)=\frac{1}{2}a'$ for $|\xi|<a'$ and $P(\xi)=0$ for $|\xi|>a'$. In this case the integration may be carried out and gives (14). Instead of integrating, we may expand as we did in the general case and obtain the Stern formula in a form more convenient for comparison with (9). This gives

$$I_0''(s)=\sum_{n=0}^{n=\infty}\frac{M(2n)}{2n!}F^{2n}(s). \qquad (15)$$

Eq. (9) may be written for comparison

$$I''(s)=\sum_{\nu=0}^{\nu=n}\left\{\sum_{n=0}^{n=\infty}\frac{M(2n)}{2n!}\frac{b^{2(\nu-n)+1}}{[2(\nu-n)+1]!}F^{2\nu}(s)\right\}. \qquad (16)$$

If the undeviated beam is a rectangle of width $2a$ this becomes

$$I''(s)=b\left\{F(s)+\frac{(b^2+a^2)}{3!}F^2(s)+\left[\frac{a^4+b^4+10a^2b^2}{5!}\right]F^4(s)+\cdots\right\}$$

expanding (15)

$$I_0''(s)=F(s)+\frac{a'^2F^2}{3!}(s)+\frac{a'^4}{5!}F^4(s)+\cdots. \qquad (17)$$

If $a'^2=a^2+b^2$ these will evidently not differ until the third term becomes of importance. It should perhaps be pointed out that under these circumstances the breadth of the *observed* undeviated beam at half-maximum intensity is a, not $(a^2+b^2)^{\frac{1}{2}}$. For any other form of $P(\xi)$ the higher moments will be larger than for the rectangle, so that the comparison is for the most favorable case.

The solid curve of Fig. 7 shows the calculated intensity while the circles show the observed points for the velocity spectrum of Fig. 5(*a*). For the evaluation of the intensity (14) was used in the region of the maximum while the first two terms of (17) were used for larger s. The higher

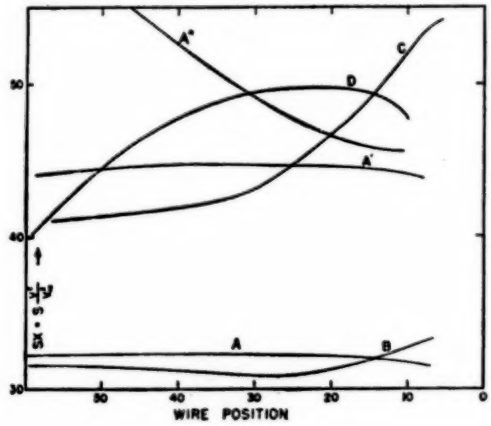

FIG. 6. Product sx as a function of s:

- *A* Beam height 3.25 mm, oven pressure 0.004 mm, magnet current 6 amp.
- *A'* Beam height 3.25 mm, oven pressure 0.004 mm, magnet current 9 amp.
- *A''* Beam height 3.25 mm, oven pressure 0.004 mm, magnet current 9 amp. (wedge).
- *B* Beam height 3.25 mm, oven pressure 0.13 mm, magnet current 6 amp.
- *C* Beam height 3.25 mm, oven pressure 1.4 mm, magnet current 9 amp.
- *D* Beam height 6 mm, oven pressure 0.004 mm, magnet current 9 amp.

[6] Stern, Zeits. f. Physik **41**, 563 (1927).

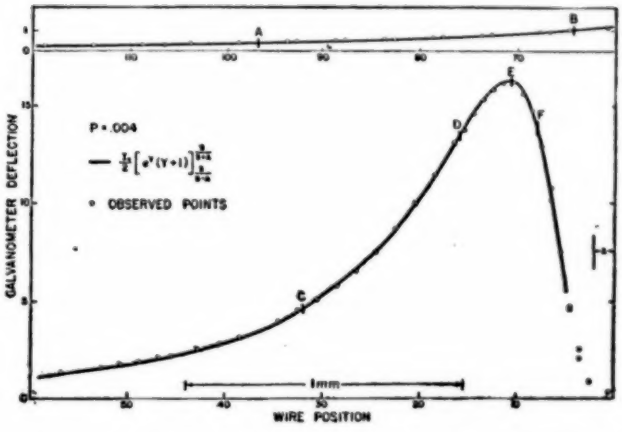

FIG. 7. Comparison between calculated and observed intensities for spectrum of Fig. 5(a). Points labeled *A*, *B*, *C*, *E* and *F* represent deflections of $(3)^{-\frac{1}{2}}$, $(2)^{-\frac{1}{2}}$, 1, $(2)^{\frac{1}{2}}$, $(3)^{\frac{1}{2}}$ and 2 times v_α.

terms in (17) are negligible when $s > s_a/3$. s_a was evaluated by the use of (12).

Unless $s_a > 20a$ the error introduced by assuming a rectangular form for $P(\xi)$ becomes significant in the region of the maximum. The agreement between the observed and calculated values is well within the experimental error for $s > s_a/3$. The difference is slightly higher for smaller s but this is probably due to the error introduced by the use of the Stern formula in this region. A trapezoidal distribution improved the fit in the one case for which the necessary calculations were carried out. Its principal effect was to shift the peak of the curve about 1/10 division farther from the center. With a higher gradient and consequent increased resolution ($s_a = 45$) the fit is satisfactory even in the region $s = s_a/3$.

The uncertainty in the observed points due to fluctuations in oven pressure and to electrical disturbances affecting the amplifier ranges from about one percent near the maximum to about ten percent beyond $2s_a$. In runs made with several values of the field gradient at oven pressures of 0.01 mm (potassium) and 0.04 mm (sodium) there is no evidence of systematic deviation from the Maxwell distribution, the calculated curves fitting the observations in substantially the same way as in Fig. 7. At the higher pressure (0.04 mm Hg) the mean free path in the oven is approximately equal to the width of the oven slit. This slit has the form of a canal 0.15 mm wide by 2 mm long so that one might very well expect forward scattering to produce some deviation from the Maxwell distribution.

Effect of Oven Pressure on Velocity Distribution

At higher pressures the effect of forward scattering becomes clearly evident. A distinct departure from the Maxwell distribution is shown by the velocity spectrum in Fig. 8. Here we have a curve taken with an oven pressure of 1.4 mm. At this pressure the mean free path is about 0.003 mm. The solid line represents the distribution as calculated for the appropriate temperature, assuming a Maxwell distribution. Clearly there is a deficiency of slow atoms. One might, at first glance, suppose that a better fit might be produced by assuming a smaller value for s_a. However, if one were to fit a theoretical curve in the region of s_a, the peak would occur at P which is clearly outside the limits of error.[7] At oven pressures of 0.13 and 0.5 mm deviations from the Maxwell distribution are observed but to a less extent than at the higher pressure. If one were to attempt to measure the atomic magnetic moment from the observed intensity distribution of Fig. (8) using the method of equal intensities,[6] the error introduced would range from 2 percent for points chosen near the maximum, to about 7 percent for points taken at three-tenths of the peak height.

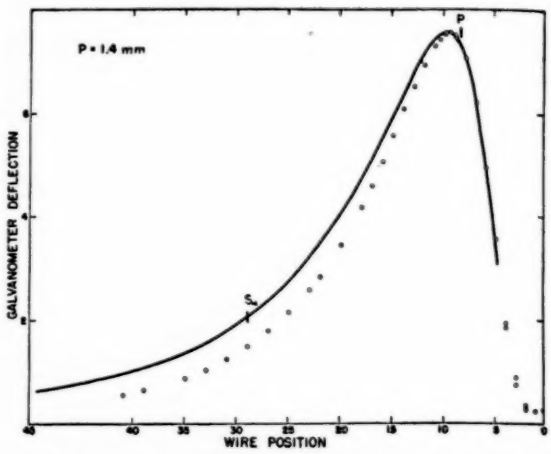

FIG. 8. Comparison of calculated and observed distributions for oven pressure of 1.4 mm Hg.

From the above results one can draw no certain inference concerning the distribution from a slit of different form. If it were desired to preserve the Maxwell distribution at high beam pressures one would expect that the use of narrow knife-edged slits would tend to eliminate forward scattering.

[7] This would also imply a change in calibration, amounting to 13 percent. A recheck of the calibration failed to reveal any such error.

Velocity Analysis of Potassium Atoms Scattered by Magnesium Oxide

A. ELLETT AND V. W. COHEN
State University of Iowa, Iowa City, Iowa
(Received June 11, 1937)

A beam of potassium atoms is scattered by an MgO crystal and the magnetic velocity analyzer used to determine the distribution in velocity of the scattered atoms. The resulting velocity spectrum agrees very well with that calculated on the assumption of a Maxwell distribution characteristic of the temperature of the crystal although the crystal temperature was varied over a wide range. A rough study made of the spatial distribution of the scattered atoms showed no evidence of specular reflection or of diffraction but merely random or cosine scattering. The scattering process appears to be one of adsorption and re-evaporation.

THE scattering of a molecular beam by a crystal is, in general, a very complex process. Only in situations where a relatively simple limiting case is approximately realized is it possible to say that we understand in any detail what takes place. One well-recognized simple process is that of adsorption and re-evaporation. Another is approximately realized in the diffraction of helium by lithium fluoride crystals studied by Stern.[1] Here the crystal behaves very much like a rigid massive grating. The general features of the diffraction spectra observed can be accounted for without taking into account the energy communicated to the crystal as a result of the change in momentum of the scattered atom. Even here, however, there are minor irregularities (small regions of anomalously low intensity), whose interpretation has only recently been given.[2] With heavier incident atoms there is still evidence of diffraction. In Fig. 1, reproduced from a paper of R. M. Zabel,[3] the knee in the helium curve is certainly due to unresolved diffraction spectra, and it seems reasonable to suppose that the form of the intensity curves for argon and neon may be accounted for in the same way. The finite angular resolution of the apparatus and the shortness of the wave-length of the heavy atoms is sufficient to account for the fact that no dip appears between the zero order (specularly reflected) beam and the spectra of higher orders. However, it is certainly also possible that the number of atoms in the crystal which scatter coherently is here much less than in the case of Stern's experiment, so that the resolving power of the crystal grating is very low. This would result in a sort of smearing of the intensity distribution, actually obliterating all its finer features. This same decrease in the number of coherently scattering atoms will result in an increase in the energy exchanged between the crystal and the rebounding atom. It is probably through this mechanism that one must seek to understand results obtained with still heavier atoms, as in the experiments of Zahl and Ellett and of Hancox on the scattering of zinc and cadmium.[4]

It is clear that data on the velocity distribution in the scattered beam as a function of crystal temperature, angle of scattering, etc. may be valuable in the further elucidation of these complex phenomena. Taylor has shown that the alkali atoms are scattered from alkali halide crystals according to the cosine law.[5] This fact is satisfactorily explained by the mechanism of adsorption and re-evaporation. But as the adsorption time becomes shorter and shorter this process must become one equally well described as random scattering. Data on the velocity distribution will again be significant. A knowledge of the accommodation coefficient and the adsorption time is of course valuable. These quantities are however of a statistical nature so that a knowledge of their values does not in general very sharply limit the mechanism.

With the velocity analyzer described in the preceding paper[6] we have studied in some detail

[1] Frisch and Stern, Zeits. f. Physik **84**, 430 (1933).
[2] A. F. Devonshire, Proc. Roy. Soc. **A156**, 37 (1936).
[3] Zabel, Phys. Rev. **42**, 218 (1932).
[4] Zahl and Ellett, Phys. Rev. **38**, 977 (1931); Hancox, Phys. Rev. **42**, 864 (1932).
[5] Taylor, Phys. Rev. **35**, 375 (1930).
[6] Preceding paper in this issue of the *Physical Review*.

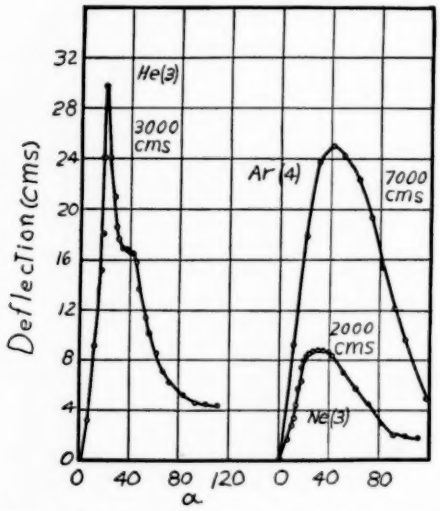

FIG. 1. Diffraction curves for He, A and Ne scattered from NaCl, specular angle 20°. (After Zabel.)

the distribution in velocity of potassium atoms scattered by a magnesium oxide crystal. This crystal was chosen for the following reasons: (1) the hope (not realized) that the scattering would not be of the diffuse type observed by Taylor,[5] (2) its very high melting point permits satisfactory outgassing, (3) its high Debye characteristic temperature[7] means less thermal disorder of the lattice presumably favoring the occurrance of recognizable diffraction phenomena, (4) its simple structure, cubic, NaCl type.

A rough study was also made of the spacial distribution of the scattered atoms.

APPARATUS

The apparatus is essentially that described in the previous paper[6] except that the oven position is changed to 0, an additional slit placed at S, and a crystal at C. The slit S, $\frac{1}{2}$ mm wide, serves to define a beam directed toward the crystal.

The crystal support and heater is shown in detail in Fig. 2. A pair of tungsten spiral filaments enclosed in holes H serve to supply heat to the block. A power input of about 50 watts will raise the temperature of the heater to 1000°C. The crystal support is free to rotate about an axis lying in the exposed surface of the crystal. Thus while the angle between the initial beam and the analyzer beam is fixed at 90°, the angle of incidence may be varied. A thermocouple T_1 is placed in contact with the crystal under one of the metal tabs covering its surface. Another thermocouple T_2 inserted into the body of the heater serves to give an estimate of the temperature gradients existing in the heater. The difference in temperature between T_2 and T_1, during runs ranges from approximately 20°C at 400°K to 50°C at 800°K. One would expect the difference in temperature between the effective surface of the crystal and the couple T_1 to be somewhat less than the difference between T_1 and T_2.

The sensitivity of the amplifier, used with the beam detector, was increased to 6×10^{-16} amp./mm. During runs with the crystal at 800°K, a pressure of about 10^{-6} mm Hg is maintained in the scattering chamber, while a pressure of about 10^{-7} is maintained in the analyzer chamber. The slit system is adjusted as in the work with the direct beam,[6] so that the calibration of the field is still valid.

ANGULAR DISTRIBUTION

The spatial distribution of the scattered atoms is determined by setting the detector wire in the center of the beam with the field off, and measuring the beam intensity as a function of crystal setting. Let us denote by θ the angle between the crystal surface and the analyzer beam. Since the incident beam is at right angles to the analyzed beam, appreciable intensity would be observed only for $\theta=45°$ if reflection were specular. If scattering consisted of low order unresolved diffraction a maximum would be observed near $\theta=45°$. If the scattering were random, hence proportional to the cosine of the angle between the normal and direction of observation, the observed intensity would be the product of three factors; (1), intensity of the incident beam per unit area, ($\cos\theta$), (2) effective crystal surface scattering to the observed beam ($1/\sin\theta$), (3) intensity of scattering per unit area [$\cos((\pi/2)-\theta)$ or $\sin\theta$] giving a resulting intensity proportional to $\cos\theta$. The result of such a measurement is illustrated in Fig. 3 which is a polar graph of intensity as a function of θ. The solid line is $I=I_0\cos\theta$, the circles are experimental points. The absence of any significant maximum at or near 45° indicates that no appreciable specular

[7] Durand, Phys. Rev. **50**, 453 (1936).

reflection or coherent scattering is taking place, and the scattering is purely random.

Velocity Analysis

In order to obtain a convenient intensity in the deflection pattern of the analyzer beam (up to 30 cm galvanometer deflection) it is necessary to operate the oven at a temperature of about 600°K, with a vapor pressure of potassium of the order of 1 mm Hg. An increase in the oven temperature would tend to clog the slit S in a short time.

Figures 4 and 5 illustrate two typical velocity spectra for crystal temperatures of 795 and 460°K. The solid curves are intensities calculated as discussed in the previous paper assuming a Maxwell distribution of velocities. The values of s_α were chosen to give the best fit to the observed data. The agreement is well within the experimental error. The effective temperatures were obtained from the equation

$$S_\alpha = (1/4KT)\mu(\partial H/\partial S)(l_1^2+2l_1l_2).$$

A summary of the results is shown in Table I in which T_0 is the oven temperature, T_c that of the crystal, and $T_{(eff)}$ the effective temperature.

In adjusting the value of s_α we find that in runs no. 1, 2, 3, 8 and 9 a change of one percent results in a decidedly poor fit. In runs 4, 5, 6 and 7 the precision of s_α is of the order of four percent. We notice that with one exception the effective temperature is consistently lower than that of the thermocouple in contact with the crystal, even when the crystal is cooler than the oven. It seems reasonable to conclude therefore, that the scattered atoms attain thermal equilibrium with the crystal, which is at a temperature slightly lower than that of the adjacent thermocouple.

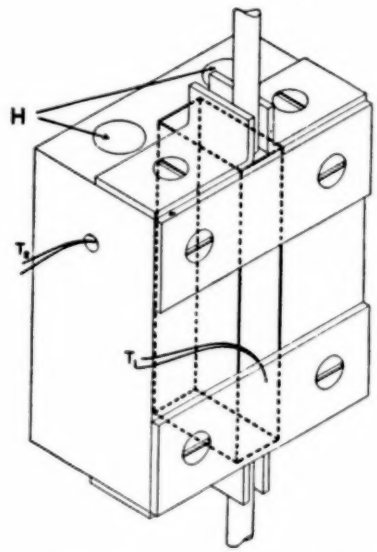

Fig. 2. Sketch of crystal support; H, holes for heating coils; T_1 and T_2, thermocouples; heavy line indicates position of the crystal.

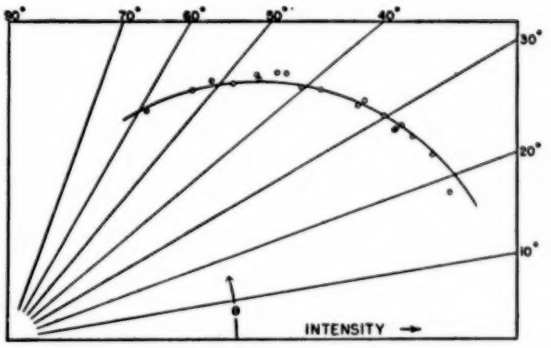

Fig. 3. Beam intensity as a function of crystal setting.

A measurement of the accommodation coefficient for K on MgO would have been sufficient to show that the average energy of the atoms after impact is that characteristic of the temperature of the crystal. The present experiment shows furthermore that the scattered atoms have attained virtually complete thermal equilibrium with the crystal, their distribution in velocity being the Maxwell distribution characteristic of the crystal temperature.

The data in Table I were obtained with MgO crystals. In addition a few less accurate runs were made using scattering surfaces of NaCl and LiF crystals, and a piece of etched polycrystalline nickel. These results are not presented in detail as in every case they showed the same behavior as

Table I. *Effective temperatures and actual oven and crystal temperatures.*

Run No.	T_0	T_c	T(eff)	T_c-T(eff)
1	592°K	481°K	469°K	12°K
2	592	636	640	−4
3	617	731	722	9
4	645	443	433	10
5	688	583	563	20
6	645	640	607	33
7	645	805	770	35
8	606	672	660	12
9	606	795	751	44

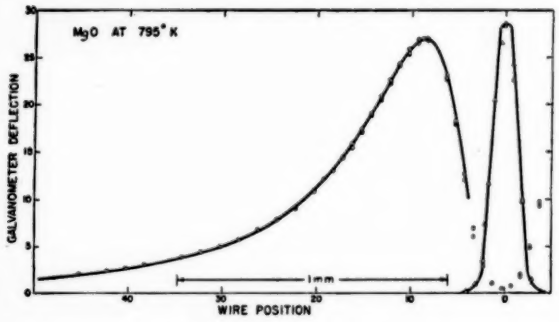

FIG. 4. Undeviated beam and velocity spectrum. Magnet current 9 amp. Solid line indicates the distribution calculated on the assumption of a Maxwell velocity distribution.

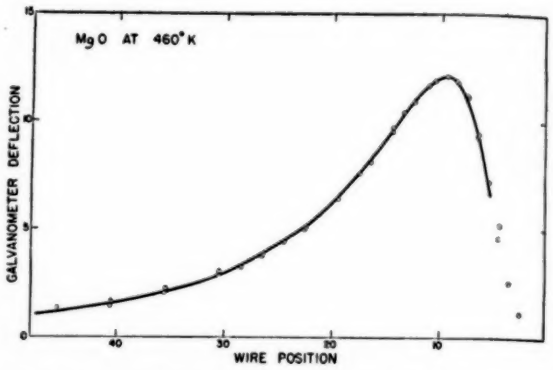

FIG. 5. Same as Fig. 4 but for a different crystal temperature and 6 amp. magnet current.

with MgO. That is, the spatial distribution of the scattered atoms was random and the velocity spectrum was a Maxwell curve calculated for a temperature equal to that of the crystal within the experimental error.

The magnesium oxide crystals used in this work, clear specimens about one or two cm on edge, were furnished through the courtesy of the Norton Company of Worcester, Mass. In particular we wish to thank Drs. R. R. Ridgeway and W. J. O'Leary of the Niagara Falls Laboratory of the Norton Company. The authors wish also to acknowledge their indebtedness to the Graduate College of the State University of Iowa for a financial grant which made this work possible, and to Mr. J. G. Sentinella, instrument maker of the physics department, for his able assistance in the construction of the apparatus.

SEPTEMBER 1, 1937 PHYSICAL REVIEW VOLUME 52

Effect of Temperature on Photoelectric Emission*

R. J. CASHMAN
Northwestern University, Evanston, Illinois

(Received June 16, 1937)

A survey of the existing theories of photoelectric emission near the threshold shows that for $\nu \ll \nu_0$, $I = \text{const}\ T^n e^{h(\nu-\nu_0)/kT}$ and for $\nu = \nu_0$, $I = \text{const}\ T^n$. Different theories demand values of n from 1/2 to 5/2. The usual method of comparing theory with experiment, by making logarithmic plots of the current, fails to give any information as to the effect of the T term and hence fails to provide a test of the theories. If, however, data are taken at the threshold for different temperatures, the equation above should yield the correct value of n. This is a situation unlike that in the Richardson equation for thermionic emission where the effect of the T term is small compared to that of the exponential term. An analysis of the existing photoelectric data shows that n lies between about 0.7 and 1.7 for the different elements. The apparent departure from a T^2 law can be adequately explained if it is assumed that the work function increases with temperature. Values of the temperature coefficient between 4 and 10×10^{-5} ev/deg. are required for the different data. A new method for determining temperature coefficients is suggested which depends on data taken at the threshold. These values predict an intersection of spectral sensitivity curves for different temperatures in agreement with experiment. This suggests an alternative method for determining temperature coefficients using data at the point of intersection. The two methods are in agreement. The value of the constant A in Richardson's thermionic equation is computed on the hypothesis that for a clean metal the departure from the theoretical value of 120 amp./cm^2 deg.^{2} is due to a temperature coefficient of the work function. The computed values are in excellent agreement with those experimentally determined from thermionic measurements on the same specimens.

---

* Presented in part at the Madison Meeting of the American Physical Society, June 22–23, 1937.

THE problem of establishing an experimental value for the exponent of T in Richardson's thermionic equation has been of interest to physicists for many years. Any value between 0 and 4 serves equally well in describing the variation of emission with temperature, a fact which is of course due to the rapid change in the exponential term. If the equation is written in the form

$$I = A_n T^n e^{-b_n/T},$$

then $$n = (dI/I)/(dT/T) - b_n/T,$$

where A_n and b_n are constants of the emitting surface for a given n. Now for tungsten at 2000°K, b_n/T is about 26, and an error of ±5 percent in either term of the right member would result in an error of about 70 percent for n if its true value were 2. The purpose of the present paper is to show that such a situation does not exist in the case of the equations of photoelectric emission and it is possible to determine the exponent of T with considerable accuracy.

Theories of Spectral Distribution Near the Threshold

It was first recognized by Fowler[1] that the emission near the threshold is dominated by the Fermi factor $1/(e^{(\epsilon - W_i)/kT}+1)$. However, the value which the temperature term has in the final expression for the current depends on the form chosen for the boundary transmission coefficient, and on the form of the absorption coefficient of electrons of given energy for light of given frequency.

(a) *Fowler's first assumption.*[1] The emission will be proportional to the number of electrons per unit volume of metal whose total energy, increased by $h\nu$, exceeds the height of the potential step W_a, at the surface. This assumption leads to an expression for the current of the form

$$I = CT(W_a - h\nu)^{\frac{1}{2}} \log \{1 + e^{(h\nu - h\nu_0)/kT}\}. \quad (1)$$

This formula was rejected because it failed to agree with experimental data.

(b) *Fowler's second assumption.*[1] The number of electrons emitted per quantum of light absorbed is proportional to the number of electrons per unit volume of metal whose kinetic energy normal to the surface augmented by $h\nu$ is sufficient to overcome the potential step at the surface. This leads to the formula

$$I = CT^2(W_a - h\nu)^{-\frac{1}{2}}\varphi(x), \quad (2)$$

where

$$x = (h\nu - h\nu_0)/kT,$$

$$\varphi(x) = \sum_{n=1}^{\infty} (-1)^{n+1} \frac{e^{nx}}{n^2} \qquad \text{for } x \leq 0,$$

$$= \frac{\pi^2}{6} + \frac{x^2}{2} - \sum_{n=1}^{\infty} (-1)^{n+1} \frac{e^{-nx}}{n^2} \qquad \text{for } x \geq 0.$$

This formula was compared with experimental data by plotting experimental $\log I/T^2$ *vs.* $h\nu/kT$ curves and comparing their shape with the theoretical $\log \varphi(x)$ *vs.* x curve. The agreement was excellent.

(c) *Fowler's third assumption.*[1] In an attempt at a more exact theory Fowler introduced a transmission probability of the form $(\frac{1}{2}mu^2 + h\nu - W_a)^{-\frac{1}{2}}$. This assumption plus the second assumption leads to

$$I = CT^{\frac{1}{2}}(W_a - h\nu)^{-\frac{1}{2}} f(x)$$

where $$f(x) = \int_0^{\infty} \frac{dy}{y^{\frac{1}{2}}} \log (1 + e^{x-y}). \quad (3)$$

The integral[2]

$$f(x) = \sqrt{\pi} \sum_{n=1}^{\infty} (-1)^{n+1} \frac{e^{nx}}{n^{\frac{1}{2}}} \quad \text{for } x \leq 0.$$

Eq. (3) was compared with experiment in the same way as Eq. (2), and was found to be in excellent agreement with the data. It has been pointed out by Mitchell,[3] however, that a transmission probability of this form rests on a mistake in normalizing the free wave function.

(d) *DuBridge's assumption.*[4] The number of electrons emitted per quantum of light absorbed is proportional to the number of electrons striking the surface per sec. per cm² whose kinetic energy normal to the surface augmented by $h\nu$ is sufficient to overcome the potential step W_a. This

[1] Fowler, Phys. Rev. **38**, 45 (1931).

[2] An apparent typographical error exists in Fowler's paper in that n appears instead of $n^{\frac{1}{2}}$.

[3] Mitchell, Proc. Camb. Phil. Soc. **31**, 416 (1935).

[4] DuBridge, *Actualités Scientifiques et Industrielles*, no. 268 (Paris, 1935).

assumption, I believe, is equivalent to Fowler's second assumption with the added statement that the probability of an electron absorbing a quantum is proportional to the normal component of velocity of the electron. The result is

$$I=\alpha A T^2\varphi(x), \tag{4}$$

where $A=120$ amp./cm^2 deg.^{2}; $\varphi(x)$ is the function defined under Eq. (2), and α is assumed constant near the threshold.

(e) *Young and Frank's assumption.*[5] The probability of emergence is

$$\frac{(\frac{1}{2}mu^2+h\nu)^{\frac{1}{2}}(\frac{1}{2}mu^2+h\nu-W_a)^{\frac{1}{2}}}{[(\frac{1}{2}mu^2+h\nu)^{\frac{1}{2}}+(\frac{1}{2}mu^2+h\nu-W_a)^{\frac{1}{2}}]^2}$$

instead of that used by Fowler. This leads to

$$I=CT^{5/2}(W_a-h\nu)^{-\frac{1}{2}}f_1(x), \tag{5}$$

where $$f_1(x)=\int_0^\infty y^{\frac{1}{2}}dy\,\log\,(1+e^{x-y}).$$

$$f_1(x)=\frac{\pi^{\frac{1}{2}}}{2}\sum_{n=1}^{\infty}(-1)^{n+1}\frac{e^{nx}}{n^{5/2}} \quad \text{for } x\leq 0.$$

(f) *Mitchell's theory.*[3] This author has modified his complete quantum-mechanical theory of the photoelectric effect in metals[6] to take into account the region near the threshold where the temperature is important. In addition the idealized square top potential barrier is replaced by one of the image field type. He gets

$$I=AT^2\varphi(x), \tag{6}$$

where A is independent of T but may depend somewhat on ν. The function $\varphi(x)$ is a series which in the vicinity of the threshold reduces to the same form as Eqs. (2) and (4) but departs from this form for high frequencies.

(g) *Classical theory.* If one makes Fowler's second assumption but uses a classical distribution of electrons in the metal an expression is obtained for the current which approaches the frequency axis asymptotically as experiments demand but which unfortunately becomes imaginary for $h\nu>h\nu_0$. Using DuBridge's assumption instead gives

$$I=CT^{\frac{1}{2}}e^{(h\nu-h\nu_0)/kT}. \tag{7}$$

The classical theory thus predicts too rapid an increase in the current for $\nu>\nu_0$.

It will be observed that all the theories reduce to an expression of the type

$$I=\text{const}\ T^n e^{(h\nu-h\nu_0)/kT} \quad \text{for } \nu\ll\nu_0 \tag{8}$$

and at the threshold to

$$I=\text{const}\ T^n. \tag{9}$$

Equations (8) and (9) serve to illustrate a point previously mentioned regarding the effect of the T term on the emission. For values of $\nu\ll\nu_0$ the change in I with T is exceedingly rapid as in thermionic emission, but as the threshold is approached the T term becomes more and more important. Thus from Eqs. (2), (4) or (6)

$$dI=I[(2dT/T)+(d\varphi/\varphi)]. \tag{10}$$

If T changes by a small amount from room temperature, the T term is about one-half the φ term for $h\nu-h\nu_0=-0.1$ ev. For $h\nu-h\nu_0=-0.02$ ev, the T term is 10 times the φ term and for $h\nu-h\nu_0=+0.1$ ev the two terms are equal.

It is to be remarked before proceeding with the analysis of experimental data that the work functions determined by the various theories will differ somewhat,[7] although for theories (b), (c), (d) and (f) the deviation is less than 0.01 ev.

Comparison with Experimental Data

The usual method of comparing theory with experiment is to make logarithmic plots like those used in testing Fowler's Eq. (2). These are isothermal plots; the T term is only an additive constant, and hence the method fails completely to give information as to the effect of the T term on the emission. DuBridge[4] has used an isochromatic method in which $\log I/T^2$ *vs.* $\log T$ curves are compared with theoretical $\log\varphi(x)$ *vs.* $\log x$ curves. The effect of the T term varies in importance for such curves depending on the frequency of the incident light.

Equation (9) should serve, however, as a direct test of the theories since current data taken at the threshold for two different temperatures bear the relation

$$n=(\log I_2/I_1)/(\log T_2/T_1). \tag{11}$$

[5] Young and Frank, Phys. Rev. **38**, 838 (1931).
[6] Mitchell, Proc. Roy. Soc. **A146**, 442 (1934); **A153**, 513 (1935).
[7] Cashman and Jamison, Phys. Rev. **50**, 568 (1936).

Table I shows the data of various authors and the values of n which result. Some of the reported data on clean metals at different temperatures could not be analyzed because the spectral sensitivity curves were not shown with sufficient accuracy at the threshold.

Morris[8] reported an eightfold increase in current between 293 and 1013°K for λ2537. This wave-length is about 5 angstroms from λ_0 and the error is small by assuming $\lambda_0 = 2537$A. On the basis of a T^2 law the currents should have the ratio 11.7 instead of 8. The data for λ_0 in the case of Ta were taken from Table I(C) of Cardwell's[9] paper. The experimental points of the spectral sensitivity curves are rather widely separated and the currents are subject to greater errors in this case. The data of DuBridge and Roehr[10] extends over many temperatures and wave-lengths. Their data at λ2482 (4.97ev) are at the threshold λ_0 and hence serve as an excellent basis for study at different temperatures. Fig. 1, curve (*a*), shows the departure of their data from a T^2 law. The author's data on barium include only a temperature range of 100°C but it is considered to be quite accurate (see Fig. 2) since a continuous source of radiation was used in conjunction with a Van Cittert double monochromator and many points were determined.

Except for the Ta result it would appear that the data favor Eq. (3) which involves T to the 3/2 power. The transmission probability, however, used to obtain this result is in error as pointed out by Mitchell.[3] The whole situation can be cleared up if one considers the effect on the emission of a work function which varies with temperature, a relationship which has been omitted from all the theories. It will be shown below that the values of the temperature coefficient of the work function required to make experimental data fit the 5/2 power equation of Young and Frank are too large when compared with values for clean metals determined indirectly from thermionic data[11, 12] and directly from photoelectric[13–15] and contact potential[16, 17] measurements. Consequently, even if it is assumed that the photoelectric process proposed by Young and Frank is in good standing theoretically, the result obtained does not represent the experimental facts as accurately as the T squared equations of Fowler, DuBridge and Mitchell, and hence is not as acceptable.

TABLE I. *Data of various authors and the values of n which result.*

	ELEMENT	$h\nu_0$	T/T_0	I/I_0 (exp)	I/I_0 (theor) $n=2$	n (exp)
Morris[8]	Au	4.84 ev	3.42	8	11.7	1.69
Cardwell[9]	Ta	4.12	3.32	2.8	11.0	.73
DuBridge and Roehr[10]	Pd	4.97	2.67	5.0	7.13	1.62
Author	Ba	2.511	1.35	1.59	1.82	1.56

EFFECT OF A TEMPERATURE COEFFICIENT OF THE WORK FUNCTION

Let $h\nu_0$ be the work function at T_0 and let it increase by an amount ΔW at T. Eqs. (2), (4) or (6) then give for $T=T_0$ and $h\nu=h\nu_0$; $x=0$ and $\varphi(x)=\pi^2/12$. For $T=T$ and $h\nu=h\nu_0$; $x=-\Delta W/kT$ and

$$\varphi(x)=e^{-\Delta W/kT}-(1/2^2)e^{-2\Delta W/kT}+(1/3^2)e^{-3\Delta W/kT}-\cdots. \quad (12)$$

The corresponding currents at the two temperatures are

$$I_0=CT_0^2\pi^2/12, \quad (13)$$

$$I=CT^2\varphi(x). \quad (14)$$

Now $\varphi(x)$ (Eq. (12)) is a universal function of the argument and hence its curve can be plotted for small arbitrary values of $\Delta W/kT$. An experimental value of $\varphi(x)$ may be obtained by substituting the experimental currents in Eqs. (13) and (14), and the corresponding $\Delta W/kT$ can be read from the curve. This gives the temperature coefficient $\alpha(=\Delta W/T-T_0)$ for this temperature range that is necessary to bring the data into

[8] Morris, Phys. Rev. **37**, 1263 (1931).
[9] Cardwell, Phys. Rev. **38**, 2041 (1931).
[10] DuBridge and Roehr, Phys. Rev. **39**, 99 (1932).
[11] Becker and Brattain, Phys. Rev. **45**, 694 (1934).
[12] Nottingham, Phys. Rev. **49**, 78 (1936).
[13] Cardwell, Phys. Rev. **47**, 628 (1935).
[14] Jamison and Cashman, Phys. Rev. **50**, 624 (1936).
[15] Unpublished data of DuBridge and his students, private discussion.
[16] Waterman and Potter, Phys. Rev. **51**, 63 (1936).
[17] D. B. Langmuir, Phys. Rev. **49**, 428 (1936).

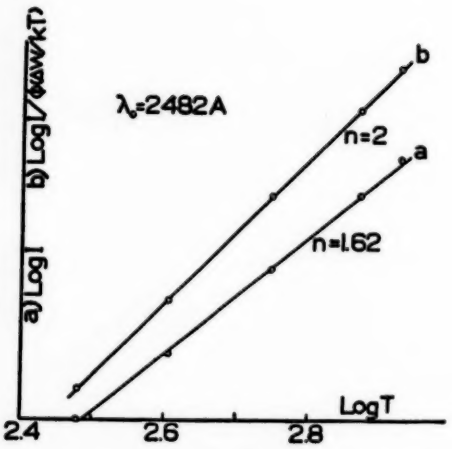

FIG. 1. Data of DuBridge and Roehr at threshold. Curve (*a*) yields the experimental exponent of T (Eq. (9)). Curve (*b*) same data with a temperature coefficient of the work function introduced into the theory equal to 6.0×10^{-5} ev/deg.

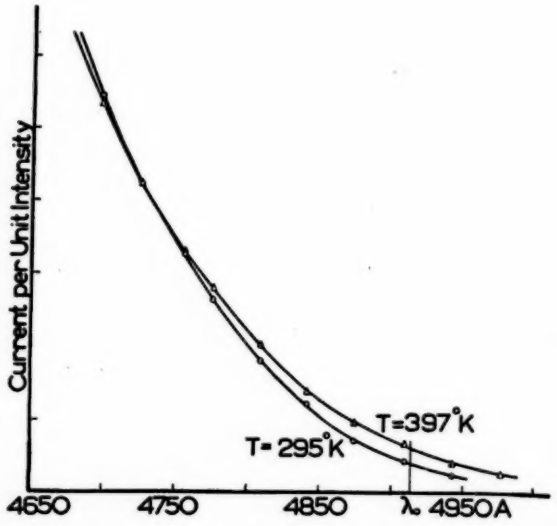

FIG. 2. Typical spectral sensitivity curves for Ba at two different temperatures showing how the emission for the higher temperature becomes *less* than that at the lower temperature below about 4700A.

agreement with a T^2 law. The data of Morris, DuBridge and Roehr and the author have been analyzed in this way and the values of α are shown in Table II. Cardwell's data on Ta and Winch's[18] on Ag have been analyzed by another method to be described in the next section.

Figure 1, curve (*b*) shows very strikingly how the data of DuBridge and Roehr are brought into agreement with a T^2 law with a temperature coefficient of only 6.0×10^{-5} ev/deg. In all cases α is extremely small and it is at first surprising that it has such a pronounced effect on the emission. The values, however, are of the same magnitude as those obtained previously by photoelectric[13–15] and contact potential[16] measurements and indirectly by thermionic measurements.[11] Attention is called, however, to the value -4.3×10^{-5} ev/deg. obtained indirectly from thermionic data by Nottingham[12] for a deactivated thoriated tungsten filament, and to the contact potential measurements on W of D. B. Langmuir[17] which agreed qualitatively with the result obtained by Nottingham. Since it appears that the temperature coefficient can be positive or negative without conflicting with thermodynamics it would be very important to make simultaneous thermionic and photoelectric measurements on a single specimen of W. This has been done by Warner[19] but the frequency range investigated does not permit a calculation of α.

If the analysis given above for the T squared equations is made for the 5/2 power equation instead one obtains the following values for the temperature coefficient: Au, 1.3×10^{-4}; Ta, 2.6×10^{-4}; Pd, 1.3×10^{-4}; Ba, 1.2×10^{-4} ev/deg. It was mentioned previously that these values are too large since the reported experimental values range from about 2 to 7×10^{-5} ev/deg. for pure metals.

The previous photoelectric method of obtaining α from Fowler plots at different temperatures requires a considerable range of wavelengths in order to get accurate fits to the theoretical curve. If the approximations made in the theories make themselves felt for $\nu \ll \nu_0$, the value of α resulting will be changed considerably. Thus in the case of barium, if one plots log (current per unit intensity) as ordinates[20] the value of α is $1.4 \pm 0.7 \times 10^{-5}$ ev/deg.; if one plots log (electrons per quantum $x(W_a - h\nu)^{\frac{1}{2}}$) the value of α is $2.2 \pm 0.7 \times 10^{-5}$ ev/deg.[14], and for a log (electrons per quantum) plot the value lies between 2 and 6×10^{-5} ev/deg., depending on what portion of the experimental data is fitted to the theoretical curve. The method described above, however, is not subject to such inconsistencies since the measurements are made at the threshold. If the

[18] Winch, Phys. Rev. **37**, 1269 (1931).
[19] Warner, Phys. Rev. **38**, 1871 (1931).
[20] Cashman and Jamison, Phys. Rev. **49**, 877 (1936).

TABLE II. *Analysis of the data of various authors and the values of α which result.*

	ELEMENT	α	$I_0=I$ (theor)	$I_0=I$ (exp)	A (comp)	A (exp)
Morris[8]	Au	5.7×10^{-5} ev/deg	2390A	2350A	62 $\frac{\text{amp.}}{\text{cm}^2\,^\circ\text{K}^2}$	
Winch[18]	Ag	4.1		2320	74	
Cardwell[9]	Ta	10.0		2890	37.5	37.2
DuBridge and Roehr[10]	Pd	6.0			60	60
Author	Ba	5.4	4650	4698	64	(60)

threshold is determined with reasonable accuracy (within ±0.01 ev) at one temperature and the temperatures themselves are fairly well known the value of α resulting should be reasonably accurate. Values of $\varphi(\Delta W/kT)$ vs $(\Delta W/kT)$ are given in Table III for the convenience of those desiring to use the method.

THE INTERSECTION OF SPECTRAL SENSITIVITY CURVES

It will be observed that all the theories predict that the effect of temperature becomes negligible for $\nu\gg\nu_0$. Thus Eqs. (2), (4) and (6) give

$$I=\text{const}\,[(h\nu-h\nu_0/k)^2+(\pi^2/3)T^2]. \quad (15)$$

For values of ν only 200A from ν_0 the second term is practically negligible, and the spectral sensitivity curves for two different temperatures should become parallel at high frequencies. Experimentally this is not observed and the curves cross at a finite angle a few tenths of a volt from the threshold. Beyond this crossing point the emission is *less* for high temperatures than for low temperatures (Fig. 2). It was this experimental fact which led to some uncertainty when Fowler's theory was proposed.[1]

It will be seen from an examination of the current expressions for $\nu>\nu_0$ that such a crossing of the curves is a natural consequence of a work function that increases slightly with temperature. The currents will be equal when

$$T_0^2\varphi(x_0)=T^2\varphi(x), \quad (16)$$

where $x_0=(h\nu-h\nu_0)/kT_0$ and

$$x=(h\nu-h\nu_0-\Delta W)/kT$$

and ν is the frequency at which the currents are equal. Thus a direct experimental proof of the hypothesis, that the departure from a T^2 law is due to a temperature coefficient of the work function, will be had if Eq. (16) is satisfied by the experimental data. This has been done for Au and Ba and the results are shown in the third and fourth columns of Table II. The agreement is excellent when one considers the experimental difficulties involved.

Equation (16) obviously provides another method for determining temperature coefficients. If the frequencies ν and ν_0 are known $\varphi(x_0)$ can be determined from Fowler's theoretical curve and the value of $\varphi(x)$ can then be calculated. By referring to the theoretical curve again x can be determined and hence ΔW. This has been done for Cardwell's data on Ta and Winch's data on Ag (Table II), since accurate current ratios could not be obtained at the threshold from their data. Cardwell[13] obtained 7.4×10^{-5} ev/deg. for the temperature coefficient of Ta from Fowler plots at two different temperatures.

DEPENDENCE OF THE RICHARDSON A ON THE TEMPERATURE COEFFICIENT OF THE WORK FUNCTION

A number of writers have pointed out that a small temperature coefficient of the work function would have a pronounced effect on the observed value of the coefficient A in the Richardson thermionic equation. This question has been examined fully by Becker and Brattain,[11] who have set forth explicitly the relations involved. Their conclusions were that a clean metal surface (as contrasted with a composite one) in the absence of strong accelerating or retarding fields would emit in such a way that any departure of A from the theoretical value 120 amp./cm^{2}deg.^{2} could be accounted for by a temperature coefficient of the work function. This implies a transmission probability for the electron at the surface which differs inappreciably from 1.0. It is thus important to examine the data in the light

TABLE III. *Values of* $\varphi(\Delta W/kT)$ *for various values of* $(\Delta W/kT)$.

$\Delta W/kT$	$\varphi(\Delta W/kT)$	$\Delta W/kT$	$\varphi(\Delta W/kT)$
−6.00	0.00248	−2.00	0.131
5.00	.00674	1.75	.167
4.50	.0111	1.50	.212
4.25	.0143	1.25	.269
4.00	.0183	1.00	.340
3.75	.0235	.75	.426
3.50	.0302	.50	.536
3.25	.0384	.387	.589
3.00	.0492	.25	.670
2.75	.0629	.2	.695
2.50	.0803	.0	.822
2.25	.1028		

of the new temperature coefficients obtained above. This is done in columns five and six, Table II. A(comp.) is determined from the relation

$$A_{\text{computed}} = 120e^{-\alpha}.$$

The assumption is made that α is constant over the photoelectric and thermionic ranges of temperature.

DuBridge and Roehr made thermionic measurements on their Pd specimen and obtained a value of 60 for A with a maximum deviation of about 30 percent from this value. It is seen that the calculated value is also 60 with $\alpha = 6.0 \times 10^{-5}$ ev/deg. Cardwell also carried out thermionic measurements on his Ta specimen and a value of 37.2 was obtained for A. The experimental value 10×10^{-5} ev/deg. for α when expressed in degrees per degree in the above equation yields 37.5 for A. This excellent agreement may be fortuitious but it is certain that a large temperature coefficient yields a low value for A. The results on Pd and Ta are particularly significant in that photoelectric and thermionic measurements were carried out on the same specimen under identical vacuum conditions.

The computed value of A for Ba was 64. Attention is called to the experiments of Ryde and Harris[21] who measured the thermionic emission from a heavy barium layer on tungsten. The method employed was to evaporate barium continuously from a side furnace onto a heated W filament, the rate of deposition on the latter being made greater than the rate of evaporation from it. They obtained a value of A of about 60 and a value for the work function of 2.11 ev. The work function is 0.4 ev lower that that obtained by the author so that a comparison of the A values is probably not justified. However, the conclusion of Becker and Brattain is given ample support by the results on Pd and Ta when analyzed on the basis of the new values for the temperature coefficient, and it seems safe to say that the variation in A for clean metals is an effect due mainly to a temperature dependence of the work function.

CONCLUSION

Experimental photoelectric data can be fitted to a T squared law provided ν_0 is regarded as a function of the temperature and this leads to a method of determining the temperature coefficient of ν_0 which is more accurate than those previously used and yields for the first time good agreement with thermionic data.

[21] Ryde and Harris, quoted by Reimann, *Thermionic Emission* (Wiley and Sons, N. Y.), 1934.

Visual Observations on the Malter Effect[1]

LEWIS R. KOLLER AND R. P. JOHNSON
Research Laboratory, General Electric Company, Schenectady, New York

(Received June 26, 1937)

The thin film field emission (Malter effect) from Al_2O_3 films on Al was investigated (1) by coating the film with a fine dust of willemite and observing the behavior of the primary beam; (2) by forming an electron image of the surface by means of the Malter current from it. The behavior of these films, while exhibiting the Malter effect, may be summarized as follows: **1.** The potential of the front surface of the electrode is a saw-tooth function of time at any point, and nonuniform over the surface at any instant. **2.** The current density of the primary beam at the surface varies, correspondingly, because of the varying electric field above the surface. **3.** A time lag exists between the application of voltage across the film and the establishment of the Malter current. **4.** The Malter current issues chiefly from a number of isolated points on the surface, and the current from any one of these points varies with time. **5.** The emitting points are scattered over the entire surface of the electrode, with some preferential grouping in the region covered by the primary beam. **6.** Some of the electrons constituting the Malter current have a kinetic energy corresponding in order of magnitude to the voltage drop across the film. **7.** The Malter electrons leave the film with a wide range of speeds.

INTRODUCTION

A NEW type of electron emitter, consisting of a thin film of insulating material on metal, has been studied by Malter. Such a film, when bombarded by electrons, emits current, many times larger than the primary current, to a collector which is held at a positive potential with respect to the metal underlying the film. Malter's explanation of the effect is that secondary emission from the surface of the film keeps it positive with respect to the metal backing. A high gradient is thus established through the film which results in the emission of electrons from the metal. Our observations agree with this explanation.

The object of these experiments was to test whether the thin film field emission from a film of Al_2O_3 on Al is proportional to the primary current density. Two methods were used. First, the surface of the film was coated with a fine dust of synthetic willemite, so that the behavior of the primary beam could be followed. So far as we could tell, this trace of fluorescent powder had no effect on the emitting properties of the electrode. Later, an electron image of the surface was formed by means of the Malter current from it.

[1] L. Malter, Phys. Rev. **49**, 478 (1936); **50**, 48 (1936). Malter calls the phenomenon "thin film field emission." We use the shorter name here for reasons of convenience.

WILLEMITE ON DISK; BEAM FOCUSED

Figure 1 shows a tube used for the first method. The Malter electrode A–M was cut from a sheet supplied us by the Aluminum Company of America. The film of electrolytic Al_2O_3 was about 10^{-3} cm thick, clear and glassy. After activation[1] with caesium and oxygen, magnesium getter was flashed and the tube was sealed off the pump.

With A–M floating, the primary beam formed a steady fluorescent spot on M. The beam was not noticeably bent after entering the collector cylinder C, and the spot did not noticeably move when A was connected to C. The floating potential of M therefore did not differ by more than a few volts from the potential of C.

The spot was focused to a diameter of about 1.5 mm, R was set at about 1/2 megohm, and A was made increasingly negative to C. At first the spot was stationary and no current flowed through the meter T. When a critical voltage near $V=50$ v was reached, the meter suddenly deflected and the spot was thrown upward off the disk onto the wall of C, indicating that M had suddenly gone strongly negative to C. The spot then drifted down the side of C slowly (seconds), flickered about at the edge of the disk, and finally returned rather rapidly across M toward its former steady position. While the spot was drifting back across M, an increasing electron current of the order of 100 μA flowed through

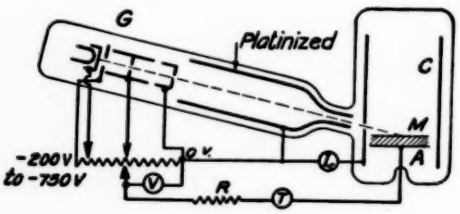

FIG. 1. Tube and circuit used in the first method of investigation. The surface M of the Malter film and the inside of the collecting cylinder C are dusted lightly with fluorescent powder.

the meter to A. Sooner or later there was another sudden deflection of the spot off the surface. The current through the meter dropped practically to zero at each such excursion. The frequency of the excursions increased with increasing V and with decreasing R.

It seems likely that after a discharge, when the primary beam is not striking M, M returns toward the potential of C by collecting positive ions formed from residual gas in the space. When M has become positive enough so that the beam again strikes it, the return is accelerated by the addition of the excess secondary emission to this small positive ion current. The spot has difficulty at the edge of the disk, probably because the bare Al, highly negative, is exposed there.

When R was increased to 5 or 10 megohms, there was a range of voltages V over which the current through T was quite steady, and the primary spot moved about only slightly and erratically on M without leaving the disk.

Willemite on Disk; Beam Defocused

The spot was defocused to cover about 1 cm² on the floating disk. When R was 1/2 megohm and V was sufficiently high, this broad spot was thrown off the disk just as the focused spot had been. With R 5 to 10 megohms and V in the range for which the focused spot moved about only slightly on M, the broad spot showed a striking "Swiss cheese pattern" (Fig. 2). In the green fluorescent patch, dark regions roughly circular and a few mm in diameter appeared suddenly and immediately began to disappear by shrinking in uniformly from the edges. At any instant the green patch was mottled with these shrinking dark areas. There was no marked limiting action of the edge of the green region—the edge was overlapped indifferently by dark holes centered out in a part of the disk which the primary beam had not been striking. The dark holes varied considerably in original size. Their maximum size and the frequency of their appearance increased with increasing V and with decreasing R. Deflection of the beam onto C was apparently a limiting case in which a single dark hole covered the entire disk.

These observations indicate that the entire surface M is "normally" at a fairly uniform potential positive to the Al beneath it. Now and then certain areas suddenly lose their positive charge. The circular shape of these areas suggests that a sudden spray of electrons is emitted from a point on M, the center of the circle, and discharges the surrounding region. The magnitude of such a spray, and hence the area discharged, is limited by the size of the ballast resistance R. The fact that the dark holes shrink inward gradually suggests that the potential of a discharged region decreases gradually toward the center. Positive ion current from the space and conduction over the surface presumably both aid in the recharging. From the time of recharging (about 1/4 sec. for completion), we can estimate the surface resistivity as, at the most, 10^{10} ohms. It seems plausible that such circular patches are being discharged suddenly and recharged gradually when the spot is focused to a small diameter, and that the changing local fields above M account for the slight erratic motion of a focused spot.

Time Lag in the Malter Effect

If the lead to A was opened and suddenly closed, the primary spot, even when R was 5 or 10 megohms, was thrown clear of the disk, and returned to its quasi-equilibrium position in the manner described above. We inferred from this that there is a time lag in the establishment of the Malter current of a greater order of magnitude than the charging time of the A–M condenser through R. When the circuit is closed the full voltage V is impressed across A–M until the Malter current sets up a drop in R. In this interval, M is discharged to A by a breakdown process. By finding what additional capacity between A and C was just large enough to

prevent these excursions, we were able to estimate that the time lag for this film was of the order of 10^{-3} sec.

Willemite on Disk; Persistent Emission

The Malter emission was excited in the normal way, with the primary spot either focused or defocused, and with R and V in the range appropriate for the existence of the Swiss cheese pattern. The primary beam was then cut off, either by biasing the grid of the gun or by cooling the cathode. The electron current through M to C persisted practically unchanged for a time ranging from seconds to hours. While this persistent current flowed, tiny bright spots of green could be seen here and there on M, together with a general very faint uniform fluorescence. The spots were somewhat concentrated in the region on which the primary beam had played, but not markedly so. The life of a spot was of the order of seconds, and longer the larger R. New spots continually appeared. A variety of experiments supported the belief that these tiny brilliant spots mark points on M from which the Malter electrons issue. For example, when a horseshoe magnet was brought up to the tube so that H ($\sim$200 gauss max.) was roughly parallel to M, these electrons were bent back and struck M, exciting it to fluorescence. New brilliant spots were apt to appear on regions thus bombarded. When a brilliant spot appeared near the edge of the disk, where the negative bare metal was exposed, the electrons were bent back toward the disk by the electric field and excited fluorescence in a fan of lines radiating from the spot (Fig. 3). In previous work with these thick films we have found that the persistent Malter current usually is unchanged until it suddenly goes to zero. In this tube, the persistent current sometimes decreased stepwise with time, the average number of bright spots decreasing with each downward step. It was sometimes possible, after the current had fallen to, say, 1/10 its initial value, to build it up by deflecting the Malter electrons back onto M with a magnet, thus exciting new emitting spots. In no case was it possible to restore the current after it had fallen to zero, other than by again bombarding the surface.

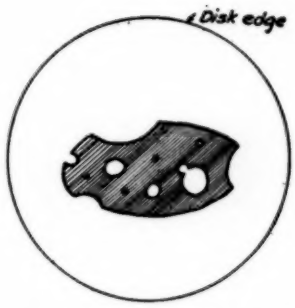

Fig. 2. Typical appearance of the surface when a fairly steady Malter current, limited by a high resistance, is flowing. The hatched region is being struck by the primary beam. The circular inclusions, which are shrinking in diameter, are areas recently discharged.

The fluorescence threshold for the willemite is about 50 v. It is evident that at least some of the electrons in the persistent Malter current leave M with kinetic energy corresponding at least in order of magnitude to the voltage drop between A and C. This is in agreement with a rough estimate of their momentum, based on the bending of their paths in the magnetic field. The positive potential of M probably is maintained partly by a small positive ion current from the space and partly by secondary emission caused by the outgoing persistent current.

Scintillations

If R was low ($<10^5$ ohms), or if a capacity $>0.1\ \mu F$ was put between A and C, when V was increased above a critical value, discharge of M occurred as a momentary bright spot or scintillation (entirely distinct from the persistent glowing green points described above). If such a scintillation occurred after the primary beam had been cut off, the persistent current immediately dropped to zero. These scintillations are apparently large-size occurrences of the same type as the dark holes in the Swiss cheese pattern.

Other Films Studied

We repeated these experiments on another electrode with a thick film ($\sim10^{-3}$ cm) and on an electrode with a much thinner film ($\sim3\times10^{-5}$ cm). With the thin film observation was harder, since the critical voltage for breakdown was lower, and hence the emerging electrons were less effective in exciting fluorescence. The re-

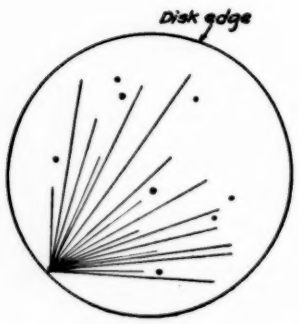

FIG. 3. Typical appearance of the surface when a persistent Malter current, limited by a high resistance, is flowing after the primary beam has been cut off.

sults with the thin film, however, were not inconsistent with those described above.

MALTER CATHODE IN AN IMAGE TUBE

The tube used for the second method of observation was similar to the image tube described by Zworykin and Morton[2] and about half as large (Fig. 4). Originally the cathode was a nickel disk with three strips of the thick-film aluminum riveted to its surface. These particular samples showed no Malter effect. However, it was possible to form a clear image of the cathode by the photoelectrons it emitted when the circular filament *F* was lighted.

We substituted for this cathode a thin-film electrode, 2 cm in diameter, surrounded by a coplanar Ni guard ring. This electrode showed a good Malter emission when we used either light from *F* or electrons from the gun to excite it, and connected the focusing rings together as a collector. Photoelectric emission from the surface is as effective as secondary emission in maintaining the surface at a positive potential.

With the usual image-tube potentials, and the film excited by light from *F*, the following cyclic behavior was observed:

At first there was a fairly sharp image of disk and guard ring, with a magnification of about 1. In the image, the disk was darker than the guard ring. The magnification began to increase, at first slowly then faster, and here and there a caustic-shaped splotch of fluorescence appeared on the screen for an instant. These splotches became more frequent and the magnification increased at a faster rate, until a blurry image of the disk alone more than covered the entire screen. Then suddenly the image reverted to its original size and sharpness, and the transient splotches ceased. This cycle occurred regularly with a period of about two seconds. Its period was less the higher the temperature of *F*. A single bright scintillation occurred on the film when the image returned to its original condition. This scintillation did not cause a burst of fluorescence on the screen.

This behavior can be explained on the same basis as the previous observations. So long as photoelectric emission from the surface continues, the surface becomes more and more positive. When the surface has charged up sufficiently, Malter current begins to flow out through the film, and reaches the screen to form the bright transient splotches. The Malter current increases rapidly with increasing potential of the film surface. Finally, the voltage across the film is so great that a scintillation occurs and the entire surface returns to the potential of the Al backing. Then the cycle is repeated.

When electrons from the gun were used as the exciting agent, the same cyclic behavior was observed. The splotchy images of the points from which the Malter emission came were apparently scattered over the disk, and were not confined to the area struck by the beam.

On removing the primary excitation, the continuous background due to photoelectric emission or to normal secondary emission vanished, as did the expansion and contraction of the image.

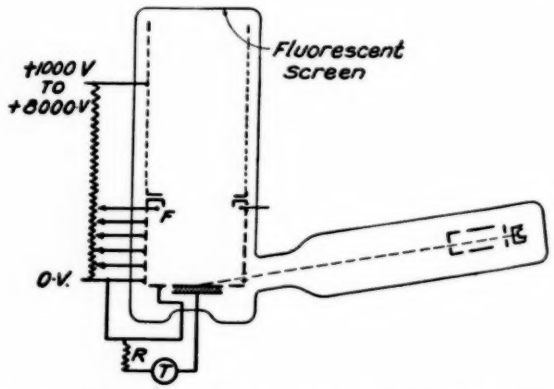

FIG. 4. Tube and circuit used for forming an electron image of Malter film on a fluorescent screen.

[2] V. K. Zworykin and G. A. Morton, J. Opt. Soc. Am. **26**, 181 (1936).

If there was no large resistance in series with the Malter electrode, the splotches corresponding to the Malter emission also disappeared. By putting 10 to 30 megohms in this circuit we could keep these splotches on the screen for a long time after stopping the primary excitation. They behaved in the same way as the fluorescent points which had marked the persistent Malter current through a film dusted with willemite.

The persistent splotches were irregular stars (Fig. 5), which could not be focused to point images of the emitting spots on the disk. We conclude that the Malter electrons have a wide range of speeds, for if their velocities differed only in direction it would be possible to bring them to a point focus.

There was no difference in appearance between the persistent splotches and the transient ones that appeared during excitation. The splotches are to be identified with the fluorescent points on a film emitting after the exciting agent has been shut off. The cyclic behavior of the image during excitation is to be associated with the sudden excursions of the primary beam mentioned above, with the sudden appearance and gradual shrinkage of the holes in the Swiss cheese pattern, and with the scintillations. It appears that the Malter emission, and the bursts that discharge the surface either wholly or in part, are two distinct types of conduction through the film.

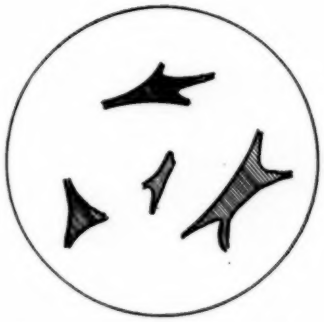

FIG. 5. Electron image of persistent Malter emission.

APPEARANCE OF THE FILMS

We examined several thick-film samples under a microscope (magnification 300), both before and after use as Malter emitters. The only visible surface irregularities were long narrow slanting cracks through the oxide, particularly near the edge of the disk, which had been cut out with shears. When the electrode was in use, there was no tendency for concentration of the emitting points along these cracks. Under the microscope, points where large scintillations had occurred appeared as craters. The existence of the Malter effect did not depend on whether scintillation breakdown had previously taken place.

LETTERS TO THE EDITOR

Prompt publication of brief reports of important discoveries in physics may be secured by addressing them to this department. Closing dates for this department are, for the first issue of the month, the eighteenth of the preceding month, for the second issue, the third of the month. Because of the late closing dates for the section no proof can be shown to authors. The Board of Editors does not hold itself responsible for the opinions expressed by the correspondents.

Communications should not in general exceed 600 words in length.

The Ratio e/m for *Primary* Beta-Rays from Radium *E*

It has recently been suggested by cloud chamber experiments, that primary beta-particles may carry with them a greater energy than that conventionally indicated by the curvature of their paths in a magnetic field.[1] Under such circumstances the mass of the beta-particles should be greater than that for normal electrons; and a measurement of the ratio e/m should give direct information in this connection.

It is of interest to note that the original experiments of Bucherer and of Neumann were made with beta-particles from radium, consisting chiefly of secondary, or internal conversion, electrons, and at a time when the primary and secondary rays had not yet been clearly identified. Therefore it appears that up to the present time no direct determination of the specific charge has been made for pure primary beta-rays as distinguished from the secondaries.

If one makes the assumption, suggested by the well-known beta-ray paradox, that all the primary beta-rays actually carry the same total energy, i.e., the energy corresponding to the upper limit of the continuous spectrum, and therefore that for momenta below the upper limit some of the total energy is "concealed" in a form other than kinetic,—then one calculates that for the beta-rays of radium E of momentum $2000H\rho$ the mass should be about twice that for normal Lorentz electrons. Therefore a rough measurement of e/m should suffice as a test for the above-mentioned assumption.

For the latter purpose we have devised a modification of the original Bucherer experiment, which consists essentially in reversing the order of the experiment. Bucherer first selected a particular velocity from the spectrum by letting the rays pass through crossed electric and magnetic fields, and then determined the momentum of the same rays by letting them pass some distance through the magnetic field alone and measuring their deflection on a photographic plate. On the other hand, with our present modification, the momentum is selected first, and then the velocity is determined by observing the value of the electric field which permits the rays to pass through the condenser. With this method the rays may be detected by means of a Geiger counter in a *fixed* position at the far end of the condenser. The experimental procedure consists simply in varying the voltage on the condenser until a "peak" of beta-rays is counted. The momentum is specified by the position of the source relative to the condenser, and by the magnetic field, which is kept constant. This arrangement seems to have a number of advantages over the original method. For example, with Bucherer's arrangement almost half of the total radiation from the source should be absorbed at the plates of the condenser; and scattering must therefore play a large rôle—while with the present modification the number of particles entering the condenser is of the same order of magnitude as the number transmitted when the voltage is adjusted for the peak. Further advantages and improvements and a discussion of the original experiments of Bucherer and Neumann will be given in a later article.

Observations have been made in the following manner: A line source of radium E of about one millicurie intensity was placed about 10 cm from one end of an electric condenser and a circular arc of about 16 cm radius. The condenser consisted of two brass plates 6 cm long and separated by about 0.5 mm. The whole was placed in vacuum and in a magnetic field of about 125 gauss, produced by a set of Helmholtz coils. The Geiger counter was placed just outside a one mil aluminum window in the vacuum chamber.

In this case one should observe a peak: for normal electrons, with about 1400 volts on the condenser; and for the "heavy" electrons, at about half this value. Actually the observations show a peak corresponding to the mass of the ordinary Lorentz electron to within about ten percent, and on the side of the heavier electrons. *Hence these results show quite definitely, that the assumption of the previously mentioned type of heavy electron is untenable,* but it is not yet quite clear whether or not the discrepancy lies within the limits of experimental error. Besides, side-peaks were observed, the one on the side of the lighter mass showing a definite maximum, and the other not quite resolved.

A complete mathematical analysis of the system of rays in this experiment has been carried out to determine the shape and intensity of the peak to be expected in the absence of scattering, but no side-peaks are predicted by these calculations. In order to determine the nature of these side-peaks and to improve the experimental accuracy a new apparatus is being constructed, with such modifications as are necessary for distinguishing between scattering and other effects.

We are indebted to Dr. J. A. Bearden and to Mr. C. M. Herget of The John Hopkins University for their generosity in supplying the radium E source; to Mr. J. L. Lawson for the loan of a Geiger counter scale-of-eight circuit and assistance with the same; and to Dr. O. S. Duffendack and to Mr. Harold Lifschutz for the loan of a Geiger counter. We also wish to express our appreciation, variously

for their interest and help, to Drs. R. L. Thornton, H. L. Crane, S. A. Goudsmit, J. Turin, D. S. Bayley, and to Mr. W. C. Parkinson and others. Finally we gratefully acknowledge support from the Horace H. Rackham School of Graduate Studies of the University of Michigan.

C. T. ZAHN
A. H. SPEES

Physics Department,
University of Michigan,
Ann Arbor, Michigan,
August 6, 1937.

[1] See reference to Crane's report on the possible difference between nuclear beta-particles and electrons, G. Breit, Third Washington Conference on Theoretical Physics, Rev. Sci. Inst. **8**, 141 (1937).

Further Search for Transmutations with Possible Emission of Negative Protons

I have been privileged to use the Berkeley cyclotron, to try again[1] to detect reactions in which there could be a chance of a negative proton being ejected during the transmutation.

The existence of the negative proton has been shown by G. Gamow[2] to be not impossible. In fact, Dirac's equation, being valid only for elementary particles of radius smaller than h/mc, does not apply to the proton whose radius is of the same order of magnitude as is its de Broglie wave-length (1.3×10^{-13} cm). Thus, no analogy to the "hole" positron theory is here required and therefore the proton—positive or negative—can be imagined as being a complex particle (neutron+positron+anti-neutrino, or, neutron +electron+neutrino).[3] Furthermore the existence of the negative proton would tentatively explain the possibility of the formation of isomeric nuclei such as: *UX*2 and *UZ*, Pb^{210}(?) and RaD, Br^{80} (18 min. and 4.2 hr.).[4] Attempts by various workers to detect the negative proton in a Wilson chamber having failed, and no evidence[5] having been found yet in any of the cosmic-ray tracks, I have looked for some process in which the detection of the negative proton was not essential to prove its existence. Radio-elements such as those formed according to the schematic reaction:

$$ {}_{Z}X^{M}+{}_{0}n^{1}\rightarrow{}_{Z+1}Y^{M}+{}_{-1}H^{1};\quad {}_{Z+1}Y^{M}\rightarrow e_{+}+{}_{Z}X^{M} \qquad (1) $$

if detected would give some support to the possible existence of the negative proton. The element bombarded should be of high isotopic content, and should not give any other positronic radioelement whose lifetime is comparable to the one looked for. The lifetime of ${}_{Z+1}Y^{M}$ should be very well established by means of a different nuclear reaction, and not be too short, so that chemical separation could be possible. Those conditions and energetic considerations lead to a very restricted choice of possible radioelements. Thus radiocarbon (C^{11}, 21.3 min.) radio-aluminum (Al^{26}, 7 sec.) or radiosilicon (Si^{27}, 2.6 min.) are favorable cases.

Attempts to detect C^{11} and Si^{27} after bombardment of boron and aluminum with fast neutrons (deuterons of about 7 Mev on Be or Li targets) have completely failed to show any activity with a thin Geiger-Müller counter, or any track in a Wilson chamber, which could not be traced to an impurity or a contamination.

The disintegration cross section for reaction (1) is therefore found to be smaller than 10^{-27} cm^2.

It is a pleasure to acknowledge my indebtedness to Professor E. O. Lawrence, Dr. D. Cooksey and co-workers for their friendly hospitality.

M. E. NAHMIAS*

Radiation Laboratory,
University of California,
Berkeley, California,
August 7, 1937.

[1] M. E. Nahmias and R. J. Walen, J. de phys., April 1937, p. 159.
[2] *Atomic Nuclei* (1937), p. 14.
[3] J. Solomon, J. de phys., May 1937, p. 182.
[4] A. H. Snell, unpublished.
[5] J. Crussard and L. Leprince-Ringuet, J. de phys., May 1937, p. 216.
* Rockefeller Fellow.

Grating Space of Barium-Copper-Stearate Films

We have recently shown[1] that films of barium stearate built according to the method of Dr. Katharine Blodgett[2] give sharp x-ray diffraction. A preliminary determination made by one of us[3] of the grating-space of several barium-copper-stearate films indicated fairly good agreement between x-ray measurements and measurements made with an interferometer from films of known numbers of layers. A more thorough investigation of these films now discloses the fact that the x-ray and optical measurements do not agree.

Interferometer measurements give 48.40A for the mean thickness of the double-layers of stearates deposited on glass. X-ray measurements, based upon the crystal wave-length[4] of 1.47336A for the tungsten $L\alpha_1$ line, give 50.31A for the grating-space of the films for an infinite order. With Bearden's[5] weighted average of 1.00248 as the ratio between ruled-grating and crystal wave-length values, the grating-space of the films in terms of the ruled-grating scale is found to be 50.43×10^{-8} cm. The observed position of the $M\alpha$ line is also consistent with these values for the grating-space. The values given are corrected for the refraction of the x-rays, our experiments giving a unit decrement of 5.4×10^{-6} for the $L\alpha_1$ line of tungsten.

We find also that the films designated by Dr. Blodgett as *X* films,[6] have approximately the same x-ray grating-space as do the *Y* films. The similarity in structure of the *X* and *Y* types of films and the lack of agreement between the x-ray and optical measurements of the grating-space, are difficult to reconcile with the idea that the crystalline structure of the films used in these experiments is imparted to them by the dipping process used in their construction.

A detailed report of the work will be given at a later date.

CLIFFORD HOLLEY
SEYMOUR BERNSTEIN

Ryerson Physical Laboratory,
University of Chicago,
Chicago, Illinois,
August 4, 1937.

[1] Clifford Holley and Seymour Bernstein, Phys. Rev. **49**, 403 (1936).
[2] Katharine B. Blodgett, J. Am. Chem. Soc. **57**, 1007 (1935).
[3] Clifford Holley, Phys. Rev. **51**, 1000 (1937).
[4] M. Siegbahn, *Spektroskopie der Röntgenstrahlen*, second edition (1931), p. 237.
[5] J. A. Bearden, Phys. Rev. **48**, 385 (1935).
[6] Blodgett, reference 2, p. 1011.

Diamagnetism of Superconducting Bodies

In connection with London's letter on the same subject[1] I should like to point out that the striking diamagnetism exhibited by superconducting metals (the so-called Meissner effect) can be interpreted, or rather described, in a way which is both simple and natural; so natural, indeed, that I am afraid it will be considered as quite obvious. Its theoretical implications, however, do not seem to be generally recognized.

Since the induction B represents the space average of the field in the molecular theory, it is difficult to believe that the idea of a superconducting phase with $B\neq 0$ inside is devoid of any meaning whatever, or, in other words, that $B=0$ is anything but an equilibrium condition. If this view is correct, then the inevitable interpretation of the Meissner effect is, that the presence of even a very small field inside the metal must cause so great an increase of the free energy, that the lines of force are pushed out of the metal. The magnetic behavior of ordinary dia-, para- and ferromagnetic bodies can of course be discussed on the same lines, starting from the expression $f=B^2/8\pi\mu$ for the free energy per unit volume. Simply to set $\mu=0$ into this expression for superconductors, would not be very satisfactory. One can easily see, instead, that in order to obtain a perfect Meissner effect at moderate field strengths, it is sufficient to postulate that f is any function of B with $(\partial f/\partial B)>0$ at $B=0$.

The possibility of a phase with $B\neq 0$ had been already considered by Peierls[2] not, however, as an unobservable instable state, but as something which could exist under suitable conditions; he identified it, therefore, with the "transition state." Casimir and Gorter, London[3] and others maintain, on the other hand, that the transition state consists of a fine texture of the pure superconducting phase with $B=0$ and of the normal phase which carries the magnetic flux; Landau's work has greatly strengthened this opinion.[4] Although, therefore, a pure superconducting phase with $B\neq 0$ is never observed experimentally, we will retain the idea of such a phase as a useful and permissible fiction, of a kind which is not unusual in thermodynamics, the best-known example being perhaps van der Waals' instable fluid. The analogy is obvious if one considers the experimental free energy curve for the transition state (Fig. 1(a)) and the corresponding "isotherm" (Fig. 1(b)) (full lines), which one is immediately tempted to accomplish in a manner analogous to van der Waals' isotherm.

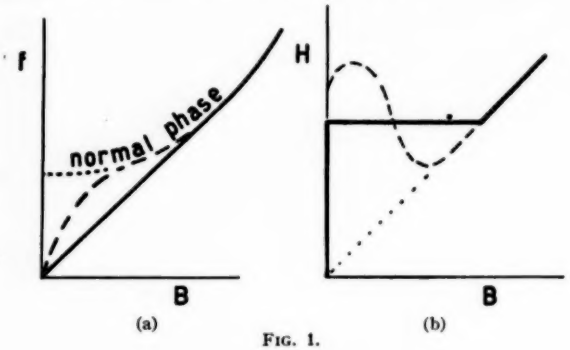

(a) (b)

FIG. 1.

(I am much indebted to Dr. Peierls for Fig. 1(a) and the discussion of the transition state contained therein.) Thus the splitting of a superconductor with $B\neq 0$ into a network of two different phases is made to depend on a general theorem about systems with a free energy curve (free energy *vs.* some additive parameter) which is concave towards the axis of abscissae (also kindly pointed out to me by Dr. Peierls), as for instance a system of two incompletely miscible liquids.

The theory will have to explain, of course, why the electronic motions should be so strongly disturbed by even a very small field. (This difficulty, however, is not specifically dependent on our assumption; it is, indeed, inescapable.) The difficulty is best seen in Fig. 1(a); the singularity at the origin ($(\partial f/\partial B)\neq 0$ at $B=0$) is particularly striking, since one would expect here a series expansion like:

$$f=a+bB^2+cB^4+\cdots$$

to be valid. We must then assume that the validity of this expansion is confined to fields so small, as to be unimportant from a macroscopic point of view. (This means that the effect of a magnetic field cannot be treated by means of perturbation theories.) We need not, perhaps be exceedingly disturbed by this fact, such singularities being indeed a common feature of "cooperative phenomena," such as superconductivity undoubtedly is. There is in fact a rather nice parallelism between the two extreme cases of magnetic behavior, the $H(B)$ curve showing a jump at $B=0$ for superconductors and the $B(H)$ curve showing a similar jump at $H=0$, if somewhat idealized, for ferromagnetic crystals.

I finally wish to express my warmest thanks to Professor Heisenberg as well as to Dr. Peierls for much kind criticism and advice.

G. C. WICK

Istituto di Fisica,
Roma, Universita,
July 28, 1937.

[1] London, Phys. Rev. **51**, 678 (1937).
[2] Peierls, Proc. Roy. Soc. **155**, 613 (1936).
[3] London, Physica **3**, 450 (1936); see also reference 2.
[4] London, Physik. Zeits. Sowjetunion **11**, 129 (1937).

Ionization of Mercury Vapor by Positive Potassium Ions

The balance space charge method of detecting ionization, reported at various times by one of the writers[1] has been improved to adapt it to experiments involving extremely feeble ionization. The ions were detected in this method by their influence on a space charge limited current of electrons flowing between a hot tungsten filament and a surrounding metal cylinder. This electron current tended to become unstable because the filament was colder near the ends than in the middle and failed to provide a space charge limited electron current at the ends. This difficulty was eliminated by lengthening the filaments about an inch at each end and placing shielding cylinders around the unusable cooler portions. The anticipated result was obtained, and with the greater stability, greater sensitivity was possible.

The system of accelerating the positive potassium ions was also altered slightly to allow a more intense ionizing

beam to enter the detector. The change amounted only to narrowing and lengthening the accelerating slits and placing the accelerators closer together.

The apparatus was tested by looking for the ionization of argon by potassium ions previously observed and reported.[1] The ionization of the argon was so intense that it was estimated conservatively that an effect one-one hundredth as large could certainly have been observed.

The argon was removed and the tube filled with mercury vapor at suitable pressure (10^{-2} to 10^{-1} mm) by closing off the tube with a mercury cut-off and heating the whole tube and cut-off to the proper temperature as given in the *International Critical Tables* for mercury vapor pressures. No ionization of the mercury was observed at all by potassium ions of energies up to 300 electron volts. The result is surprising in view of the fact that ionization of mercury by sodium ions had previously been observed.[2] It now appears as if the ionization by sodium ions if it really exists is the result of a purely fortuitous interaction which can occur between Na^+ and Hg. The work is being checked.

The senior writer wishes to express his indebtedness to Professor R. T. Birge and Professor Leonard B. Loeb for the privilege of working in the physics laboratory of the University of California.

ROBERT N. VARNEY

New York University,
University Heights.

MILTON E. GARDNER
A. C. COLE

University of California,
Berkeley, California,
August 16, 1937.

[1] R. N. Varney, Phys. Rev. **47**, 483 (1935).
[2] Varney and Cole, Phys. Rev. **50**, 261 (1936).

Disintegration of Boron by Deuterons

In a previous experiment, Bonner and Brubaker[1] investigated the neutrons from the disintegration of boron by 0.9 MV deuterons. From the measurement of the energies of recoil protons it was shown that there were neutron lines at 4.35, 6.35, 9.1 and 13.2 MV. When recoil helium nuclei were used to measure the neutron energies, the same lines were observed with the possible exception of the one at 13.2 MV. At that time it was suggested that the absence of high energy recoils might be due to the fact that 13 MV neutrons do not make elastic head-on collision with helium nuclei. The present experiment has been done to clear up the question as to whether the expected high energy helium recoils are missing.

3500 pairs of stereoscopic pictures were taken when boron was bombarded with 0.9 MV deuterons. For this series of pictures the cloud chamber was filled with helium at a pressure of 10.5 atmospheres. The energy distribution of the recoils in the forward direction (0−10°) indicated neutron lines with energies of about 4.3, 6.3, 9.1 and 13.2 MV, the last three having relative intensities of 1, 3, and 1, respectively. Thus it seems certain that 13 MV neutrons do make elastic collisions with helium nuclei.

The relative intensity of the 13.2 MV line (as compared to the 9.1 MV group) appears somewhat weaker when detected with recoil helium nuclei than with recoil protons. If this small effect is not due to experimental error it may be due to a difference in the variation of the collision cross section with energy for helium and hydrogen nuclei.

W. E. STEPHENS
T. W. BONNER

Kellogg Radiation Laboratory,
California Institute of Technology,
Pasadena, California,
August 4, 1937.

[1] Bonner and Brubaker, Phys. Rev. **50**, 308 (1936).

Errata: Magnetic Quadrupole Field and Energy in Cubic and Hexagonal Crystals

(Phys. Rev. **44**, 38 (1933))

and

Magnetic Interaction and Resultant Anisotropy in Strained Ferromagnetic Crystals

(Phys. Rev. **52**, 18, (1937))

In analyzing the effects of strain on magnetic interaction in crystals I have had occasion to recompute S_{40}, a coefficient fixing the magnitude of so-called quadrupole energy terms,[1] and have discovered a mistake, made in 1933, in reducing correct lattice sums of fourth-order zonal harmonics to the form chosen for publication. The mistake does not affect any conclusion yet based upon the erroneous values since the resulting discrepancies lie within the present accuracy of measurements. The following are the changes that should be made in the interest of accuracy.

In Phys. Rev. **44**, 38–42 (1933) in the last paragraph on page 40 write $A_0' = (21/2)R_\epsilon$ and $A' = -(105/4)R_\epsilon$ for $A_0 = (21/2)NR_\epsilon$ and $A = -(105/4)NR_\epsilon$. In Table III on page 41 the last two entries in the last column should be -1.77512 and -4.30040 instead of -1.77562 and -4.11336.

In Phys. Rev. **52**, 18–30 (1937), in Table II on page 21, the values of S_{40} under "Body-Centered Cubic" and "Face-Centered Cubic" should be -3.10646 and -7.52569 instead of -3.10734 and -7.19838. In Table III, part 1, and in Table IV, the "First Anisotropy Coefficient" (quadrupole part) should be multiplied by 0.99972 for body-centered crystals, by 1.04547 for face-centered crystals, and K_1 changed as necessary to correspond.

L. W. MCKEEHAN

Sloane Physics Laboratory,
Yale University,
New Haven, Connecticut,
August 5, 1937.

[1] For an explanation of this notation see Phys. Rev. **52**, 18–30 (1937).

Important Notice

THE American Institute of Physics will pay $2.00 per copy for each of the following issues of the *Physical Review:*

Volume 1, No. 6—June, 1913
Volume 2, No. 2—August, 1913
Volume 2, No. 4—October, 1913
Volume 2, No. 5—November, 1913
Volume 7, No. 1—January, 1916
Volume 7, No. 2—February, 1916
Volume 7, No. 3—March, 1916
Volume 7, No. 4—April, 1916
Volume 7, No. 5—May, 1916
Volume 9, No. 2—February, 1917

Copies should be in good condition. They should be addressed to the Publications Manager, American Institute of Physics, 175 Fifth Avenue, New York, New York, with the name and address of sender and with a covering letter.